

FORSCHUNGSZENTRUM ROSSENDORF



WISSENSCHAFTLICH-TECHNISCHE BERICHTE

FZR-318

Mai 2001

Annual Report 2000
Institute of Radiochemistry

Editor: Prof. Dr. Th. Fanghänel

Editorial staff: Dr. H.-J. Engelmann
Prof. Dr. G. Bernhard

Preface

The Institute of Radiochemistry (IRC), one of the five institutes of the Forschungszentrum Rossendorf (FZR) performs basic and applied research in the fields of radiochemistry and radioecology. Main goal is the quantification of the interaction and mobility of radionuclides in the geo- and biosphere. Because of their high radiotoxicity and long half-life the actinides are of special interest. Among the actinides uranium and its manifold interactions plays a major role in the institute's research activities. In addition the interactions of some important long-lived fission and decay products are studied.

More than 60 scientists, technicians and PhD students are employed in the Institute of Radiochemistry. The research is focused on understanding the fundamental processes relevant for the behavior of radionuclides in the environment. Main topics are:

- Aquatic chemistry
- Radionuclide interaction with mineral surfaces
- Radionuclide interaction with biological materials (microbes and plants)
- Modeling the radionuclide transport
- Development of spectroscopic speciation methods

We accomplished many new scientific results in the past year, which are presented in this Annual Report. Among them only a very few can be highlighted in this preface.

Further progress was achieved in understanding the interaction mechanism of actinides with humic acids. The coordination numbers and bond distances of the coordinated oxygens have been determined by X-ray absorption spectroscopy for tetra- and pentavalent actinides (Np(IV) and Np(V)). It was shown that the carboxylic groups of the humic acid form monodentate complexes with the neptonyl ions.

We extended our laser spectroscopic capabilities by installing a new laser system with ultra-short pulses (130 fs) for fluorescence measurements of organic substances. We intend to gain information on actinide complexes with organic ligands by studying the fluorescence properties of the organics with very short life times. The laser system and the method were successfully validated by the determination of the well-known uranyl-salicylic acid complexation.

Although surface complexation concepts are more and more used to describe the interaction of trace metals on aqueous / mineral surfaces, their application in environmental engineering and risk assessment is still scarce. To bridge this gap, we started to create a mineral-specific database for surface complexation. A prototype of this database has already been set up as Microsoft Access application. It is not a mere data collection but allows data processing and gives links to spectroscopic species evidence and theoretical background for surface complexation models.

A new radio-analytical tool was developed which allows the direct and fast determination of α -emitting radionuclides in concrete. By a special treatment of the sample and a special evaluation procedure α - emitting radionuclides in multi-element spectra can be detected as low as 0,02Bq/g within 30 h. The large amounts of concrete potentially contaminated with α -active nuclides which pile up during the decommissioning of nuclear installations can be characterized more efficiently by the application of this method. Its application for the decommissioning of the WAK, Karlsruhe is under discussion.

The institute organized two large international conferences in the past year: The 2nd Euroconference Bacterial-Metal/Radionuclide Interactions: Basic Research and Bioremediation, August/September 2000, Rossendorf/Dresden, Germany and The Second Euroconference and NEA Workshop on Speciation Techniques, and Facilities for Radioactive Materials at Synchrotron Light Sources, September 2000, Grenoble, France.

Since February 2000 I have the honor to be appointed as the new director of the Institute of Radiochemistry. I wish to thank Prof. Dr. Gert Bernhard who has been acting director until February 2000.

I would like to express many thanks to our numerous national and international research partners, visitors and collaborators. Special thanks are due to the Executive Board of the Forschungszentrum Rossendorf, the Ministry of Science and Arts of the State of Saxony, the Federal Ministry of Education and Research of

Germany, the Federal Ministry of Economics and Technology of Germany, the Deutsche Forschungsgemeinschaft, the Bundesamt für Strahlenschutz, the European Commission and other organizations for their support of our research and last, but not least, to the staff and guests of the IRC for performing excellent research and administration.



A handwritten signature in black ink that reads "Thomas Fanghänel". The signature is written in a cursive style.

Prof. Dr. Thomas Fanghänel

CONTENTS

I. SCIENTIFIC CONTRIBUTIONS

1. AQUATIC CHEMISTRY OF ACTINIDES/RADIONUCLIDES

Thorium(IV) Complexation by Humic Acids Studied by EXAFS S. Pompe, K. Schmeide, T. Reich, C. Hennig, H. Funke, A. Roßberg, H. Moll, K.H. Heise, G. Bernhard	1
Complex Formation in the System Uranium(VI) - Alpha-Substituted Carboxylic Acids Studied by UV-vis Spectroscopy; Part I: Glycolic Acid H. Moll, G. Geipel, G. Bernhard, Th. Fanghänel, I. Grenthe	2
Complex Formation in the System Uranium(VI) - Alpha-Substituted Carboxylic Acids Studied by UV-vis Spectroscopy; Part II: α -Hydroxyisobutyric Acid H. Moll, G. Geipel, G. Bernhard, Th. Fanghänel, I. Grenthe	3
Complex Formation of Uranium(VI) with Adenosine Triphosphate G. Geipel, G. Bernhard	4
Formation of $\text{Ca}_2[\text{UO}_2(\text{CO}_3)_3]$ in Dependence on the Concentration of UO_2^{2+} , Ca^{2+} and CO_3^{2-} S. Amayri, L. Baraniak, G. Bernhard	5
Synthesis and Characterization of Barium Uranyl Carbonate, $\text{Ba}_2[\text{UO}_2(\text{CO}_3)_3] \cdot 6\text{H}_2\text{O}$ S. Amayri, G. Geipel, G. Bernhard, K. Henkel	6
Synthesis and Characterization of Strontium Uranyl Carbonate, $\text{Sr}_2[\text{UO}_2(\text{CO}_3)_3] \cdot 8\text{H}_2\text{O}$ S. Amayri, G. Geipel, G. Bernhard, K. Henkel	7
Structural Comparison of $\text{Cu}[\text{UO}_2\text{AsO}_4]_2 \cdot 12\text{H}_2\text{O}$ and $\text{Cu}[\text{UO}_2\text{AsO}_4]_2 \cdot 8\text{H}_2\text{O}$ C. Hennig, M. Rutsch	8
Complex Formation of Uranium(VI) with 5-Sulfosalicylic Acid Studied by TRLFS Part I: Nanosecond Laser Pulses as Excitation Source G. Geipel, G. Bernhard	9
Complex Formation of Uranium(VI) with 5-Sulfosalicylic Acid Studied by TRLFS Part II: Femtosecond Laser Pulses as Excitation Source G. Geipel, G. Bernhard	10
Comparison of Several Hydroxybenzoic Acids in Terms of Complex Formation with Uranium(VI) G. Geipel, G. Bernhard	11
Complex Formation of Uranium(VI) with Benzoic Acid D. Vulpus, L. Baraniak, G. Bernhard, Th. Fanghänel	12
Synthesis and Characterization of Np(VII) in Strong Alkaline Solution H. Moll, T. Reich, G. Geipel, C. Hennig, H. Funke, S. Pompe, K. Schmeide, Th. Fanghänel, I. Grenthe	13
Neptunium(IV) Humate Complexation Studied by XAFS Spectroscopy K. Schmeide, S. Pompe, T. Reich, C. Hennig, H. Funke, A. Roßberg, G. Geipel, V. Brendler, K.H. Heise, G. Bernhard	14
EXAFS Study of the Neptunium(V) Complexation by Humic Acids in Neutral Solution S. Pompe, K. Schmeide, T. Reich, C. Hennig, H. Funke, A. Roßberg, G. Geipel, V. Brendler, K.H. Heise, G. Bernhard	15
First XAFS Measurements of Plutonium Complexation by Humic Substances K. Schmeide, S. Pompe, T. Reich, C. Hennig, H. Funke, A. Roßberg, G. Geipel, K.H. Heise, G. Bernhard	16
Solvent Extraction of Uranium(VI) by Calix[6]arene K. Schmeide, B. Barz, K.H. Heise, G. Bernhard, K. Gloe	17

2. INTERACTION OF ACTINIDES/RADIONUCLIDES WITH SURFACES OF ROCKS, MINERALS AND COLLOIDS	
Inorganic Colloids in Mine Waters H. Zänker	19
Acid Rock Drainage (ARD) Samples from the 'Himmelfahrt Fundgrube' at Freiberg Studied by XAS H. Moll, H. Zänker, W. Richter, V. Brendler, C. Hennig, A. Roßberg, H. Funke, T. Reich	20
Colloid-Borne U(VI) in the Flooding Water of an Abandoned Uranium Mine W. Richter, H. Zänker	21
SEM of Colloid Particles on Nuclear Track Filters: The Influence of Dissolved Salts G. Hüttig, W. Richter, H. Zänker	22
Detection of Iron Colloids on Filter Membranes after Weathering of an Iron-rich Chlorite in Neutral pH-Range E. Krawczyk-Bärsch, G. Hüttig, H. Zänker, T. Arnold, G. Bernhard	23
Uranium Sorption on Iron-rich Chlorite and the Effect of Humic Acid E. Krawczyk-Bärsch, T. Arnold, G. Bernhard	24
The Dissolution of Chlorite in Acid pH-Region E. Krawczyk-Bärsch, T. Arnold, F. Brandt, D. Bosbach, G. Bernhard	25
Adsorption of Hexavalent Uranium onto Phyllite as a Function of the Concentration of Calcium and Carbonate L. Baraniak, S. Amayri, G. Bernhard	26
Uranium(VI) Adsorption onto Phyllite and Granite in the Presence of Calcium and Carbonate S. Amayri, L. Baraniak, G. Bernhard	27
Studying the Sorption of Uranium(VI) onto Muscovite by Atomic Resolution Transmission Electron Microscopy T. Arnold, E. Krawczyk-Bärsch, G. Bernhard	28
Time-Resolved Laser Fluorescence Spectroscopy (TRLFS) Study of the Sorption of Curium(III) onto Smectite and Kaolinite Th. Stumpf, A. Bauer, F. Choppin, J.I. Kim	29
Sorption of Curium(III) onto γ -Alumina - A TRLFS Study Th. Stumpf, Th. Rabung, R. Klenze, H. Geckeis, J.I. Kim	30
Synthesis of ^{14}C -Labeled and Unlabeled Humic Acid Type M42 S. Pompe, M. Bubner, M. Meyer, R. Nicolai, K.H. Heise, G. Bernhard	31
Redox Equilibria in Natural Aquatic Systems Caused by Decomposition of Organic Matter A. Abraham, L. Baraniak, G. Bernhard	32
Redox Equilibria in Natural Aquatic Systems Including Dissolved Organic Matter A. Abraham, L. Baraniak, G. Bernhard	33
3. INTERACTION OF ACTINIDES/RADIONUCLIDES WITH BIOLOGICAL SYSTEMS	
Comparison of the Structures of the Natural Bacterial Communities in one Uranium Mining Waste Pile and in one Uranium Mill Tailings K. Flemming, G. Satschanska, S. Selenska-Pobell	35
EXAFS Investigations of Uranium(VI) Complexes Formed at the Cell Surfaces of <i>Acidithiobacillus ferrooxidans</i> Types M. Merroun, T. Reich, C. Hennig, G. Geipel, G. Bernhard, S. Selenska-Pobell	36

Characterization of the Uranium(VI) Complexes Formed at the Cells of Three <i>A. ferrooxidans</i> Types by the Use of Infrared Spectroscopy M. Merroun, R. Nicolai, K.H. Heise, S. Selenska-Pobell	37
Sequence Analysis of the Surface Layer (S-Layer) Proteins of the Uranium Mining Waste Pile Isolate <i>B. sphaericus</i> JG-A12 and of <i>B. sphaericus</i> NCTC 9602 J. Raff, K. Flemming, S. Selenska-Pobell	38
Bacteria Cultured from Soil Samples of Uranium Mining Waste Piles I. Tzvetkova, Tz. Tzvetkova, V. Groudeva, S. Selenska-Pobell	39
Scanning Electron Microscopy Investigations of Uranium Complexes in Plant Samples A. Günther, E. Christalle, H. Reuther, G. Bernhard	40
4. MODELING OF RADIONUCLIDE TRANSPORT	
RES ³ T - Rossendorf Expert System for Surface and Sorption Thermodynamics V. Brendler	41
Chemical Modeling of Sorption onto Colloids in Mine Waters V. Brendler, H. Zänker	42
5. DEVELOPMENT OF SPECTROSCOPIC SPECIATION METHODS AND OTHER ANALYTICAL TOOLS	
A SPLICE Program to Connect Two EXAFS Spectra of the Same Sample H. Funke, H. Böttger	43
Test Experiments to Verify the 'SPLICE' Program H. Funke, T. Reich, C. Hennig, A. Roßberg	44
EXAFS Study of U(VI) Compounds: A new Approach to Data Analysis Yu.A. Babanov, T.Ye. Zayarnaya, T. Reich, H. Funke	45
Application of the Tikhonov Regularization Method to the EXAFS Analysis of $UO_2(H_2AsO_4)_2 \cdot H_2O$ T.Ye. Zayarnaya, T. Reich, C. Hennig, H. Funke	46
The Application of Iterative Transformation Factor Analysis for the Decomposition of Multicomponent EXAFS Spectra of Uranium(VI) Complexes with Acetic Acid A. Roßberg, T. Reich	47
Combination of EXAFS and XRD for Solving Heavy-Atom Structures Part I: X-Ray Powder Diffraction of $UO_2[H_2AsO_4]_2 \cdot H_2O$ C. Hennig, T. Reich, F. Prokert, N. Schell, G. Reck, W. Kraus	48
Combination of EXAFS and XRD for Solving Heavy-Atom Structures Part II: EXAFS Measurements of $UO_2[H_2AsO_4]_2 \cdot H_2O$ C. Hennig, T. Reich, F. Prokert, N. Schell, G. Reck, W. Kraus	49
FTIR Spectroscopy of Water Solutions R. Nicolai, K.H. Heise	50
Laser Induced Breakdown Detection of Colloids C. Walther, G. Geipel	51
The Use of Deflocculants and Surfactants to Stabilize Concrete Suspensions for the Preparation of Alpha-Sources C. Nebelung, B. Barz	52
Minimizing of the Background Spectrum of a Grid Ionization Chamber C. Nebelung	53

6. CHEMISTRY OF THE HEAVIEST ELEMENTS	
A First Attempt to Chemically Identify Element 112	55
A.B. Yakushev, G.V. Buklanov, M.L. Chelnokov, V.I. Chepigin, S.N. Dmitriev, V.A. Gorshkov, V.Ya. Lebedev, O.N. Malyshev, Yu.Ts. Oganessian, A.G. Popeko, E.A. Sokol, S.N. Timokhin, V.M. Vasko, A.V. Yeremin, I. Zvara, S. Hübener, A. Türler	
Attempt to Characterize Elemental Lawrencium by Thermochromatography	56
S. Taut, S. Hübener, A. Vahle, B. Eichler, A. Türler, D.T. Jost, H.W. Gäggeler, C.A. Laue, K.E. Gregorich	
Adsorption Studies with Homologs of Superheavy Elements	57
A. Vahle, S. Hübener, S. Taut, E. Jäger, M. Schädel, B. Schausten, B. Eichler	
A Geometric Model for Direct Condensation	58
A. Vahle, R. Dressler	
Semi-Empirical Calculation of Metal Adsorption Entropies and Enthalpies	59
S. Taut, S. Hübener, B. Eichler	
Volatility Studies of Actinide Oxide Hydroxides	60
S. Hübener, S. Taut, A. Vahle	
II. PUBLICATIONS, PATENTS, LECTURES AND POSTERS	61
III. SEMINARS, CONFERENCES AND WORKSHOPS	71
IV. PERSONNEL	75
V. ACKNOWLEDGMENTS	77

I. SCIENTIFIC CONTRIBUTIONS

Aquatic Chemistry of Actinides/Radionuclides

THORIUM(IV) COMPLEXATION BY HUMIC ACIDS STUDIED BY EXAFS

S. Pompe, K. Schmeide, T. Reich, C. Hennig, H. Funke, A. Roßberg, H. Moll, K.H. Heise, G. Bernhard

The near-neighbor surroundings of Th(IV) complexed with Aldrich humic acid and Bio-Rex70, a cation exchange resin having only carboxyl groups as proton exchanging sites, were studied by EXAFS.

We determined the structural parameters of a Th(IV) complex with natural humic acid (HA) from Aldrich by EXAFS. The results were compared with those obtained for Th(IV) sorbed onto Bio-Rex70, a cation exchange resin having solely carboxyl groups. Furthermore, we compared our results with EXAFS data for the HA and Bio-Rex70 interaction with Th(IV) /1/ and Np(IV) /2/ as well as with structural data of Th(IV) hydrate /3/ and carboxylates /4/.

Experimental

Aldrich HA (AHA) and pre-equilibrated Bio-Rex70 from Bio-Rad (pH 1) were suspended in 0.1 M HClO₄. After addition of a 0.052 M Th(IV) stock solution, the pH was adjusted to pH 1 and the suspensions were stirred for 48 hours. The separated Th(IV) sorbates were studied in the form of wet pastes. The resulting loadings were 41 mg Th/g AHA and 2 mg Th/g Bio-Rex70.

Thorium L_{III}-edge EXAFS spectra were recorded at room temperature in fluorescence mode at the Rosendorf Beamline at the ESRF in Grenoble.

Results and discussion

Fig. 1 shows the Th L_{III}-edge k³-weighted EXAFS oscillations and their Fourier transforms (FT) that are not corrected for EXAFS phase shifts causing peaks to appear at shorter distances relative to the true distance.

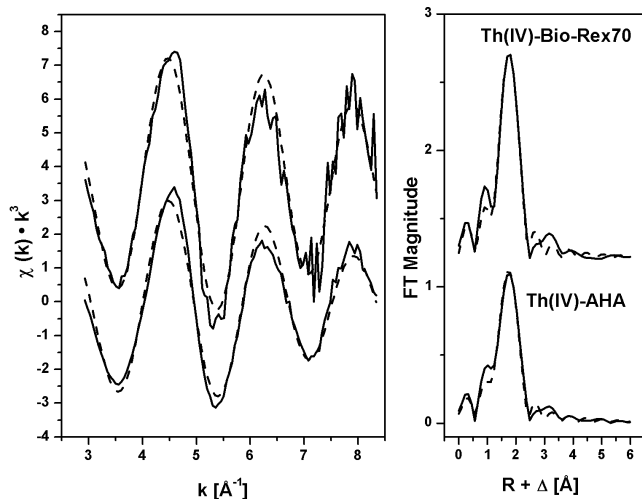


Fig. 1: Th L_{III}-edge k³-weighted EXAFS spectra and their corresponding FT. Solid lines: experiment, dashed lines: fit.

The EXAFS oscillations and FT are comparable for both samples. The FT are dominated by a peak at about 1.8 Å which represents oxygen atoms coordinated to Th(IV). The EXAFS oscillations were fitted to the EXAFS equation involving one coordination shell of Th with oxygen as the backscatterer. The structural data obtained are summarized in Tab. 1.

Th(IV)-AHA and Th(IV)-Bio-Rex70 show comparable coordination numbers (N) and Th-O bond lengths (R). In both samples Th(IV) is surrounded by 11 oxygen

atoms at a distance of 2.44 Å. Since Bio-Rex70 shows solely carboxyl groups as proton exchanging sites, we concluded that under the applied experimental conditions the interaction between AHA and Th(IV) is dominated by humic acid carboxyl groups, as expected for pH 1. However, the higher EXAFS-Debye-Waller factor, σ^2 , for the oxygen coordination shell of Th(IV)-AHA compared to Th(IV)-Bio-Rex70 and Th⁴⁺ (aq) indicates a greater bond lengths distribution in Th(IV)-AHA.

Sample	Th-O			ΔE_0 (eV)	Ref.
	N	R (Å)	σ^2 ^a		
Th(IV)-AHA	10.6 ± 1.5	2.44 ± 0.01	1.3	-17.3	
Th(IV)-Bio-Rex70	11.0 ± 2.1	2.45 ± 0.02	0.9	-17.3	
Th(IV)-AHA	10.1	2.43	1.3	1.0	/1/
Th(IV)-Bio-Rex70	9.4	2.44	1.2	1.0	/1/
Th ⁴⁺ (aq)	10.8 ± 0.5	2.45 ± 0.01	0.7	4.0	/3/

^a σ^2 in units of 10⁻² Å².

Tab. 1: EXAFS structural parameters in comparison to literature data.

Within the experimental error, the results obtained agree with those determined by Denecke et al. /1/. In addition, the coordination number and bond length of Th(IV)-AHA are comparable to those reported for Th⁴⁺ (aq) /3/. This means that the interaction of Th(IV) with humic acid carboxyl groups induces no shortening of the Th-O bond lengths. Thus, a differentiation between coordinated water molecules and carboxylate groups of the HA is not possible. To identify the predominant binding mode of humic acid carboxylate groups onto Th(IV), the Th-O bond length is compared with those of Th(IV) model compounds. Monodentate coordinated carboxylate groups in various Th(IV) malonates /4/ show Th-O bond distances between 2.337 Å and 2.469 Å. The Th-O distance of 2.44 Å obtained for Th(IV)-AHA lies in this range, indicating a predominantly monodentate coordination of humic acid carboxylate groups.

The comparison of the Th(IV) data with those determined for the interaction of Np(IV) with AHA and Bio-Rex70 /2/ shows that both tetravalent actinides are coordinated by about 11 oxygen atoms. However, the Np-O bond length is shorter (R=2.36±0.01 Å) than the Th-O bond distance. The bond length difference of 0.08 Å is close to the difference of the effective ionic radii of Th⁴⁺ and Np⁴⁺ in aqueous solution (0.06±0.02 Å) /5/.

Acknowledgment

This study was supported by BMWi (no. 02E9299).

References

- /1/ Denecke, M.A. et al., J. Synchr. Rad. **6**, 394 (1999)
- /2/ Schmeide, K. et al., this report, p. 15
- /3/ Moll, H. et al., Inorgan. Chem. **38**, 1795 (1999)
- /4/ Zhang, Y.-J. et al., Polyhedron **19**, 1757 (2000)
- /5/ Neck, V. et al., Radiochim. Acta **88**, 815 (2000)

COMPLEX FORMATION IN THE SYSTEM URANIUM(VI) – ALPHA-SUBSTITUTED CARBOXYLIC ACIDS STUDIED BY UV-vis SPECTROSCOPY; PART I: GLYCOLIC ACID

H. Moll, G. Geipel, G. Bernhard, Th. Fanghänel, I. Grenthe¹

¹Department of Chemistry, Inorganic Chemistry, The Royal Institute of Technology, 10044 Stockholm, Sweden

We studied the complex formation of uranium(VI) with glycolic acid at a uranium concentration of 0.005 M at pH = 2. The absorption spectra show an isosbestic point at 394 nm. The formation constant of $\text{UO}_2(\text{HOCH}_2\text{COO})^+$ at 1 M NaClO_4 was calculated to be $\log k_{1:1} = 2.32$.

The complex formation of uranium(VI) with glycolic acid (H_2Gly) was mainly investigated by potentiometry and NMR techniques in the past /1-3/. There are no information about spectroscopic properties of the species involved. The study of organic ligands having a alpha OH group is challenging due to the ability of forming chelates even at low pH.

The experiments were carried out using a conventional CARY5G UV-vis spectrometer (Varian Co.). The experimental conditions were chosen in this form that only the first complex and the free uranyl ion are present in the test solutions /1/. Fig. 1 depicts the UV-vis spectra of uranium(VI) as a function of the total glycolic acid concentration at pH=2.

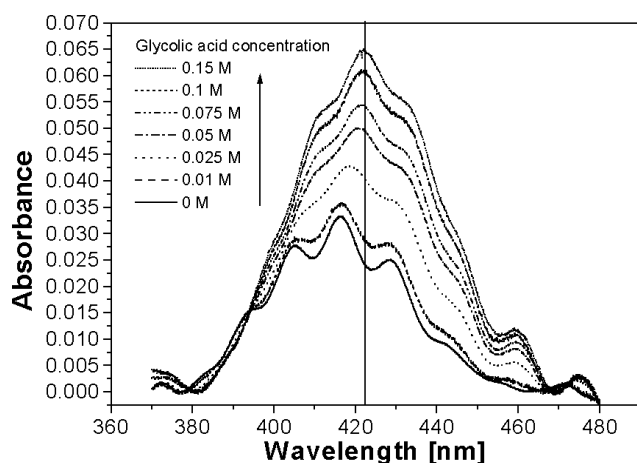


Fig. 1: UV-vis spectra of uranium(VI) as a function of the glycolic acid concentration at pH=2

The spectra shown in Fig. 1 are background corrected. One isosbestic point was detected at 394 nm. Two features are showing the complex formation of uranium(VI) with glycolic acid: a) an increase in the absorbance, and b) a red shift of the absorption maxima. The measured absorption at a certain wavelength (e.g. 405, 416, 422, and 433 nm) of a test solution containing UO_2^{2+} and $\text{UO}_2(\text{HOCH}_2\text{COO})^+$ is given by:

$$A = \varepsilon_{10}[\text{UO}_2^{2+}] + \varepsilon_{11}[\text{UO}_2(\text{HOCH}_2\text{COO})^+] \quad (1)$$

We used a least square fit algorithm to calculate the molar extinction coefficients and concentrations of the two species. The information from potentiometry /1/ were used as starting values.

$\text{UO}_2^{2+}, \lambda$ [nm]				$\text{UO}_2(\text{HOCH}_2\text{COO})^+, \lambda$ [nm]			
405	416	422	433	405	416	422	433
5.5	6.7	4.9	3.8	11.0	18.0	26.0	22.0

Tab. 1: Molar extinction coefficients [$\text{L mol}^{-1} \text{cm}^{-1}$]

The first complex has a five times larger absorbance at 422 nm compared to the free uranyl ion. A deconvolution of the measured sum spectra is shown in Fig. 2.

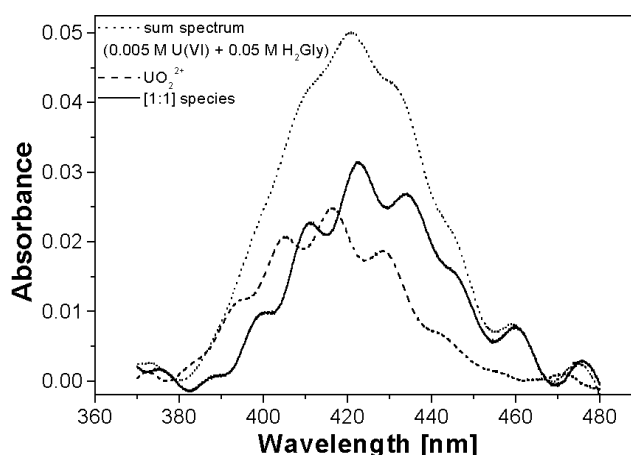
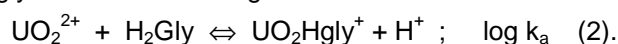
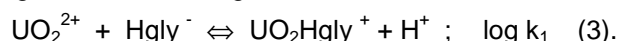


Fig. 2: Spectra of the single components

We investigated the complex formation of uranyl and glycolic acid according to



Taking the dissociation of glycolic acid into account, $\log K = 3.61$ /1/, we get



To validate reaction (2) we performed a slope analysis (Fig. 3). The slope of 1.05 ± 0.1 indicates a predominant 1:1 complex formation. The stability constant of reaction (3), $\log k_1 = 2.32 \pm 0.13$, is in good agreement with literature data.

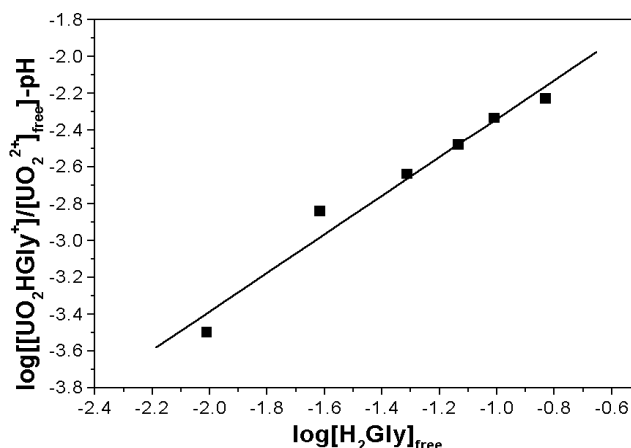


Fig. 3: Slope analysis for reaction (2)

Further investigations especially on the structure and fluorescence properties of the main species are in progress.

Acknowledgements

The studies were funded by the European Union (EU) under contract number HPMF-CT-1999-00342.

References

- /1/ Magnon, L. et al., Gazz. Chim. Ital. **104**, 967 (1974)
- /2/ Kakahana, M. et al., J. Phys. Chem. **91**, 6128 (1987)
- /3/ Szabó, Z. et al., Inorg. Chem. **39**, 5036 (2000)

COMPLEX FORMATION IN THE SYSTEM URANIUM(VI) – ALPHA-SUBSTITUTED CARBOXYLIC ACIDS STUDIED BY UV-vis SPECTROSCOPY; PART II: α -HYDROXYISOBUTYRIC ACID

H. Moll, G. Geipel, G. Bernhard, Th. Fanghänel, I. Grenthe¹

¹ Department of Chemistry, Inorganic Chemistry, The Royal Institute of Technology, 10044 Stockholm, Sweden

The complex formation of uranium(VI) in the α -hydroxyisobutyrate system was studied at a uranium concentration of 0.005 M at pH 2 and 4. The formation constants of $\text{UO}_2(\text{HOCHCH}_3\text{COO})^+$ and $\text{UO}_2(\text{HOCHCH}_3\text{COO})_3^-$ at 1 M NaClO_4 were determined.

Potentiometric and NMR data are indicating a stronger complex formation of α -hydroxyisobutyric acid (H_2IBA) with uranyl compared to H_2Gly /1,2/. To our knowledge there are no information published regarding the spectroscopic properties of the main species formed.

The experiments in this system were performed using a conventional CARY5G UV-vis spectrometer (Varian Co.). The experimental conditions were chosen in this form that only two species are present in the test solutions /1/ at each pH. The experiments were carried out at $[\text{UO}_2^{2+}]$ of 0.005 M in 1 M NaClO_4 as a function of the ligand concentration.

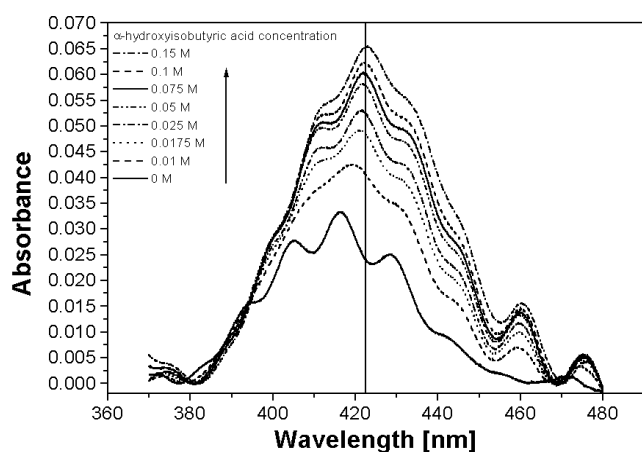


Fig. 1: UV-vis spectra of uranium(VI) as a function of the H_2IBA concentration at pH=2

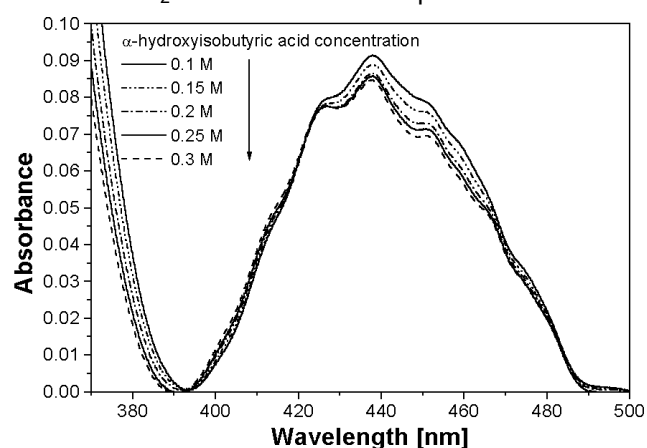


Fig. 2: UV-vis spectra of uranium(VI) as a function of the H_2IBA concentration at pH=4

The absorption spectra at both pH values are summarized in Fig. 1 and 2. An increase in absorbance and a red shift of the absorption maxima, 5 nm compared to the free UO_2^{2+} , are indicating the interaction of UO_2^{2+} and H_2Gly already at pH=2. If we are moving to pH 4 the red shift of the absorption maxima is even larger, 20 nm, perhaps due to a stronger involvement of the OH group in the complex formation. On the other hand the absorption decreases as a function of the ligand concentration.

We calculated in a similar way as described in /3/ the molar extinction coefficients and species concentrations at given wavelengths (405, 416, 422, and 433 nm at pH=2; 425, 438, 452, and 466 nm at pH=4) by a least square fit algorithm. The species concentrations calculated from ref. /1/ were used as starting values. The first complex has a six times larger absorbance at 438 nm compared to the free uranyl ion. Whereas the second and third complex showed a eight times larger absorbance.

The complex formation reactions investigated were, pH=2:



pH=4:

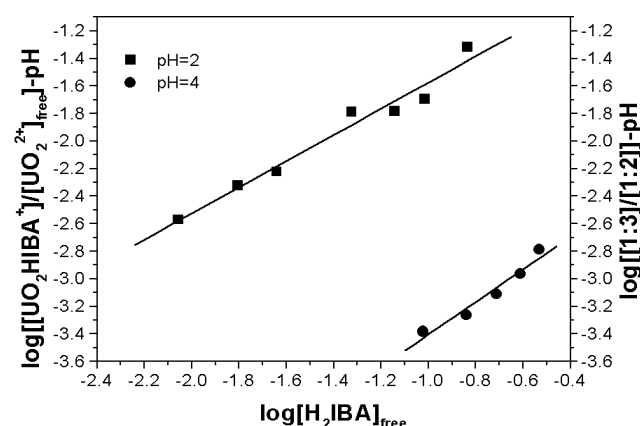


Fig. 3: Slope analysis for reactions 1 and 2

To validate the reactions (1, 2) we performed a slope analysis (Fig. 3). The slopes of 0.95 ± 0.08 and 1.2 ± 0.2 for reaction 1 and 2, respectively, indicate a predominant 1:1 complex formation in both cases. Taking the dissociation of H_2IBA of $\log K = 3.79$ /2/ and



into consideration, we get:



We could show the extraction of single component absorption (not shown here, /3/) as well as the calculation of stability constants at 1 M NaClO_4 in agreement with literature values /1,2/.

Further investigations on the structure and fluorescence properties of the main species are in progress.

Acknowledgements

The studies were founded by the European Union (EU) under contract number HPMF-CT-1999-00342.

References

- /1/ Magnon, L. et al., Gazz. Chim. Ital. **104**, 967 (1974)
- /2/ Szabó, Z. et al., Inorg. Chem. **39**, 5036 (2000)
- /3/ Moll, H., et al., this report p.2

COMPLEX FORMATION OF URANIUM(VI) WITH ADENOSINE TRIPHOSPHATE

G. Geipel, G. Bernhard

We studied the interaction of uranium(VI) with adenosine triphosphate (ATP). A 1:1 complex with a formation constant of $\log K = -3.8 \pm 0.44$ was found.

Adenosine triphosphate is an important enzymatic compound, which can transfer the phosphate and diphosphate groups between molecules. Heavy metal ions bound to the adenosine phosphates can be transported into living cells and then deposited. In addition to studies of the soil-to-plant transfer factors /1/ and interaction of the uranyl ion with microorganisms /2/, we investigated the complex formation of the uranyl ion with adenosine triphosphate (ATP).

We found that adenosine phosphates are very strong quenchers of the fluorescence of the uranyl ion and also of the complexes formed. In the uranyl - adenosine triphosphate system fluorescence emission was only observed in a small range of adenosine concentration. The deconvoluted fluorescence spectra show other emission maxima than both the uranyl ion and phosphate complexes. This suggests that a complex between uranyl and adenosine triphosphate is formed.

Fig. 1 shows a set of fluorescence spectra of the uranyl - adenosine triphosphate complex formed. No change was observed in the emission maxima with the delay time. We observed only two fluorescence lifetimes. The shorter one ($<1.8\mu s$) was assigned to the free uranyl ion and the longer lifetime ($>3\mu s$) to the complex formed.

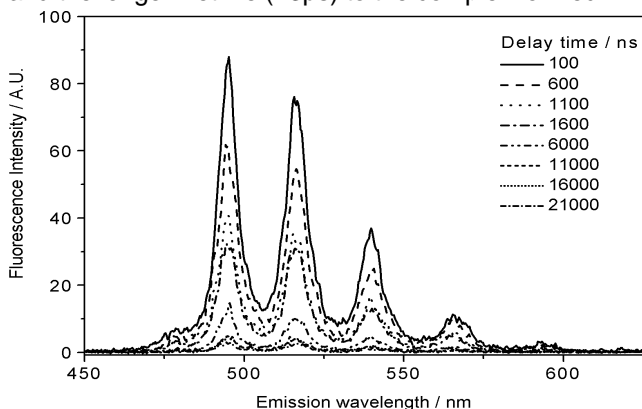


Fig. 1: Time resolved fluorescence spectra of the uranyl adenosine triphosphate complex

Starting with low concentrations of adenosine triphosphate, first we found a strong decrease in the fluorescence of the uranyl ion combined with a decrease in the fluorescence lifetime. This is typical for fluorescence quenching. The quench constant derived from lifetime data was about $3 \cdot 10^8$. By using the data from the quenching experiments we were able to recalculate the fluorescence intensity of the complex formed when no quencher was present in the solution. These data were used to calculate the concentrations of the complex formed and the residual noncomplexed uranium(VI) in the solution, using the measured intensities of the complex. The complex formation reaction can be written

$$x \text{ ATP} + \text{UO}_2^{2+} = \text{UO}_2\text{-ATP}_x^{(2-y)+} + y \text{ H}^+ \quad (1)$$

Applying the mass action law and transformation to the logarithmic scale, we obtain:

$$\log \frac{[\text{UO}_2\text{-ATP}_x^{(2-y)+}]}{[\text{UO}_2^{2+}]} = \log K + x \log [\text{ATP}_{\text{noncompl.}}] - y \log [\text{H}^+] \quad (2)$$

At constant pH the left-hand side of Equation (2) is a

linear function of $\log [\text{ATP}_{\text{noncompl.}}]$. This is illustrated in Fig. 2. The slope x of the linear fit was determined to be 1.58 ± 0.10 . Hence the stoichiometry of reaction (1) remains unclear. The slope of 1.5 indicates that at least two complexes are formed.

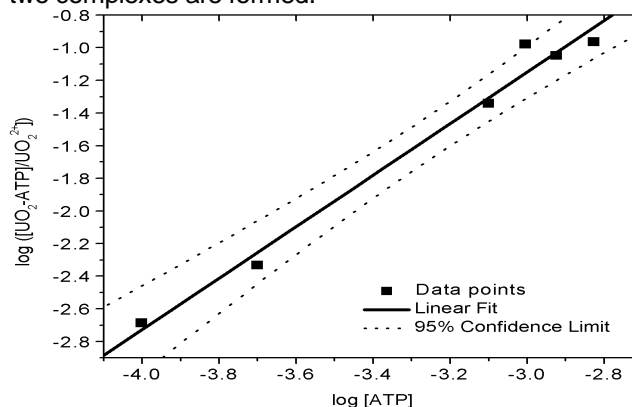


Fig. 2: Logarithm of the concentration ratio $[\text{UO}_2\text{-ATP}] / [\text{UO}_2^{2+}]$ as function of the free ATP concentration

Using a constant concentration of UO_2^{2+} ($1 \cdot 10^{-4} \text{ M}$) and ATP ($8 \cdot 10^{-4} \text{ M}$), the fluorescence intensity was measured as a function of pH. A maximum of the fluorescence intensity was found at $\text{pH} = 3.4$.

Equation (2) can be rearranged as

$$\log \frac{[\text{UO}_2\text{-ATP}_x]}{[\text{UO}_2^{2+}] \cdot [\text{ATP}_{\text{noncompl.}}]^x} = \log K - y \log [\text{H}^+] = \log K + y \cdot \text{pH} \quad (3)$$

The analysis of Equation (3) in the pH range from 2.2 to 3.2 is shown in Fig. 3. Using a linear fit of the data points, a slope y of 2.35 ± 0.26 was calculated.

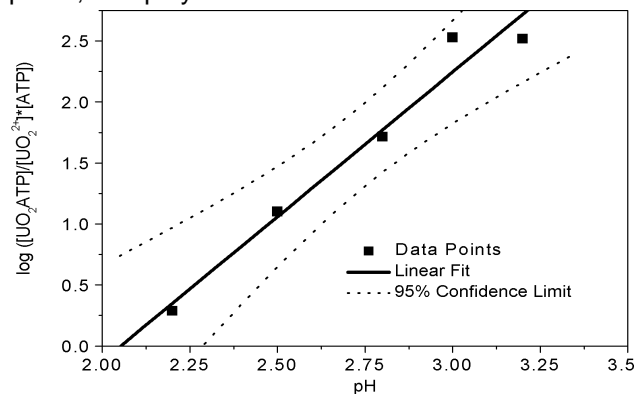


Fig. 3: Logarithm of the ratio $([\text{UO}_2\text{-ATP}] / [\text{UO}_2^{2+}] \cdot [\text{ATP}])$ as function of pH

This can be interpreted as a predominant release of two hydrogen ions, if one uranyl ion is bound to the ATP complex. Equation (1) can now be written



The complex formation constant for reaction (4) strongly depends on the x -value. A preliminary formation constant was calculated to be $\log K_{(I=0.1 \text{ M})} = -3.80 \pm 0.44$, considering that a 1:1 complex was formed ($x=1$).

Additional experiments are in progress to validate the stoichiometry and the complex formation constant.

References

- /1/ Günther, A., Bernhard, G. et al., submitted to NRC5
/2/ Panak, P. et al., Radiochim. Acta **84**, 183-186 (1999)

FORMATION OF $\text{Ca}_2[\text{UO}_2(\text{CO}_3)_3]$ IN DEPENDENCE ON THE CONCENTRATION OF UO_2^{2+} , Ca^{2+} AND CO_3^{2-}

S. Amayri, L. Baraniak, G. Bernhard

The formation of $\text{Ca}_2[\text{UO}_2(\text{CO}_3)_3]$ in aqueous solution was calculated as a function of pH, considering the main uranium(VI) hydroxo and carbonato complexes. The complex is stable in the pH region from 7.5 to 11.5 and is the dominant uranium(VI) species in the natural waters of uranium mining areas which are rich in calcium and carbonate. In a saturated aqueous solution the mineral *liebigite* $\text{Ca}_2[\text{UO}_2(\text{CO}_3)_3] \cdot 10 \text{H}_2\text{O}$ is in equilibrium with the pure complex $\text{Ca}_2[\text{UO}_2(\text{CO}_3)_3]$ in the pH range from 6.0-12.0

Introduction

In natural aquatic systems uranium(VI) ions are usually coordinated by inorganic ligands, e.g. by carbonate and hydroxide ions. In natural mining-related waters in the south of Saxony (Germany) uranium contamination amounts up to 0.02 mmol/L in the presence of relatively high concentrations of calcium, magnesium, carbonate and sulphate (in the order of 10^{-2} mol/L). The pH ranges from 7.0 to 8.0. In a former study /1/ the complex $\text{Ca}_2[\text{UO}_2(\text{CO}_3)_3]$ was found to be the dominant species in such waters.

Calculations and results

Uranium(VI) speciations were carried out using the RAMESSES code (Leung, 1988). The uranium(VI) hydrolysis constants and the stabilities of the carbonato complexes used in the calculations are listed in Table 1.

Species	$\log \beta$ $I=0 \text{ M}$	$\log \beta$ $I=0.1 \text{ M}$	$\log \beta$ $I=0.2 \text{ M}$
$\text{UO}_2(\text{OH})_2$	-10.30	-10.51	-10.55
$[\text{UO}_2(\text{OH})_3]^-$	-19.20	-19.20	-19.20
$[(\text{UO}_2)_2(\text{OH})_2]^{2+}$	-5.62	-5.83	-5.87
$[(\text{UO}_2)_3(\text{OH})_5]^+$	-15.55	-16.19	-16.31
$[\text{UO}_2(\text{CO}_3)]$	9.68	8.82	8.67
$[\text{UO}_2(\text{CO}_3)_2]^{2-}$	16.94	16.08	15.93
$[\text{UO}_2(\text{CO}_3)_3]^{4-}$	21.60	21.60	21.60
$\text{Ca}_2[\text{UO}_2(\text{CO}_3)_3]$	30.79	28.23	27.75
$[(\text{UO}_2)_2\text{CO}_3(\text{OH})_3]^-$	-19.01	-19.22	-19.26
$[(\text{UO}_2)_3\text{CO}_3(\text{OH})_3]^+$	-17.5	-18.14	-18.26

Tab. 1: U(VI) hydrolysis constants and formation constants of the U(VI) carbonato complexes /2/

The stability constant of the species $\text{Ca}_2[\text{UO}_2(\text{CO}_3)_3]$ was taken from /1/. The stabilities were recalculated for the various ionic strengths by the *Davies* equation.

The speciation in Fig. 1 shows that in case of a low uranium(VI) content in a calcite-rich water (characteristic of the environment of a primary uranium deposit) more than 99% of uranium(VI) is bound as the species $\text{Ca}_2[\text{UO}_2(\text{CO}_3)_3]$ (A). If the calcium and carbonate contents are lower (in the order of 10^{-3} mol/L), only about 50% of this species (B) appears due to the preferred formation of carbonato complexes, especially $[\text{UO}_2(\text{CO}_3)_3]^{4-}$. The complex $\text{Ca}_2[\text{UO}_2(\text{CO}_3)_3]$ is stable in the pH range from 6.5 to 12.0. The complex is hydrolysed at a lower and higher pH, forming $[\text{UO}_2(\text{OH})_2]$, $[(\text{UO}_2)_2\text{CO}_3(\text{OH})_3]^-$, $[(\text{UO}_2)_3\text{CO}_3(\text{OH})_3]^+$ and $[\text{UO}_2(\text{OH})_3]^-$. The stable carbonato complexes $[\text{UO}_2\text{CO}_3]$, $[\text{UO}_2(\text{CO}_3)_2]^{2-}$ and $[\text{UO}_2(\text{CO}_3)_3]^{4-}$ appear at low calcium concentrations.

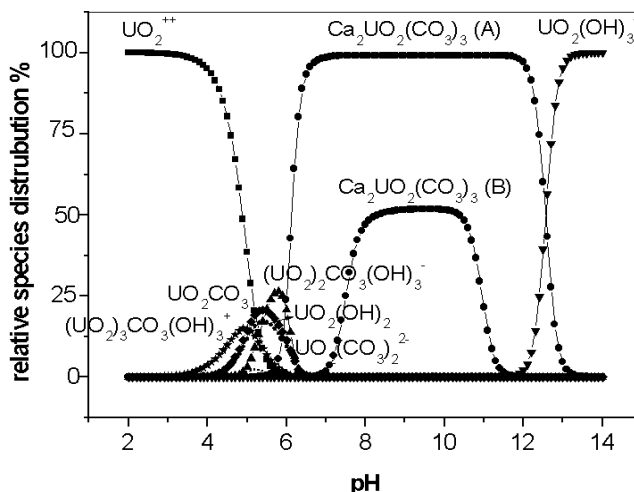


Fig. 1: U(VI) species distribution as a function of pH ($[\text{UO}_2^{2+}] = 2.0 \cdot 10^{-5}$ mol/L; (A): $[\text{Ca}^{2+}] = 0.69 \cdot 10^{-2}$ mol/L, $[\text{CO}_3^{2-}] = 1.89 \cdot 10^{-2}$ mol/L; (B): $[\text{Ca}^{2+}] = 0.69 \cdot 10^{-3}$ mol/L, $[\text{CO}_3^{2-}] = 1.89 \cdot 10^{-3}$ mol/L at $I = 0.1 \text{ M}$)

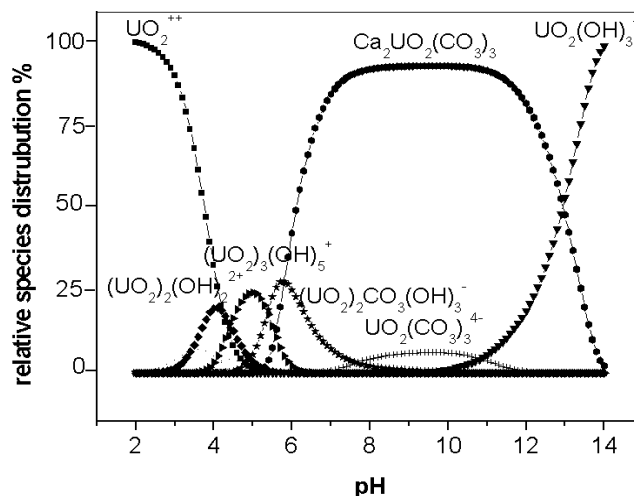


Fig. 2: U(VI) species distribution as a function of pH ($[\text{UO}_2^{2+}] = 0.014$ mol/L, $[\text{Ca}^{2+}] = 0.027$ mol/L, $[\text{CO}_3^{2-}] = 0.042$ and $I = 0.2 \text{ M}$)

The speciation in Fig. 2 shows that if *liebigite* is in equilibrium with its solution, $\text{Ca}_2[\text{UO}_2(\text{CO}_3)_3]$ is the dominant species (more than 90%). Therefore *liebigite* precipitates from such a solution in the pH range from 7.0 to 11.5. The species $[(\text{UO}_2)_3(\text{OH})_5]^+$ and $[(\text{UO}_2)_2\text{CO}_3(\text{OH})_3]^-$ are present between pH 4.0 and 6.0. Above pH 12.0 the complex $\text{Ca}_2[\text{UO}_2(\text{CO}_3)_3]$ hydrolyses to $[\text{UO}_2(\text{OH})_3]^-$.

References

- /1/ Bernhard, G. et al., Radiochim. Acta submitted
- /2/ Grenthe, I. et al., NEA-TDB *Chemical Thermodynamics of Uranium*. Data Bank: Issyles-Moulineaux. France (1992)

SYNTHESIS AND CHARACTERIZATION OF BARIUM URANYL CARBONATE, $Ba_2[UO_2(CO_3)_3] \cdot 6H_2O$

S. Amayri, G. Geipel, G. Bernhard, K. Henkel

Two methods for the synthesis of barium uranyl carbonate, $Ba_2[UO_2(CO_3)_3] \cdot 6H_2O$, are described. TRLFS, XRD, ICP-MS, AAS, IR and thermoanalysis were used to characterize this compound.

To complete the systematic study of earth alkaline uranyl tricarbonate complexes, it was our aim to develop a procedure for the preparation of barium uranyl carbonate (BaUC), $Ba_2[UO_2(CO_3)_3] \cdot 6H_2O$. The well analytically characterized substance will be used for solubility and speciation investigations.

Experimental and results

Synthesis of $Ba_2[UO_2(CO_3)_3] \cdot 6H_2O$

BaUC was synthesized according to the two following methods:

1) Double Anion Exchange Method (DAEM): An excess of $BaCl_2$ is added to magnesium uranyl carbonate solution or saturated ammonium uranyl carbonate solution. The obtained light yellow crystalline powder is filtered off, washed with deionized water and dried at room temperature. The yield was about 99%.

2) Direct Synthetic Method (DSM) /1/: A solution of $2 \cdot 10^{-3}$ M uranyl nitrate with a solution of $6 \cdot 10^{-3}$ M sodium carbonate and a solution of $4 \cdot 10^{-3}$ M barium chloride is mixed. The yield of this method was about 97%.

Chemical analysis

Element	U	Ba	U/Ba
DAEM	28.50±0.1	32.80±0.6	0.50
DSM	28.57±0.3	32.98±0.1	0.50
Calculated	28.58	32.98	0.50
Analysis	ICP-MS	AAS	

Tab. 1: Chemical analysis of $Ba_2[UO_2(CO_3)_3] \cdot 6H_2O$, prepared using various methods

X-ray analysis

For the first time a X-ray powder diagram of BaUC is recorded. The X-ray powder diffraction diagram (Fig. 1) shows that the synthesized substance seems to be crystalline with amorphous parts. Up to now, it was impossible to get single crystals of BaUC. The experimental conditions are described in /1/.

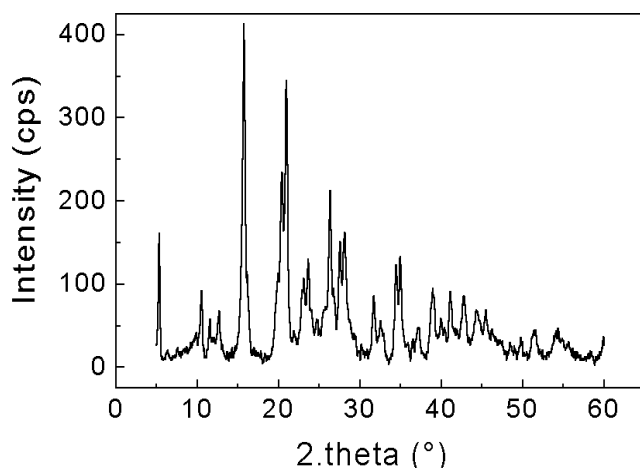


Fig. 1: X-ray diffractogram of BaUC

Thermal decomposition of BaUC

The thermal stability of BaUC was investigated by thermoanalyser STA-92 (Setaram, France) with an applied heating of 30 °C/min and a flow of O_2 of 3L/min. Tab. 2 gives the interpretation and assignment of mass decrease of TG and DTA measurements. The thermal decomposition of BaUC is characterized by four steps and the final product was analyzed by X-ray to be Ba_2UO_5 .

Temp. °C	Decrease masse %	Assignment	Interpretation
22-121	5.03	2.31 H_2O	2.31 H_2O
121-306	7.82	3.60 H_2O	3.60 H_2O
306-571	9.66	1.82 CO_2	1.82 CO_2
571-829	5.59	1.11 CO_2	1.11 CO_2

Tab. 2: Results of the thermo-analysis of BaUC

The results summarized in Tab. 2 show that one mol of BaUC contains 5.91 ± 0.17 moles H_2O and 2.93 ± 0.09 moles CO_2 , this is in good agreement with our elemental analysis of $Ba_2[UO_2(CO_3)_3] \cdot 6H_2O$ (Tab. 1).

TRLFS measurements

The used Nd-YAG-laser system is described in /2/. Using TRLFS we have found that the determined fluorescence lifetime of solid BaUC ($16.3 \pm 0.4 \mu s$) is smaller than the lifetime of liebigite ($146 \pm 0.5 \mu s$). The main emission wavelengths are at 469.9, 487.7, 507.3, 528.9, 552.2, 570.5 nm (Fig. 2) and present a shift of about +5 nm to liebigite. BaUC was not investigated by TRLFS before.

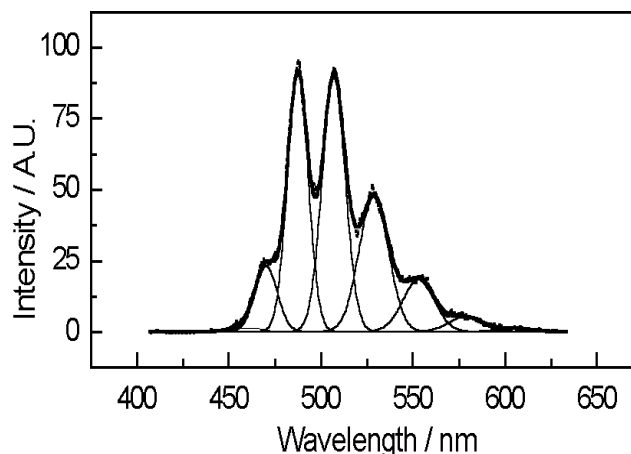


Fig. 2: TRLFS spectrum of $Ba_2[UO_2(CO_3)_3] \cdot 6H_2O$

Conclusion

The results of our analysis confirm the identity of our product with $Ba_2[UO_2(CO_3)_3] \cdot 6H_2O$. This synthesized BaUC will be used for solubility experiments.

References

- /1/ Amayri, S., PhD Thesis, TU Dresden, in prep.
- /2/ Brachmann, A., Thesis, TU Dresden (1997)

SYNTHESIS AND CHARACTERIZATION OF STRONTIUM URANYL CARBONATE, $\text{Sr}_2[\text{UO}_2(\text{CO}_3)_3]\cdot 8\text{H}_2\text{O}$

S. Amayri, G. Geipel, G. Bernhard, K. Henkel

Pure strontium uranyl carbonate, $\text{Sr}_2[\text{UO}_2(\text{CO}_3)_3]\cdot 8\text{H}_2\text{O}$, was synthesized. Several analytical methods such as XRD, ICP-MS, AAS, TRLFS, IR spectroscopy and thermoanalysis were used to characterize this compound.

Concerning systematic study of uranyl carbonate minerals and related synthetic compounds [1], strontium uranyl carbonate was of interest.

Our goal was to synthesize strontium uranyl carbonate (SrUC) with the composition $\text{Sr}_2[\text{UO}_2(\text{CO}_3)_3]\cdot 8\text{H}_2\text{O}$ and to characterize the final product regarding its composition and purity. Such well characterized substance will be used for solubility and speciation investigations.

Experimental and results

Synthesis of $\text{Sr}_2[\text{UO}_2(\text{CO}_3)_3]\cdot 8\text{H}_2\text{O}$

We have synthesized large amount of SrUC in short time by applying this method in the manner described below: A solution containing 5.02 g $\text{UO}_2(\text{NO}_3)_2\cdot 6\text{H}_2\text{O}$ (p.a. Merck) in 10 mL water is added slowly with constant stirring to a solution containing 3.18 g Na_2CO_3 (p.a. Merck). After that a solution containing 5.32 g $\text{SrCl}_2\cdot 6\text{H}_2\text{O}$ (p.a. Merck) in 10 mL of water is added slowly to the uranyl carbonate solution. Yellow crystals (≤ 3 mm), stable in air, are grown at room temperature from this mixture by slow evaporation of the solvent water.

Chemical analysis

The U content was determined using an inductively coupled plasma (Ar-plasma) mass spectrometer and Sr content was determined using a flame-atomic absorption spectrometer. SrUC with the composition $\text{Sr}_2[\text{UO}_2(\text{CO}_3)_3]\cdot 8\text{H}_2\text{O}$ contains 30.94% uranium, 22.78% Strontium and U/Sr ratio of 0.5. ICP-MS analysis showed that the synthesized SrUC contains $30.61\pm 0.35\%$ U and $22.45\pm 0.40\%$ Sr. That is in good agreement with the theoretical stoichiometry.

X-ray analysis

Powder diffraction data of synthetic SrUC were indexed for monoclinic structure with the space group P2/c and the calculated lattice parameters were: $a=11.328\pm 0.164$ Å, $b=11.407\pm 0.139$ Å, $c=25.617\pm 0.424$ Å, $\beta=93.53^\circ$ and $V=3303.9\pm 146.8$ Å³. The unit cell constants were found to be similar to literature data [2]. The diffraction pattern of SrUC shows Fig. 1.

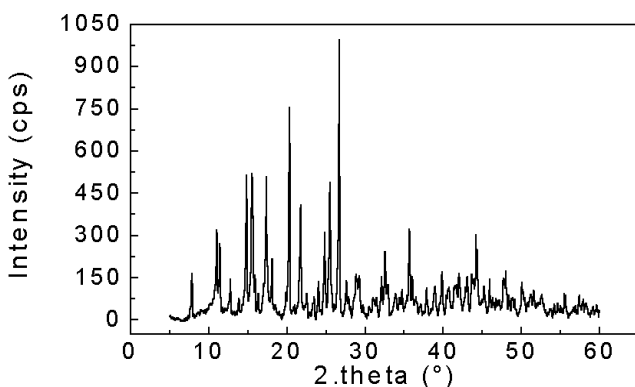


Fig. 1: X-ray diffractogram of the synthesized SrUC

Thermal decomposition of SrUC

SrUC dehydrates in one step in the range of 22-226 °C

(one endothermic peaks at 137 °C Fig. 2), then the composition of the anhydrous phase take place, with decarbonization in two steps in the range of 226-728 °C (two endothermic peaks at 340 °C and 484 °C), the complete decarbonization is finished at 729.3 °C. Sr_2UO_5 was the final product of the thermal decomposition of SrUC confirmed by X-ray analysis.

The result shows that one mol of SrUC contains 7.97 ± 0.24 moles H_2O and 3.00 ± 0.09 moles CO_2 , this is in excellent agreement with our analysis of $\text{Sr}_2[\text{UO}_2(\text{CO}_3)_3]\cdot 8\text{H}_2\text{O}$.

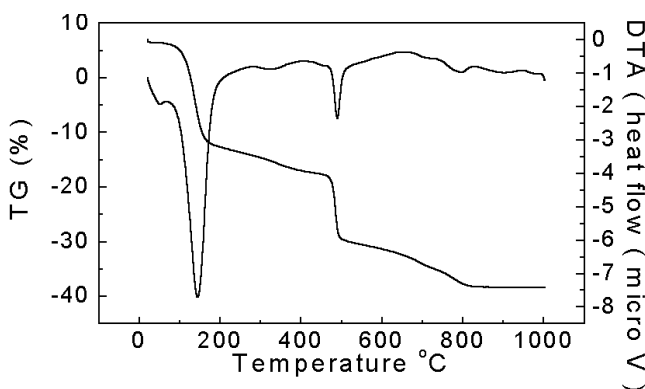


Fig. 2: Thermo-analysis diagrams of synthetic SrUC

TRLFS measurements

The used Nd-YAG-laser system is described in [3]. From TRLFS the fluorescence lifetime of solid SrUC is determined to be 77.3 ± 1.1 µs and the main emission wavelengths were at 488.8, 502.8, 522.9, 545.4, 569.2 and 600.1 nm (Fig. 3).

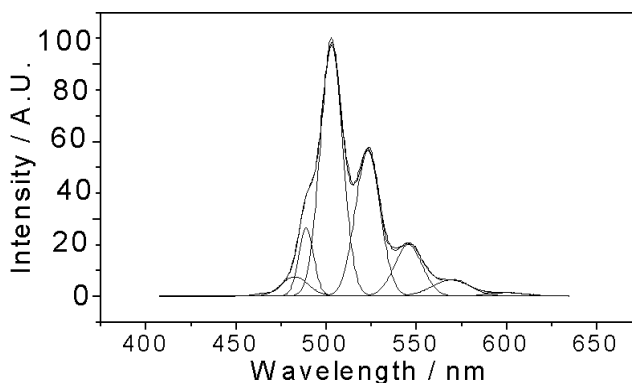


Fig. 3: TRLFS spectrum of $\text{Sr}_2[\text{UO}_2(\text{CO}_3)_3]\cdot 8\text{H}_2\text{O}$

Conclusion

The results of our analysis confirm the identity of our product with $\text{Sr}_2[\text{UO}_2(\text{CO}_3)_3]\cdot 8\text{H}_2\text{O}$. This synthetic SrUC will be used for solubility experiments.

References

- [1] Amayri, S., et al., Report FZR-218, p.14-15 (1998), FZR-247, p.12 (1999), and FZR-285, p.6-7 (2000)
- [2] Mereiter, K., Acta Cryst. **C42**, 1678-1681 (1986)
- [3] Brachmann, A., Thesis, TU Dresden (1997)

STRUCTURAL COMPARISON OF $\text{Cu}[\text{UO}_2\text{AsO}_4]_2 \cdot 12\text{H}_2\text{O}$ AND $\text{Cu}[\text{UO}_2\text{AsO}_4]_2 \cdot 8\text{H}_2\text{O}$

C. Hennig, M. Rutsch

Cu K-edge EXAFS measurements at 15K were used to characterize the main structural difference between zeunerite, $\text{Cu}[\text{UO}_2\text{AsO}_4]_2 \cdot 12\text{H}_2\text{O}$ (1) and meta-zeunerite $\text{Cu}[\text{UO}_2\text{AsO}_4]_2 \cdot 8\text{H}_2\text{O}$ (2) and compared with X-ray diffraction measurements.

Sample **1** is obtained by synthesis and consists of pure $\text{Cu}[\text{UO}_2\text{AsO}_4]_2 \cdot 12\text{H}_2\text{O}$. The structure contains two symmetry-inequivalent Cu positions. In the EXAFS analysis only one Cu atom position is considered (Fig. 1), because the second one has only an occupation factor of 0.075.

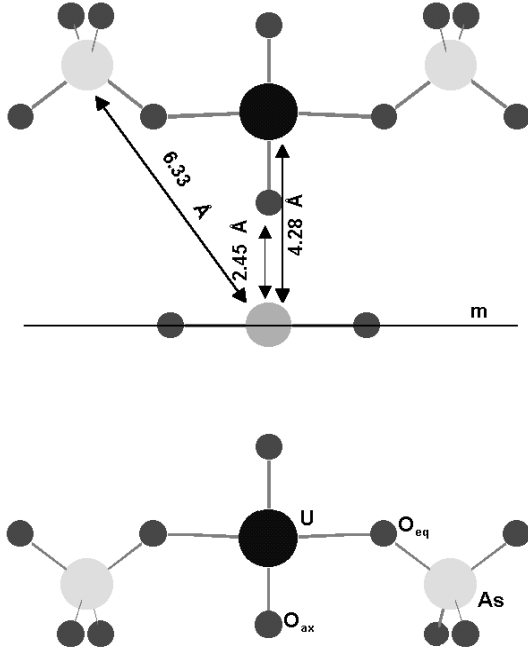


Fig. 1: Structure from XRD data [1] of sample **1**, zeunerite, $\text{Cu}[\text{UO}_2\text{AsO}_4]_2 \cdot 12\text{H}_2\text{O}$, m = mirror plane.

Sample **2** is originated by a natural meta-zeunerite mineral. This structure contains one symmetry-independent Cu atom position (Fig. 2).

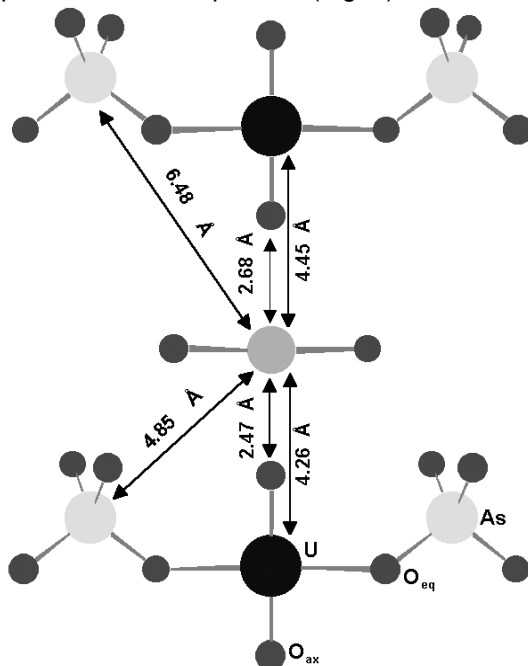


Fig. 2: Structure from XRD data [1] of sample **2**, meta-zeunerite, $\text{Cu}[\text{UO}_2\text{AsO}_4]_2 \cdot 8\text{H}_2\text{O}$.

The powdered sample contains 14% $\text{Cu}[\text{UO}_2\text{AsO}_4]_2 \cdot 12\text{H}_2\text{O}$. However, the EXAFS is dominated by the scattering contribution of $\text{Cu}[\text{UO}_2\text{AsO}_4]_2 \cdot 8\text{H}_2\text{O}$. Due to the damping of thermal oscillations, a lot of backscattering shells occur in the Fourier transform (FT). For simplifying the data analysis, the FT between $R+\Delta=5.5-10\text{\AA}$ was Fourier filtered, back transformed and subtracted from raw EXAFS data of each spectra.

	Shell	R [Å] ^a	N ^b	σ ² [Å ²]	ΔE ₀ [eV]
1	Cu-OW	1.94	3.1(2)	0.0016	-4.4
	Cu-O _{ax}	2.46	1.1(2)	0.0016**	
	Cu-U	4.22	1.3(5)	0.0013	
	Cu-U _{MS}	4.22**	2.7**	0.0026**	
2	Cu-OW	1.94	2.4(1)	0.0018	-13.9
	Cu-O _{ax}	2.46	1.2(1)**	0.0018**	
	Cu-U1	4.04	0.8(1)	0.002*	
	Cu-U2	4.52	0.7(1)*	0.002*	
	Cu-As	4.84	1.6(2)	0.002*	

^aErrors in distances R are ± 0.02 Å, ^berrors in coordination numbers N are ± 25 % with standard deviations in parentheses, *value fixed during the fit, **dependent from the previous variable

Tab. 1: EXAFS structural parameters

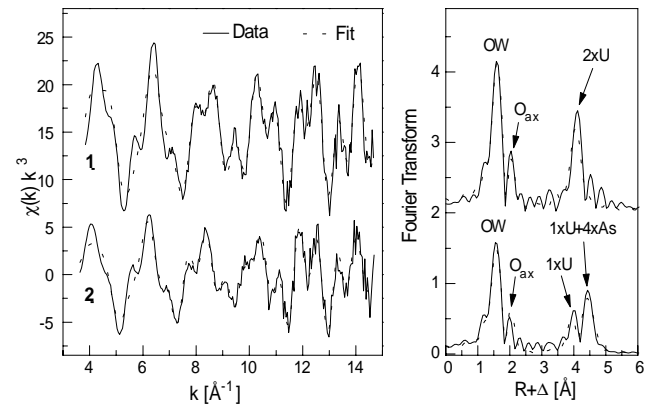


Fig. 3: Cu K-edge k^3 -weighted EXAFS spectra (left) and corresponding Fourier transform (right) for sample **(1)** and **(2)** at T = 15 K.

The $[\text{Cu}(\text{H}_2\text{O})_4]^{2+}$ group causes dominant FT peaks with Cu-O distances of 1.94Å for sample **1** and **2**. Sample **1** shows one Cu-U peak at a distance of 4.22Å. A strong Cu-U-O_{ax}-Cu MS contribution appears because the involved atoms are arranged linearly. This observation points to a highly symmetric arrangement of the $[\text{UO}_2\text{AsO}_4]_\infty$ layers concerning Cu. In contrast, the spectrum of sample **2** shows two FT peaks in that region. The first peak is originated by one uranium atom in a distance of 4.04Å. The second peak consists of arsenic atoms in a distance of 4.84Å and one uranium atom in a distance of 4.52Å. These observations indicate that in meta-zeunerite one $[\text{UO}_2\text{AsO}_4]_\infty$ layer is arranged closer to the Cu atom.

References

/1/ Hennig, C. et al., unpublished

COMPLEX FORMATION OF URANIUM(VI) WITH 5-SULFOSALICYLIC ACID STUDIED BY TRIFS PART I: NANOSECOND LASER PULSES AS EXCITATION SOURCE

G. Geipel, G. Bernhard

We studied the complex formation of uranium(VI) with 5-sulfosalicylic acid by time-resolved laser-induced fluorescence spectroscopy. As fluorescent component in this study the light emitting properties of the uranyl ion were used. The complex formation constant was found to be $\log K = -0.73 \pm 0.40$.

The conventional time-resolved laser-induced spectroscopy (TRLFS) was used to investigate the influence of 5-sulfosalicylic acid onto the fluorescence properties of uranium. The goal was to compare the results of this method with results using the femtosecond system (see Part II). To avoid hydrolysis of uranium the studies were carried out at pH 3.8. The uranium concentration of all measured solutions was $5 \cdot 10^{-5}$ M and the ionic strength was kept to be 0.1 M.

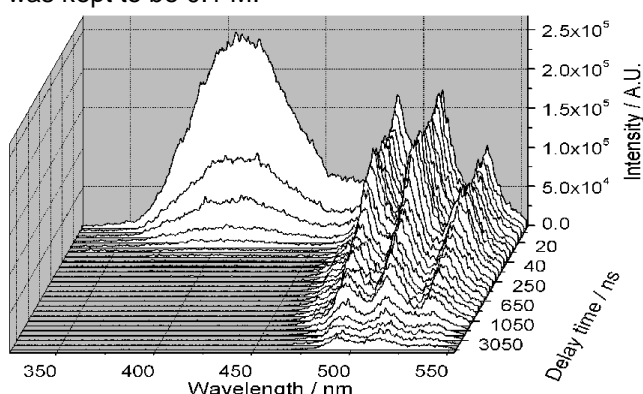


Fig. 1: Time-resolved fluorescence spectrum of $8 \cdot 10^{-5}$ M sulfosalicylic acid and $5 \cdot 10^{-5}$ M uranium(VI)

Fig. 1 shows a time-resolved spectrum of including the fluorescence spectrum of the 5-sulfosalicylic acid with a very short fluorescence lifetime. There are collected only five spectra with different delay times, therefore only a rough estimate of the fluorescence lifetime can be given (~ 5 ns). In the wavelength range of the uranium fluorescence we found besides the residual emission of the 5-sulfosalicylic acid more than one fluorescence lifetime. The conclusion of this behavior could be that the formed complex shows fluorescence properties in the wavelength range for uranyl fluorescence but not in the emission range of the organic ligand.

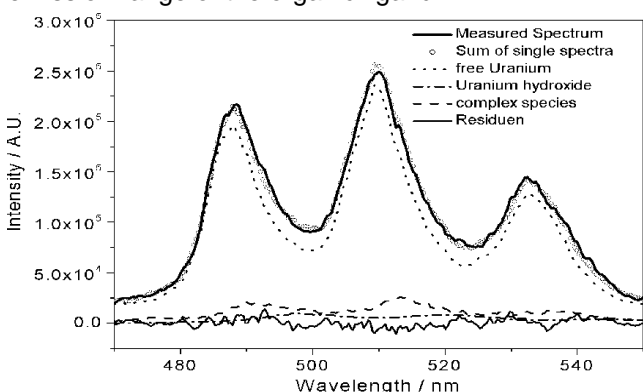


Fig. 2: Deconvolution of spectra, conditions see text
In Fig. 2 the deconvolution of the fluorescence spectrum of a solution containing $3 \cdot 10^{-4}$ M 5-sulfosalicylic acid is shown measured 650 ns after application of the laser pulse. Besides the emission of the free uranyl ion two other fluorescence spectra could be detected. If we assign one of these spectra to residual hydrolysis products the other one should be the spectrum of the formed

complex. The main fluorescence emission bands were found at 475.2 nm, 492.6 nm, 513.6 nm and 535.2 nm, respectively. The fluorescence lifetime of the uranyl-5-sulfosalicylate species is smaller than $1 \mu\text{s}$. Further measurements are necessary.

The complex formation constant was calculated using only the fluorescence intensity of the free uranyl ion. The fluorescence intensity for the free uranyl ion was calculated by deconvolution of the spectra recorded 150 ns after laser pulse application. Assuming that only one complex species will be formed and that the concentration of hydrolysis products can be neglected, a simple algorithm for the calculation can be established.

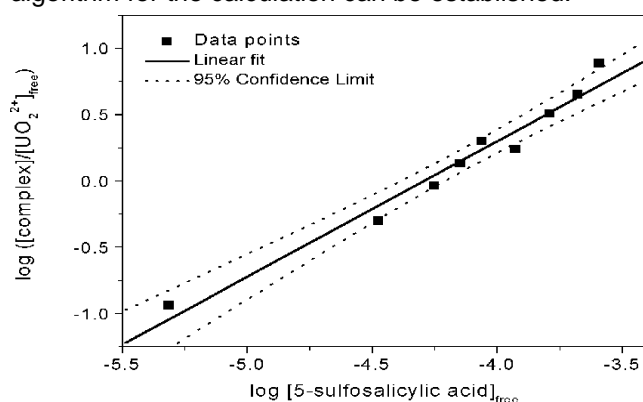
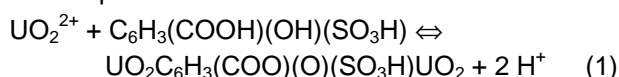


Fig. 3: Validation of the stoichiometry of the complex formation at pH 3.8

Fig. 3 shows the validation of the stoichiometry of the complex formation. The slope of the fit was calculated to be 1.02 ± 0.07 . This clearly confirms the formation of a 1:1 complex.

The complex formation reaction can be written



The calculation of the complex formation constant can be done in two modes. First we use the fluorescence intensity of the formed complex. We calculate a formation constant of $\log K' = 3.07 \pm 0.37$ considering that under the experimental conditions uranium is complexed up to a maximum of 30% [1]. To get the overall formation constant for reaction (1) we have to take into account the dependence on the concentration of H^+ and the dissociation of the 5-sulfosalicylic acid. The formation constant for reaction (1) is calculated to be $\log K = -0.73 \pm 0.40$.

On the other hand the formation constant can be calculated from the data of the free uranyl ion. The constant was found to be $\log K' = 4.39 \pm 0.30$. This is a relatively large discrepancy, which is probably caused by a dynamic quench effect. Studies to evaluate this quench effect are in progress.

References

- [1] A.E. Martel, R.M. Smith, R.J. Motekaitis: *NIST Critically Selected Stability Constants of Metal Complexes*, Database Version 5.0 (1998)

COMPLEX FORMATION OF URANIUM(VI) WITH 5-SULFOSALICYLIC ACID STUDIED BY TRFLS PART II: FEMTOSECOND LASER PULSES AS EXCITATION SOURCE

G. Geipel, G. Bernhard

Using Time-Resolved Laser-Induced Fluorescence Spectroscopy (TRLFS) with femtosecond pulses as excitation source we studied the complex formation between uranium(VI) and 5-sulfosalicylic acid using the fluorescence properties of the organic ligand. The complex formation constant was found to be $\log K = -0.67 \pm 0.08$.

In a previous contribution we reported the result of studies on the complex formation between uranium and 5-sulfosalicylic acid using the fluorescence properties of uranium(VI). We want to compare these results with data obtained from measurements of the fluorescence of 5-sulfosalicylic acid (2-hydroxy-5-sulfobenzoic acid; HSBA-H). HSBA-H has itself strong fluorescence emission. The fluorescence lifetime is relatively short (5.39 ± 0.26 ns). Fig. 1 shows the time-resolved fluorescence spectra of pure $5 \cdot 10^{-5}$ M 5-sulfosalicylic acid at pH 4.00.

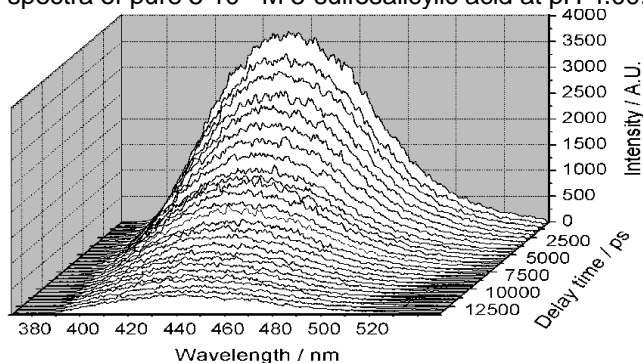


Fig. 1: Fluorescence spectra of 5-sulfosalicylic acid

Due to static quenching, the fluorescence intensity decreases as function of the concentration of added uranium(VI). Considering that the formed complex does not emit any fluorescence we can formulate the following scheme:



The fluorescence emissions $h\nu_1$ and $h\nu_2$ can be measured by TRFLS, the excited complex does not show any fluorescence emission, it reaches the ground state by radiation less deactivation. Fig. 2 shows the results of the measurement of the deactivation kinetics for $5 \cdot 10^{-5}$ M 5-sulfosalicylic acid at several concentrations of added uranium(VI).

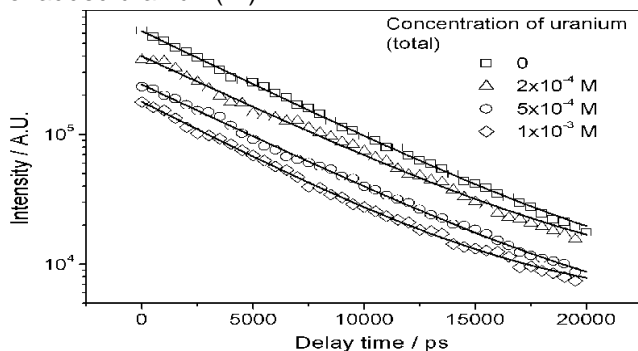


Fig. 2: Fluorescence decay of 5-sulfosalicylic acid at several uranium concentrations

Discriminating the emitted fluorescence of the free uranyl ion we can calculate the formation constant according to equation (6).

$$K = \frac{[\text{HSBA-UO}_2^+][\text{H}^+]}{[\text{UO}_2^{2+}][\text{HSBA-H}]} \quad (3)$$

$$K = K'[\text{H}^+] \quad (4)$$

$$\frac{I_0}{I} = \frac{[\text{HSBA-UO}_2^+][\text{HSBA-H}]}{[\text{HSBA-H}]} \quad (5)$$

$$\frac{I_0}{I} = 1 + K'[\text{UO}_2^{2+}] \quad (6)$$

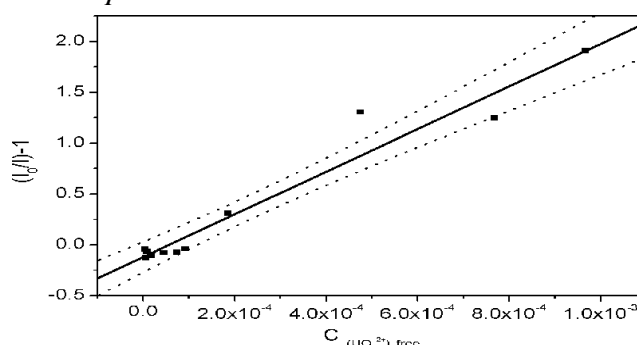


Fig. 3: Stern-Vollmer plot of the fluorescence behavior of 5-sulfosalicylic acid as function of free uranium concentration

The calculated fluorescence intensities at the relative delay time 0 ps were used for the Stern-Vollmer plot shown in Fig. 3. The slope of the Stern-Vollmer plot is equivalent to the complex formation constant. It is found to be $\log K' = 3.32 \pm 0.02$.

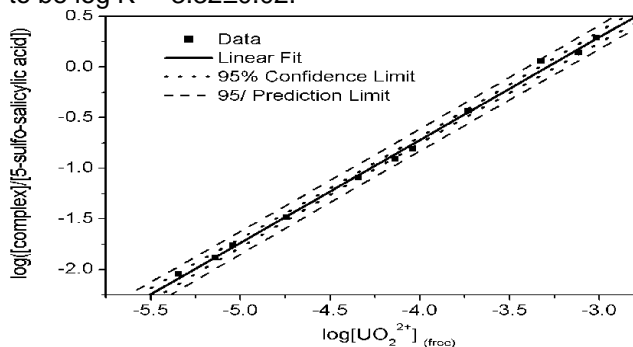


Fig. 4: Validation of the complex formation of uranium(VI) with 5-sulfosalicylic acid

Fig. 4 shows the validation of the complex formation in concentration units. The slope of the fitted straight line is 1.016 ± 0.018 , confirming the proposed stoichiometry of a 1:1 complex. The intersection gives us the complex formation constant to be $\log K' = 3.34 \pm 0.07$.

Taking into account the release of one proton during the complex formation, we have to insert the pH of the studied solutions. The pH was 4.00 ± 0.01 . Finally we calculate the complex formation constant at an ionic strength $I = 0.1$ M to be $\log K = -0.67 \pm 0.08$. Comparing these data with the results in Part I we find a very good agreement between the results of both methods. The data are also in agreement with the formation constant compiled in the NIST database /1,2/.

References

- 1/ A.E. Martel, R.M. Smith, R.J. Motekaitis: *NIST Critically Selected Stability Constants of Metal Complexes*, Database Version 5.0 (1998)
- 2/ Abdel-Gaber, A.A. et al., *J. Chinese Chem. Soc.* **34**, 291 (1987)

COMPARISON OF SEVERAL HYDROXYBENZOIC ACIDS IN TERMS OF COMPLEX FORMATION WITH URANIUM(VI)

G. Geipel, G. Bernhard

We studied the complex formation of salicylic acid, resorcylic acid and gallic acid with uranium(VI), using TRLFS with femtosecond laser pulses. We found a decrease in fluorescence lifetime with an increasing number of OH groups. The complex formation constants also differed from each other, although there was no clear dependence on the OH groups.

We studied the interaction of three hydroxybenzoic acids with uranium(VI), using their fluorescence properties. The fluorescence was excited by the femtosecond laser system described in a previous paper /1/.

The concentration of the hydroxybenzoic acids was $5 \cdot 10^{-5}$ M for salicylic acid, $1 \cdot 10^{-4}$ M for α -resorcylic acid and $3 \cdot 10^{-4}$ M for gallic acid. The pH of the solutions was kept constant at 4.00 ± 0.01 . The concentration of uranium was varied from $1 \cdot 10^{-6}$ M to $5 \cdot 10^{-3}$ M.

The various concentrations of the hydroxybenzoic acids are caused by their different fluorescence properties. In the series 2-hydroxy benzoic acid (salicylic acid), 3,5-dihydroxy benzoic acid (α -resorcylic acid) and 3,4,5-trihydroxy benzoic acid (gallic acid) the fluorescence lifetime decreases. We determined the fluorescence lifetime to be 4.05 ± 0.10 ns, 0.94 ± 0.13 ns (shorter by two measured lifetimes) and 0.284 ± 0.013 ns in the series salicylic, α -resorcylic and gallic acid. The fluorescence intensities of the noncomplexed acids showed a comparable decrease in this series.

For evaluation of the measured fluorescence data we used the same mechanism as described in /2/.

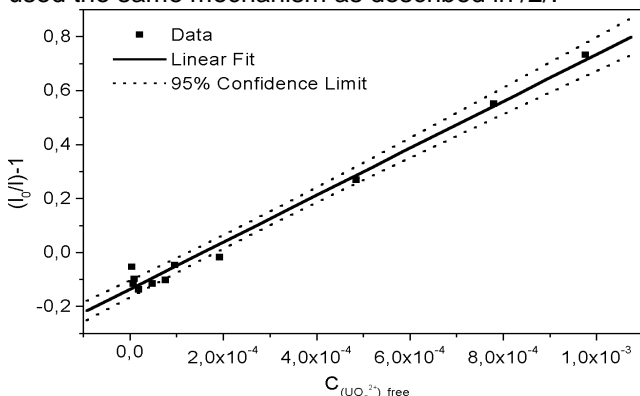


Fig. 1: Stern-Vollmer plot for interaction of uranium(VI) with salicylic acid

Fig. 1 shows the Stern-Vollmer plot for salicylic acid. The slope of the linear fit represents the complex formation constant at pH 4.0. We calculated the formation constant to be $\log K' = 2.88 \pm 0.02$. Considering the complex formation reaction to be

$$C_6H_4(OH)(COO)^- + UO_2^{2+} = C_6H_4(O)(COOUO_2) + H^+$$

the formation constant at the ionic strength $I = 0.1$ M was found to be $\log K = -1.12 \pm 0.03$.

The fluorescence behavior of the α -resorcylic acid was different from that of the other two hydroxybenzoic acids. We found at least two fluorescence emissions with lifetimes of 4.45 ± 1.20 ns and 0.94 ± 0.13 ns. This is due to the existence of the undissociated ligand and its first dissociation product. For calculation of the complex formation we used the data of the shorter fluorescence lifetime. The results for α -resorcylic acid are plotted in Fig. 2. The formation constant was calculated to be $\log K' = 2.57 \pm 0.03$.

As in the fluorescence properties of α -resorcylic acid, gallic acid should also be expected to have two lifetimes.

Due to the low fluorescence intensity only one relatively short fluorescence lifetime was detected by us.

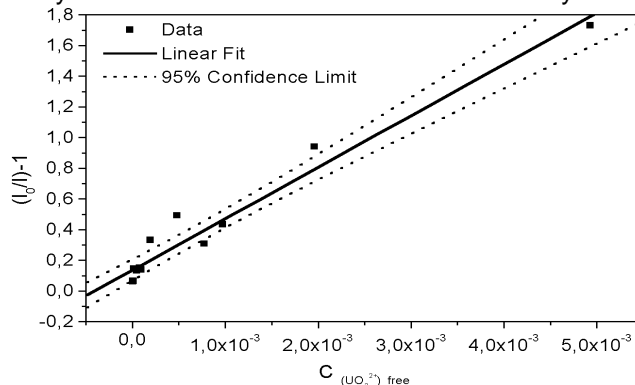


Fig. 2: Stern-Vollmer plot for interaction of uranium(VI) with α -resorcylic acid (data for short lifetime)

Fig. 3 shows the Stern-Vollmer plot for interaction of uranium(VI) with gallic acid. From the slope of the linear fit we calculated the formation constant to be $\log K' = 3.22 \pm 0.04$.

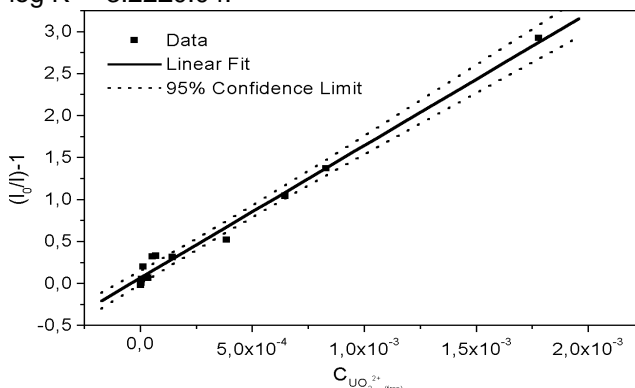


Fig. 3: Stern-Vollmer plot for interaction of uranium(VI) with gallic acid

Fig. 4 shows the validation of the complex formation of the three hydroxybenzoic acids studied. In all three cases the considered 1:1 complex formation was confirmed.

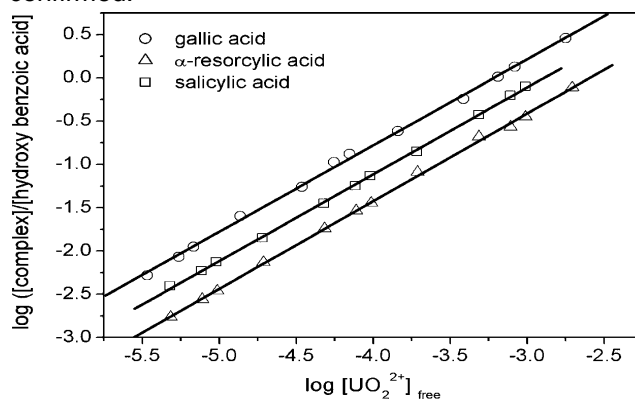


Fig. 4: Validation of complex formation of hydroxy benzoic acids

Further studies are in progress.

References

- /1/ Rutsch, M. et al., Report FZR-285 (2000) p. 9-10
- /2/ Geipel, G., Bernhard, G., this report p. 4

COMPLEX FORMATION OF URANIUM(VI) WITH BENZOIC ACID

D. Vulpius, L. Baraniak, G. Bernhard, Th. Fanghänel

The complexation of uranium(VI) with benzoic acid was studied by potentiometric pH titration. Only the formation of the 1:1 complex with $\log \beta_{11} = 2.92 \pm 0.05$ was found at an ionic strength of 0.1 M (NaClO_4) and at 25.0 °C. The dissociation constant of benzoic acid was redetermined to be $\text{p}K = 4.06 \pm 0.01$.

Experimental

0.01 M benzoic acid (Merck, AR) and 0.001 M uranyl nitrate (Chemapol, AR) in 0.01 M HClO_4 (Merck, AR) were used as stock solutions. The uranium concentration was determined by ICP-MS. The samples were titrated with carbonate-free 0.01 M NaOH (Merck, Titrisol) whose ionic strength was adjusted to 0.1 M by adding 0.09 mol/L NaClO_4 (Merck, AR). The analytical concentration of this solution was determined by titration with 0.01 M HCl (Merck, Titrisol). All solutions were prepared with CO_2 -free, deionized water in a glove box under nitrogen. The experiments were performed with an automatic titrator (GP-Titrino 736, Metrohm), using an Orion Ross 81-02 combination electrode with ceramic diaphragm and a Schott BlueLine 11 pH combination electrode with platinum diaphragm. Both electrodes were calibrated before each experiment with NBS buffers at pH 4.01 and 6.87 (Wissenschaftlich-Technische Werkstätten), and the pH meter readings were converted to values of pCH by an acid-base titration. After each experiment the electrodes were recalibrated to determine the drift. The titration vessel was flushed with nitrogen. The sample temperature was held at 25.0 ± 0.1 °C. The titration method was the following: After an initialization time of 15 min, 0.05 mL of NaOH solution was added and stirred for one minute. After waiting for another minute without stirring, the pH was measured and the next titration step was taken. The titration curves were evaluated by the computer program SCOGS2 /1/.

Results

The value of the dissociation constant of benzoic acid depended on the pH electrode used. While the Orion electrode reproduced the literature value, the Schott electrode produced a value with a small deviation (Tab. 1). This was accounted for by the different diaphragm types. The new platinum diaphragm of the Schott electrode has a constant electrolyte discharge and consequently a very stable potential which is fast adjusted. This does not apply to the electrode with ceramic diaphragm. In the present case this causes a smaller rise of the pH in the titration curve which leads to a smaller dissociation constant. The dissociation constant of benzoic acid is therefore 4.06 ± 0.01 at $I = 0.1$ M (NaClO_4) and 25.0 °C.

Reference	pK
CRITICAL Database 5.0 /2/	4.01 ± 0.02
This work, Orion electrode	4.00 ± 0.01
This work, Schott electrode	4.06 ± 0.01

Tab. 1: Dissociation constant of benzoic acid at $I = 0.1$ M (NaClO_4) and 25.0 °C

To study the complexation behavior of uranium(VI) with benzoic acid, solutions of uranium(VI) and benzoic acid were titrated in concentration ratios of 1:5,

1:10, and 1:20 ($[\text{UO}_2^{2+}] = 1 \cdot 10^{-4}$ to $2 \cdot 10^{-4}$ M, $[\text{C}_6\text{H}_5\text{COOH}] = 1 \cdot 10^{-3}$ to $2 \cdot 10^{-3}$ M). The titration curves show only the formation of a weak 1:1 complex in the pH range from 3.0 to 5.5 (Tab. 2, Fig. 1). Strong evidence for this complex is supplied by the results with a metal ligand ratio of 1:10. The uranium(VI) hydrolysis was included in all calculations in accordance with the NEA Thermodynamical Database /3/. The hydrolysis constants were converted to an ionic strength of 0.1 M (NaClO_4), using the specific ion interaction theory /3/.

Reference	I / mol/L	T / °C	$\log \beta_{11}$
Ramamoorthy /4/	0.1	31.0	2.59
This work	0.1	25.0	2.92 ± 0.05

Tab. 2: Stability constant of the 1:1 uranyl benzoate complex

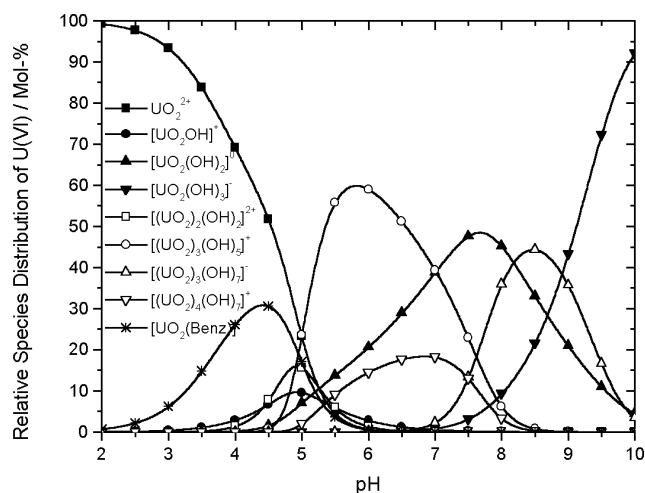


Fig. 1: Relative species distribution of uranium(VI) in benzoic acid as a function of pH ($[\text{UO}_2^{2+}] = 1 \cdot 10^{-4}$ M, $[\text{C}_6\text{H}_5\text{COOH}] = 1 \cdot 10^{-3}$ M, $I = 0.1$ M (NaClO_4), 25.0 °C)

Acknowledgment

This study was supported by the Deutsche Forschungsgemeinschaft under Contract No. BE 2234/3-1.

References

- /1/ Perrin, D.D. et al., in: *Computational Methods for the Determination of Formation Constants*, Leggett, D.J., Ed., Plenum Press, New York, 1985, pp. 71–97
- /2/ Martell, A.E. et al., *NIST Critically Selected Stability Constants of Metal Complexes Database*, Version 5.0, U.S. Department of Commerce, Gaithersburg, 1998
- /3/ Grenthe, I. et al., *Chemical Thermodynamics of Uranium*, OECD NEA, North-Holland, 1992, pp. 107, 683–698
- /4/ Ramamoorthy, S. et al., *Bull. Chem. Soc. Jpn.* **41**, 1330 (1968)

SYNTHESIS AND CHARACTERIZATION OF Np(VII) IN STRONG ALKALINE SOLUTION

H. Moll, T. Reich, G. Geipel, C. Hennig, H. Funke, S. Pompe, K. Schmeide, Th. Fanghänel, I. Grenthe¹

¹Department of Chemistry, Inorganic Chemistry, The Royal Institute of Technology, 10044 Stockholm, Sweden

Dark green Np(VII) was successfully synthesized using ozone. EXAFS analysis showed that in contrast to Np(V) and Np(VI) 4 oxo oxygens are bound to the central Np atom, $\text{NpO}_4(\text{OH})_2^{3-}$.

Experimental

For synthesis of Np(VII), we followed in general the description given by Clark et al. /1/. First, Np(VI) was produced by electrochemical oxidation of Np(V) in diluted HNO_3 . Np(VI) was analyzed spectrophotometrically (strong absorption band at 1220 nm). A dark brown/red precipitate, presumably $\text{NpO}_2(\text{OH})_2$, was obtained by adding NaOH. Ozone was bubbled through a mixture of $\text{NpO}_2(\text{OH})_2$ and 2.5 M NaOH. The solid dissolved to dark green Np(VII). The characteristic absorption maxima at 412 nm and 618 nm, and the molar absorption coefficients published in /2/ were used to determine the Np(VII) concentration, 0.015 M, of the solution measured at ROBL. The absorption spectra of the solution measured before and after the XAS measurement showed no difference.

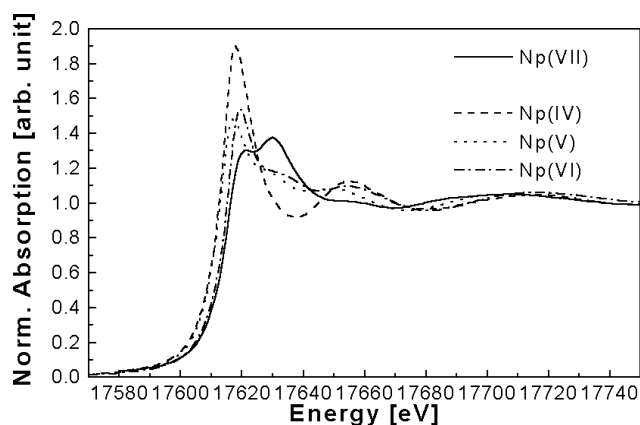


Fig. 1: Normalized Np L_{III} -edge XANES spectra. Spectra of Np(IV), Np(V), and Np(VI) were taken from /5/

The alkaline Np(VII) solution was hermetically sealed under O_3 atmosphere in a polyethylene cuvette of 3 mm diameter. The EXAFS transmission spectra were recorded at room temperature using a water-cooled Si(111) double-crystal monochromator of fixed-exit type ($E = 5\text{-}35$ keV) at the Rossendorf Beamline (ROBL) at ESRF, Grenoble. The energy scale was calibrated using the first inflection point of the absorption spectrum of a Y foil (17038 eV). The scattering phases and amplitudes were calculated for a cluster of $\text{NpO}_4(\text{OH})_2$ using FEFF7. The atomic co-ordinates were taken from $\text{Co}(\text{NH}_3)_6\text{NpO}_4(\text{OH})_2 \cdot 2\text{H}_2\text{O}$ reported in /3/.

Results and Discussion

The XANES spectrum of Np(VII) in alkaline solution is significantly different compared to those of Np(IV), Np(V), and Np(VI) /5/. The Np(VII) species shows different symmetry properties indicating that no actinyl unit is present as in Np(V) and Np(VI). Soderholm et al. /4/ reported a similar XANES spectrum of their Np(VII) sample /4/. The bond lengths and co-ordination numbers obtained are summarized in Tab. 1. The EXAFS spectra and the corresponding Fourier transforms (FT) are summarized in Fig. 2.

Sample	Shell	N	σ^2 (\AA^2)	R (\AA)	ΔE_0 (eV)
0.015M Np(VII) in 2.5M NaOH	Np=O	3.6 ± 0.3 (4.0)	0.0020	1.89_4 (1.88 ₆)	-5.0
	Np-O	3.3 ± 1.3 (2.0)	0.0133	2.32_6 (2.32 ₃)	

Tab. 1: EXAFS structural parameters measured for dark-green Np(VII) in 2.5 M NaOH. In parenthesis XRD values are given that were taken from Ref. /3/

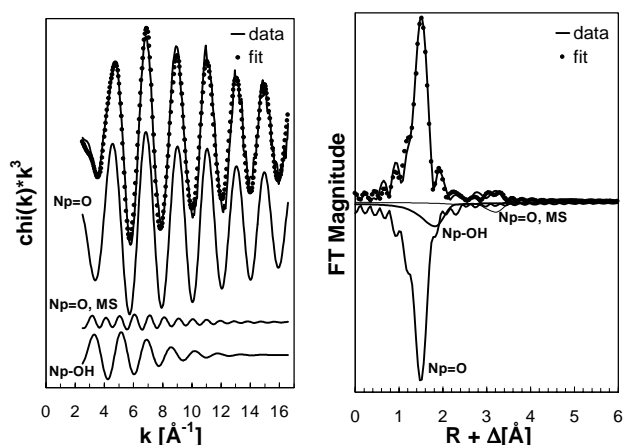


Fig. 2: Np L_{III} -edge k^3 -weighted EXAFS data including the best fit and corresponding FT measured for 0.015 M Np(VII) in 2.5 M NaOH

Four oxygen atoms at 1.89 \AA are coordinated in the first shell around Np. The Debye-Waller factor of 0.0020 \AA^2 is typical for actinyl compounds indicating a short and strong bond. The distance of these oxygens is significantly longer compared to Np(V), 1.82 \AA , and Np(VI), 1.75 \AA /5/. The amplitude of this shell is larger compared to "normal" actinyl compounds /5/. An average co-ordination number of 3 and a distance of 2.33 \AA were determined for the second shell. The error of N is large because of the low amplitude and the strong interference with the "yl" oxygens. The atomic surrounding of Np(VII) in solution measured by EXAFS is in excellent agreement with the XRD results (see Tab. 1) of $\text{Co}(\text{NH}_3)_6\text{NpO}_4(\text{OH})_2 \cdot 2\text{H}_2\text{O}$ /3/. To summarize, the XAS experiments and additional information from XRD lead to the conclusion that the structure of Np(VII) in alkaline solution is most likely $\text{NpO}_4(\text{OH})_2^{3-}$.

We will compare our experimental findings with new quantum chemical calculations.

References

- /1/ Clark, D.L. et al., J. Am. Chem. Soc. **119**, 5259 (1997)
- /2/ Spitsyn, V.I. et al., J. Inorg. Nucl. Chem. **31**, 2733 (1969)
- /3/ Grigorev, M.S. et al., Radiokhimiya **28**, 690 (1986)
- /4/ Soderholm, L. et al., in press (2000)
- /5/ Reich, T. et al., Radiochim. Acta **88**, 633 (2000)

NEPTUNIUM(IV) HUMATE COMPLEXATION STUDIED BY XAFS SPECTROSCOPY

K. Schmeide, S. Pompe, T. Reich, C. Hennig, H. Funke, A. Roßberg,
G. Geipel, V. Brendler, K.H. Heise, G. Bernhard

For the first time, structural parameters of the near-neighbor surrounding of Np(IV) sorbed onto natural and synthetic humic and fulvic acids (HA, FA) were determined at pH 1 by X-ray absorption fine structure (XAFS) spectroscopy. Bio-Rex70, a cation exchange resin having solely carboxylic groups as metal binding functional groups, was used as reference substance for humic substances. The structural parameters of humates are compared with literature data of Np(IV) hydrates and carboxylates.

Experimental

Np(IV) samples were prepared as wet pastes at pH 1 from Aldrich HA (AHA), Kranichsee FA (KFA), synthetic HA type M42, and Bio-Rex70 (from Bio-Rad) /1/. The Np loading was between 4 and 41 mg Np per g sorbent. The samples were measured in transmission mode at the Rossendorf Beamline at the ESRF in Grenoble.

Results and discussion

The tetravalent oxidation state of Np and its stability in the humate and Bio-Rex70 complexes within the time of our experiment is verified by XANES spectroscopy. In Fig. 1, the XANES spectrum of Np(IV)-AHA is shown in comparison to that of the corresponding Np(V) sample. The spectrum of Np(IV) humate shows the characteristic near-edge features of Np(IV) compounds: A more intense 'white line' peak, but no additional shoulder on the high energy side of the peak as generally observed for Np(V) samples.

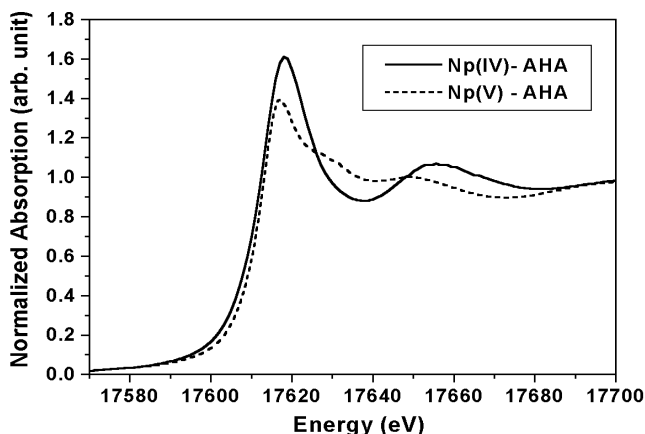


Fig. 1: Normalized Np L_{III} -edge XANES spectra

The Np L_{III} -edge k^3 -weighted EXAFS spectra of the Np(IV) samples and the corresponding Fourier transforms (FTs) are shown in Fig. 2. Both the EXAFS oscillations and the FTs of all Np(IV) complexes are similar.

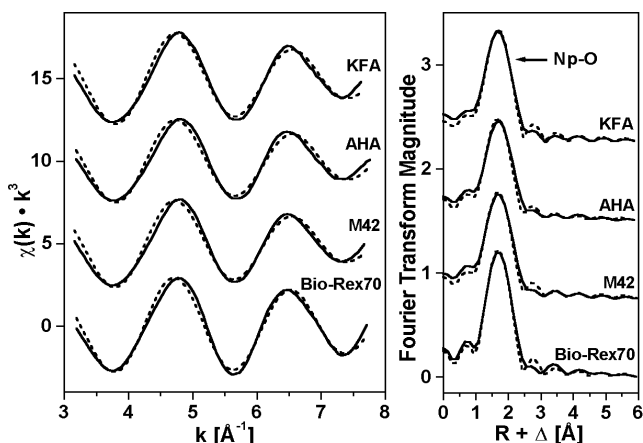


Fig. 2: Raw Np L_{III} -edge k^3 -weighted EXAFS spectra and corresponding Fourier transforms of Np(IV) samples

The structural parameters are given in Tab. 1.

Sample	Shell	N	R [Å]	σ^2 [Å ²]
Np(IV)-KFA	Np-O	11.3±1.7	2.36	0.0162
Np(IV)-AHA	Np-O	10.1±1.7	2.36	0.0159
Np(IV)-M42	Np-O	11.0±1.7	2.36	0.0166
Np(IV)-Bio-Rex70	Np-O	10.2±1.3	2.37	0.0127
Np(IV) in 1 M HCl /2/	Np-O	11.2±1.1	2.40	0.0075
Np(IV) in 2 M H ₂ SO ₄ /3/	Np-O	11±1	2.39	0.0118
	Np-S	2.2±0.9	3.07	0.0070

$\Delta E_0 = -11.1$ eV; $R \pm 0.01$ Å; The 95 % confidence limits are given for N and R as estimated by EXAFSPAK.

Tab. 1: Structural parameters of Np(IV) samples

In the Np(IV) humate complexes, the Np ion is surrounded by about 11 oxygen atoms at a distance of 2.36 Å. Similar parameters are determined for the Np(IV) complex with Bio-Rex70, which has solely carboxylic groups as metal binding functional groups. This verifies that in the humate complexes predominantly the carboxylic groups are responsible for binding Np ions at pH 1. This was expected.

Compared to the hydrated Np(IV) ion in hydrochloric or sulfuric medium /2,3/, the coordination number of the humates is similar, only the Np-O bond length is shortened by about 0.04 Å due to humate complexation. Since no carbon atoms of the binding humic acid carboxylate groups could be detected, it is not possible to determine separate coordination numbers for carboxylate groups and water molecules coordinated to Np by EXAFS analysis.

To identify the binding mode of the carboxylate groups, the bond distances of the Np(IV) humates are compared to those of Np(IV) model compounds which contain carboxylic groups. The results show that the bond distance of the Np(IV) humates is smaller than found for bridging and chelate forming carboxylate groups in Np(IV) oxalate ($R=2.39$ Å, 2.51 Å) /4/ or for bidentate binding carboxylate groups in Np(IV) formate ($R=2.50$ Å) /5/. From this we conclude that the humic acid carboxylate groups are predominantly monodentately bound to Np(IV) ions. This has to be verified by future studies with additional Np(IV) model compounds.

Acknowledgment

This work was supported by the BMWi (no. 02 E 9299).

References

- Schmeide, K. et al., Proceedings of Internat. Conf. Actinide-XAS-2000, Grenoble, France, in press
- Allen, P.G. et al., Inorg. Chem. **36**, 476 (1997)
- Reich, T. et al., Radiochim. Acta **88**, 633 (2000)
- Grigoriev, M.S. et al., Radiokhim. **39**, 419 (1997)
- Hauck, J., Inorg. Nucl. Chem. Lett. **12**, 617 (1976)

EXAFS STUDY OF THE NEPTUNIUM(V) COMPLEXATION BY HUMIC ACIDS IN NEUTRAL SOLUTION

S. Pompe, K. Schmeide, T. Reich, C. Hennig, H. Funke, A. Roßberg, G. Geipel, V. Brendler, K.H. Heise, G. Bernhard

The structure of Np(V) humic acid complexes at pH 7 was studied by EXAFS. The results were compared to structural parameters of a Np(V) hydrate and Np(V) carboxylates reported in the literature.

Structural parameters for Np(V) humic acid (HA) complexes were determined by EXAFS. For the first time, the influence of phenolic OH groups on the Np(V) complexation by HA was studied using a chemically modified HA with blocked phenolic OH groups and Bio-Rex70, a cation exchange resin having only carboxyl groups as proton exchanging sites.

Experimental

Np(V) complexes were prepared under N₂ atmosphere from commercially available natural HA Aldrich (AHA), modified Aldrich HA with blocked phenolic OH groups (AHA-PB) /1/, synthetic HA type M42, and Bio-Rex70 from Bio-Rad. The phenolic OH group content of AHA and AHA-PB amounts to 3.1 meq/g and 1.1 meq/g. Np(V) humate solutions were prepared at pH 7 with Np and HA concentrations of 0.88-0.90 mmol/L and of 8.1-10.8 g/L, respectively (0.1 M NaClO₄). For all samples the formation of the Np(V) humate complexes was verified by NIR absorption spectroscopy. In addition, Np(V) was sorbed onto Bio-Rex70 at pH 7 in 0.1 M NaClO₄. The resulting sorbate had a loading of 121.3 mg Np/g Bio-Rex70. The Np(V) humates were studied in form of solutions, the Bio-Rex70 sorbate in form of a wet paste.

Np LIII-edge EXAFS spectra were recorded at room temperature in fluorescence mode (Np(V) humates) and in transmission mode (Np(V)-Bio-Rex70) at the Rossendorf Beamline at the ESRF in Grenoble.

Results and discussion

The Np LIII-edge k³-weighted EXAFS oscillations and their Fourier transforms (FT) are shown in Fig. 1.

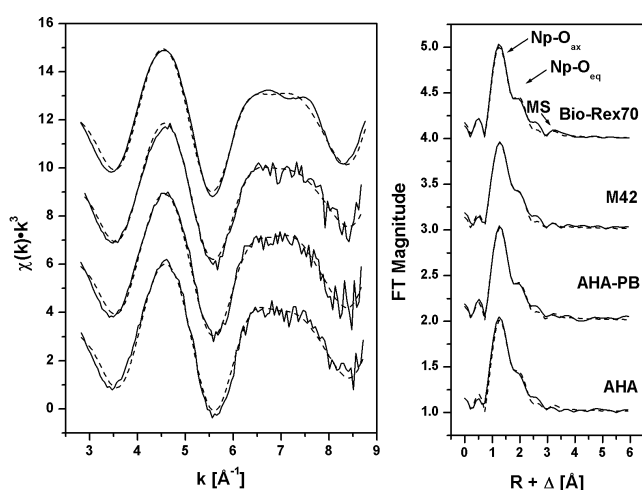


Fig. 1: EXAFS oscillations and their corresponding FT. Solid lines: experiment, dashed lines: fit, MS: multiple scattering along the NpO₂⁺ unit.

EXAFS oscillations were fitted to the EXAFS equation using a structural model with two Np coordination shells containing oxygen as backscatterer and including multiple scattering effects along the neptunyl unit.

The structural data obtained are summarized in Tab. 1.

Np(V)-Sample	Np-O _{ax}		Np-O _{eq}			ΔE ₀ (eV)
	R(Å) ^a	σ ^{2b}	N ^c	R(Å) ^a	σ ^{2b}	
AHA	1.84	3.5	2.9	2.48	4.7	-7.8
AHA-PB	1.85	3.4	2.8	2.49	5.4	-8.0
M42	1.84	4.8	3.3	2.48	7.8	-8.8
Bio-Rex70	1.85	3.4	2.9	2.50	4.6	-8.2
NpO ₂ (H ₂ O) _x ^{+d}	1.82	2.3	3.6	2.49	6	

^a R ± 0.01 Å, ^b σ² in units of 10⁻³ Å², ^c N ± 25 %, ^d /2/

Tab. 1: EXAFS structural parameters. N_{ax}=2

Independent of the HA origin and their functionality, the axial (ax) and equatorial (eq) coordination numbers (N) and Np-O bond lengths (R) for all Np(V) humates are comparable with each other as well as with the EXAFS data of the Np(V)-Bio-Rex70 sorbate. Due to the fact that the Np(V) humates of AHA-PB and AHA show comparable structural parameters it can be concluded that the blocking of phenolic OH groups of the HA has no influence on the local structure around Np in the Np(V) humates. Since Bio-Rex70 solely has carboxyl groups as proton exchanging sites, similar coordination numbers and bond lengths of Np(V) humates and of Np(V)-Bio-Rex70 indicate that carboxylate groups dominate the interaction between Np(V) and HA at pH 7. However, a contribution of phenolic OH groups to the interaction between HA and Np(V) cannot completely be excluded by these results, because they represent average values over all interactions between HA and Np(V). There is the possibility that phenolic OH groups interacting with Np(V) show equatorial bond lengths similar to those of carboxylate groups. The equatorial Np-O bond lengths (R_{Np-Oeq}) of the humates are comparable with R_{Np-Oeq} of monodentate coordinated carboxylate groups in a Np(V) malonate complex /3/. Due to the fact that R_{Np-Oeq} of the humates are also comparable with R_{Np-Oeq} of NpO₂(H₂O)_x⁺ (Tab. 1) /2/, a differentiation between monodentate coordinated carboxylate groups and water molecules is not possible. A predominant bidentate coordination of humic acid carboxylate groups to Np(V) can be excluded. R_{Np-Oeq} of 2.60 Å was found for bidentate coordinated carboxylate groups in a Np(V) formate complex /4/.

Acknowledgment

This work was supported by BMWi under contract no. 02E9299.

References

- /1/ Pompe, S. et al., Radiochim. Acta **88**, 553 (2000)
- /2/ Reich, T. et al., Radiochim. Acta **88**, 633 (2000)
- /3/ Grigoriev, M.S. et al., Radiokhim. **4**, 24 (1993)
- /4/ Grigoriev, M.S. et al., J. Neorgan. Chim. **39**, 1328 (1994)

FIRST XAFS MEASUREMENTS OF PLUTONIUM COMPLEXATION BY HUMIC SUBSTANCES

K. Schmeide, S. Pompe, T. Reich, C. Hennig, H. Funke, A. Roßberg,
G. Geipel, K.H. Heise, G. Bernhard

The near-neighbor surrounding of Pu(III,IV) sorbed onto humic substances and Bio-Rex70 was studied at pH 2 by XAFS spectroscopy. The structural parameters of the humates are compared with literature data of Pu(III) and Pu(IV) hydrates.

The objective was to investigate the interaction of Pu(III) with humic and fulvic acid (HA, FA) and Bio-Rex70.

Experimental

A Pu(III) stock solution (^{242}Pu), prepared by electrochemical reduction of a Pu(VI) solution, was used to prepare Pu(III) samples from synthetic HA type M42, Kranichsee FA (KFA), and Bio-Rex70 (from Bio-Rad) at pH 2 under inert gas conditions. The Pu loading of the resulting wet pastes of M42, KFA and Bio-Rex70 was 61, 71 and 6 mg Pu per g sorbent, respectively. Pu L_{III} -edge XAFS spectra were collected in fluorescence mode at the Rossendorf Beamline at the ESRF in Grenoble.

Results and discussion

The trivalent oxidation state of Pu in the stock solution as well as in the supernatants obtained during preparation of the Pu humate, fulvate and Bio-Rex70 samples was verified by UV-vis absorption spectroscopy using the absorption band at 600 nm. Pu(IV) could not be detected (at 470 nm) in the solutions stored under inert gas conditions, even 4 months after sample preparation. That means, an oxidation of Pu(III) by humic substances or Bio-Rex70 can be excluded.

However, according to the XANES spectra of the humate, fulvate and Bio-Rex70 sorbates the samples contain predominantly Pu(IV) with small amounts of Pu(III). That means, the trivalent oxidation state of Pu was not stable within the time of our experiment. The most likely reason is that during the sample transport to the beamline oxygen diffused through the PE bags and the Kapton tape window used for sealing the Teflon sample holders for pastes.

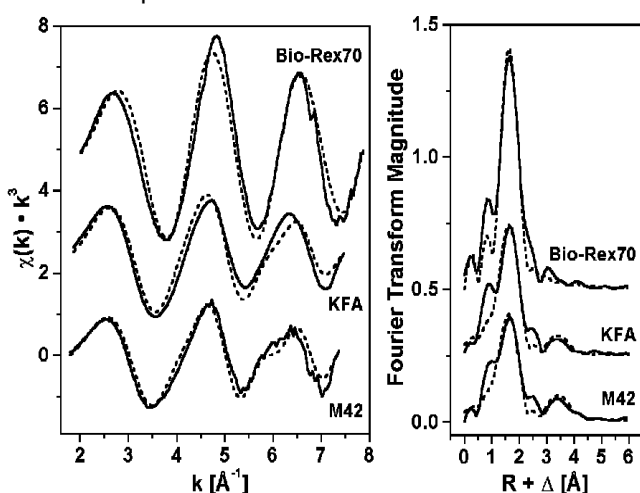


Fig. 1: Raw Pu L_{III} -edge k^3 -weighted EXAFS spectra of Pu samples and corresponding Fourier transforms (without phase corrections). Solid lines: experiment, dashed lines: fit

The EXAFS oscillations and the Fourier transforms of M42 and KFA, shown in Fig. 1, are similar to each other but different from those of Bio-Rex70.

The structural parameters are given in Tab. 1.

Sample	Shell	N	R [Å]	σ^2 [Å ²]
Pu-M42	Pu-O	7.8±1.7	2.38±0.03	0.0250
	Pu-Pu	1.9±1.9	3.78±0.04	0.0086
Pu-KFA	Pu-O	8.3±1.8	2.38±0.03	0.0228
	Pu-Pu	1.5±2.4	3.77±0.05	0.0112
Pu-Bio-Rex70	Pu-O	6.8±1.2	2.34±0.01	0.0098
Pu(III)·nH ₂ O /1/	Pu-O	7.6±0.6	2.48±0.01	0.0102
Pu(IV)·nH ₂ O /2/	Pu-O	8	2.39	0.0118

The 95 % confidence limits are given for N and R as estimated by EXAFSPAK.

Tab. 1: Structural parameters of Pu samples

Within the experimental error, the coordination number of the Pu-O shell of all samples is comparable with those of Pu(III) and Pu(IV) hydrates. The bond length of the Pu-Bio-Rex70 sorbate, which contains the highest amount of Pu(IV), is about 0.05 Å shorter than that of Pu(IV) hydrate. A similar shortening (0.04 Å) was found for Np(IV) samples due to complexation by humic substances and Bio-Rex70 /3/.

According to the XANES results, the Pu sorbates of M42 and KFA contain a slightly higher amount of Pu(III) compared to the Pu-Bio-Rex70 sorbate. This results in a slightly larger bond length ($R_{\text{Pu-O}}=2.38$ Å) which is due to the larger ionic radius of Pu^{3+} (1.12 ± 0.02 Å) compared to Pu^{4+} (1.01 ± 0.02 Å) /4/. The broader bond length distribution due to the two oxidation states is evident in the larger Debye-Waller factor determined for the humate and fulvate samples.

The Fourier transforms of the M42 and KFA samples (cf. Fig. 1) show an additional broad peak at about 3.4 Å which points to a strong backscatterer. Fitting a Pu-Pu shell, 1 to 2 Pu atoms were found at a bond distance of 3.78 Å. This indicates the formation of polynuclear Pu species which is characteristic for Pu(IV). This effect was not observed for Pu-Bio-Rex70, probably due to the lower Pu loading of Bio-Rex70 compared to the humic substances.

The results have shown that in case of humate and Bio-Rex70 sorbates of such redox sensitive actinide ions as Pu much attention has to be paid to the selection of sample containers to minimize diffusion of oxygen. Another possibility is to prepare the samples on-site directly before the XAFS measurements.

Acknowledgment

This work was supported by the BMWi (no. 02 E 9299).

References

- 1/ Reich, T. et al., Report FZR-285, p.72 (2000)
- 2/ Ankudinov, A.L. et al., Phys. Rev. B **57**, 7518 (1998)
- 3/ Schmeide, K. et al., this report, p.14
- 4/ Neck, V., Kim, J.I., Radiochim. Acta **88**, 815 (2000)

SOLVENT EXTRACTION OF URANIUM(VI) BY CALIX[6]ARENE

K. Schmeide, B. Barz, K.H. Heise, G. Bernhard, K. Gloe¹

¹Institute of Inorganic Chemistry, Technische Universität Dresden, 01062 Dresden, Germany

The extraction efficiency of carboxymethoxy-*p*-*tert*-octyl-calix[6]arene towards uranium(VI) was studied in a two phases solvent extraction system in dependence on pH value, ligand concentration and solvent.

Introduction

Calixarenes are macrocyclic molecules formed by 4 to 8 para-substituted phenolic units linked by methylene bridges ortho to the OH functions. Especially calix[6]arenes functionalized with carboxylic or hydroxamic groups on the lower rim have attracted considerable attention as efficient reagents for selective separation of uranium from aqueous solution /e.g., 1-3/.

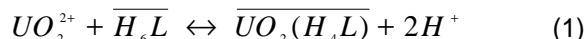
We studied the binding properties of carboxymethoxy-*p*-*tert*-octyl-calix[6]arene /4/ towards uranium(VI) by means of solvent extraction.

Experimental

The calixarene was dissolved in 1,2-dichlorobenzene and dichloromethane (10^{-3} M), respectively, and shaken with the aqueous uranium solution (10^{-5} M) for 8 hours. The phase ratio $V_{(org)}:V_{(w)}$ was 1:1. The two phases were separated and the uranium content was determined in the aqueous phase by ICP-MS. The pH of the aqueous solution was initially adjusted and measured after reaching equilibrium.

Results

The equilibrium of the uranium extraction by the calix[6]arene (H_6L) can be written according to the following equation, where the solid line denotes the species in the organic phase:



The distribution coefficient (D), defined as the ratio of uranium concentration in the organic and in the aqueous phase, is a measure of uranium extractability and of complex stability.

$$D = \frac{[\overline{UO_2(H_4L)}]}{[UO_2^{2+}]} \quad (2)$$

From the definition of D and of the extraction constant (K) follows:

$$\log D = \log K + \log[\overline{H_6L}] + 2 \cdot pH \quad (3)$$

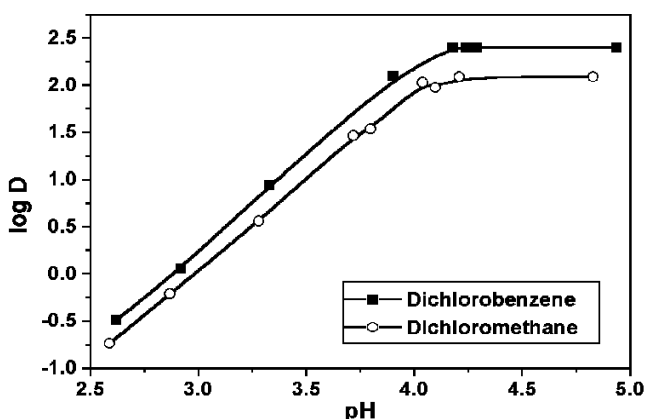


Fig. 1: Extraction of uranium by carboxymethoxy-*p*-*tert*-octyl-calix[6]arene in 1,2-dichlorobenzene and dichloromethane as a function of pH.

The dependence of uranium extraction on pH and solvent is shown by the plots of $\log D$ versus pH in Fig. 1. Between pH 2.6 and about 4.1 the extraction efficiency increases constantly with pH. The curve slope of two indicates that two carboxylic groups are deprotonated upon extraction of uranium, thereby forming a neutral complex. At pH values higher than pH 4.1 in the aqueous phase, the maximum of extraction is reached. The uranium extraction is higher for dichlorobenzene than for dichloromethane as solvent.

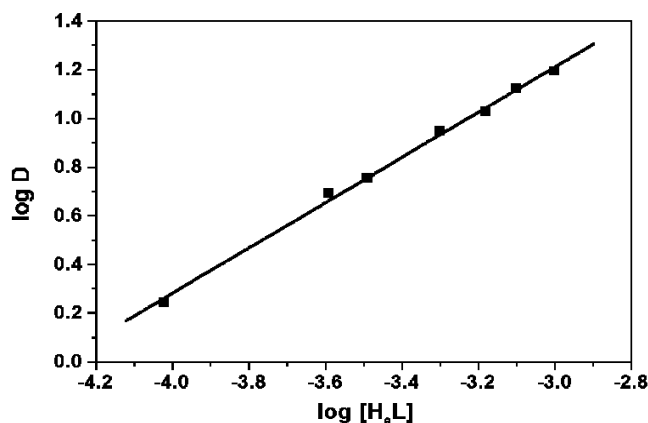


Fig. 2: Extraction of uranium by carboxymethoxy-*p*-*tert*-octyl-calix[6]arene in dichloromethane as a function of ligand concentration at constant pH in the aqueous phase (pH 3.7).

The stoichiometry of the extraction species follows from Fig. 2. The plot of $\log D$ versus $\log [H_6L]$ for pH 3.7 shows a slope of unity. This means that a single calixarene molecule is involved during extraction.

Conclusion

Since two protons are released and one calixarene molecule is involved during extraction, the extraction scheme given in eq. (1) is verified.

The results of solvent extraction indicate that carboxymethoxy-*p*-*tert*-octyl-calix[6]arene is an excellent uranophile even in the acidic pH region.

Acknowledgment

This work was supported by the BMBF (no. 0339917).

References

- 1/ Shinkai, S. et al., J. Chem. Soc., Chem. Commun., 233 (1986)
- 2/ Nagasaki, T. et al., J. Chem. Soc., Perkin Trans. 2, 1063 (1991)
- 3/ Baglan, N. et al., J. Radioanalyt. Nucl. Chem. 226, 261 (1997)
- 4/ Ohto, K. et al., Analyt. Sciences 11, 893 (1995)

**Interaction of Actinides/Radionuclides with
Surfaces of Rocks, Minerals and Colloids**

INORGANIC COLLOIDS IN MINE WATERS

H. Zänker

A broad variety of inorganic colloidal particles is found in mine waters. The size, concentration and mineralogy of these particles and their tendency to adsorb heavy metal ions depend on the chemical conditions in the specific water body (section of the mine).

Inorganic colloids in mine waters (emphasis is laid on the waters in abandoned uranium mines here) are mainly produced by the formation of oxyhydroxides and oxyhydroxy sulfates of iron(III) and aluminum due to the oxidation of Fe^{2+} and the hydrolysis of Fe^{3+} and Al^{3+} . Seen from the point of view of colloid chemistry, all mine waters lie between two extremes which are represented by the following two water types:

(i) Type "acidic pore water"

These waters can be separated from the rock by centrifugation or can be collected in the mines as acid rock drainage (ARD) samples. The colloid chemistry of ARD solutions was extensively studied by us. The waters possess high salt concentrations and are very acidic (pH 1 to 3). Ultrafine particles of <5 nm are the main colloidal component. The colloid concentration reaches the range of >1 g/L. The particles consist of hydroniumjarosite and schwertmannite. As and Pb show a high tendency to adsorb onto these particles.

(ii) Type "bulk water"

This type mainly refers to the flowing mine waters such as adit waters which possess a near-neutral pH. Typical colloid contents of such waters lie around 1 mg/L, typical particle sizes are 100 to 300 nm. The particles consist of Fe(III) and Al oxyhydroxides (ferrihydrite, alumogel, possibly jurbanite or alunite). Their electrostatic stabilization is weak (zeta potential only about -10 mV), i.e. they show a greater tendency to coagulate and flock than do the colloids of the type (i) waters. Contaminants such as As, Pb, Cu, Th, ^{210}Po , ^{210}Pb are strongly bound onto these particles.

Colloidal particles in mine waters deserve attention because of their ability to adsorb heavy metals and to influence heavy metal transport. However, heavy metal adsorption is strongly dependent on pH. The adsorption conditions are therefore very different for type (i) and type (ii) waters. Type (i) solutions have pH values at the left of the heavy metal "adsorption edges". Only elements that possess a tendency to precipitate in sulfate-rich waters (Pb, Ra) or that have a special chemical affinity to iron(III) oxyhydroxy sulfates (As) are attached to the colloids in these waters. Type (ii) solutions lie at the right of many "adsorption edges." Many heavy metals, including U(IV) and Th, are therefore scavenged by the colloid particles in these waters. In carbonate-free solutions also U(VI) is adsorbed to iron(III) oxyhydroxides at pHs above 6. In geochemical samples, however, this U(VI) adsorption is often suppressed due to the formation of uranyl carbonate complexes.

An interesting colloid chemistry is observed during the transition of type (i) waters to type (ii) waters which occurs in the course of the flooding of abandoned ore mines (dilution of the type (i) waters). Huge amounts of iron (III) particles of 100 to 300 nm are formed in such situations due to O_2 ingress and pH increase.

The adsorption rises drastically as soon as the pH of the "adsorption edge" of a heavy metal is reached. The adsorption behavior of U(VI) in flooding waters differs significantly from that of U(VI) in both typical acidic "pore waters" and typical steady-state "bulk waters". Typical pH values of the flooding waters lie in the range between 4 and 6 after some flooding time. Uranyl adsorption to the iron(III) particles is neither suppressed by high acidity nor by uranyl carbonate complexation in this pH region. Therefore, most of the uranium(VI) is colloid-borne in such waters.

The consequences of neglecting the colloids when assessing the long-term behavior of contaminants in abandoned mines differ for the individual heavy metals. The following possibilities exist:

(a) The modeling description is correct.

The heavy metal ion under study is not adsorbed onto solid phases, i.e., it is "mobile": Neglecting the colloid-facilitated transport is justified.

(b) The modeling description is "over-conservative".

The heavy metal ion is regarded as mobile in the model but adsorbs in reality onto solid phases: Scavenging and removal by colloid filtration and/or aggregation plus aggregate sedimentation come into play; the model is "over-conservative" (too pessimistic).

(c) The modeling description is "under-conservative".

The heavy metal ion is regarded as immobile due to adsorption onto solid phases (rock walls) in the model. However, a certain fraction of the heavy metal inventory may be bound to colloidal particles and thus be mobile in reality. The model is "under-conservative" (too optimistic).

Case (a) is, for example, given for U(VI) at pH values below 4 and above 6 (carbonate-containing waters).

Case (b) applies to U(VI) in the pH range from 4 to 6.

Case (c) might apply to U(IV).

The influence of inorganic colloids on the uranium transport can currently be assessed quite well for oxic mine waters. Very little knowledge exists for anoxic mine waters where the uranium is tetravalent. U(IV) is usually regarded as "immobile" due to sorption to the rock walls. It is not known to what degree the scenario of case (c) can counteract this "immobility".

The open questions are:

Can Fe(III) colloids act as carrier colloids for U(IV), i.e., is there a significant field of coexistence of Fe(III) and U(IV)?

Can siderite (FeCO_3) particles act as carrier colloids for U(IV)?

Can intrinsic U(IV) colloids play a role?

Investigations into the colloid-chemical behavior of U(IV) in mine waters under in-situ conditions are in preparation.

ACID ROCK DRAINAGE (ARD) SAMPLES FROM THE "HIMMELFAHRT FUNDGRUBE" AT FREIBERG STUDIED BY XAS

H. Moll, H. Zänker, W. Richter, V. Brendler, C. Hennig, A. Roßberg, H. Funke, T. Reich

This XAS investigation deals with the in-situ characterization of the near-order surrounding of As in ARD solutions containing colloidal particles as well as with the determination of the particle mineralogy.

Experimental

The ARD solutions were transferred into polyethylene cuvettes of 3 mm diameter to measure Fe K-edge XAS spectra. The path length was 10 mm for As K-edge experiments. All model substances and the precipitate were analysed using XRD and/or REM/EDX /1/. Appropriate amounts of the solid samples were mixed with Teflon and then pressed to give pellets with a diameter of 13 mm.

Sample	Fe [M]	As [M]	[As]/[Fe]
Raw sample	0.080	$5.2 \cdot 10^{-3}$	0.065
5 μm filtrate	0.070	$4.8 \cdot 10^{-3}$	0.068
1 kD retentate	0.368	0.080	0.217
1 kD filtrate	0.054	$1.4 \cdot 10^{-3}$	0.026
	Fe [mg/g]	As [mg/g]	
Precipitate	324	68	0.210

Tab. 1: Chemical analysis of the ARD samples

XAFS data were recorded at the Rossendorf Beamline (ROBL) at the ESRF in Grenoble. Transmission and/or fluorescence spectra were measured at room temperature using a water cooled Si(111) double-crystal monochromator of fixed-exit type ($E = 5 - 35$ keV). For energy calibration of the sample spectra, the spectrum from a Fe or Pt foil was recorded simultaneously. The data were treated using the EXAFSPAK software. Theoretical backscattering phase and amplitude functions, $\delta(k)$ and $F(k)$, used in data analysis were calculated using FEFF6.

Results and Discussion

Fig. 1 depicts the EXAFS spectra measured at the As K-edge.

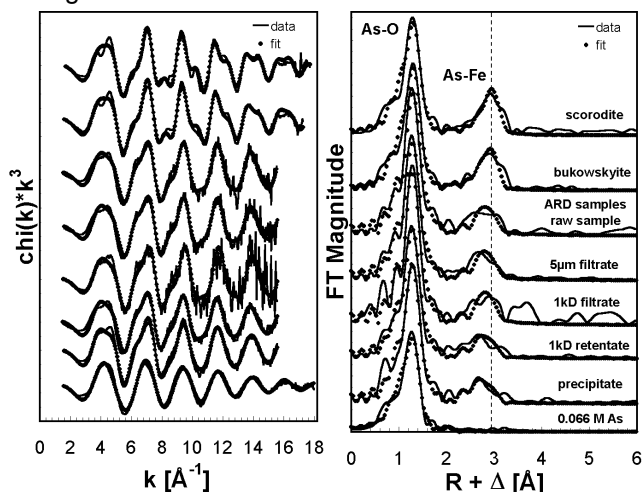


Fig. 1: Experimental EXAFS oscillations and corresponding Fourier Transforms of the model compounds and the ARD fractions at the As K-edge

The Fe EXAFS data (not shown here) of the freshly formed colloids suggest that an amorphous Fe phase dominates the colloidal matrix. On the other hand, the EXAFS oscillation of the precipitate shows the presence of a more crystalline Fe phase. The data of the 5 μm filtrate indicate an intermediate between these

two stages. The Fe-Fe distance of ≈ 3.60 Å suggests a relatively close relationship between the ARD samples and the jarosite. Considering the REM/EDX analysis of particle agglomerates on a Nucleopore filter /1/ and the EXAFS results, we assume that the colloidal particles represent an intermediate in the precipitate formation process having a mineralogy similar to that of the precipitate, i.e., consisting of H-jarosite and amorphous Fe phases.

Sample	Shell	N	R [Å]	σ^2 [Å ²]
Scorodite (mineral) FeAsO ₄ ·2H ₂ O	As-O	5.0 (4)	1.68 (1.68)	0.0027
	As-Fe	3.7 (4)	3.34 (3.33)	0.0048
Bukowskyite (mineral) Fe ₂ AsO ₄ SO ₄ OH·7H ₂ O	As-O	5.2	1.68	0.0025
	As-Fe	3.2	3.33	0.0042
ARD solution raw sample	As-O	4.3	1.69	0.0013
	As-Fe	2.2	3.28	0.0047
ARD solution (5 μm filtrate)	As-O	4.5	1.69	0.0017
	As-Fe	2.2	3.27	0.0046
ARD solution (1 kD filtrate)	As-O	4.4	1.68	0.0011
	As-Fe	1.9	3.26	0.0032
ARD solution (1 kD retentate)	As-O	4.7	1.69	0.0021
	As-Fe	2.5	3.29	0.0067
ARD solution precipitate	As-O	5.0	1.68	0.0022
	As-Fe	4.5	3.28	0.0110
0.066 M As solution	As-O	5.2	1.68	0.0025

Tab. 2: Summary of the EXAFS structural parameters. In parenthesis XRD values /2/

The As K-edge XANES data, the intensive white line and the As K-edge energies of 11875.0 eV indicate the +5 oxidation state of As in all ARD samples. Taking the EXAFS results alone (Fig. 1, Tab. 2), one might draw the conclusion that arsenate interacts with the solid iron hydroxy sulfates in a similar way in all fractions. The pronounced As-Fe contribution at 3.28 Å (see Fig. 1) measured in the ARD raw sample and the different filtrates shows that arsenate is bound to the colloids (iron hydroxy sulfate) in a similar way to that of arsenate onto ferrihydrite, i.e., by inner-sphere surface complexation /3/. The picture is different for the precipitate. The relatively large arsenic content and the small particle surface of the precipitate make surface complexation unlikely. A better explanation is an epitaxial growth of a scorodite phase within/on the iron hydroxy sulfate. Relaxation processes of the As-Fe bond occurring in such small scorodite zones could explain the atypical As-Fe distance of 3.28 Å.

References

- /1/ Zänker, H. et al., submitted to Appl. Geochem.
- /2/ Hawthorne, F.C., Acta Cryst. B **32**, 2891 (1976)
- /3/ Waychunas, G.A. et al., Geochim. Cosmochim. Acta **57**, 2251 (1993)

COLLOID-BORNE U(VI) IN THE FLOODING WATER OF AN ABANDONED URANIUM MINE

W. Richter, H. Zänker

The colloids result primarily from the oxidation of Fe(II) due to the access of oxygen. Whereas U(VI) was not adsorbed onto the colloids in the acidic mine waters of the past, significant adsorption occurs in the more recent flooding waters of higher pH.

The most abundant colloid particles in the waters of the Königstein uranium mine are Fe(III) oxyhydroxide particles and Fe(III) oxyhydroxy sulfate particles. These iron compounds are known for their ability to adsorb heavy metals such as U(VI) /1,2/. However, heavy metal adsorption is strongly dependent on pH. In the past, very acidic waters were typical of the Königstein mine /3/. Heavy metal adsorption onto the above-mentioned iron compounds is only marginal in such waters. Now, with the flooding process well advanced, this mine contains more and more waters of lower acidity. Uranyl binding to ferric oxyhydroxides and oxyhydroxy sulfates shows a sharp adsorption edge between pH 4 and 5.5 /1,2/, i.e. uranyl adsorption onto ferric iron particles should play an increasing role. On the other hand, Fe concentrations and U concentrations are much lower in the more recent (more dilute) flooding waters and the colloidal state is less stable than in the strongly acidic pore waters and leaching waters: the colloids show an increasing tendency to coagulate and sediment (zeta potential: -7 mV). Furthermore, the groundwaters mixing with the mine waters are partly oxid. Thus, also Fe(III) particle production due to the oxidation of Fe(II) plays an increasing part.

Component	Raw sample concentration [$\mu\text{Mol/L}$]	Concentration removable by a 50-nm filter [$\mu\text{Mol/L}$]
Al	12.7	9.15
As	0.27	0.194
Ca	913	< 0.6
Ce	0.037	0.025
Fe	383	212.6
Mg	151.2	0.11
Mn	7.65	0.058
Si	160	< 1.9
U	2.41	1.45
Zn	9.88	0.17
Sulfate	1130	na
Bicarbonate	1000*	na
Chloride	280	na

* Value of a sample taken two months later. na: Not analyzed

Tab. 1: Results of ICP-MS, AAS and ion chromatography on the raw sample and on the filter cake. Filter cake was washed three times with Milli-Q-water.

Column 2 of Tab. 1 shows the chemical analysis of a typical example of the more dilute type of flooding water. The pH of the sample was 5.5, the Eh 446 mV, the O_2 content 3.5 mg/L. One can see that the cation concentrations are dominated by Ca and Fe. The most important anions are sulfate and bicarbonate. The Fe concentration is much lower than in the highly mineralized pore waters /3/, but significantly higher than in the bulk water of a fully flooded ore mine at steady state (see mine at Freiberg /4/). A large fraction of the iron was divalent. Storage in a refrigerator significantly reduced the iron oxidation rate; 52.3 % of the iron was still ferrous iron after 7 d (determination with 1,10 phenanthroline). Based on the Eh measured we assume that only hexavalent uranium plays a role.

The elemental concentrations removable by 50-nm filtration (Nuclepore filter) two days after sampling are given in Column 3 of Tab. 1. About 50% of the iron is filterable, which is in accordance with the results of the Fe(II)/Fe(III) analysis. Ferric iron is the main component of the colloids, followed by Al and U (about 60% of the U is colloid-borne). Minor contributions are associated with As and Ce. Fig. 1 gives an SEM micrograph of the filter cake.

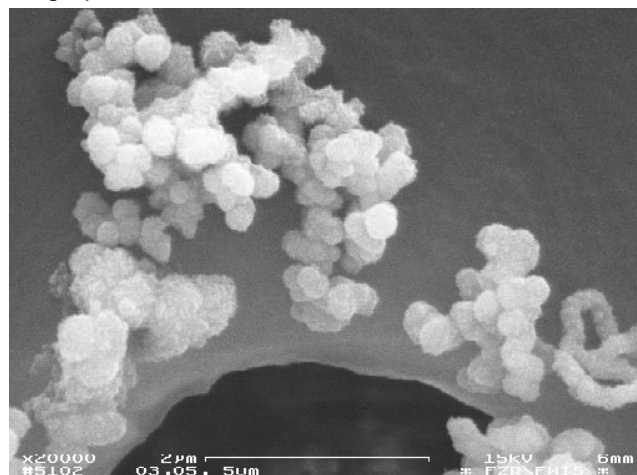


Fig.1: SEM micrograph of Fe(III) particles on a 5- μm Nuclepore filter. Filter cake washed three times with Milli-Q water. Coating with gold

Particles of about 200 nm are visible. Experience shows that Fe(III) particles of the colloidal size range are ubiquitous in the waters of the Königstein mine. These particles are produced as soon as oxygen has access to Fe^{2+} solutions that are not too acidic. Whereas uranyl adsorption onto Fe(III) particles does not occur at very low pHs /5/, extensive uranyl adsorption is encountered at pH above 4. We assume from previous experiments /4/ that uranyl adsorption can be suppressed again at pH values above 6 due to the formation of uranyl carbonate complexes.

The uranyl ion is normally regarded as a "mobile" (dissolved) in geochemical calculations. The most common effect of uranyl adsorption onto ferric particles in the pH range from 4 to 6 should therefore be migration mitigation rather than migration enhancement, i.e. the assumption of an unhindered uranyl migration is often over-conservative for this pH region. This is due to scavenging of the uranyl ions by Fe(III) particles and removing them by colloid coagulation and sedimentation.

References

- /1/ Waite, T.D. et al., *Geochim. Cosmochim. Acta* **58**, 5465 (1994)
- /2/ Webster, J.G. et al., *Environ. Sci. Technol.*, **32**, 1361 (1998)
- /3/ Jenk, U.: Thesis TU Bergakademie Freiberg (1994)
- /4/ Zänker, H. et al., *Radiochim. Acta* **88**, 619 (2000)
- /5/ Zänker, H. et al., Submitted to *Appl. Geochem.*

SEM OF COLLOID PARTICLES ON NUCLEAR TRACK FILTERS: THE INFLUENCE OF DISSOLVED SALTS

G. Hüttig, W. Richter, H. Zänker

The depiction of environmental particles on filter membranes by SEM was tested for its susceptibility to artifacts due to salt crystallization on the drying filter.

The range of 50 to 400 nm is the typical particle size range of environmental colloids /1/. Particles of this size can very well be visualized by scanning electron microscopy (SEM). They can also be analyzed by energy-dispersive X-ray analysis (EDX). The preparation of the colloid particles for SEM and EDX is rather easily done by separating them from the water with the help of a nuclear track filter, drying the filter cake and coating it with gold or carbon. The filtered sample volume should be such that not more than one third of the filter membrane becomes covered with particles.

Figs. 1a and 2a show examples of SEM micrographs of environmental particles on Nuclepore filters (Costar, Cambridge, USA). They were obtained from mine drainage gallery water which was described in more detail in /2/. The water was saturated with air and had a pH value of 7.2. The salt content was dominated by sulfates, carbonates and chlorides of Ca, Na and Mg which had a total concentration of several hundred mg/L (electrical conductivity: 1055 $\mu\text{S}/\text{cm}$). A colloid concentration of about 1 mg/L was found (oxyhydroxides of Fe and Al). Particles of about 100 nm are visible on the filters (also filter pores are to be seen).

It is the routine procedure in our group to rinse filter cakes three times with 20 mL of Milli-Q water before drying and coating them in order to remove soluble salts. The question arose whether this rinsing is sufficient to prevent falsification of the SEM micrographs by crystallizing electrolytes. The following tests were carried out to answer this question.

First, we analyzed the three washing waters by means of ICP-MS and ion chromatography. 97.8% of the removable calcium, for instance, was found in the first washing water, 1.7% in the second and 0.6% in the third, indicating the effectiveness of our three-step washing procedure. The behavior of the other major components such as the Mg^{2+} or the SO_4^{2-} ions was similar.

Then we replaced three-step rinsing by ten-step rinsing. Figs. 1b and 2b show that this rigorous rinsing causes hardly any change in the appearance of the filter cakes. The latter consisted almost entirely of separated colloid particles no matter which of the two rinsing procedures was used. This was also confirmed by EDX spectra of the filter cakes that identified Fe and Al as the major constituents of the particles for both rinsing methods (coating with carbon).

It is also remarkable that the amount of particles on the filter membrane is only little reduced if a 5 μm filter (Fig. 2) is used instead of the 50 nm filter (same filtered sample volumes). This is due to the fact that filtration is not a 'sieving' process such as sieving of powders in air but a process also governed by particle aggregation in the fluid-to-membrane interface layer and by adsorption of particles onto the membrane /3/.

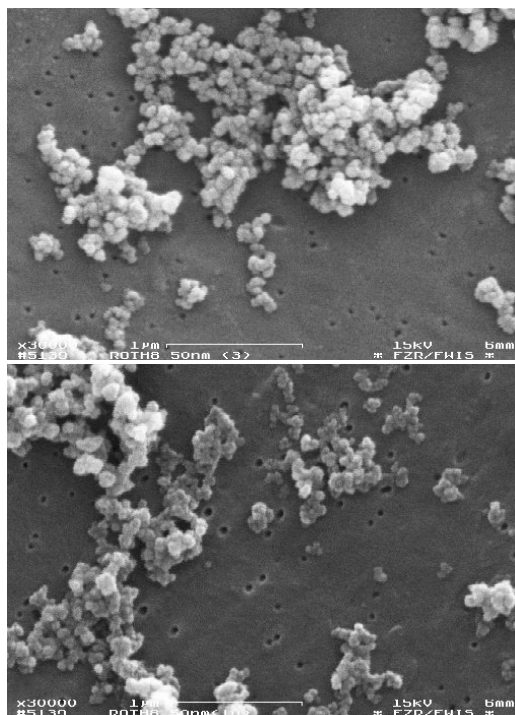


Fig. 1a/b: SEM micrograph of particles on a 50 nm Nuclepore filter. (a) triplicate rinsing; (b) tenfold rinsing

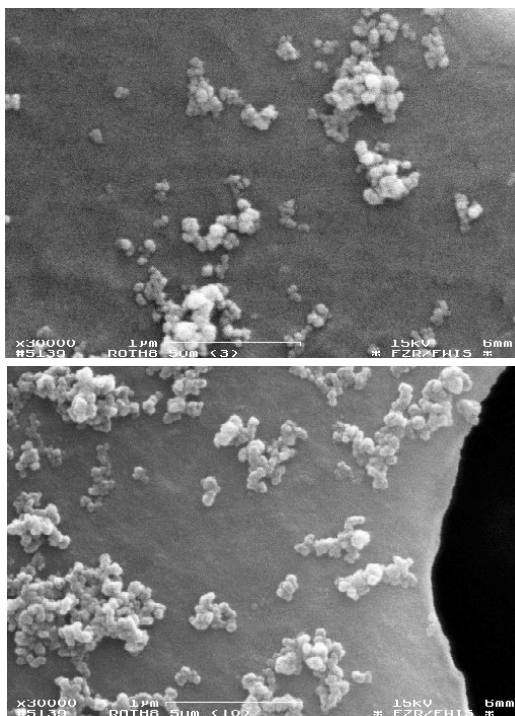


Fig. 2a/b: SEM micrograph of particles on a 5 μm Nuclepore filter. (a) triplicate rinsing; (b) tenfold rinsing

Conditions: Sample volume = 12 mL; coating with gold; magnification = 1 : 30,000, i.e. total length of the depicted filter membrane sections 3.75 μm .

References

- /1/ Buffle, J. et al., *Env. Sci. Techn.* **32**, 2887 (1998)
- /2/ Zänker, H. et al., *Radiochim. Acta* **88**, 619 (2000)
- /3/ Stumm, W.: *Chemistry of the Solid-Water Interface* Wiley, 1992, p. 282

DETECTION OF IRON COLLOIDS ON FILTER MEMBRANES AFTER WEATHERING OF AN IRON-RICH CHLORITE IN NEUTRAL PH-RANGE

E. Krawczyk-Bärsch, G. Hüttig, H. Zänker, T. Arnold, G. Bernhard

During the weathering of chlorite in aqueous solution of neutral pH range, colloids were formed as spherical particles of 30-80 nm in diameter. After centrifugal acceleration of the suspension the agglomerated particles were directly detected as Fe colloids by SEM/EDS investigations.

Introduction

Chlorite is one of the most abundant phyllosilicates, commonly found in sedimentary and low grade metamorphic rocks of the greenschist facies. The layered structure consists of regularly alternating talc and brucite like layers /1/, where a wide range of substitution of Fe, Mg and Al may occur in the octahedral layers. During weathering of chlorite in aqueous solution these elements are released. Dissolved ferrous iron oxidizes to ferric iron and forms insoluble Fe hydroxides or Fe carbonates. In previous investigations /2/ stable iron and aluminium hydroxide colloids were detected in a suspension of ground phyllite in which chlorite was one of the main mineralogical components.

Experimental

An iron-rich chlorite (ripidolith) from Flagstaff Hill (California, USA) was split into powder particles by freezing small chlorite samples with N₂ and subsequent heating at 40°C. Half a gram of chlorite (grain size 63-200 µm) was added to 40 mL of deionized water, which had previously been adjusted to an ionic strength of 0.1 M. The suspension was rotated end-over-end during the batch experiment for 2 months. No pH adjustment of the suspension was carried out. The final pH value of 7.04 was taken at the end of the experiment. The aqueous phase and the solid phase were separated by centrifugal acceleration (2500 x g, 1h and 3500 x g, 1h) in a Centricon T 124 high-speed centrifuge as described in [2]. A defined volume of the centrifugate was filtrated through a 50 nm Nuclepore filter in order to fix the ultrafine particles on a substrate. After washing the filter cake three times with MILLIQ-H₂O the filters were dried and prepared for scanning electron microscopy (SEM) and energy dispersive microanalysis (EDS) by sputtering the filters with gold and coating them with carbon.

Results and discussion

In SEM investigations colloids were imaged on the filter as spherical particles. They mainly formed agglomerates (Fig. 1); individual colloids were only rarely observed. The size of the spherical colloids ranged from 30 to 80 nm in diameter. EDS analyses were performed on several large agglomerates in order to obtain information about the chemistry of these colloids. Since the primary electronic beam is 2 µm in diameter, analyses of the small agglomerated colloids may partly be influenced by the electronic stimulation of their surroundings. However, some EDS analyses were successful. Fig. 2 shows an EDS spectrum in which only iron was detected. The detection of Fe colloids was described before in /2/, using a combined technique of centrifugation at varying centrifugal speed and ICP-MS/AAS of the centrifugates.

Fe colloids of a forming chlorite suspension were directly detected in our study at pH 7 by SEM/EDS.

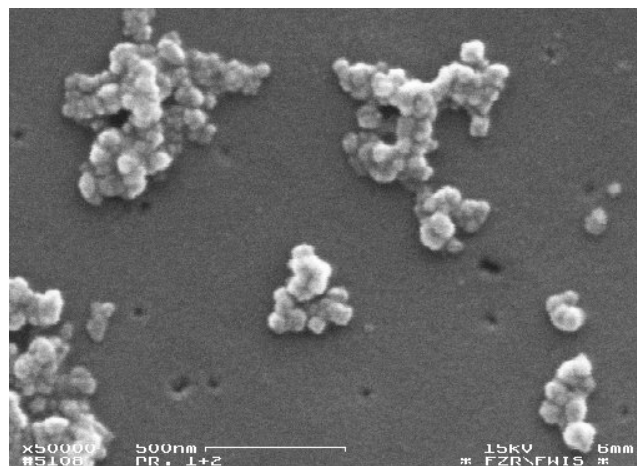


Fig. 1: Agglomerates of spherical colloids on a filter membrane. SEM-picture

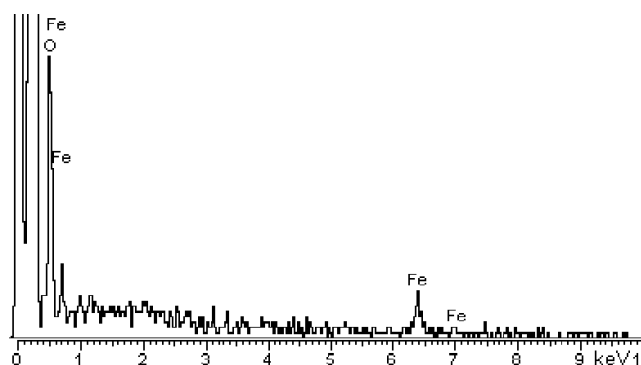


Fig. 2: EDS-spectrum of spherical iron colloids

In the acid region (pH < 4) the formation of Fe colloids was prevented because of the higher solubility of Fe in this pH region. With decreasing solubility in the neutral and alkaline media the released Fe precipitates and forms Fe colloids, mostly ferrihydrite particles /3/. Despite their small weight, these Fe colloids are highly significant for sorption experiments because of their huge specific surface area and have to be considered in sorption experiments

Acknowledgments

This work was supported by DFG(BE 2234/4-1). The authors wish to thank E. Christalle for the SEM and EDS investigations.

References

- /1/ Deer, W.A. et al., *An Introduction to the Rock Forming Minerals*. (1977)
- /2/ Zänker, H. et al., *Aquatic Geochemistry* (submitted).
- /3/ Arnold, T. et al., *Chemical Geology* **151**, 129 (1998)

URANIUM SORPTION ON IRON-RICH CHLORITE AND THE EFFECT OF HUMIC ACID

E. Krawczyk-Bärsch, T. Arnold, G. Bernhard

The sorption behavior of uranium on an iron-rich chlorite in the presence of humic acid differs from the sorption behavior investigated on sheet silicates, such as biotite and muscovite. The difference seems to depend on the formation of secondary iron minerals, such as ferrihydrite, which strongly influence the sorption of uranium in the presence of humic acid.

Introduction

Chlorite is a common accessory mineral commonly found in sedimentary and low-grade metamorphic rocks such as the phyllite in the former uranium mining area of Saxony (Germany). During the weathering of chlorite the main constituents of the octahedral sheets are leached out. Fe, for example, precipitates as secondary iron mineral coatings or forms iron colloids. In previous investigations the newly formed secondary iron mineral was described as ferrihydrite which significantly influences the sorption behavior of uranium on chlorite /1/. In the present study the effect of humic acid on the sorption behavior of uranium on an iron-rich chlorite is compared with the sorption behavior in the absence of HA due to the formation of secondary iron minerals.

Experimental

The batch sorption experiments were carried out in the same way as the experiments described in /2/ with the iron-rich Flagstaff Hill Chlorite from California. Half a gram of chlorite of a fraction size of 63-200 μm was added to 20 ml of 0.1 M NaClO_4 solution and altered for 24 h under atmospheric conditions before 18 ml of the solution was added. The final volume was adjusted to the desired pH value until the pH was stable. Then 2 ml of a humic acid ("Kleiner Kranichsee") stock solution and after 14 days an $\text{UO}_2(\text{ClO}_4)_2$ solution were added to achieve an initial humic acid (HA) concentration of 5 mg/L and an initial U(VI) concentration of 1×10^{-6} M. In batch experiments without HA the same U(VI) initial concentration was used.

Results and discussion

The results of the batch experiments for chlorite in the absence and in presence of HA are depicted in Fig. 1.

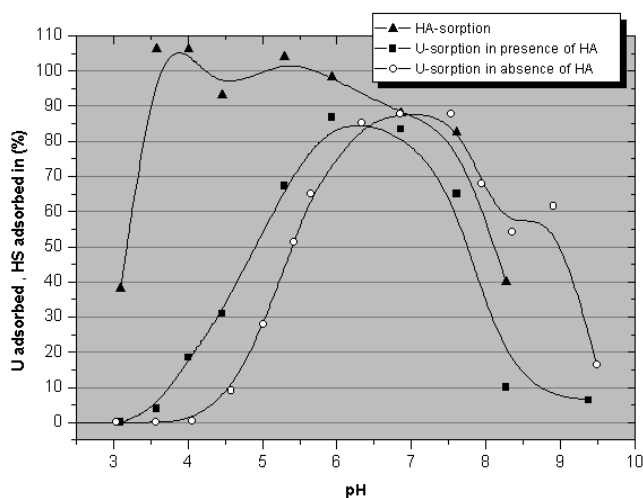


Fig. 1: U(VI) and HA uptake on chlorite.
Added: U(VI) = $1 \cdot 10^{-6}$ M; HA = 5 mg/L

In the absence of HA the sorption behavior of U(VI) on chlorite is similar to the sorption behavior on minerals studied in previous investigations. The sorption begins at pH values > 4.0 and takes place in the near neutral pH range. Chlorite has its sorption maximum at pH 6.8 with 88 %. Compared with biotite /3/ and muscovite /2/, U(VI) sorption on the iron-rich chlorite is the highest, followed by biotite. With increasing pH U(VI) sorption decreases but it is still active at pH 9.5 with 16,5 %. The sorption intensity of chlorite differs strongly from that of biotite and muscovite.

In the presence of HA the curve of U(VI) sorption on chlorite is similar to the curve obtained in the absence of HA. Only the beginning, the maximum and the end of U(VI) sorption are shifted towards lower pH values by about 0.5. The sorption maximum of 87% is reached at pH 6.0 and is as high as the maximum obtained in the absence of HA. In comparison with biotite and muscovite the sorption maxima are lower in the presence of HA.

Previous studies carried out on phyllite /1/ showed that the intensive sorption behavior of U(VI) on the iron-rich chlorite is due to the formation of secondary iron minerals, such as ferrihydrite, during the weathering process of chlorite. These iron minerals seem to be responsible for sorbing most of the U(VI) because of its large specific surface area.

In the presence of HA the U(VI) sorption on chlorite is lower than to the U(VI) sorption on biotite and muscovite when HA is present in the neutral pH range. This difference may be explained by the results of the kinetic studies carried out on ferrihydrite /4/. According to these results U(VI) sorption on ferrihydrite is slower when ferrihydrite is first coated with HA. In that case the sorbed HA probably blocks some major sorption sites of ferrihydrite, preventing the sorption of U(VI).

As the formation of secondary iron minerals during the weathering process of iron-rich chlorite is significant the sorption behavior of ferrihydrite has to be taken into account when interpreting the sorption behavior of U(VI) on chlorite in the presence of HA.

Acknowledgments

This work was supported by DFG (BE 2234/4-1). The authors wish to thank U. Schaefer for the ICP/MS analysis.

References

- /1/ Arnold, T. et al., Chemical Geology **151**, 129-141 (1998)
- /2/ Schmeide, K. et al., Radiochim. Acta **88**, 723-728 (2000).
- /3/ Krawczyk-Bärsch, E. et al., Report FZR **285** (2000) p.26
- /4/ Schmeide, K. et al. Report FZKA **6524** (2000) p.149-169

THE DISSOLUTION OF CHLORITE IN ACID pH-REGION

E. Krawczyk-Bärsch, T. Arnold, F. Brandt¹, D. Bosbach¹, G. Bernhard

¹ Institute of Mineralogy, University of Münster

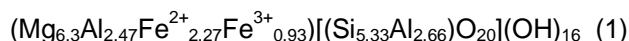
The dissolution of chlorite was studied in laboratory systems with flow-through reactor in the acid pH-region. The early stage of the dissolution of chlorite is highly non-stoichiometric with the highest release of the elements. A quasi linear release of the elements Mg, Al, Si and Fe is obtained after ten hours, indicating a steady-state kinetic.

Introduction

The migration of long-lived radionuclides from the geosphere to the biosphere depends on hydrogeological and chemical processes, including mineral dissolution. One of the important mineral is iron-rich chlorite, which is one of the main mineralogical components of phyllite. Chlorite contains ferrous and ferric iron, which may be leached out during weathering and form secondary iron hydroxides minerals, which do have a special sorption behavior of uranium [1]. In laboratory experiments the chlorite dissolution had been studied with a continuous flow-through reactor in the acid pH region. The received release rates of Fe, Si, Al and Mg may show the kinetics of chlorite dissolution.

Experimental

The chlorite used for the laboratory experiments was an iron-rich chlorite from Mangalapur (India). Electron microprobe, X-ray diffraction and Mössbauer investigations defined the chlorite composition and give the following chemical formula:



with an analyzed amount of FeO and Fe₂O₃ of about 13,3 % and 6,07 %. Chlorite is a 2:1 sheet silicate with an interlayer octahedral brucite sheet. The most octahedral cations are Mg, Fe²⁺, Fe³⁺ and Al. To prevent the destruction of the crystal faces, the mineral powder had to be prepared by freezing small fresh samples with N₂ and a subsequent heating (40°C). The flow-through experiments were carried out at room temperature, using a solution of known composition and a pH of 4. The solution was pumped at a specified rate through the reactor. Half a gram of the chlorite powder (grain size 63-200 μm) was kept between two membrane filters in the reactor. Reacted solution samples were taken for four days during the experiment. They were analyzed for Fe, Si, Al and Mg using ICP/MS (Inductively Coupled Plasma Mass Spectrometry). The pH of the reactor outflow and the temperature were recorded during the experiment.

Results and discussion

The analyses of the reacted solution samples were used to determine the dissolution rate DR (moles of element h⁻¹ s⁻²). The dissolution rate was calculated for Fe, Si, Al and Mg, using the following equation [2]:

$$DR = \frac{(\Delta ppm) \cdot V}{M_A \cdot r_A \cdot S} \quad (2)$$

where (Δppm) = concentration of element A in reacted solution sample - concentration of element A in blank solution, A = dissolved component (Fe, Si, Al and

Mg), V = flow rate (g h⁻¹), M_A = molecular weight of A, r_A = number of moles of A, and S = specific surface area of chlorite (m²/g).

Fig. 1 shows the dissolution rates calculated for each element. The highest release of the elements from the chlorite was observed during the first eight hours of the experiment. In this early stage the dissolution of chlorite is highly non-stoichiometric with a slow Fe and Al release and a fast Mg release.

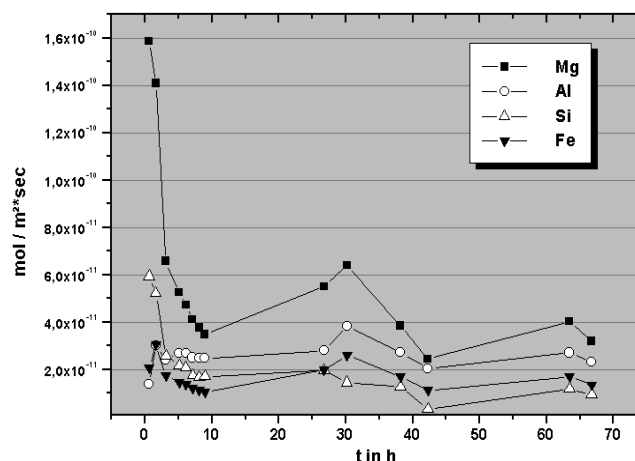


Fig. 1: Dissolution rate of chlorite calculated for each element and each reacted solution at pH 4.0.

After ten hours a quasi linear release is obtained, indicating equilibrium (steady-state), which may be due to steady-state kinetics and is expected for a surface-chemical-reaction-controlled dissolution mechanism [3]. The dissolution rates obtained for the elements at the end of the experiment will be proved by further dissolution runs. Finally, we will know, if the dissolution rate of chlorite will really slow and stabilize to steady-state kinetics or if it will remain incongruently.

Acknowledgments

This work was supported by DFG (BE 2234/4-1). The authors thank U. Schaefer for ICP/MS analysis.

References

- /1/ Arnold, T. et al., Chemical Geology **151**, 129 (1998)
- /2/ Knauss, K.G. et al., Geochim. Cosmochim. Acta **53**, 1493-1501 (1989)
- /3/ Malmström, M. et al., Journal of Contaminant Hydrology **21**, 201-213 (1996)

ADSORPTION OF HEXAVALENT URANIUM ONTO PHYLLITE AS A FUNCTION OF THE CALCIUM AND CARBONATE CONCENTRATION

L. Baraniak, S. Amayri, G. Bernhard

U(VI) adsorption from 10^{-6} M $UO_2(ClO_4)_2$ onto phyllite decreases from more than 98% to 30% if $[Ca^{2+}]$ increases from $2.5 \cdot 10^{-3}$ to $1.0 \cdot 10^{-2}$ M. The adsorption is not reduced in the presence of 0.1 M CO_3^{2-} . There is no U(VI) adsorption from mine water rich in Ca^{2+} , Mg^{2+} and CO_3^{2-} as it is the case in the flooded mines of the Erzgebirge Mountains (Germany).

Introduction

In a laboratory study of the adsorption of U(VI) onto *phyllite*, Arnold et al. /1/ found that more than 98% of uranium is strongly bound by surface complexation with superficial functional groups. In contrast no U(VI) is adsorbed onto *phyllite* from the water of the abandoned uranium mines in the Erzgebirge Mountains (Saxony) /2/. Major constituents of this mine water are: 448 mg/L Na^+ (0.02 M), 266 mg/L Mg^{2+} (0.011 M), 282 mg/L Ca^{2+} (0.007 M), 36.7 mg/L K^+ ($9.4 \cdot 10^{-4}$ M), 6.8 mg/L UO_2^{2+} ($2.5 \cdot 10^{-5}$ M), 1230 mg/L CO_3^{2-} (0.02 M) and 1960 mg/L SO_4^{2-} (0.02 M).

Experimental

Samples of crushed *phyllite* (0.5 g, 63-200 μm) from the Schlema mining site were pre-equilibrated over three weeks with aqueous solutions (40 mL 0.1 M $NaClO_4$), which contained increasing concentrations of $Ca(ClO_4)_2$ and $NaHCO_3$. A small amount of $UO_2(ClO_4)_2$ was added to produce an initial concentration of $1.0 \cdot 10^{-6}$ M UO_2^{2+} . The liquid phase was further spiked by a trace amount of ^{234}U to determine the adsorbed U(VI) by liquid scintillation counting (LSC). For three days the samples were gently agitated under inert gas at room temperature to establish the adsorption equilibrium. The final pH was 7.6 ± 0.1 . The U(VI) distribution ratio (R_d) was calculated from α -LS-counting of the ^{234}U activity concentration in the solution prior to and after equilibration. The measurements were performed with an LS-counter (Beckman), using a 3-mL aliquot of the liquid phase (percolated through a 0.2- μm Nalgene® filter) mixed with 4-mL Ready-Gel® scintillator in small LS vials. The percentage adsorption was the mean value of 5 determinations with an error of $\pm 0.5\%$.

Ca^{2+} [mol/L]	U(VI) adsorption [%]	R_d [mL/g]
$\leq 10^{-4}$	≥ 98	≥ 5266
$1.0 \cdot 10^{-4}$	98.2	4375 ± 1740
$1.0 \cdot 10^{-3}$	96.5	2211 ± 334
$5.0 \cdot 10^{-3}$	94.3	1327 ± 124
$1.0 \cdot 10^{-2}$	88.0	588 ± 29
$5.0 \cdot 10^{-2}$	55.3	99.2 ± 2.0
$1.0 \cdot 10^{-1}$	29.7	33.9 ± 0.8

Tab. 1: Uranium(VI) adsorption as a function of $[Ca^{2+}]$

Results

The U(VI) adsorption as a function of the concentration of Ca^{2+} shows (1) a small decrease of about 4% to $5.0 \cdot 10^{-3}$ M Ca^{2+} and (2) a strong decrease in ad-

sorption to 30% if the concentration of Ca^{2+} is increased up to 0.1 M (Table 1).

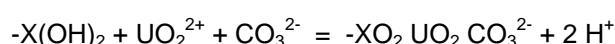
In the presence of carbonate in the liquid phase almost no influence on U(VI) adsorption was found. If the concentration of CO_3^{2-} was increased by 4 orders of magnitude (from $1.0 \cdot 10^{-5}$ M to 0.1 M), the loss in U(VI) adsorption was smaller than 1% (Table 2) and considering the error of $\pm 5\%$, this loss was completely insignificant.

CO_3^{2-} [mol/L]	U(VI) adsorption [%]	R_d [mL/g]
$\leq 10^{-5}$	≥ 98.5	≥ 5280
$1.0 \cdot 10^{-5}$	≥ 98.5	≥ 5280
$1.0 \cdot 10^{-4}$	98.3	4649
$1.0 \cdot 10^{-3}$	98.5	5280
$1.0 \cdot 10^{-2}$	97.9	3748
$1.0 \cdot 10^{-1}$	97.8	3574

Tab. 2: Uranium(VI) adsorption as a function of $[CO_3^{2-}]$

Conclusions

(1) The formation of the strong U(VI) carbonate complexes does not prevent U(VI) adsorption onto *phyllite*. This is in agreement with the adsorption mechanism proposed by Waite et al. /3/ according to which U(VI) can be bound as a carbonate complex onto rock and mineral surfaces:



(2) The decrease in U(VI) adsorption is accounted for by the competition between the two-valent cations for the surface binding sites, with UO_2^{2+} being bound strongly and Ca^{2+} much more weakly. A more than 10^4 -fold excess of Ca^{2+} is therefore required to desorb UO_2^{2+} from the *phyllite* surface ($[Ca^{2+}]/[UO_2^{2+}] = 10^{-2}/10^{-6}$). This is the case in the mine water and that is why UO_2^{2+} is not adsorbed at the huge *phyllite* surface, which is in contact with the water inside the flooded uranium mines.

References

- /1/ Arnold, T., Zorn, T., Bernhard, G., Nitsche, H., Chemical Geology **151**, 129-141 (1998)
- /2/ Baraniak, L., Bernhard, G., Nitsche, H., Report FZR-218 (1998) p. 6
- /3/ Waite, T.D. et al., Geochim. Cosmochim. Acta **58**, 5465-5478 (1994)

URANIUM(VI) ADSORPTION ONTO PHYLLITE AND GRANITE IN THE PRESENCE OF CALCIUM AND CARBONATE

S. Amayri, L. Baraniak, G. Bernhard

The adsorption of uranium(VI) onto phyllite and granite in the presence of Ca^{2+} and CO_3^{2-} was studied by batch experiments in the pH range from 6.0 to 12.0 at $I=0.1 \text{ M NaClO}_4$ and 25°C . The concentration of uranium was $1.0 \cdot 10^{-6} \text{ M}$ and that of Ca^{2+} and CO_3^{2-} $1.0 \cdot 10^{-3} \text{ M}$. We found that in addition to the well-known strong adsorption maximum between pH 5.5 and pH 7.0, adsorption is also evident in alkaline media at $\text{pH} \geq 10.0$.

Introduction

The adsorption of U(VI) onto the metamorphic rocks phyllite and granite of the Westerzgebirge (Saxony) is of interest for the restoration of former uranium mining sites. U(VI) adsorption onto phyllite and granite was studied by Arnold et al. /1/. They found that U(VI) is almost quantitatively adsorbed from pure U(VI) solution in micromolar concentration in the pH range of from 5.5 to 7.5 at $I=0.1 \text{ M NaClO}_4$.

Experimental

The metamorphic rocks of the Westerzgebirge are rich in calcite and dolomite and all natural waters are consequently highly mineralized by Ca^{2+} , Mg^{2+} , and CO_3^{2-} . We studied the U(VI) adsorption from $1.0 \cdot 10^{-6} \text{ M UO}_2(\text{ClO}_4)_2$ solutions containing two concentration levels of Ca^{2+} and CO_3^{2-} (10^{-6} and 10^{-3} M). To determine the adsorption we used batch experiments, taking 0.5 g solid and 40 mL solution. The U(VI) distribution was measured by applying ^{234}U tracer (120 Bq/sample) and by liquid scintillation counting of 4.78 MeV α particles in the liquid phase (after filtration through a 450 nm cellulose acetate membrane).

Results and Discussion

In the presence of $2.0 \cdot 10^{-6} \text{ M Ca}^{2+}$ and $3.0 \cdot 10^{-6} \text{ M CO}_3^{2-}$ we found almost equal degrees of U(VI) adsorption onto phyllite and granite ($\geq 90\%$) in the pH range from 5.5 to 8.0 (Fig. 1). Adsorption was from a solution containing $\text{UO}_2(\text{OH})_2(\text{aq})$ as the major species.

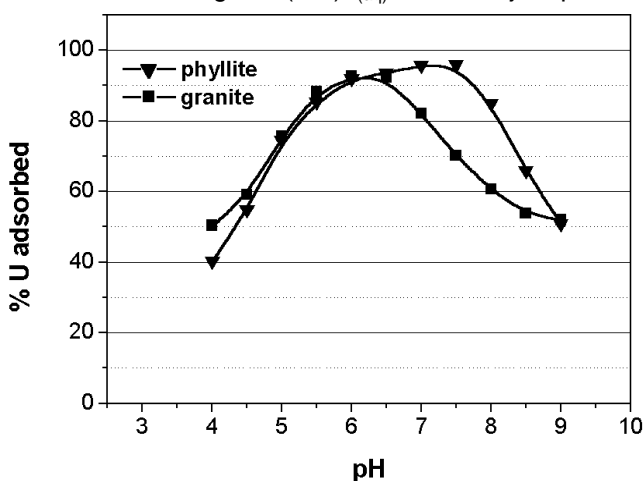


Fig. 1: U(VI) adsorption onto phyllite and granite from solutions of $2.0 \cdot 10^{-6} \text{ M Ca}^{2+}$ and $3.0 \cdot 10^{-6} \text{ M CO}_3^{2-}$

In further experiments we increased the concentration of Ca^{2+} and CO_3^{2-} to $1.0 \cdot 10^{-3} \text{ M}$. We found that above pH 7.0 adsorption decreased (onto phyllite to 50% and onto granite to 35%) and reached its minimum at pH 9.0. In this range the species $\text{UO}_2(\text{OH})_2(\text{aq})$ was unstable and about 75% of it are transferred to $\text{Ca}_2\text{UO}_2(\text{CO}_3)_3$. Then adsorption increased again to about 85% at pH 11 on both phyllite and granite (Fig.

2, Fig. 3) because in this pH range the species $\text{Ca}_2\text{UO}_2(\text{CO}_3)_3$ was converted into $\text{UO}_2(\text{OH})_3^-$. To assess the influence of Ca^{2+} and CO_3^{2-} on U(VI) adsorption, the adsorption from pure U(VI) solution, i.e., from Ca^{2+} and CO_3^{2-} free solution, was determined at $\text{pH} \geq 7.0$ (Fig. 2, Fig. 3).

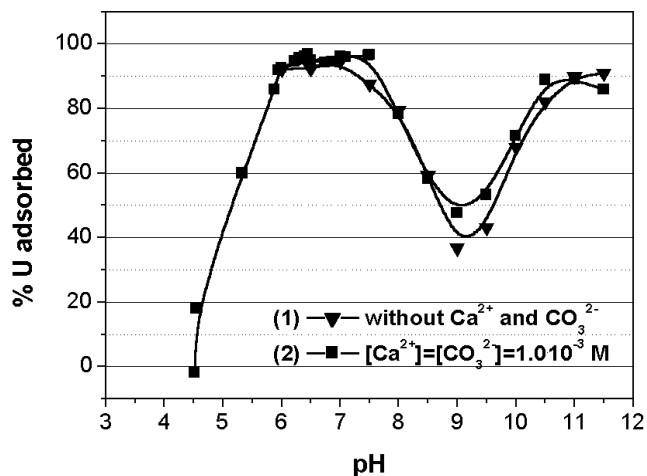


Fig. 2: U(VI) adsorption onto phyllite from solutions without (1) and with (2) Ca^{2+} and CO_3^{2-}

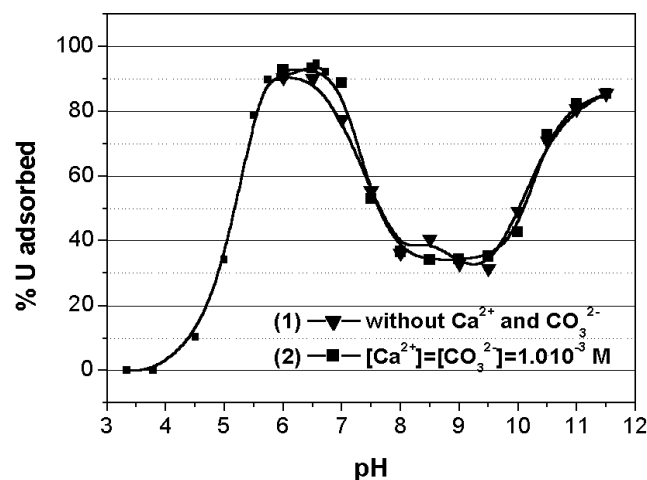


Fig. 3: U(VI) adsorption onto granite from solutions without (1) and with (2) Ca^{2+} and CO_3^{2-}

Conclusion

- (1) At concentrations below $1.0 \cdot 10^{-3} \text{ M}$, Ca^{2+} and CO_3^{2-} have no influence on U(VI) adsorption in the pH range from 6.0 to 12.0. Under these conditions U(VI) is strongly bound to the surface of the rocks.
- (2) Increasing adsorption takes place if U(VI) hydroxo complexes are formed (pH 5-6 and pH 9-12). The pH range of the adsorption minimum (pH 8-10) is dominated by the U(VI) carbonate species and the recently mentioned $\text{Ca}_2\text{UO}_2(\text{CO}_3)_2$ /2/.

References

- /1/ Arnold, T. et al., Chem. Geol. **151**, 129-141 (1998)
- /2/ Bernhard, G. et al., Radiochim. Acta, submitted

STUDYING THE SORPTION OF URANIUM(VI) ONTO MUSCOVITE BY ATOMIC RESOLUTION TRANSMISSION ELECTRON MICROSCOPY

T. Arnold, E. Krawczyk-Bärsch, G. Bernhard

Uranium sorbed onto muscovite was studied with High Resolution Transmission Electron Microscopy (HRTEM). Small uranium clusters, 5 -10 nm in size, were observed on the muscovite surface. Based on their diffraction pattern they were related to metallic uranium and schoepite.

Introduction

Surface complex formation constants are usually obtained by using a surface complexation model and optimizing the formation constants from experimental sorption data /1/. This is a pure modeling efforts and the sorbed surface species may or may not exist. To verify or to disregard such modeled surface species they have to be identified by appropriate techniques, e.g. EXAFS /2,3/. Because of its atomic resolution TEM seems to be a promising technique to directly detect sorbed surface species.

Experimental

Two muscovite samples were prepared by adding 0.5g of muscovite powder with the grain size fraction of <20 μm to 40 mL of deionized water. The pH of the suspension was adjusted to 6.3 - 6.5 and checked every day and if necessary readjusted with the appropriate acid or base until the pH was stable. Afterwards uranium was added to one sample to set the uranyl(VI) concentration to $5 \cdot 10^{-4}$ M. Uranium precipitation as schoepite could therefore not be excluded. The Blank sample and the uranium sample were then studied as a dry powder by High Resolution Transmission Electron Microscopy (HRTEM).

Results and discussion

It was found that the blank sample and the uranium sample showed differences. Small clusters were observed on the uranium sample which could not be seen on the blank sample, clearly indicating that the clusters have to be related to precipitated or sorbed uranium. The particles size of these clusters was approximately 5 to 10 nm in diameter. The clusters, however, were not recognizable at the beginning of the HRTEM measurement, but formed after a few seconds of electron irradiation. This observation was related to lateral diffusion with subsequent agglomeration and formation of larger particles which then were large enough to be detected by HRTEM. Furthermore, it seems very likely that that the sorbed and precipitated uranium undergoes a further change. The hydration sphere probably will be stripped off during the high vacuum or latest during the heavy electron bombardment on the sample surface. The electron bombardment may further change the sorbed uranium by reducing the uranium(VI) to uranium (IV) or even down to metallic uranium. Five clusters were also studied by selected area electron diffraction (SAED) patterns and compared to well known diffraction pattern of metallic uranium, various uranium minerals, and in addition, diffraction patterns of muscovite and some secondary minerals, which may have formed during sample preparation. The diffraction pattern of the five clusters are shown in Fig. 1.

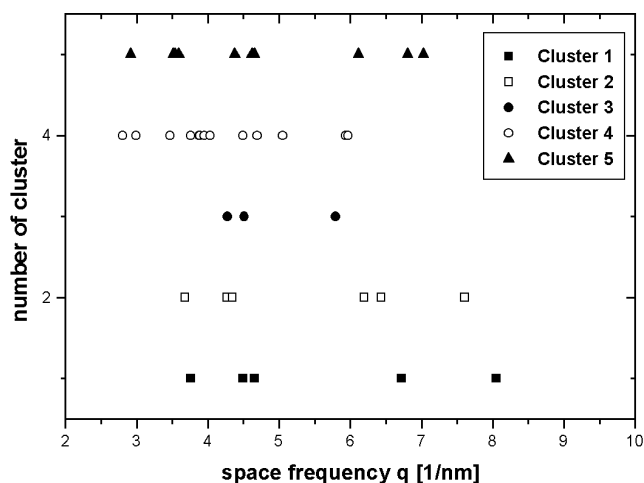


Fig. 1: Diffraction pattern of five uranium cluster sorbed to muscovite

It is obvious that these clusters do not show the same diffraction pattern indicating that these clusters may represent different mineralogies. The diffraction patterns seem to best match diffraction pattern of metallic uranium, schoepite, and muscovite. However, at present the results are not unequivocal and further TEM investigations have to be performed.

Acknowledgment

HRTEM was carried at the "Institute für Angewandte Physik und Didaktik der Physik" at the Technical University Dresden by H. Lichte. The studies were funded by the Deutsche Forschungsgemeinschaft (DFG) under the project number Ni 210/6-2.

References

- /1/ Arnold, T. et al., Journal of Contaminant Hydrology **47**, 219-231 (2001)
- /2/ Reich, T. et al., J. Elec. Spec. Rel. Phe. **96**, 237-243 (1998)
- /3/ Moyes, L. et al., Environ. Sci. & Technol. **34**, 1062-1068 (2000)

TIME-RESOLVED LASER FLUORESCENCE SPECTROSCOPY (TRLFS) STUDY OF THE SORPTION OF CURIUM(III) ONTO SMECTITE AND KAOLINITE

Th. Stumpf, A. Bauer¹, F. Choppin², J.I. Kim¹

¹Forschungszentrum Karlsruhe, Institut für Nukleare Entsorgung, D-76021 Karlsruhe, Germany

²Univ. Paul Sabatier, UMR 5563-LMTG, 38 rue des 36-Ponts, F-31400 Toulouse, France

The surface sorption process of Cm(III) onto smectite and kaolinite was investigated by TRLFS in the trace concentration range. At low pH Cm(III) is sorbed as an outer-sphere complex and retains its complete primary hydration sphere. With increasing pH, inner-sphere adsorption onto kaolinite and smectite occurs via the aluminol edge sites [1].

Sorption to mineral surfaces is a major process controlling the concentration, mobility and bioavailability of radionuclides in nature. Oxide and clay minerals are the main constituents in groundwater and soil systems responsible for metal ion sorption. For the case that actinides in a nuclear waste repository are set free, clays as back-fill material will be the technical barrier for their spreading. Consequently it is essential for the long-term performance assessment of nuclear waste repositories to know about the interactions of actinide ions with clay minerals. Therefore it is necessary to identify the surface species that are formed during the sorption process. For this purpose, the speciation of surface sorbed metal ions was studied by time-resolved laser fluorescence spectroscopy (TRLFS) in the nanomolar concentration range, as a function of pH, at low ionic strength. The high fluorescence spectroscopic sensitivity of curium enables studying the complexation process of Cm(III) onto kaolinite and smectite as a model ion for the surface sorption behavior of trivalent actinides. The evolution of the fluorescence emission spectra of $3 \cdot 10^{-7}$ mol/L Cm(III) with 0.25 g/L smectite in aqueous suspension at various pH is shown in Fig. 1.

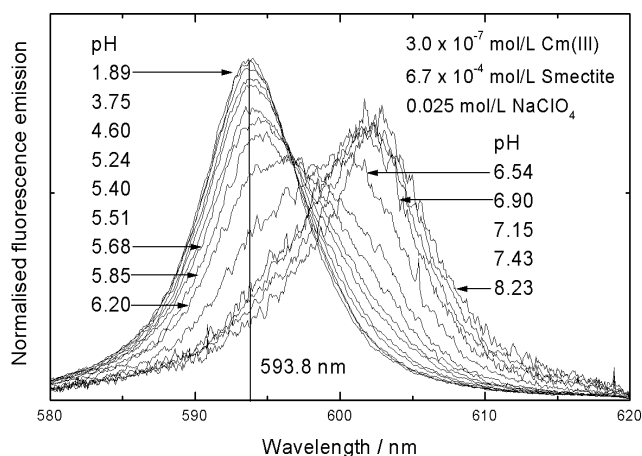


Fig. 1: Fluorescence emission spectra of Cm(III) in aqueous smectite suspension at various pH; spectra are scaled to the same peak area.

At $pH \leq 4.6$ only the signal of the Cm(III) aquo ion is detected. At $pH \geq 5.24$, the intensity of the 593.8 nm peak decreases and two other peaks appear with maxima at 598.8 nm ($pH \geq 5.24$) and 603.3 nm (for $pH \geq 7.15$). Comparable evolution is observed for the kaolinite suspension. It is remarkable that, in case of smectite and kaolinite, the spectra of the sorbed Cm(III) species at low pH (≤ 5) show no difference to spectra of the Cm(III) aquo ion. This observation indicates that at pH values ≤ 5 the sorbed Cm(III) ion retains its hydration sphere. Such a sorption process

suggests outer-sphere complex formation on the interlayer sites.

The red shift of the fluorescence emission of Cm(III) at higher pH (> 5) in the smectite suspension is caused by a change in the ligand field of the Cm(III) ion and indicates inner-sphere complex formation. A peak deconvolution was carried out to resolve the individual species from the composite fluorescence emission spectra at $pH \geq 5$. Three different species have been identified. In addition to the Cm(III) aquo ion, two different inner-sphere Cm(III) surface complexes are formed. All measured spectra have been deconvoluted using pure component spectra with peak maxima at 598.8 nm and 603.3 nm. The results are illustrated in Fig. 2.

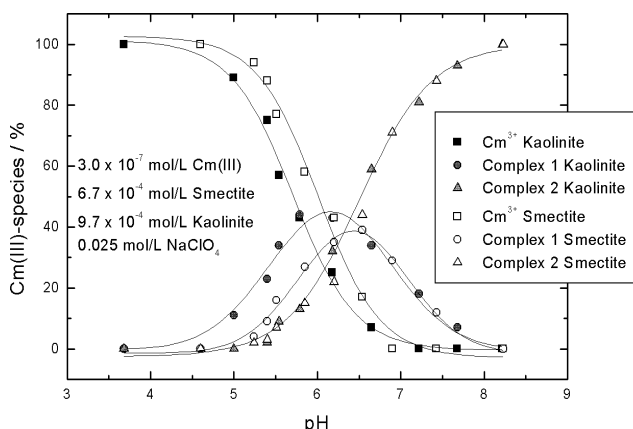


Fig. 2: Speciation plot of the Cm(III)/clay system.

The similarity of spectra of sorbed curium at $pH > 8.2$ measured in $\gamma\text{-Al}_2\text{O}_3$ [2] and clay suspensions and their difference from the spectrum of sorbed Cm(III) in silica [3] suspension suggest that inner-sphere complexation occurs via the aluminol sites. The fluorescence emission lifetime of Cm(III) in the clay suspensions at various pH was determined. In both cases at $pH \leq 5$, the number of water molecules in the first co-ordination shell of the Cm(III) was found to be 9. This proves that the outer-sphere complex has not only the same fluorescence emission spectrum as the Cm(III) aquo ion, but also the same number of water molecules in the first co-ordination shell of curium. The fluorescence lifetimes of the formed kaolinite, smectite and γ -alumina inner-sphere complexes are very similar. The lifetime of $110 \pm 7 \mu\text{s}$ corresponds to five water molecules in the first co-ordination shell of the sorbed Cm(III).

References

- 1/ Stumpf, T. et al., Environ. Sci. Technol., submitted
- 2/ Stumpf, T. et al., this report p.30
- 3/ Chung, K. H. et al., Radiochim. Acta **82**, 215-219 (1998)

SORPTION OF CURIUM(III) ONTO γ -ALUMINA - A TRLFS STUDY

Th. Stumpf, Th. Rabung¹, R. Klenze¹, H. Geckeis¹, J.I. Kim¹

¹Forschungszentrum Karlsruhe, Institut für Nukleare Entsorgung, D-76021 Karlsruhe

The sorption process of Cm(III) onto γ -Al₂O₃ is structurally investigated at the trace concentration range by using time-resolved laser fluorescence spectroscopy (TRLFS). For the Cm(III)-alumina system, just one surface site for metal ion sorption could be found; however, two different surface complexes exist, depending on pH /1/.

For the long-term performance assessment of nuclear waste repositories, knowledge concerning the interactions of actinide ions with mineral surfaces is imperative. The mobility of released radionuclides is strongly dependent on the sorption/desorption processes at mineral surfaces. Therefore, it is necessary to characterise the surface species formed and to elucidate the reaction mechanisms involved. Insight into the sorption mechanisms and identification of surface species is of cardinal importance for a reliable predictive modeling of sorption reactions. Time-resolved laser fluorescence spectroscopy (TRLFS) allows due to its high fluorescence yield speciation studies of Cm(III) in the nanomolar concentration range.

Fluorescence emission spectra of $2.7 \cdot 10^{-7}$ mol/L Cm(III) in 0.6 g/L γ -alumina suspension, recorded at pH values ranging from 4.4 to 9.6, are shown in Fig. 1 together with the spectrum for pure Cm(III) solution at pH 2. The emission band with a peak maximum at 593.8 nm corresponds to the Cm³⁺ aquo ion. With increasing pH, the intensity of this peak decreases and two other red-shifted peak maxima appear at 601.2 nm (starting at pH 4.93) and 603.3 nm (for pH ≥ 7) indicating inner-sphere complex formation. These two peaks are ascribed to curium species sorbed onto the alumina surface.

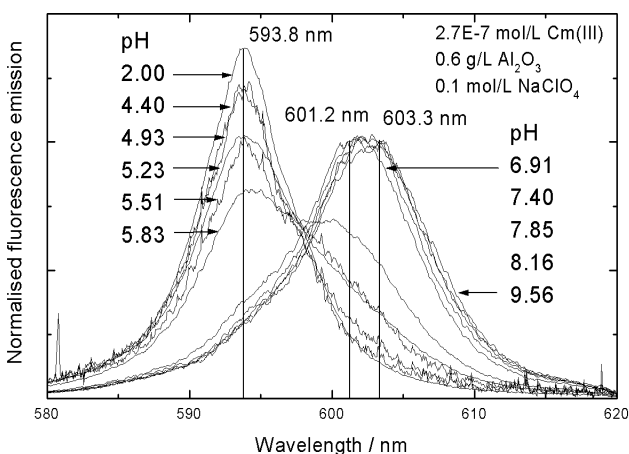


Fig. 1: Fluorescence emission spectra of Cm(III) in aqueous alumina suspension at various pH; spectra are scaled to the same peak area.

Fluorescence decay rates are caused by radiative and non-radiative processes. For the ${}^6D_{7/2} \rightarrow {}^8S_{7/2}$ transition of Cm(III) in 1 M HClO₄, the decay rate is calculated to be 770 s^{-1} this corresponds to a radiative lifetime (reciprocal decay rate) of 1.3 ms. Non-radiative decay is mainly due to energy transfer from the excited state to ligand vibronics, e.g., OH vibration of coordinated H₂O or OH⁻ molecules. A linear correlation between the decay rate and the number of H₂O molecules in the first co-ordination shell of Cm(III)

complexes exists /2/. A lifetime of 68 μs , determined for the Cm(III) aquo ion, corresponds to 9 water molecules and a value of 1.3 ms corresponds to zero H₂O molecules in the first co-ordination shell of Cm(III). In Fig. 2 the time dependency of the emission decay of Cm(III) in alumina suspension at pH 4, 5 and 7.67 is shown. For the Cm(III) fluorescence emission at pH 7.67 a lifetime of 110 μs is obtained, corresponding to 5 water molecules in the Cm(III) first co-ordination shell. This observation is confirmed by measurement of the fluorescence lifetime at pH 5 which exhibits bi-exponential decay. This finding indicates that the lifetime of the excited state of Cm(III) is shorter than the exchange kinetic between the Cm³⁺ aquo ion and the surface complex species. The decay for spectra at pH 7.67, where only the two Cm(III) surface species with emission peak maxima at 601.2 nm and 603.3 nm are present, is mono-exponential. For spectra recorded at a pH of 9.63 where the second Cm(III) surface complex predominates, also a lifetime of 110 μs is obtained.

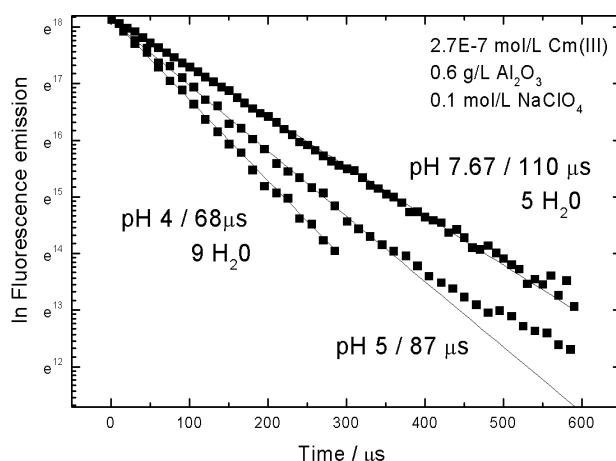


Fig. 2: Time dependency of emission decay of Cm(III) in aqueous alumina suspension at various pH.

Further studies show that the second Cm(III)/alumina complex is a hydrolyzed surface species, with one H₂O substituted by a hydroxyl group. Both Cm(III) surface species are not imbedded into the bulk alumina structure, unlike results obtained from investigations of Cm(III) sorption at the silica surface /3/. Apparently, there is a fundamental difference in the processes occurring at the solid/water interface during sorption of Cm(III) in these two model systems.

References

- /1/ Stumpf, T. et al., J. Colloid Interface Sci., accepted
- /2/ Kimura, T. et al., J. Alloys Comp. **213/214**, 313-317 (1994)
- /3/ Chung, K. H. et al., Radiochim. Acta **82**, 215-219 (1998)

SYNTHESIS OF ^{14}C -LABELED AND UNLABELED HUMIC ACID TYPE M42

S. Pompe, M. Bubner, M. Meyer, R. Nicolai, K.H. Heise, G. Bernhard

Unlabeled and ^{14}C -labeled synthetic humic acids type M42 were synthesized as model substances for complexation and migration studies. The humic acids were characterized regarding their structure and functionality.

Introduction

In order to get a more profound knowledge about the influence of humic acids on the speciation of metal ions in the environment we developed different well-defined humic acid model substances, e.g., humic acid type M1 and type M42 according to the melanoidin concept /1/. In addition, we developed methods for the synthesis of ^{14}C -labeled humic acids with stable labeling in the molecular structure /2/. Due to the fact that these humic acids can be quantified in very low concentrations they can be used in migration experiments, e.g., to study kinetic processes /3/. In the present study we synthesized humic acid type M42 which has a carboxyl group content comparable to natural humic acids as well as ^{14}C -labeled humic acid type M42 (^{14}C]M42) for the use in complexation and migration experiments. Both humic acids were characterized regarding their structure and functionality.

Experimental

The basic synthesis of humic acid type M42 is described in detail in /1/. It starts from a mixture of 22 g glutamic acid monohydrate, 33 g xylose and 60 mL water which is heated for 92 hours at 80 ± 2 °C under reflux and inert gas. During the reaction a dark-brown solid and solution are formed. The humic acid-like fraction of the reaction product is extracted from the solid with NaOH under inert gas. The humic acid is precipitated from the alkaline solution with HCl, washed, dialyzed, and lyophilized. For the synthesis of 52 g humic acid seven synthesis sequences, each with six basic batches, were necessary. ^{14}C]M42 is synthesized according to humic acid type M42, however, by addition of [^{14}C]glutamic acid to the precursor substances. We synthesized 0.9 g humic acid ^{14}C]M42 with a specific radioactivity of 2.38 MBq/g which represents a ^{14}C -yield of 2 % (starting activity: 3 mCi [^{14}C]glutamic acid). Evaluating this radiochemical yield it has to be taken into account that the humic acid-like fraction of the reaction product is small compared to the other fractions that are formed during the synthesis, e.g., the humin- and fulvic acid-like fraction.

Proton exchange capacity (PEC) and carboxyl group content of both humic acids were determined by direct titration and calcium acetate exchange /4/, respectively. The structure was studied by FTIR spectroscopy.

Results and discussion

Fig. 1 shows the FTIR spectra of both humic acids. The comparison of the spectra regarding the position of the IR absorption bands and the band intensities shows that both spectra are nearly identical. Thus, it can be concluded that humic acid type M42 and ^{14}C]M42 show a comparable structure as expected. Tab. 1 summarizes the carboxyl group content and PEC of both humic acids. Under consideration of the experimental error the corresponding data agree very

well with each other. Humic acid type M42 and ^{14}C]M42 show a carboxyl group content that is comparable to most natural humic acids, e.g., comparable to Aldrich humic acid which has 4.41 ± 0.11 meq/g carboxyl groups /1/.

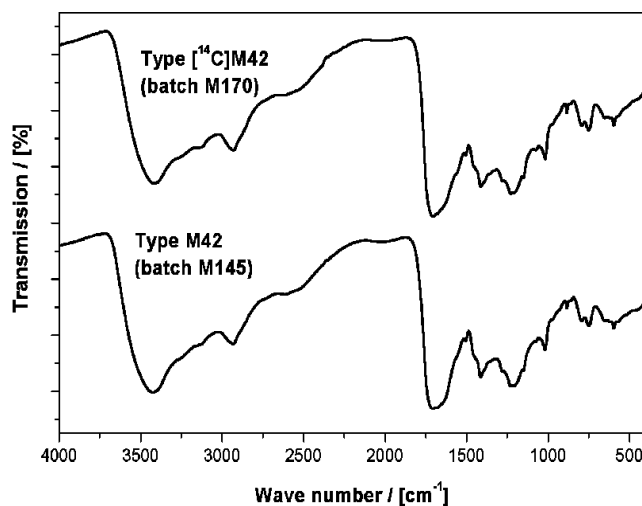


Fig. 1: FTIR spectra of the ^{14}C -labeled and unlabeled synthetic humic acid type M42. The spectra are shifted along the y-axis for clarity.

Humic Acid	COOH (meq/g)	PEC ^a (meq/g)
Type M42 (batch M145)	3.76 ± 0.09	3.51 ± 0.07
Type ^{14}C]M42 (batch M170)	3.63 ± 0.02	3.55 ± 0.05

^aPEC: Proton exchange capacity.

Tab. 1: Functional group content of synthetic humic acid type M42 and ^{14}C]M42.

From the obtained results it can be concluded that both humic acids agree very well in structure, PEC and carboxyl group content. In spite of the different batch sizes used for preparation of humic acid type M42 and ^{14}C]M42 the synthesis is reproducible regarding the humic acid properties. The high reproducibility offers the possibility to synthesize comparable ^{14}C -labeled and unlabeled humic acid model substances for the use in migration and complexation experiments.

Acknowledgment

This work was supported by BMWi under contract number 02E9299.

References

- /1/ Pompe, S. et al., Report FZR-290 (2000) p.29
- /2/ Bubner, M. et al., J. Labeled Compd. Radiopharm. **XLI**, 1057 (1998)
- /3/ Schmeide, K. et al., Report FZKA 6524 (2000) p. 149
- /4/ Schnitzer, M. et al., *Humic substances in the environment*. New York 1972

REDOX EQUILIBRIA IN NATURAL AQUATIC SYSTEMS CAUSED BY DECOMPOSITION OF ORGANIC MATTER

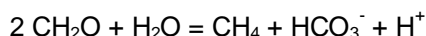
A. Abraham, L. Baraniak, G. Bernhard

The free standard enthalpy (G^0) as a sum parameter for dissolved organic matter (DOM) is derived from the point of co-existence of the species HCO_3^- , CO_3^{2-} , DOM and $\text{CH}_{4(\text{aq})}$ in the Eh-pH diagram of the system C-O-H. Using this G^0 the redox potential in environmental waters can be calculated from the content of DOM, carbonate and methane.

Introduction

The anoxic, microbially mediated degradation of dissolved organic matter (DOM) generates reducing environments in natural aquatic systems /1/. DOM in environmental waters consists for the most part of wood and plant decomposition products (carbohydrates, $(\text{CH}_2\text{O})_n$) and humic acids. The redox milieu arises from the disproportionation of organic carbon into methane and carbon dioxide.

The following equation describes this phenomenon:



The redox potential (Eh) caused by this process can be calculated from the methane content of the bog gas and the carbonate concentration in the corresponding water layer according to



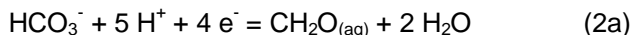
with $\lg K_a = 27,887$ and

$$p\varepsilon = 1/8 \lg[\text{HCO}_3^-] - 1/8 \lg[\text{CH}_{4(\text{aq})}] - 9/8 \text{pH} - 1/8 \lg K_a$$

In order to include the DOM content in the calculation of Eh, we determined K_a for the processes:



$$\lg K_{a(1)} = \lg[\text{CH}_{4(\text{aq})}] - \lg[\text{CH}_2\text{O}] + 4 \text{pH} + 4 p\varepsilon \quad (1b)$$



$$\lg K_{a(1)} = \lg[\text{CH}_2\text{O}] - \lg[\text{HCO}_3^-] - 5 \text{pH} + 4 p\varepsilon \quad (2b)$$



$$\lg K_{a(2)} = \lg[\text{CH}_2\text{O}] - \lg[\text{CO}_3^{2-}] - 6 \text{pH} + 4 p\varepsilon \quad (3b)$$

Thermodynamic reflections

Gibbs free energy G^0 of DOM is required for K_a calculation as a sum parameter that reflects all the dissolved organic compounds. We derived G^0 from the Eh-pH diagram of the C-O-H system which was calculated using the G^0 values of Wagman et al. /2/. In this diagram we find that at the point with the coordinates

$$\text{pH} = 10.35 \text{ and } p\varepsilon = -8.159 \text{ (Eh} = -0.4827 \text{ V)}$$

the species $\text{CH}_{4(\text{aq})}$, HCO_3^- , CO_3^{2-} and CH_2O (DOM) are in co-existence, i.e. this point (P1) represents the inter-section of the Eh-pH boundaries of the species HCO_3^- , CO_3^{2-} , DOM and $\text{CH}_{4(\text{aq})}$ (equilibria $\text{HCO}_3^-/\text{DOM}$, $\text{DOM}/\text{CH}_{4(\text{aq})}$, $\text{HCO}_3^-/\text{CO}_3^{2-}$ and $\text{CO}_3^{2-}/\text{CH}_{4(\text{aq})}$) (Fig. 1).

The equilibrium constants of reactions 1a to 3a can be calculated by applying Eqs. 1b to 3b for P1 on the condition that $[\text{CH}_{4(\text{aq})}]$ is equal to $[\text{CH}_2\text{O}]$ and that $[\text{HCO}_3^-]$ and $[\text{CO}_3^{2-}]$ are equal to $[\text{CH}_2\text{O}]$. Gibbs free energy G^0 of DOM then results from

$$\Delta_R G^0_{(1)} = -2.303 \text{ RT } \lg K_{a(1)}$$

$$G^0_{\text{DOM}} = G^0_{\text{CH}_{4(\text{aq})}} + G^0_{\text{H}_2\text{O}} - \Delta_R G^0_{(1)}$$

Results

The $\lg K_a$ values for the reduction and oxidation of DOM (Eqs. 1a to 3a) amount to 8.764, 19.11 and 29.46 (Tab. 1). As the mean value for the free standard enthalpy of dissolved organic matter we found:

$$G^0 = -221.6 \pm 1.1 \text{ kJ/mol } (-52.96 \pm 0.26 \text{ kcal/mol})$$

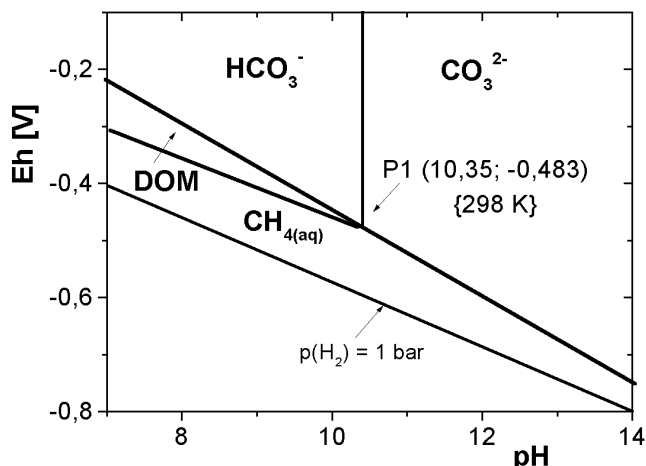


Fig. 1: Intersection of Eh-pH boundaries of the species HCO_3^- , CO_3^{2-} , DOM and $\text{CH}_{4(\text{aq})}$, according to /3/

The G^0_{DOM} derived is correct because (1) the boundaries of the DOM stability field are exactly reflected and (2) in our field experiments we found the same redox potentials from the carbonate-methane ratio and the ratios including the DOM content.

Redox-Equilibrium	$\lg K_a$	G^0_{DOM} [kJ/mol]
DOM / $\text{CH}_{4(\text{aq})}$	8.764	-221.56
HCO_3^- / DOM	19.114	-221.51
CO_3^{2-} / DOM	29.464	-221.67

Tab. 1: Equilibrium constant for the reduction of DOM to methane and the oxidation of DOM to carbonate and the resulting free standard enthalpy for DOM

References

- /1/ Baraniak, L., Abraham, A., Bernhard, G., Report FZR-285 (2000) p. 38
- /2/ Wagman, D.D. et al., J. Phys. Chem. Ref. Data 11, Suppl. 2 (1965) p. 392
- /3/ Brookins, D.G., Eh-pH Diagrams for Geochemistry, Springer-Verlag, 1988, p. 35

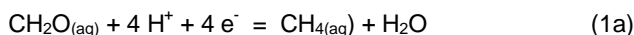
REDOX EQUILIBRIA IN NATURAL AQUATIC SYSTEMS INCLUDING DISSOLVED ORGANIC MATTER

A. Abraham, L. Baraniak, G. Bernhard

The equilibrium constants of redox reactions involving dissolved organic matter (DOM) were calculated for temperatures other than 298 K from the shift of the boundary intersection point of the species $\text{CH}_{4(\text{aq})}$, HCO_3^- , CO_3^{2-} and DOM in the Eh-pH diagram as a function of the temperature difference.

Introduction

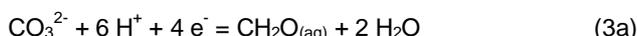
The equilibrium constants of redox reactions involving dissolved organic matter (mainly carbo-hydrates $\text{CH}_2\text{O}_{(\text{aq})}$) can be calculated from Gibbs free energy of the reactants. They are therefore valid under standard conditions, i.e. at 298 K. For the following equilibria we found:



$$\lg K_{a,1} = \lg[\text{CH}_{4(\text{aq})}] - \lg[\text{CH}_2\text{O}] + 4 \text{pH} + 4 \text{p}\varepsilon = 8.764 \quad (1\text{b})$$



$$\lg K_{a,1} = \lg[\text{CH}_2\text{O}] - \lg[\text{HCO}_3^-] - 5 \text{pH} + 4 \text{p}\varepsilon = 19.11 \quad (2\text{b})$$



$$\lg K_{a,2} = \lg[\text{CH}_2\text{O}] - \lg[\text{CO}_3^{2-}] - 6 \text{pH} + 4 \text{p}\varepsilon = 29.46 \quad (3\text{b})$$

Using these equilibria for characterization of redox conditions in environmental studies, we have to recalculate the equilibrium constants for the specific site temperature. That is usually done by applying van't Hoff reaction isobar. But in our case the reaction enthalpy is un-known. A way out was found by determining the point of co-existence of $\text{CH}_{4(\text{aq})}$, HCO_3^- , CO_3^{2-} and CH_2O (DOM) in the Eh-pH diagram for the temperature under review. Using the coordinates of this point, the equilibrium constants for the reactions involving DOM can be calculated as demonstrated in the preceding article.

Thermodynamic reflections

The point of co-existence of the species $\text{CH}_{4(\text{aq})}$, HCO_3^- , CO_3^{2-} and DOM at a temperature other than 298 K was found from the pH dependence of Eh on the stability field boundaries between $\text{CH}_{4(\text{aq})}$ and HCO_3^- and between $\text{CH}_{4(\text{aq})}$ and CO_3^{2-} (Fig. 1). This is possible because the reaction enthalpies are well known and the equilibrium constants can therefore be calculated for any temperature (Tab.1).

	Redox-reaction	$\Delta_R G^0$ [kJ/mol]	$\Delta_R H^0$ [kJ/mol]	$\lg K_a$ ^{1) 298 K} ^{2) 277 K}
1	$\text{HCO}_3^- / \text{CH}_{4(\text{aq})}$	-159.13	-254.53	27.887 ¹⁾ 35.675 ²⁾
2	$\text{CO}_3^{2-} / \text{CH}_{4(\text{aq})}$	-218.03	-269.43	38.209 46.453
3	$\text{H}_2\text{CO}_{3(\text{aq})} / \text{CH}_{4(\text{aq})}$	-122.73	-246.93	21.508 24.789

Tab. 1: Characterization of the carbonate-methane equilibria

Results

In our case, i.e. for a temperature of 277 K, we found the point of co-existence from the intersection of the $\text{p}\varepsilon$ -pH dependence of the carbonate-methane boundaries according to:

$$(1) \text{p}\varepsilon = 1/8 \lg K_{a,1} - 9/8 \text{pH}$$

in the case of $\text{HCO}_3^- + 9 \text{H}^+ + 8 \text{e}^- = \text{CH}_{4(\text{aq})} + 3 \text{H}_2$ and

$$(2) \text{p}\varepsilon = 1/8 \lg K_{a,2} - 10/8 \text{pH}$$

in the case of $\text{CO}_3^{2-} + 10 \text{H}^+ + 8 \text{e}^- = \text{CH}_{4(\text{aq})} + 3 \text{H}_2\text{O}$.

The coordinates of this point of co-existence are:

$$\text{pH} = 10.79 \text{ and } \text{p}\varepsilon = -7.666 \text{ (Eh} = -0.4215 \text{ V).}$$

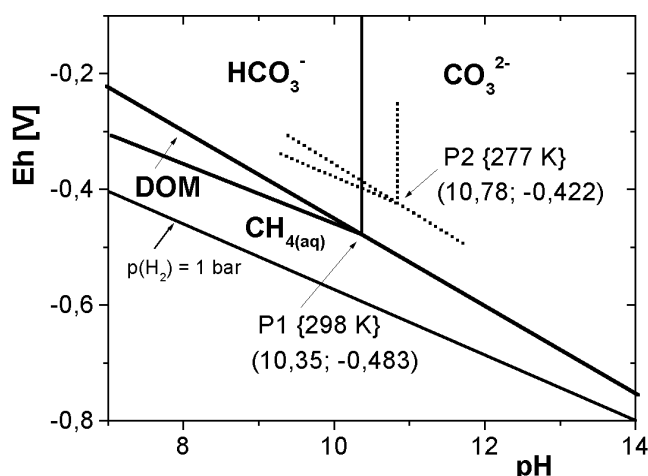


Fig. 1: Intersection of Eh-pH boundaries of the species HCO_3^- , CO_3^{2-} , DOM and $\text{CH}_{4(\text{aq})}$ at 298 K and 277 K

Now the equilibrium constants of reactions 1a to 3a can be calculated by inserting pH and $\text{p}\varepsilon$ of P2 into Eqs. 1b to 3b on the condition that $[\text{CH}_{4(\text{aq})}]$ is equal to $[\text{CH}_2\text{O}]$ and that $[\text{HCO}_3^-]$ and $[\text{CO}_3^{2-}]$ are equal to $[\text{CH}_2\text{O}]$. The results for $\lg K_{a(1-3)}$ for 277 K in comparison with 298 K are given in Tab. 2. In case that H_2CO_3 is involved in the redox reaction (at pH 6.2) according to



$$\lg K_{a,4} = \lg[\text{CH}_2\text{O}] - \lg[\text{H}_2\text{CO}_{3(\text{aq})}] - 4 \text{pH} + 4 \text{p}\varepsilon \quad (4\text{b})$$

the equilibrium constant was calculated as the difference of the reactions H_2CO_3 to $\text{CH}_{4(\text{aq})}$ (3 in Tab. 1) and DOM to $\text{CH}_{4(\text{aq})}$ (1a) with the result of $\lg K_{a,4} = 12.341$ (Tab. 2).

	Redox-equilibrium	$\lg K_a$ (298 K)	$\lg K_a$ (277 K)
1	DOM / $\text{CH}_{4(\text{aq})}$	8.764	12.448
2	HCO_3^- / DOM	19.114	23.226
3	CO_3^{2-} / DOM	29.464	34.004
4	H_2CO_3 / DOM	12.744	12.341

Tab. 2: Equilibrium constants for the reduction of DOM to methane and the oxidation of DOM to carbonate at 298 K and 277 K

**Interaction of Actinides/Radionuclides
with Biological Systems**

COMPARISON OF THE STRUCTURES OF THE NATURAL BACTERIAL COMMUNITIES IN ONE URANIUM MINING WASTE PILE AND IN ONE URANIUM MILL TAILINGS

K. Flemming, G. Satschanska, S. Selenska-Pobell

Significant differences were found in the structures of the bacterial communities in soil samples collected from one uranium mining waste pile and from one uranium mill tailings. Both environments, however, share populations which are highly related to *Pseudomonas migulae* and to *Acidithiobacillus ferrooxidans*.

Composition of the natural bacterial communities was studied in soil samples collected from one uranium mining depository site, namely the "Haberland Pile" situated near the town of Johanngeorgenstadt (JG) and from one uranium mill-tailings, Gittersee / Co-schütz (Gitt2), near the town of Dresden. For this the 16S rDNA retrieval was applied. The JG samples were collected from two sites of the pile, one possessing the highest concentrations of uranium and other toxic metals (JG36, 2 to 3 m below the land surface) and the second one which was less polluted (JG30, 4 to 5 m below the surface). The Gitt2 samples were collected from a highly contaminated coal-like part of the tailings at depths between 2 and 3.5 m below the surface. The composition of the natural bacterial populations in the studied habitats was extremely diverse and site specific. Analysing 100 to 150 clones per sample we have found only several repeated RFLP types which were considered as predominant.

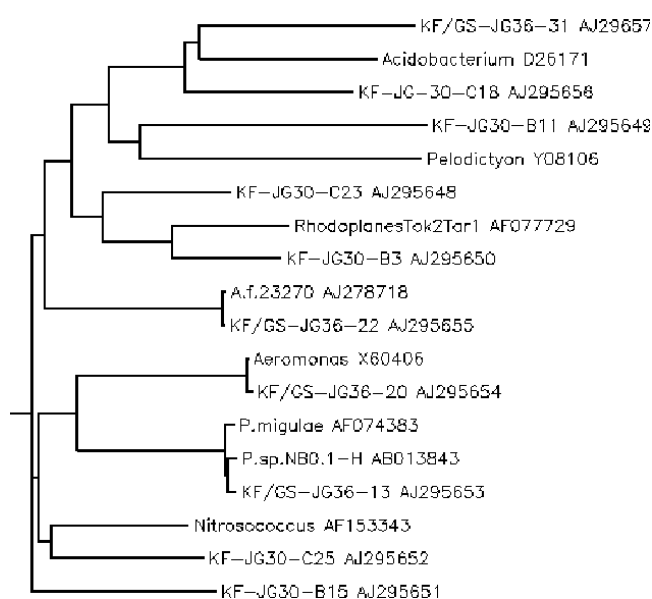


Fig. 1: Phylogenetic tree of the predominant bacterial groups in the uranium mining waste pile JG.

In Figure 1 a phylogenetic tree derived on the basis of the predominant 16S rRNA gene sequences found in the two analysed JG sites is presented. As evident from the Figure 1 the predominant bacterial groups identified in the site JG36 are clustered in the γ -Proteobacteria with *Pseudomonas migulae*, *Aeromonas*, and the chemolithoautotroph *Acidithiobacillus ferrooxidans* (type strain A.f. 23270). Several clones were affiliated to the phylum Acidobacterium/Holophaga. Representatives of the latter phylum were found also at the site JG30. In this less contaminated site the presence of two groups of α -Proteobacteria related to *Rhodoplanes* and a cluster

of bacteria related to the ammonia oxidiser *Nitrosococcus* was indicated. In contrast to the highly polluted site JG36, the JG30 was not predominated by *A. ferrooxidans* and γ -*Pseudomonas/Aeromonas* groups. However, representatives of these two groups were found in the Gitt2 site which was polluted in a grade similar to those of the JG36.

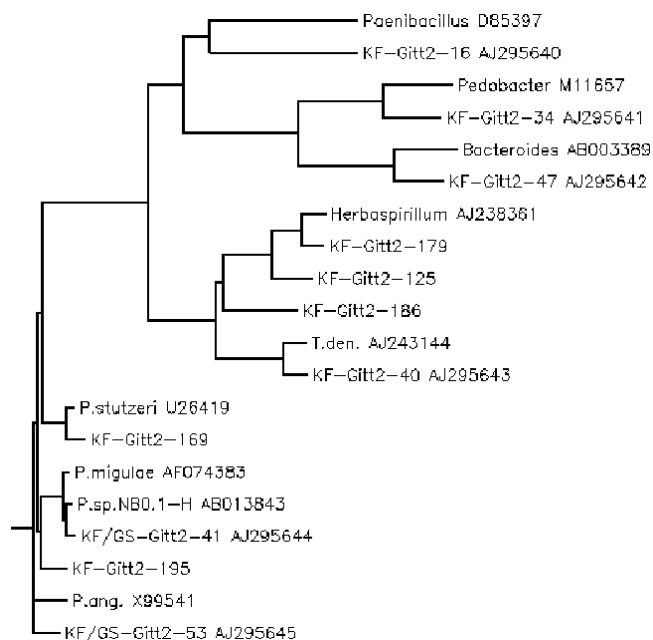


Fig. 2: Phylogenetic tree of the predominant bacterial groups in the uranium mill-tailings Gitt2.

As evident from Figure 2 in Gitt2 several closely related γ -*Pseudomonas* groups affiliated to *P. stutzeri* and *P. anguiliseptica* were found in addition to the cluster of *P. migulae*. Interestingly, in the cases of JG36 and Gitt2 this cluster has an identical structure (see Fig. 1 and Fig. 2). The representatives of *A. ferrooxidans* were identified in Gitt2 using RFLP-typing. No *Holophaga* and α -Proteobacteria were identified among the predominant bacteria in Gitt2. Instead, two groups of *Bacteroides*, several β -Proteobacterial groups related to *Hebraspirillum* and *Thiobacillus denitrificans* and a community of Gram positive *Paenibacillus* were indicated. The observed differences in the composition of the bacterial communities in the samples studied most probably due to their different geological origin and also to their different grade of contamination with heavy metals. The presence of *A. ferrooxidans* in the highly contaminated samples is indicative for bioleaching activities in those sites.

Acknowledgments

This work was supported by grant 4-7531.50-03-FZR/607 from the Sächsisches Staatsministerium für Wissenschaft und Kunst, Dresden, Germany.

EXAFS INVESTIGATIONS OF URANIUM (VI) COMPLEXES FORMED AT THE CELL SURFACES OF *Acidithiobacillus ferrooxidans* TYPES

M. Merroun, T. Reich, C. Hennig, G. Geipel, G. Bernhard, S. Selenska-Pobell

The structural parameters of the uranium complexes formed at the surfaces of three *A. ferrooxidans* eco-types were studied, using extended X-ray absorption fine structure (EXAFS) spectroscopy. The EXAFS spectra demonstrated that the phosphorus or sulphur-containing residues of *A. ferrooxidans* cells are involved in interaction with uranium.

Sequence analysis of the 16S rRNA genes of several reference strains and uranium-mining waste-pile isolates of *A. ferrooxidans* revealed specific signatures which distinguish three types within the species /1/. These types differ in their capability to accumulate and tolerate uranium /2/.

In this study applying EXAFS spectroscopy, we analysed the nature of the uranium complexes formed at the cell surfaces of the three *A. ferrooxidans* types.

The samples were measured at the Rossendorf Beamline (ROBL) at the European Synchrotron Facility (ESRF), Grenoble, France.

The samples studied were:

Dry biomass samples of *A. ferrooxidans* W1, 33020 and D2, (a), (c) and (e), and wet paste samples of *A. ferrooxidans* W1, 33020 and D2, (b), (d) and (f), respectively.

oxygen atoms (Oeq) is 2.35 Å. The coordination number of Oeq is 5-6.

SAMPLE	SHELL	N	R [Å]	σ^2 [Å ²]
a	U-O _{ax}	2 ^a	1.78	0.0014
	U-O _{eq}	4.7(5)	2.35	0.0071
	U-C	1.6(4)	2.92	0.0037 ^a
	U-P	0.9(3)	3.58	0.0070
b	U-O _{ax}	2 ^a	1.77	0.00126
	U-O _{eq}	5.4(5)	2.35	0.0089
	U-C	1.6(3)	2.92	0.002 ^a
	U-P	1.3(3)	3.56	0.007 ^a
c	U-O _{ax}	2 ^a	1.77	0.0015
	U-O _{eq}	4.5(4)	2.35	0.0076
	U-C	1.0(3)	2.92	0.004 ^a
	U-P	0.8(3)	3.59	0.008 ^a
d	U-O _{ax}	2 ^a	1.78	0.00127
	U-O _{eq}	5.1(5)	2.35	0.0082
	U-C	1.6(4)	2.90	0.0033 ^a
	U-P	0.9(4)	3.58	0.008 ^a
e	U-O _{ax}	2 ^a	1.77	0.00155
	U-O _{eq}	5.7(5)	2.35	0.0093
	U-C	1.2(4)	2.90	0.004 ^a
	U-P	1.4(3)	3.59	0.007 ^a
f	U-O _{ax}	2 ^a	1.77	0.00146
	U-O _{eq}	5.2(3)	2.35	0.0087
	U-C	1.4(2)	2.91	0.003 ^a
	U-P	1.0(1)	3.59	0.004 ^a

^a value fixed for calculation

Tab. 1: Structural parameters of the *A. ferrooxidans* uranium complexes

In all samples uranium is coordinated by two axial oxygen atoms (Oax) at a distance of 1.77-1.78 Å. The average distance between uranium and the equatorial

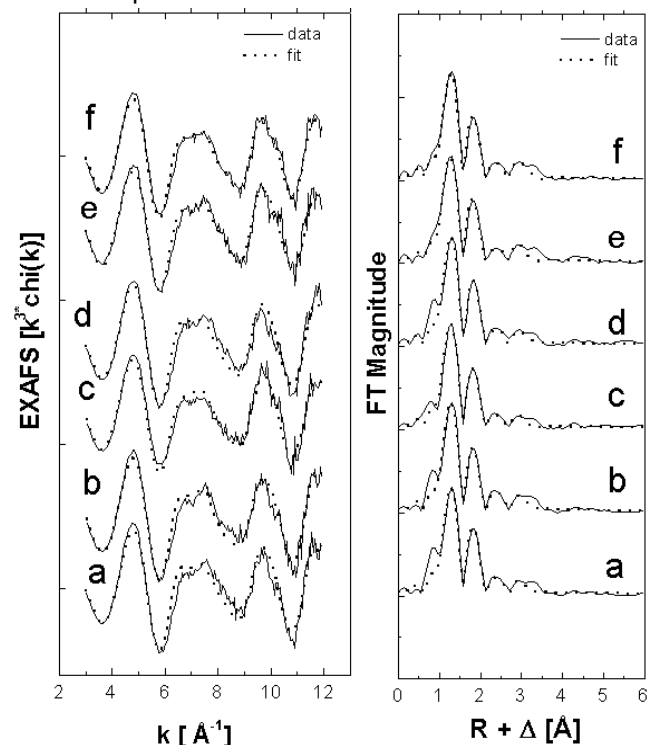


Fig.1: Uranium L_{III}-edge k³-weighted EXAFS spectra (left) and corresponding FT (right) of the *A. ferrooxidans* uranium complexes

Using U-C and U-P phase and amplitude functions, the third and fourth peaks in the FT of *A. ferrooxidans* indicate a distance of 2.91 and 3.58 ± 0.02 Å, respectively. The latter is the same U-P bond distance as for the organic uranyl phosphate (U(VI)-ATP complex). But we do not exclude the possibility of implication of sulphur because these 2 elements (P and S) are close to each other in the periodic system of elements and EXAFS cannot distinguish between them. In addition, P (or S) is bonded in a monodentate mode to the uranyl ion. Bidentate bonding would result in an atomic distance of approximately 3.2 Å. No structural differences were observed between the uranium complexes formed by the 3 types of *A. ferrooxidans*. However, the EXAFS spectra indicate a formation of uranium complexes different from those formed by Bacilli /3/.

Acknowledgments

This study was supported by grant 4-7531.50-03-FZR/607 from the Sächsisches Staatsministerium für Wissenschaft und Kunst, Dresden, Germany.

References

- /1/ Selenska-Pobell, S. et al., Antonie van Leeuwenhoek (in press).
- /2/ Merroun, M. et al., Report FZR-285 (1999) p.53
- /3/ Hennig, C. et al., Radiochim. Acta (in press)

CHARACTERIZATION OF THE URANIUM (VI) COMPLEXES FORMED AT THE CELLS OF THREE *A. ferrooxidans* TYPES USING INFRARED SPECTROSCOPY

M. Merroun, R. Nicolai, K.H. Heise, S. Selenska-Pobell

Infrared (IR) spectroscopy was used to study the functional groups of three *A. ferrooxidans* ecotypes involved in uranium complexation. The results indicated that uranium was bound by phosphorus or sulphur-containing groups of the cells of *A. ferrooxidans* types.

Bacteria express on their surfaces a wide variety of complex molecules which at physiological pH values contain numerous charged functional chemical groups (such as phosphoryl, carboxyl, and amino groups) that usually impart to the cell surface a net of anionic (negative) charge densities. Since the cell surface is in direct contact with the environment, the charged groups within the surface layers can interact with ions or charged molecules present in the external milieu. As a result, metal cations may become electrostatically attracted and bound to the cell surface. Only little information is available on the microbial functional groups involved in interaction with uranium and other heavy metals under highly acidic conditions. In such environments 3 types of *A. ferrooxidans* were identified /1/ which can accumulate and tolerate uranium in a different way /2/.

The aim of this study was to determine the nature of *A. ferrooxidans* chemical groups involved in uranium complexation, using infrared spectroscopy.

The FTIR spectrum (50 to 4,000 cm^{-1}) of native biomass of *A. ferrooxidans* type I (without uranium) is presented in Fig.1.

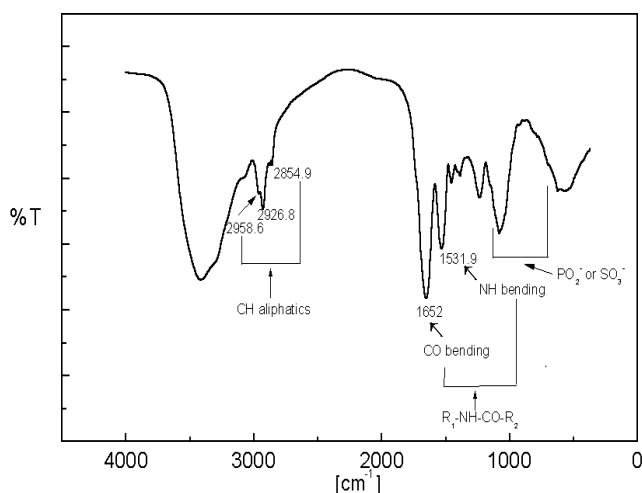


Fig. 1: IR spectrum of *A. ferrooxidans* type I cells.

There are distinct stretching frequencies; the band at 1,532 cm^{-1} is assignable to NH bending of the secondary amide group CONH (amide II band), while the band between 1,700 and 1,600 cm^{-1} (1,652 cm^{-1}) is indicative of the presence of CO groups.

The groups of bands in the range from 3,000 to 2,800 cm^{-1} are attributable to C-H stretching modes, indicating the presence of the alkyl groups CH_3 , CH_2 and CH.

In addition, the region from 1,000 to 1,300 cm^{-1} contains contributions from phosphate or sulphate groups.

These groups belong to various cellular components, such as peptides, phospholipids, peptidoglycan, etc., which are able to complex metals.

Fig. 2 shows the IR spectra for native and uranium treated *A. ferrooxidans* types. The absorption band at 925.6 cm^{-1} (Type II), 925.8 cm^{-1} (Type I), and 927.5 cm^{-1} (Type III) originates from the asymmetric stretching vibration of the uranyl unit.

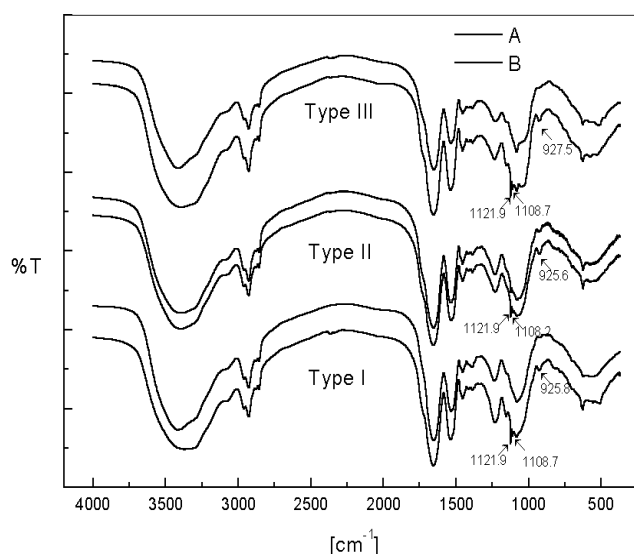


Fig. 2: IR spectra of the three *A. ferrooxidans* types. (A) without uranium, (B) treated with uranium

The IR spectra of the 3 types of *A. ferrooxidans* treated with uranium have a similar nature and revealed a shift in phosphorus or sulphur groups to higher wave numbers (IR cannot distinguish between these 2 elements due to the close proximity of such elements in the periodic table). This indicates interactions of these bacterial functional groups with uranium. The results of IR spectroscopy are in good agreement with those found using extended x-ray absorption fine structure (EXAFS) spectroscopy /3/.

Acknowledgments

This study was supported by grant 4-7531.50-03-FZR/607 from the Sächsisches Staatsministerium für Wissenschaft und Kunst, Dresden, Germany.

References

- /1/ Selenska-Pobell, S. et al., Antonie van Leeuwenhoek (in press)
- /2/ Merroun, M. et al., Report FZR-285 (1999) p.53
- /3/ Merroun, M. et al., this report p.36

SEQUENCE ANALYSIS OF THE SURFACE LAYER (S-LAYER) PROTEINS OF THE URANIUM MINING WASTE PILE ISOLATE *B. sphaericus* JG-A12 AND OF *B. sphaericus* NCTC 9602

J. Raff, K. Flemming, S. Selenska-Pobell

The N-terminal domains of the S-layer proteins of the uranium waste pile isolate *Bacillus sphaericus* JG-A12 and of its genomic analogue, *B. sphaericus* NCTC 9602, were investigated using PCR and sequence analysis. The primary structure of both proteins differs significantly from those of the other S-layers studied up to date.

Genes of the S-layer proteins of *B. sphaericus* JG-A12 and 9602 were analyzed partially. The strain JG-A12 was recovered from a uranium mining waste pile near the town of Johanngeorgenstadt and classified using the 16S rDNA retrieval to the species *B. sphaericus* /1/. In the same work /1/ it was demonstrated that the closest phylogenetic relative to the uranium waste isolate JG-A12 is the strain of *B. sphaericus* NCTC 9602. Both strains belong to the sero-group I of the species and possess almost undistinguishable genomic fingerprints /1/. Parts of the S-layer genes corresponding to the N-terminal domain of the matured proteins were amplified and sequenced using primers designed as described in /2/.

also the lengths of the two proteins differ significantly from those of the other S-layers deposited to the EMBL Gene Bank.

On the basis of their ability to accumulate selectively and reversibly large amounts of U, Pb, Cd, Cu, and Al the strains *B. sphaericus* JG-A12 and 9602 were chosen for construction of biological ceramics for bioremediation of heavy metal polluted environments. Moreover, the strain JG-A12 which is well adapted to the rather complex conditions of the uranium wastes might be used for an *in situ* decontamination of the latter. This biotechnological approach, however, requires monitoring of the strain JG-A12 during the production of the bioceramic and also after its release into the environment.

Because the strains JG-A12 and 9602 possess identical 16S rDNA and their genomic fingerprints are highly related /1/ it is impossible to discriminate them by the usually used standard approaches of 16S ARDREA or genomic PCR.

In this work we suggest an alternative method for monitoring the strains which exploits the differences between their S-layers genes. Our analysis demonstrated that the two above mentioned strain-specific amino acids of the S-layers are coded by specific stretches in the corresponding genes which affect the site for the restriction endonuclease *Mse*I. The latter allows fast and reliable discrimination of the strains carrying the genes (see Fig. 2).

conserved aa	1	-----*	-----*	-----*	-----*
SLH consensus		--FKDVXX-D	HWAAKYINAL	VKLGIIVKGX	GDGXFGEKXK
<i>B. sph. JGA12</i>		AGFSDVAGND	HEV--AINAL	ADAGII-NGY	ADG SFKPNQT
<i>B. sph. 9602</i>		AGFSDVAGND	HEV--AINAL	ADAGII-NGY	ADGTFKPNQT
<i>B. firmus</i>		AKFSDVSS-S	HWAIDDINYL	VERGAL-QGY	PDGTFKPNNS
<i>B. stea. PV72</i>		ASFTDVADP--	-QYKDAIDEL	VSTGAT-KGK	TETKFGVYDE
<i>B. sph. 2362</i>		AQLNDFNKIS	GYAKEAVQSL	VDAGVI-QGD	ANGNFNPLKT
<i>B. sph. P-1</i>		AQVNDYKNIS	GYAKEAVQAL	VDQGVV-QGD	TNGNFNPLNT
<i>B. sph. 4525</i>		AQVNDYKNIS	GYAKEAVQSL	VDQGVV-QGD	TNGNFNPLNT
	41	*****-*	-----*	-----*	-----*
conserved aa		-----*	-----*	-----*	-----*
SLH consensus		ITRAEAAXII	VRAXA----	--LKLXXXX-	--XFKDVX--
<i>B. sph. JGA12</i>		INRGQVVKLL	GRYLEAQGQE	IPADWNSKQ-	--RFNDLPVT
<i>B. sph. 9602</i>		INRGQVVKLL	GRYLEAQGQE	IPADWNSKQ-	--RFNDLPVT
<i>B. firmus</i>		ITRAEIAVYL	ARTLGL----	--LDVDSVET	TDKE SDVPE
<i>B. stea. PV72</i>		ITRRLDAVIL	ARVLK----	--LDVDNAKD	A-GFTDVP--
<i>B. sph. 2362</i>		ISRAEAATIF	TNALE----	--LEAEGDVI	--NFKDVK--
<i>B. sph. P-1</i>		VTRAQAEIF	TKALE----	--LEANGDVI	--NFKDVK--
<i>B. sph. 4525</i>		VTRAQAEIF	TKALE----	--LEADGDVI	--NF SDVK--
	81	-----*	-----*	-----*	-----*
conserved aa		-----*	-----*	-----*	-----*
SLH consensus		XDHWAAYKIN	ALVK--LGII	VKXGDXGXF	EKKXITRAEA
<i>B. sph. JGA12</i>		AEEELVKY-A	ALAKD-AGVF	-NG-SNGNLN	ASQTMQRQOM
<i>B. sph. 9602</i>		AEEELVKY-A	ALAKD-AGVF	-NG-SNGNLN	ASQTMQRQOM
<i>B. firmus</i>		ATHWANPYIA	ATVDQTEGVI	-DGYENGTFR	PSNTITRQEM
<i>B. stea. PV72</i>		--KDRAKYVN	ALVE--AGVL	-NGKAPGKFG	AYDLPLTRVEM
<i>B. sph. 2362</i>		ADAWYYDAITA	ATVE--NGIF	-EGVSATBEFA	PNKQLTRSEA
<i>B. sph. P-1</i>		AGAWYYNSIA	AVVA--NGIF	-EGVSATBEFA	PNKSLTRSEA
<i>B. sph. 4525</i>		AGAWYYNSIA	AVVA--NGIF	-EGVSANBEFA	PNKSLTRSEA
	121	-----*	-----*	-----*	-----*
conserved aa		-----*	-----*	-----*	-----*
SLH consensus		AXIIVRAK-A	LKLXXXX--X	FKDVX----X	DHWAAYK---
<i>B. sph. JGA12</i>		AVVLVRAIKE	IAGVDLV-AE	YKKANFVTEI	GDDLKAYSAE
<i>B. sph. 9602</i>		AVVLVRAIKE	IAGVDLV-AE	YKKANFVTEI	GDDLKAYSAE
<i>B. firmus</i>		AKMVVEAY-D	LLELVEGKDL	FTDVS----	GLWSTDY---
<i>B. stea. PV72</i>		AKIIANRY-K	LKADDVK-LP	FTDVN----	DTWA-PY---
<i>B. sph. 2362</i>		AKILVDAF-E	LEGECDL-SE	FADAS---TV	KPWAKSY---
<i>B. sph. P-1</i>		AKILVEAF-G	LEGEADL-SE	FADAS---QV	KPWAKKY---
<i>B. sph. 4525</i>		AKVLVDAF-G	LEGEESL-SQ	FADAS---QV	KGWAKSA---
	161	-----*	-----*	-----*	-----*
conserved aa		-----*	-----*	-----*	-----*
SLH consensus		----INALVK	LGIIVKXGSD	G--XFGPKXK	ITRAEAAXII
<i>B. sph. JGA12</i>		QRTAIVALEY	AGITNVAH--	----FNPGNS	VTRGQFASSI
<i>B. sph. 9602</i>		QRTAIVALEY	AGITNVAH--	----FNPGNS	VTRGQFASS
<i>B. firmus</i>		----INILAS	NGVAAGMTAT	T---FAPRGE	VLRAQTAAFI
<i>B. stea. PV72</i>		----VKALYK	YEVTKGKTEP	S---FGAYQN	ITRGDFAEVY
<i>B. sph. 2362</i>		----LETAVA	NGVIKGSAN	GKTNLNPNAP	ITRQDFAVVF
<i>B. sph. P-1</i>		----LETAVA	NGIFEGTDAN	K---LNPNSN	ITRQDFALVF
<i>B. sph. 4525</i>		----LETAVA	NGIFTGSEEN	GKLNLPNAA	ITRQDFAVVF

Fig. 1: Alignment of the N-terminal domains of the S-layers of: *B. sphaericus* JG-A12 (AJ292965) and *B. sphaericus* NCTC 9602 (AJ292964) to those of the mostly related S-layer proteins found in EMBL: *B. firmus* OF4 (AF242295), *B. stearothermophilus* PV72 (X98095), *B. sphaericus* WHO 2362 (M28361), *B. sphaericus* P-1 (A45814) and *B. sphaericus* ATCC 4525 (AF211170). Highly conserved amino acids are indicated with asterisks /3/.

As evident from the Fig. 1 the N-terminal domains of the S-layers of *B. sphaericus* JG-A12 and 9602 share extremely high homology. Only two of 182 analysed amino acid residues are not identical (underlined in the Fig. 1). However, the amino acid sequences and

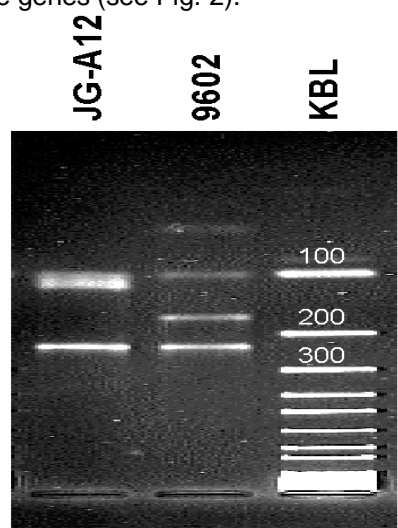


Fig. 2: *Mse*I profiles of the S-layer amplicons of the *B. sphaericus* strains JG-A12 and the 9602.

Acknowledgements

This work was supported by grant Se 671/7-1 from the Deutsche Forschungsgemeinschaft.

References

- /1/ Selenska-Pobell S. et al., FEMS Microbiol. Ecol. **29**, 59-69 (1999)
- /2/ Raff, J. et al., Report FZR-285 (2000) p. 55
- /3/ Engelhardt et al., J. Struct. Biol. **124**, 276 (1998)

BACTERIA CULTURED FROM SOIL SAMPLES OF URANIUM MINING WASTE PILES

I. Tzvetkova, Tz. Tzvetkova, V. Groudeva, S. Selenska-Pobell

Several pure and mixed cultures from uranium waste piles were recovered and analyzed by the use of classical and molecular methods. The predominant bacterial groups cultured from the wastes are able to biotransform metals.

Bacteria play a role in transformations and transport of radionuclides and other toxic metals in nature. Different bacterial species are able to affect mobilization and immobilization of uranium in the uranium waste piles. In this study we used enrichment cultures to recover bacteria from two uranium mining wastes. We did classify the obtained individual and/or mix cultures using classical and molecular approaches. Because the majority of bacteria in the extreme environments are living in consortia which are described as symbiotic /1, 2/, it is a compromise to use the 16S rDNA retrieval for analysis of enriched biofilm or mixed cultures instead of pure ones /3/.

The main bacterial groups defined in the samples of the uranium waste piles are the chemolitho-autotrophic *Acidithiobacillus ferrooxidans* and *Leptospirillum ferrooxidans*. These bacteria play a significant role in the dissolution and the mobilization of many metals and radionuclides in the wastes.

In addition, the following heterotrophic bacteria have been cultured: strains of the genus *Desulfovibrio*, namely *Desulfovibrio vulgaris* subspecies *oxamicus* (Dv. vulg. ox.) and *Desulfovibrio intestinalis* (Dv. int) which reduce a large variety of metals, strains belonging to γ -*Pseudomonas*, strains related to *Agrobacterium* and *Sphingomonas* (α -Proteobacteria) as well as isolates related to uncultured Gram positive bacilli. In Fig. 1 a phylogenetic tree based on the 16S rDNA sequences of the recovered individual strains is shown.

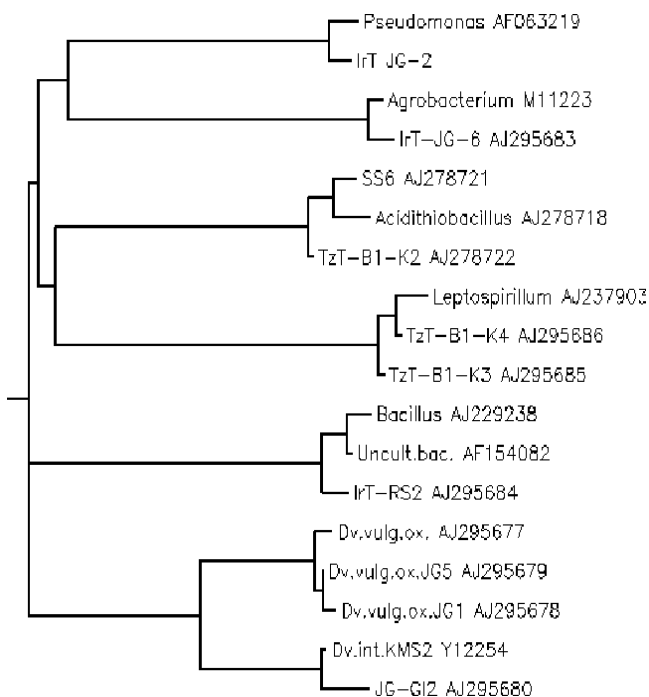


Fig. 1: Phylogenetic tree of the bacterial isolates cultured from the uranium waste piles.

Two enrichment mixed cultures were recovered and analyzed as well. Fig. 2 shows a phylogenetic tree based on the 16S rDNA sequences of these two bacterial consortia. One of them, called initially "JG1", from which the sulfate reducing isolate Dv. vulg. ox. JG1 was purified, consisted of two additional metal reducing strains, IrT-JG1-71 and IrT-JG1-58 (not shown), closely related to Dv. vulg. ox. JG1, and eleven diverse representatives of *Clostridium*. The members of this bacterial consortium are involved in different interaction with metals such as reduction, bio-precipitation, biosorption and bio-mineralisation. In this way they are influencing the geochemistry of the sedimentary environments from which they were recovered. In addition, the JG1 consortium may be used for removing metals from contaminated liquid wastes.

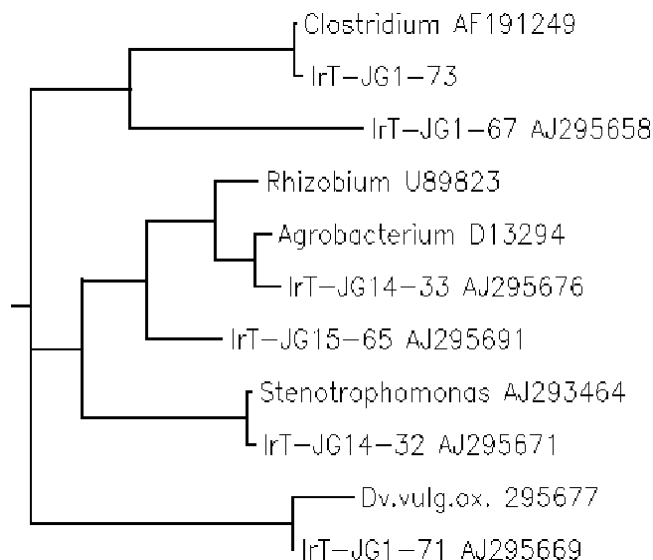


Fig. 2: Phylogenetic tree of the members of the isolated bacterial consortia.

Another mixed culture "JG14" consisted of different α -Proteobacteria (*Agrobacterium* and *Rhizobium*) and one microdiverse population of environmental strains of *Stenotrophomonas maltophilia* (β - γ -Proteobacteria). *S. maltophilia*, agrobacteria and rhizobia represent different kinds of rhizospheric bacteria interacting with plants. Their presence in the samples is an indication for bacteria-plant symbiotic interactions. The latter might be considered as a positive step towards a natural bioremediation.

References

- /1/ Schlöttenburg, C. et al., Int. J. Syst. Environ. Microbiol. **50**, 1505-1511 (2000)
- /2/ Strous, M. et al., Nature **400**, 446-449 (1999)
- /3/ Selenska-Pobell, S. et al., Microbiology and Radiochemistry (in press)

SCANNING ELECTRON MICROSCOPY INVESTIGATIONS OF URANIUM COMPLEXES IN PLANT SAMPLES

A. Günther, E. Christalle¹, H. Reuther¹, G. Bernhard
¹Institute of Ion Beam Physics and Materials Research

Scanning electron microscopy (SEM) and energy-dispersive X-ray microanalysis (EDS) were used for verification and more detailed characterization of uranyl complexes in uranium-containing cross and longitudinal sections of root and shoot axis samples of the blue lupin.

Introduction

The chemical characterization of species is needed for a reliable assessment of the migration of radionuclides and heavy metals into the geological and biological environment. The summary transfer factor has to be replaced by chemically well-defined parameters. Previously some experiments were performed by time-resolved laser-induced fluorescence spectroscopy and X-ray absorption spectroscopy to determine the chemical speciation of uranium in plants [1]. Scanning electron microscopy makes it possible to optically detect uranium species in plant samples and to determine the elements involved.

Experimental

Blue lupins were grown in the laboratory on uranium containing soils and as hydroponics in uranium-containing solutions (uranium concentration: 10^{-2} - 10^{-4} M). Fresh root and shoot axis sections (cross and longitudinal) of contaminated plants were prepared for scanning electron microscopical investigations. After the drying process in air at room temperature, the samples were fixed onto conductive adhesive films and coated with carbon or sputtered with gold. The scanning electron microscopy were carried out with a ZEISS DSM 962. For the SEM measurements secondary (SE) and backscattering electrons (BSE) were used, whereby acceleration voltages up to 30 kV were applied. The chemical composition of the uranium-containing depositions in plant cells and walls were determined by energy-dispersive X-ray microanalysis (EDS).

Results

Uranium-containing depositions in plant cells and walls were documented by means of scanning electron microscopy (Fig.1).

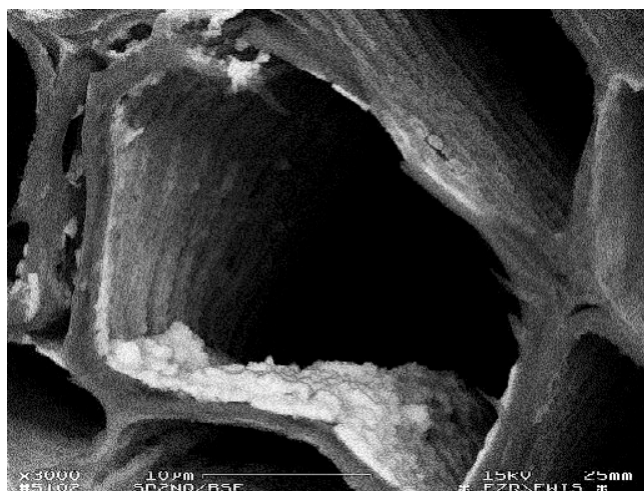


Fig. 1: SEM picture (BSE) of uranium containing plant cell of a shoot axis selection

Differences in grey tone reflections indicating differences in elementary composition were confirmed by the detection of backscattering electrons. Compared with other elements, such as C, O and N, uranium with the atomic number 238 seems to be lightreflecting. The uranium-containing depositions are not equally distributed in the samples. Fig.1 shows that there are larger accumulations as well as areas with less or no uranium.

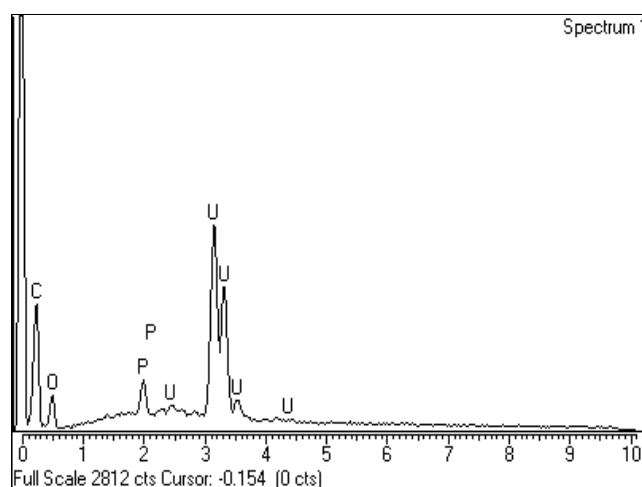


Fig. 2: EDS spectrum of selected points of uranium containing deposition in a plant cell

The EDS analyses (example in Fig.2) of selected points or areas of the uranium-containing depositions showed oxygen and phosphorus, in some cases even sulphur and silicon (cell wall) when the plant was offered high initial uranium concentrations (10^{-2} M). The uranium-phosphorus ratio lies in the range from 2:1 to 8:1.

This excess of uranium results from the high uranium concentration offered to the plant.

With lower and more environmentally relevant uranium concentrations (10^{-4} M), calcium, potassium and chlorine also appeared in the uranium-containing depositions in plant cells. The uranium-phosphorus ratio is clearly smaller in the range from 1:1 to 1:5. It is independent of the kind of uranium species offered to the plant by variation of the pH value of the hydroponics solution during growth. Determination of the element phosphorus supports the result of the EXAFS (Extended X-ray Absorption Fine Structure) investigations in which the U-P atomic distance of uranium complexes in various plant samples was determined.

References

/1/ Günther, A., Bernhard, G.: Zwischenbericht DFG-BE 2234/1-1

Modeling of Radionuclide Transport

RES³T - ROSSENDORF EXPERT SYSTEM FOR SURFACE AND SORPTION THERMODYNAMICS

V. Brendler

A prototype of a digitized version of a thermodynamic sorption database has been implemented as a relational database with MS Access. It is mineral-specific and can therefore also be used for additive models of more complex solid phases such as rocks or soils. An integrated user interface helps users to access selected mineral and sorption data, to extract internally consistent data sets for sorption modeling, and to export them into formats suitable for other modeling software.

It becomes increasingly evident that the sole use of distribution coefficients to describe sorption phenomena in reactive transport models is a too simplistic approach. A big improvement is to treat surface reactions as complexation reactions analogous to such reactions in homogeneous aqueous solutions. Therefore such models are called Surface Complexation Models (SCM) /1/.

As to the knowledge of the author, however, there is no digital thermodynamic database for surface complexation equilibria existing world-wide, despite the vast amount of available data. This induces several severe drawbacks:

- There is a lack of systematic screening and filling of data gaps.
- Only rarely critical reviews of alternative (and sometimes mutually excluding) data sets exist. Consequently, no broadly accepted set of recommended values exists, complicating comparisons of sorption experiments or modeling results.
- Every sorption problem relies on its own case-specific and often incomplete or inconsistent data set.
- Only very few of the abundant surface complexes proposed in the literature (mostly resulting just from best-fit considerations) are actually validated by spectroscopic evidence or supported by theoretical (quantum-chemical) calculations.

The RES³T database is designed as a Relational DataBase System (RDBS) and implemented in Microsoft Access on PC. All information is structured into logical subunits, stored into separate tables which are logically connected by the RDBS. This ensures that every piece of information is only stored once, all occurrences of a data record in other, more complex data sets is managed by references. Other benefits are high efficiency and internal consistency. The data records contain information about:

- Chemical ligands which can be both inorganic or organic ones: constituting elements, stoichiometry, charge, radius, redox state, molar mass;
- Minerals: names (official and trivial ones), formula, density, molar mass, reaction paths (aging, weathering, secondary phase formations) with chemical equation, thermodynamic and kinetic constants;
- Mineral surface properties: specific surface area (with associated grain size fraction), point of zero charge;
- Surface binding sites: concentration, affinity or coordination type, protolysis constants, applied SCM type, capacitance values, ion exchange capacity;
- Surface complexes: species, spectroscopic or theory-based evidence, reaction equation, formation constant, chemical structure.

For any value the used experimental method is stored, together with the respective ionic strength, the background media, and other information necessary to evaluate the data or derive other values. If published, errors for numerical data are included as a prerequisite for sensitivity and uncertainty analysis.

In addition to such "hard" data items an extensive bibliography is provided with both original citations and secondary literature references. The cited literature comprises also model evaluations with respect to theoretical limitations, thermodynamic consistency and parameter sensitivity. Moreover, it covers questions of experimental methods (design, error ranges and application areas) and interpretation of results from sorption experiments. All this means a transition from a pure data collection towards a "smart" database, that finally will turn into a sorption expert system. This is supported by a broad variety of offered user interactions:

- Users can easily extract specific data sets, e.g. all records relevant for the combination of a specific mineral and a specific SCM, or all sorption data available for a certain element / ligand / ion, or all published surface area data of a mineral, with output to screen or printer.
- Data selections can be exported into a file to be used in other geochemical speciation or reactive transport codes. Then, the output format will automatically be adapted to the specific requirements of the different software packages.
- Original bibliographic references can be traced back with access to other parameter sets originating from the same source.
- Each data record has a time stamp and editing remarks. Thus it is easy to reconstruct past data set assemblages at any later time, or to compare alternative data sets for a given scenario.
- The user is supplied with an integrated online help in addition to a printed documentation.

The database contains 134 specific surface area values, 246 surface site property data sets, and 341 records for surface complexation reactions for a total of 77 solid phases.

Major future development directions are towards the implementation of a world wide web (WWW) gateway to allow easy external access to the data base via the Internet, and towards an automatic data conversion between various units or reaction formulations.

Reference

/1/ Stumm, W., *Chemistry of the solid-water interface*. Wiley, New York (1992)

CHEMICAL MODELING OF SORPTION ONTO COLLOIDS IN MINE WATERS

V. Brendler, H. Zänker

Geochemical modeling including surface complexation were used to interpret observations of pH dependence of the distribution of uranium in complex water samples from the mine gallery "Rothschönberger Stolln" at Freiberg / Saxony. The major obstacle is the lack of an appropriate sorption database covering all occurring elements in good quality.

Risk assessment studies and the planning of restoration measures for contaminated water supplies have to rely on conservative assumptions on the mobility of the potentially hazardous compounds. In many cases this is not only determined by solubility products and the complexation in the aqueous phase, but also by migration pathways in colloidal form, either pseudo- or eigencolloids. This study should explore to which degree such phenomena observed on water samples from the "Rothschönberger Stolln" mine drainage gallery in Freiberg/Saxony can be explained by surface complexation models (SCM) /1/. The respective analytical results and the colloid characterization (mainly hydrous ferric oxide - HFO) were presented in previous articles /2/.

The MINTEQA2 /3/ geochemical speciation software was used for the modeling. From the various data sets available in the literature, only two, both based on the Diffuse Double Layer Model (DDL), incorporate uranium(VI) surface species. The first one originates from Dzombak and Morell /1/, where the uranyl surface species is not correctly described (Scenario 1), sorption of carbonate is missing and no ternary uranium-carbonate-surface species are included. The second one was published by Arnold et al. /4/ (Scenario 2) and is lacking data for all competing sorption reactions of the other major solution components. To discriminate the effects caused by the binary and ternary carbonate surface species, in a 3rd scenario the data set from /1/ has been stripped off of all reactions containing ions other than uranyl. The idea of a combined data base from /1/ and /4/ has to be abandoned due to different surface site densities (SSD) and surface protolysis constants applied in the two basic data sets, rendering them mutually inconsistent.

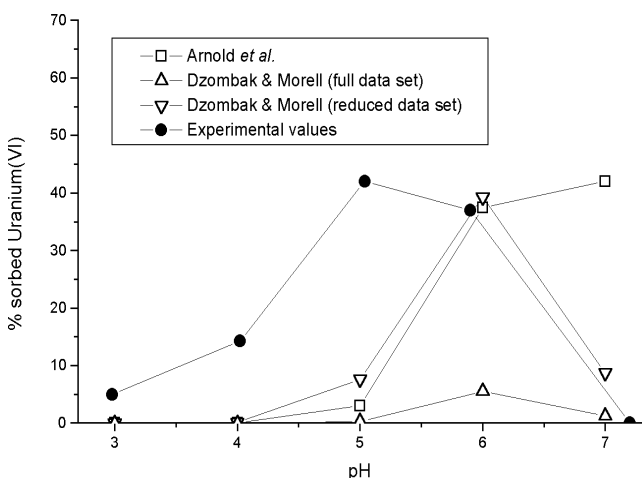


Fig. 1: Comparison of experimental and modeled uranium sorption onto HFO colloids

From the species distribution shown in Fig.1 it is obvious that the analytical determined distribution is not properly reflected by the modeling results.

This can have several reasons:

- In the acidic range (pH 3 -5), all data sets heavily underestimate the effect of sorption. Even a tenfold increasing of the surface site densities did not reverse this effect, so the reason must be some missing (ternary ?) surface complexes of uranium. There are enough free surface sites available, see Fig. 2.

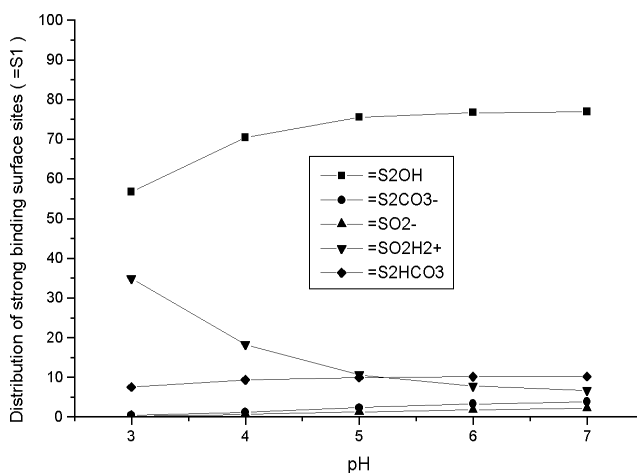


Fig. 2: Distribution of strong binding sites of HFO colloids

- At the highest investigated pH, the inclusion of ternary uranyl-carbonate surface species overcompensates the carbonate sorption in /4/ and yields too much sorption. Most probably a strong competing surface species is missing.
- The addition of competing surface reactions in /1/ for the other major cations in solution reduces the uranyl sorption too much. The same effect transferred to the data from /4/ would also give too strong a reduction in uranyl sorption. A closer look on the speciation shows that mainly lead and zinc bind to the strong binding sites, but the weak binding sites are occupied only to a small amount, similar to Fig. 2.

This work very distinctly demonstrates the need for comprehensive and consistent sets of SCM data when real-world scenarios with their complexity of chemical interactions have to be modeled.

References

- /1/ Dzombak, D.A., Morel, F.M.M., *Surface complexation modeling. Hydrous ferric oxide*, Wiley, New York (1990)
- /2/ Zänker, H. et al., Report FZR-272 (1999) p.106
- /3/ Allison, J.D. et al., Report EPA/600/3-91/021 (1991), U.S. EPA Environ. Res. Lab.
- /4/ Arnold, T. et al., *Chemical Geology* **151**, 129 (1998)

Development of Spectroscopic Speciation Methods and Other Analytical Tools

A SPLICE PROGRAM TO CONNECT TWO EXAFS SPECTRA OF THE SAME SAMPLE

H. Funke, H. Böttger¹

¹Communication and Data Processing Department

A computer program is presented that is able to connect (to "splice") two EXAFS spectra of the same sample if they have an overlapping energy region. This will be a useful tool in many situations where a spectrum cannot be measured over the desired energy range by a single scan.

Introduction

Among other purposes, the radiochemical experimental station at ROBL was designed to perform EXAFS experiments, using a closed cycle He cryostat by which the sample can be cooled to 15 K. In the first commissioning experiments with the cryostat in the autumn of 1999, the technical problem arose that sometimes it was impossible to obtain a continuous low-noise EXAFS scan over a wide k range. Thus, the idea of connecting two parts of an EXAFS scan in an unique way was born. The computer program SPLICE was developed to merge two EXAFS spectra of the same sample in an overlapping energy region. The word "splice" was chosen because of the analogy of the old sailing term "splicing".

The SPLICE program may be a useful tool in overcoming difficulties due to the shortness of time during an EXAFS experiment. Such problems may be caused by various situations, such as:

- any perturbation of the synchrotron beam,
- too frequent refill times,
- only the noisy part (in general the rear part of the spectrum) has to be repeated for an amendment of the statistics of the EXAFS scan.

Program description

The idea underlying the Fortran program SPLICE will be described with reference to Fig. 1. Two raw EXAFS scans (F_1 and F_2) are recorded in separate energy regions with an overlap of about 50 data points. Each scan is represented by the energy E and the attached absorption values.

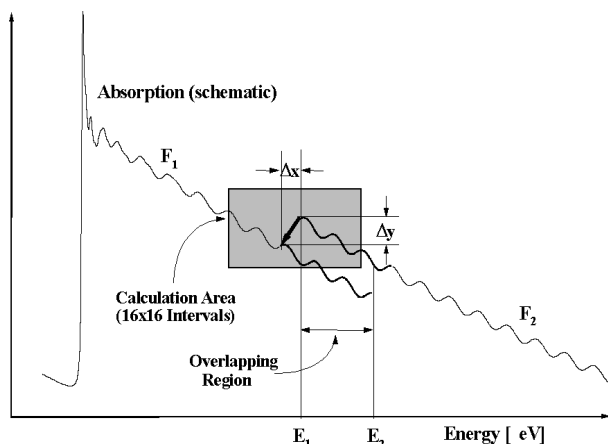


Fig. 1: Illustration of the program SPLICE

Ideally, within this overlapping area both scans should be identical. However, by reason of physical and technical conditions there are some small differences of the second scan relative to the first.

The object now was to find three parameters Δx , Δy , and λ that would minimize the area between the overlapping parts of the spectra $S(\Delta x, \Delta y)$:

$$S(\Delta x, \Delta y) = \int_{E_1}^{E_2} \|F_1(x) - (F_2(x - \Delta x) - \Delta y) \cdot \lambda\| dx \Rightarrow \min$$

A dilatation parameter λ was introduced to correct some calibration differences between the two absorption functions F_1 and F_2 caused by small changes in the experimental conditions. Otherwise it would not have been possible to find a unique minimum of S . Note that the only fit parameters in the search for the minimum are Δx and Δy . λ must therefore be chosen so that it holds for each Δx and Δy that:

$$\int_{E_1}^{E_2} (F_1(x) - (F_2(x - \Delta x) - \Delta y) \cdot \lambda) dx = 0.$$

The initial placement of the points of F_2 means that $\Delta x=0$, $\Delta y=0$, and $\lambda=1$. After working out a special iteration procedure to define the optimal values of Δx , Δy , and λ , the program generates the spliced scan that consists of two parts:

- 1) All measured points (x, y) of F_1 with energy values below the first point of the overlapping area. These data will not be changed.
- 2) The corrected points (x^{spl}, y^{spl}) of the spliced function F_2 , beginning with the first point of the overlapping area. These data are changed according to our objective:

$$x^{spl} = x - \Delta x \text{ and } y^{spl} = (y - \Delta y) \cdot \lambda.$$

More detailed information to follow the optimization process is stored in a result file. Some first experience shows that the results are practically not dependent on the type of chosen interpolation, integration, and norm. The crucial point for the iteration procedure to find a unique minimum is the introduction of the dependent calibration parameter λ .

If the iteration process cannot find a stable minimum as a result of too much noise or other defects of the spectra, the user receives a message that splicing of the two scans is impossible.

The final range of the parameters found is usually:

$$\begin{aligned} |\Delta x| &< 1 \text{ eV,} \\ |\Delta y| &< 0.005, \\ |\lambda - 1| &< 0.001. \end{aligned}$$

The functionality of the program is demonstrated by application to a set of real EXAFS spectra which is described in the following paper /1/.

References

- /1/ Funke, H. et al., this report, p.44

TEST EXPERIMENTS TO VERIFY THE “SPLICE” PROGRAM

H. Funke, T. Reich, C. Hennig, A. Roßberg

The SPLICE program, which is able to merge two EXAFS spectra of the same sample, was evaluated by test experiments. The measurements were performed at the U L_{III} edge using EXAFS spectra of an uranyl arsenate sample measured up to k of 22 \AA^{-1} at a temperature of 15 K.

Experiments were performed to test the SPLICE program, presented in /1/, using real EXAFS spectra of an uranyl arsenate sample with the sum formula $\text{H}_2[\text{UO}_2\text{AsO}_4]_2 \cdot 8\text{H}_2\text{O}$. To reduce thermal vibrations, the sample was cooled to 15 K using a closed-cycle He cryostat. The measurements were carried out on ROBL at the ESRF. The data were analyzed by standard methods using EXAFSPAK and FEFF8. Aspects of the structure and co-ordination chemistry of the EXAFS studies on uranyl arsenates and similar compounds are discussed elsewhere /2/.

Three different EXAFS spectra were compared. The first two spectra consist of two different scans merged by SPLICE. The third spectrum consists of one uninterrupted continuous scan.

- Splice A: Two absorption spectra, both scanned with an equal step in k -space of $\Delta k = 0.05 \text{ \AA}^{-1}$ are spliced at $k = 15 \text{ \AA}^{-1}$ to give an entire EXAFS-spectrum with a length of $k = 22 \text{ \AA}^{-1}$.

- Splice B: Two absorption spectra, the first scanned with an equal step in k -space of $\Delta k = 0.05 \text{ \AA}^{-1}$ and the second with an equal step of $\Delta k = 0.02 \text{ \AA}^{-1}$ are spliced at $k = 15 \text{ \AA}^{-1}$ to give an entire EXAFS spectrum with a length of $k = 22 \text{ \AA}^{-1}$. This is a demonstration of the ability of the SPLICE program to connect two scans recorded with different steps in k -space.

- Without splicing C: For comparison with the spliced spectra, one entire spectrum was recorded over the whole range of $k = 22 \text{ \AA}^{-1}$ with an equal step of $\Delta k = 0.05 \text{ \AA}^{-1}$.

The relevant graphs of the three test spectra are compared in Fig. 1. The values of the fit-results using EXAFSPAK are shown in Tab. 1. The present fit model was chosen in analogy to /2/ to demonstrate the equality of the three spectra A, B, and C. A detailed fit analysis is also presented in /2/.

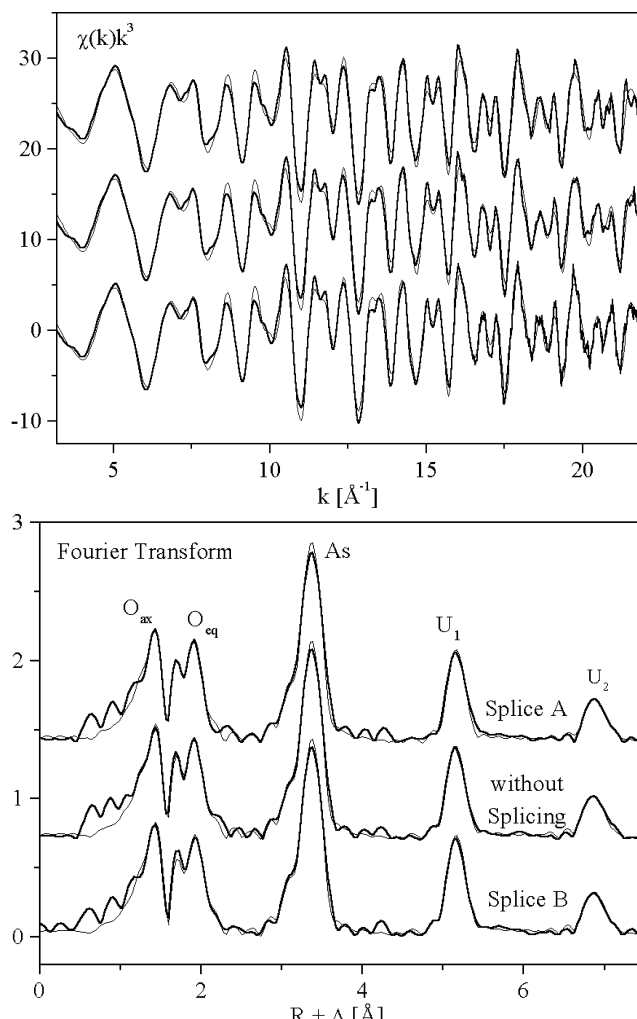


Fig. 1: Uranium L_{III} -edge k^3 -weighted EXAFS spectra and corresponding Fourier transforms of the spliced spectra A and B in comparison with the spectrum C (without splicing). Experimental data - solid lines; fit – thin solid lines.

Coord. shell	N			R [Å]			$\sigma^2 \cdot 10^3$ [Å ²]			ΔE_0		
	A	B	C	A	B	C	A	B	C	A	B	C
O _{ax}	1.9	2.0	1.8	1.79	1.79	1.79	1.46	1.62	1.20	-8.9	-8.8	-9.0
O _{ax} ^{ms}	5.0	4.4	4.0	3.64	3.63	3.63	2.80	3.20	2.40	-14.1	-16.6	-16.6
O _{eq}	4.7	4.4	4.8	2.30	2.30	2.30	2.33	1.99	2.45	-16.7	-14.5	-15.4
As	3.7	4.2	4.0	3.70	3.70	3.70	1.55	1.65	1.52	-14.5	-15.0	-14.8
U ₁	5.9	5.2	5.4	5.40	5.40	5.40	3.05	2.63	2.84	-13.1	-13.8	-14.0
U ₂	6.4	6.3	6.4	7.21	7.20	7.20	3.64	3.39	3.37	-24.8	-25.3	-25.2

Tab. 1: Comparison of fitted co-ordination numbers, distances, Debye-Waller factors and ΔE_0 shifts of the three test spectra (including the multiscattering path U-O_{ax}-U-O_{ax}-U). The rounding errors of the fitted data are two orders lower than the data compared in this table.

Significant differences are not visible between the graphs of the three spectra. The differences between the fit results are covered by the usual experimental uncertainties of EXAFS measurements.

References

- /1/ Funke, H., Böttger, H., this report, p.43
 /2/ Hennig, C. et al., J. Synch. Rad. **8**, 695-697 (2001)

EXAFS STUDY OF U(VI) COMPOUNDS: A NEW APPROACH TO DATA ANALYSIS

Yu.A. Babanov¹, T.Ye. Zayarnaya¹, T. Reich, H. Funke

¹Institute of Metal Physics, Ekaterinburg, Russia

The mathematical procedure of the regularization method is discussed and applied to the EXAFS analysis of uranyl arsenate $\text{UO}_2(\text{HAsO}_4) \cdot 4\text{H}_2\text{O}$.

The structure of a system consisting of n types of atoms can be described by $N = n(n+1)/2$ partial pair correlation functions (PCF's), $g_{ij}(r)$. A PCF $g_{ij}(r)$ is the density of the probability to find a pair of atoms i and j at an interatomic distance r (Fig. 1).

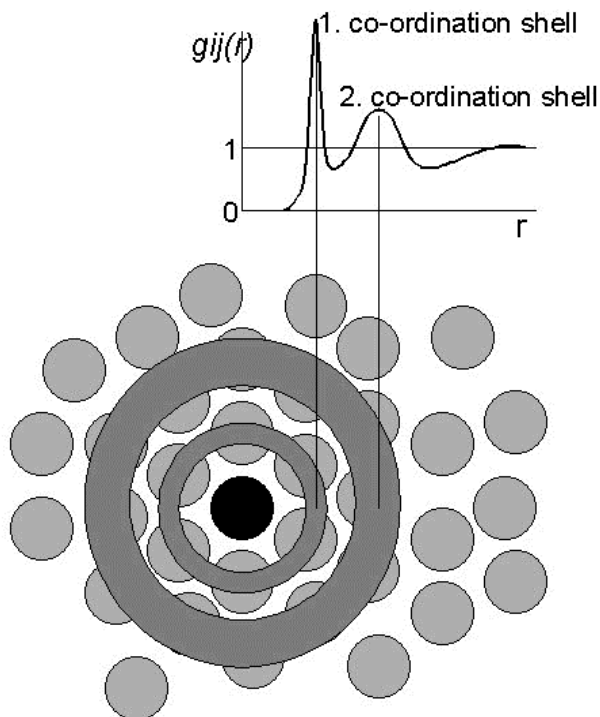


Fig. 1: Scheme of the statistical meaning of the partial pair correlation function $g_{ij}(r)$.

In single-scattering approximation, the EXAFS signal is described by an integral equation containing n PCF's. To numerically solve this integral equation, the Tikhonov regularization method /1/ has been applied successfully to the EXAFS analysis of metallic single-component and binary systems /2/.

This approach has been developed further by including a special iterative procedure to allow the simultaneous determination of several PCF's from one EXAFS spectrum /3/. To evaluate this new algorithm, we analyzed the U L_3 -edge and As K-edge EXAFS spectra of a reference compound, $\text{UO}_2(\text{HAsO}_4) \cdot 4\text{H}_2\text{O}$, which had been measured previously at the Rossendorf Beam Line (ROBL) at the ESRF in Grenoble /4/.

From the U L_3 -edge EXAFS spectrum, we obtained the PCF's for the pairs U-U, U-As (Fig. 2), and U-O. The PCF's of the pairs As-U, As-As, and As-O were obtained from the As K-edge EXAFS spectrum. The structural parameters for the first two U-As coordination shells can be determined directly from the PCF $g_{UAs}(r)$ given in Fig. 2. From the maximum and the area of the Gaussian peak labeled As₁, one obtains the following parameters: U-As distance of 3.73 Å, coordination number of 4, and Debye-Waller factor of 0.002 Å². As one can see from Fig. 2, these param-

eters agree with the model calculation based on neutron-scattering data /5/. Quantitative agreement was also observed for the first coordination shells of the other five PCF's.

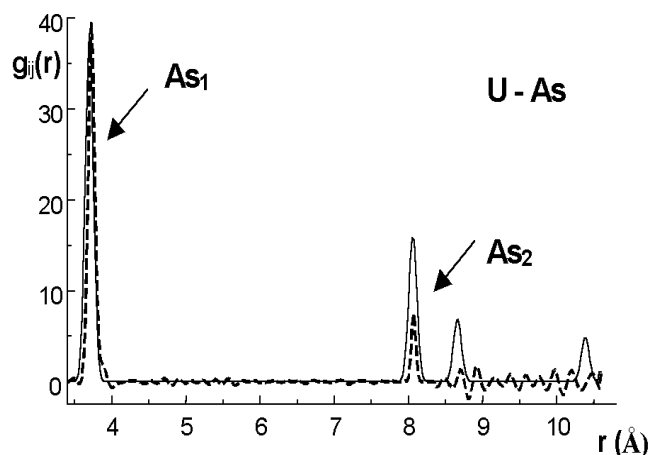


Fig. 2: The experimental PCF $g_{ij}(r)$ for the pair U-As of $\text{UO}_2(\text{HAsO}_4) \cdot 4\text{H}_2\text{O}$ (dashed line). The model calculation (solid line) used the atomic coordinates of $\text{UO}_2(\text{DAsO}_4) \cdot 4\text{D}_2\text{O}$ /5/ and a global Debye-Waller factor of 0.003 Å.

Compared to other methods for EXAFS analysis, the main advantage of this new approach is that the presence of a certain coordination shell can be detected and its distance determined without any structural model. Therefore, this method has great potential, especially for the EXAFS analysis of systems with closely spaced coordination shells of the same or different type of atoms.

References

- /1/ Tikhonov, A.N., Arsenin, V.Ya., *Solution of Ill-Posed Problems*, John Wiley and Sons Inc., New York, 1981
- /2/ Babanov, Yu.A. et al., *Phys. stat. sol. (b)* **105**, 747 (1981); Ershov, N.V. et al., *Phys. stat. sol. (b)* **108**, 103 (1981)
- /3/ Babanov, Yu.A. et al., *Proceedings of the 2nd Euro-conference and NEA Workshop on Speciation, Techniques, and Facilities for Radioactive Materials at Synchrotron Light Sources*, Grenoble, France, Sept. 10-12, 2000 (accepted for publication)
- /4/ Hennig, C. et al., *J. Synchrotron Rad.* **8**, 695 (2001)
- /5/ Fitch, A.N. et al., *Acta Cryst.*, **C39**, 159 (1983)

APPLICATION OF THE TIKHONOV REGULARIZATION METHOD TO THE EXAFS ANALYSIS OF $\text{UO}_2(\text{H}_2\text{AsO}_4)_2 \cdot \text{H}_2\text{O}$

T.Ye. Zayarnaya¹, T. Reich, C. Hennig, H. Funke
¹ Institute of Metal Physics, Ekaterinburg, Russia

The possibility to determine structural parameters from partial pair correlation functions (PCF's) for $\text{UO}_2(\text{H}_2\text{AsO}_4)_2 \cdot \text{H}_2\text{O}$ is considered assuming that its crystal structure is unknown.

In the present investigation it has been assumed that the crystal structure of $\text{UO}_2(\text{H}_2\text{AsO}_4)_2 \cdot \text{H}_2\text{O}$ is unknown. Therefore, a chemically similar compound with a known atomic structure, i.e., $\text{UO}_2(\text{HAsO}_4) \cdot 4\text{H}_2\text{O}$, has been chosen to calculate the scattering amplitude and phases by FEFF8 /1/. The aim was to evaluate the capability of the Tikhonov regularization method further.

After solving the inverse ill-posed problem using the algorithm described in /2/, we obtained three partial pair correlation functions (PCF's) both from U L_3 -edge and As K-edge EXAFS spectra. These spectra had been measured at 15 K in transmission mode at the Rossendorf Beam Line ROBL and have been analyzed also by standard EXAFS procedures using the EXAFSPAK software package /3/ (see Tab. 1).

Shell	Least-square fit /3/	Tikhonov regularization method	XRD /4/
U-U ₁	5.38	5.26	5.27
U-U ₂	5.73	5.77	5.75
U-As ₁	3.70	3.73	3.70
U-O ₁	1.79	1.76	1.76
U-O ₂	2.35	2.40	2.39
As-U ₁	3.71	3.70	3.70
As-As ₁	-	4.11	4.13
As-O ₁	1.69	1.68	1.69

Tab. 1: Interatomic distances in Å for $\text{UO}_2(\text{H}_2\text{AsO}_4)_2 \cdot \text{H}_2\text{O}$ (15K)

In contrast to the conventional method of a nonlinear least-square fit, which relies on a structural model to describe the experimental EXAFS spectrum, the Tikhonov regularization method was able to detect the presence of the As-As₁ shell. The inter-atomic distances for the coordination shells obtained from the peak maximum in the partial PCF's agree within ± 0.02 Å with recently published XRD values /4/ (Tab. 1). The difference of 0.12 Å between our results and the least-square fit for the U-U₁ shell is probably due to the influence of As atoms at this distance, which were not included in the least-square fit /3/.

The differences in the uranium near-neighbor surrounding in $\text{UO}_2(\text{H}_2\text{AsO}_4)_2 \cdot \text{H}_2\text{O}$ and $\text{UO}_2(\text{HAsO}_4) \cdot 4\text{H}_2\text{O}$ become evident in the U-O₂ coordination shell. For $\text{UO}_2(\text{HAsO}_4) \cdot 4\text{H}_2\text{O}$, the average bond distance to four equatorial oxygen atoms is 2.30 Å. In $\text{UO}_2(\text{H}_2\text{AsO}_4)_2 \cdot \text{H}_2\text{O}$ five oxygen atoms surround the uranium in the equatorial plane with an average dis-

tance 2.39 Å (Fig.1). The changes both in coordination number and inter-atomic distance are reproduced by our analysis.

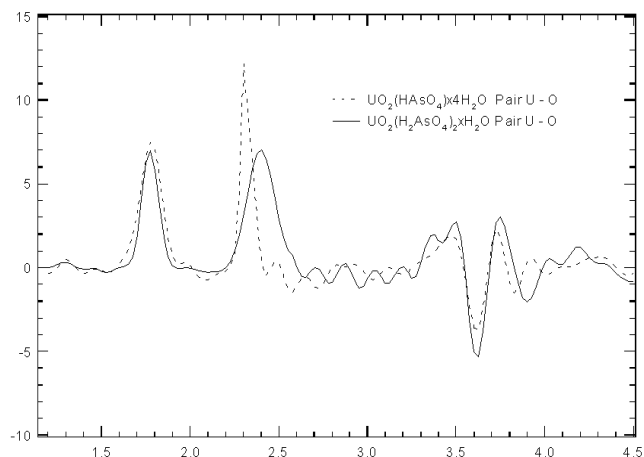


Fig. 1: The PCF $g_{ij}(r)$ as a function of r in Å for the pair U-O obtained from the U L_3 -edge EXAFS spectrum of $\text{UO}_2(\text{HAsO}_4) \cdot 4\text{H}_2\text{O}$ (dashed line) and $\text{UO}_2(\text{H}_2\text{AsO}_4)_2 \cdot \text{H}_2\text{O}$ (solid line).

In summary, the calculations show that it is possible to extract structural information, i.e., inter-atomic distances and coordination numbers, from U L_3 -edge and As K-edge EXAFS spectra of $\text{UO}_2(\text{H}_2\text{AsO}_4)_2 \cdot \text{H}_2\text{O}$ without a structural model as it is necessary in a least-square fit. The Tikhonov regularization method will be extremely useful for obtaining EXAFS structural parameters in complicated systems where exact structural information, e.g., single-crystal XRD data, is unavailable.

References

- /1/ Ankudinov, A.L. et al., Phys. Rev.B, **58**, 7565 (1998)
- /2/ Babanov, Yu.A. et al., *Proceedings of the 2nd Euroconference and NEA Workshop on Speciation, Techniques, and Facilities for Radioactive Materials at Synchrotron Light Sources*, Grenoble, France, Sept. 10-12,2000 (accepted for publication)
- /3/ Hennig, C. et al., this report p.49
- /4/ Gelsing, T.M. et al., Z. Anorg. Allg. Chem., **626**, 1414 (2000)

THE APPLICATION OF ITERATIVE TRANSFORMATION FACTOR ANALYSIS FOR THE DECOMPOSITION OF MULTICOMPONENT EXAFS SPECTRA OF URANIUM(VI) COMPLEXES WITH ACETIC ACID

A. Roßberg, T. Reich

To isolate the spectra of the pure spectroscopic components (factors) and their distribution in a mixture, it is necessary to measure a series of samples where their composition is changed by variation of one physicochemical parameter (e.g. pH, concentration, temperature ect.). The variation of the spectra can be quantified with the application of Eigenanalysis and the orthogonal and nonorthogonal rotation by using the VARIMAX-rotation and the iterative targettest. In this investigation the result is the pH-speciation of the structural units from the uranyl acetate complexes. Our factor analysis algorithm can be especially important for environmental samples.

Experimental

Eight solutions were prepared with 0.05 mol/L U(VI) and 1.0 mol/L acetic acid under norm conditions. The pH was varied in the interval from pH 0.10 to pH 4.48. The ionic strength was 1.2 mol/L. Fig. 1 shows the pH-speciation of the complexes according to stability constants from [1]. The U L_{III} -edge EXAFS spectra were measured in transmission mode at ROBL.

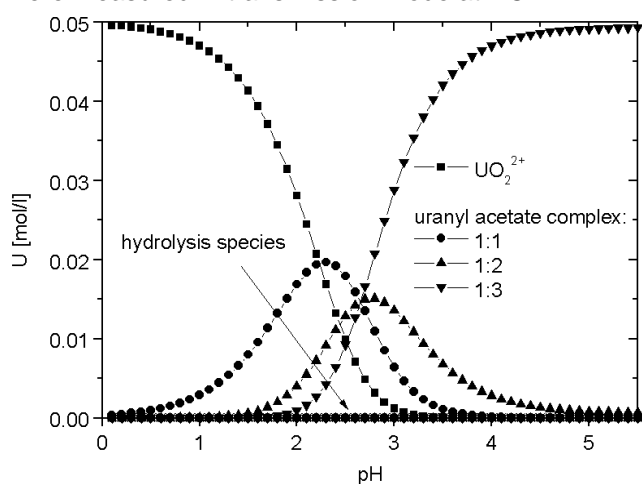


Fig. 1: Calculated pH speciation (conditions: see experimental)

Results and Discussion

The Eigenanalysis yields that only two factors are necessary to describe the variance in the spectra. By employing the VARIMAX rotation [2] and the iterative targettest (ITT), the relative concentrations (matrix **C**) and the EXAFS spectra (matrix **R**) of the two factors result. The measured spectra (matrix **D**) can be reproduced with two factors (Fig. 2).

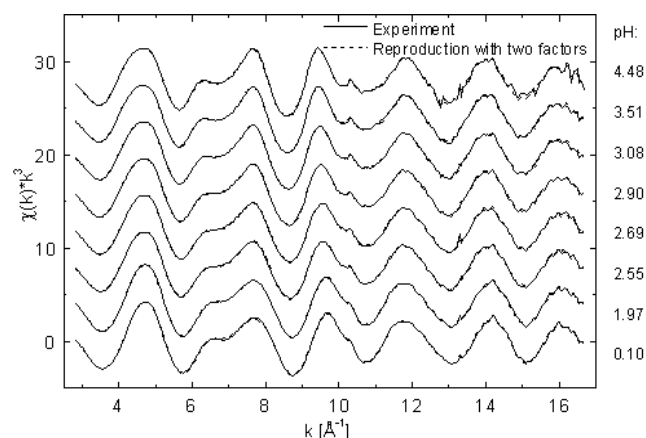


Fig. 2: The raw k^3 -weighted U L_{III} -edge EXAFS spectra and their reproductions with $\mathbf{D} = \mathbf{RC}$.

All complex species must consist of the fractions of the two isolated factors. The EXAFS spectra from the isolated factors were analyzed with EXAFSPAK [3]. Factor 1 consists of five equatorial oxygen atoms ($O_{eq,1}$) at a short distance (2.41 Å). Factor 2 consists of six equatorial oxygen atoms ($O_{eq,2}$) at a longer distance (2.46 Å) to the uranyl unit. The structural parameters from factor 1 are in agreement with those of the uranylhydrate. For factor 2 the structural parameters indicate that the carboxylic groups of three acetate ligands are bidentate coordinated to the uranyl unit. Only two chemical different equatorial oxygen atoms (O_{eq}) determine the data. Therefore, the EXAFS spectra of the 1:1 and 1:2 uranyl acetates cannot be isolated since these complexes coordinate water and acetate simultaneously. By multiplying the relative concentration of factors 1 and 2 by 5 and 6, respectively, one can plot the coordination numbers for $O_{eq,1}$ and $O_{eq,2}$ as a function of pH (Fig. 3).

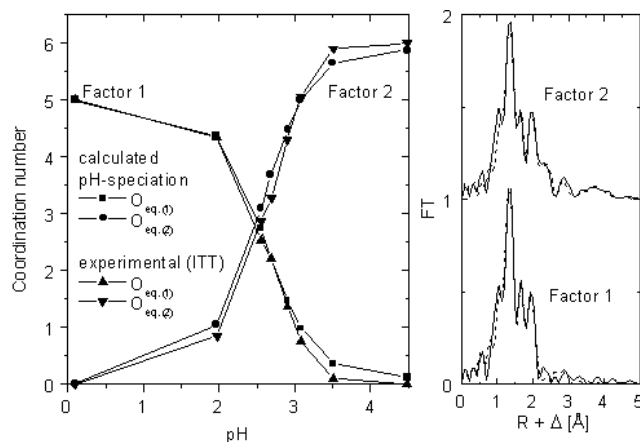


Fig. 3: The result of the ITT and the calculated pH-speciation (left). The Fouriertransforms (FT) and the best fit (dotted line) of the EXAFS spectra of the isolated factors (right).

To compare our results (Fig. 3) with the calculated speciation (Fig. 1), we assumed that 4 and 2 water molecules are coordinated in the 1:1 and 1:2 uranyl complexes, respectively. Then, the average $O_{eq,1}$ and $O_{eq,2}$ coordination numbers can be calculated from the speciation diagram for all pH values. As one can see from Fig. 3, these calculated values are in agreement with the experimental results.

References

- [1] Ahrland, S., Acta Chemica Scandinavica **5**, 199 (1951)
- [2] Kaiser, H.F., Psychometrika **23**, 187 (1958)
- [3] George, G.N. et al., SSRL, Stanford, CA. USA

COMBINATION OF EXAFS AND XRD FOR SOLVING HEAVY-ATOM STRUCTURES: PART I: X-RAY POWDER DIFFRACTION OF $\text{UO}_2[\text{H}_2\text{AsO}_4]_2 \cdot \text{H}_2\text{O}$

C. Hennig, T. Reich, F. Prokert¹, N. Schell¹, G. Reck², W. Kraus²

¹Institut für Ionenstrahlphysik und Materialforschung

²Bundesanstalt für Materialforschung und Materialprüfung, D-12489 Berlin

Determination of heavy-atom structures using X-ray powder diffraction is difficult because the reflection intensities are mainly influenced by the heavy scatterers. The atomic coordinates of light atoms remains often uncertain. The probability to obtain the complete structure increases if one includes parameters derived from EXAFS measurements as restraints into the procedure of structure solving.

In crystal structures containing uranium atoms, the X-ray scattering process is only weakly influenced by light atoms, whereas the contribution of heavy atoms dominates. Therefore, it is no problem to determine the atomic coordinates of uranium using X-ray powder diffraction. But it is difficult to locate the light atoms. On the other hand, a method like EXAFS, sensitive on short range order, gives reliable atomic distances in the surroundings of heavy atoms /1/ and allows to characterize the coordination polyhedra. These results can elucidate the main structure motif. In part II of this annual report the procedure is demonstrated using $\text{UO}_2[\text{H}_2\text{AsO}_4]_2 \cdot \text{H}_2\text{O}$ as example. Including the information from EXAFS as restraints in the structure solving procedure, the probability increases to obtain the complete structure.

In order to avoid crystallite orientation effects, the sample was prepared in a glass capillary and measured by sample rotation in Debye-Scherrer geometry. The high angle resolution was achieved by X-ray powder diffraction measurement carried out at the materials research end station at ROBL in a 2θ range of $8.0 - 34.7^\circ$ using a wavelength of $\lambda = 1.05070\text{\AA}$. The diffraction pattern is given in Fig. 1. Details of data collection and cell parameters obtained after a profile refinement are given in Tab. 1.

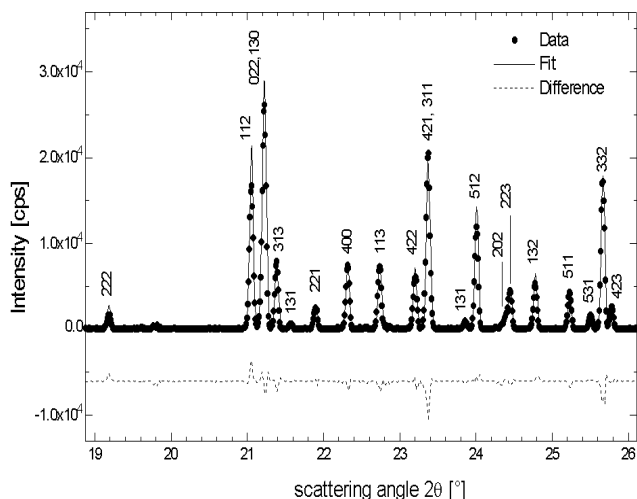


Fig. 1: Detail of X-ray powder diffraction pattern on $\text{UO}_2[\text{H}_2\text{AsO}_4]_2 \cdot \text{H}_2\text{O}$

The proposed procedure starts with the determination of cell parameters (a, b, c, β) and space group from XRD powder data. In a second step the absolute values of the structure factor $|F|$ are separated by iterating a decomposition formula /2,3/ starting from $|F|$ values arbitrarily set to be equal. In the third step the coordination polyhedra and their connections are determined using EXAFS. Heavy-atom positions will be found by direct methods using atomic scattering factors obtained from International Tables for X-ray crystallography /4/. The position of light atoms are determined by including the EXAFS results as help for the interpretation of the first difference Fourier synthesis. Subsequently, the complete coordination polyhedron geometry obtained by EXAFS is used as restraints in the first cycles of structure refinement. The final step is the refinement of all structural parameters by releasing the restraints.

Diffractometer	6-circle (Huber)
Radiation / λ [\AA]	Synchrotron / 1.05070
Scan geometry	Debye-Scherrer
Z	4
Space group	C2/c
a [\AA]	13.1650
b [\AA]	8.8583
c [\AA]	9.0475
β [$^\circ$]	124.512
2θ range [$^\circ$]	8.0-34.7
$\Delta 2\theta$ [$^\circ$]	0.01
No. of reflections	82
Profile function	Gauss
W	0.0043

W - reflex profil parameter

Tab. 1: Details of data collection and crystallographic data of $\text{UO}_2[\text{H}_2\text{AsO}_4]_2 \cdot \text{H}_2\text{O}$

The algorithm described above was successfully used to solve the structure. A refinement of the structure should be possible with data from extended 2θ range. The lattice constants (Tab. 1) are in agreement with the literature data /5,6/.

This methodical development demonstrates that the combination of EXAFS with powder diffraction allows a complete crystal structure determination of heavy atom structures also when no single crystals are available.

References

- /1/ Hennig, C. et al., J. Synchrotron Rad., in press
- /2/ Le Bail, A. et al., Mater. Res. Bull. **23**, 447 (1988)
- /3/ Reck, G. et al., Suppl. Z. Krist. **17**, 95 (2000)
- /4/ International Tables for X-ray Crystallography, Kluwer Academic Publishers, Dordrecht (1995)
- /5/ Barten, H., J. Appl. Cryst. **15**, 119 (1982)
- /6/ Gelsing, T.M. et al., Z. Anorg. Allg. Chem. **626**, 1414 (2000)

COMBINATION OF EXAFS AND XRD FOR SOLVING HEAVY-ATOM STRUCTURES: PART II: EXAFS MEASUREMENTS OF $\text{UO}_2[\text{H}_2\text{AsO}_4]_2 \cdot \text{H}_2\text{O}$

C. Hennig, T. Reich, F. Prokert¹, N. Schell¹, G. Reck², W. Kraus²

¹Institut für Ionenstrahlphysik und Materialforschung

²Bundesanstalt für Materialforschung und Materialprüfung, D-12489 Berlin

EXAFS is a short range order method and allows the analysis of coordination polyhedra in the surrounding of heavy atoms. The analysis of coordination is demonstrated on $\text{UO}_2[\text{H}_2\text{AsO}_4]_2 \cdot \text{H}_2\text{O}$.

Fig. 1 depicts the As K-edge k^3 -weighted EXAFS spectra of $\text{UO}_2[\text{H}_2\text{AsO}_4]_2 \cdot \text{H}_2\text{O}$ and the corresponding fit results are presented in Tab. 1. The measurement at room temperature (298 K) shows that As is surrounded by four oxygen atoms in an average distance of 1.68 Å indicating a $[\text{AsO}_4]$ tetrahedron. In order to reduce the thermal atomic movement, the same sample was measured at 15 K. This measurement shows that each $[\text{AsO}_4]$ tetrahedron is surrounded by two uranium atoms at a distance of 3.71 Å. This bond length points to a monodentate connection between the arsenate and the uranyl polyhedra. Corresponding to the $[\text{H}_2\text{AsO}_4]$ sequence of the chemical formula, two of the oxygen atoms are protonated.

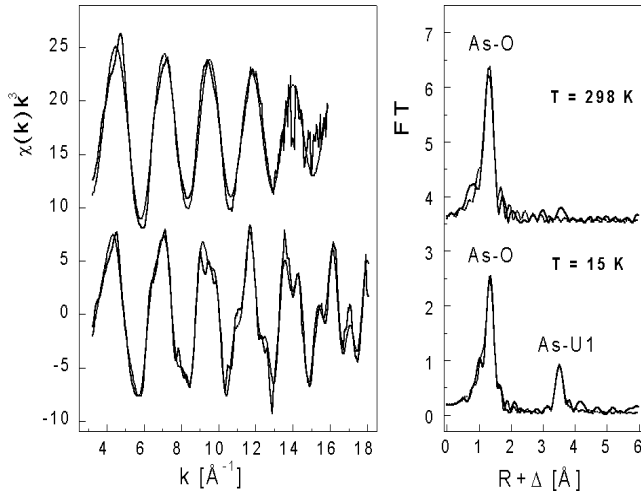


Fig. 1: As K-edge k^3 -weighted EXAFS spectra of $\text{UO}_2[\text{H}_2\text{AsO}_4]_2 \cdot \text{H}_2\text{O}$ (on the left) and their Fourier transform (on the right).

T [K]	shell	R [Å]	N	σ^2 [Å ²]	ΔE [eV]
298	As-O	1.68	3.8(2)	0.0017	2.3
15	As-O	1.69	4.2(1)	0.0016	-4.9
	As-U1	3.71	1.9(2)	0.0029	-11.0

Tab. 1: EXAFS structural parameters of the As K-edge of $\text{UO}_2[\text{H}_2\text{AsO}_4]_2 \cdot \text{H}_2\text{O}$ at 289 K and 15 K (see Fig. 1).

EXAFS measurements of $\text{UO}_2[\text{H}_2\text{AsO}_4]_2 \cdot \text{H}_2\text{O}$ at the U L_{III} -edge are shown in Fig. 2 and the fit results are given in Tab. 2. Two axial oxygen atoms are at a distance of 1.77 Å and five equatorial oxygen atoms are detected at an average distance of 2.38 Å. That they are not symmetry-equivalent is indicated by the high Debye-Waller factor of 0.0069 Å². The U-As distance is determined to be 3.70 Å with a coordination number of three. Taking into consideration that the errors in coordination numbers of distant shells are reduced at low temperatures, the uranium atom is coordinated by

four As atoms via oxygen atoms. Therefore, the fifth equatorial oxygen atom belongs to a H_2O molecule given in the chemical formula.

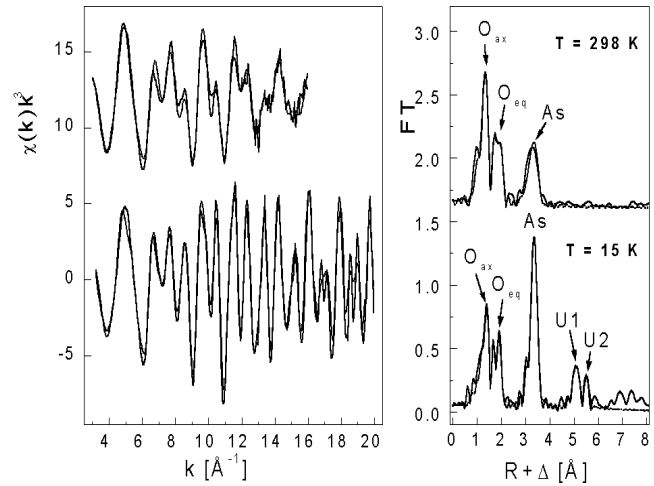


Fig. 2: U L_{III} -edge k^3 -weighted EXAFS spectra of $\text{UO}_2[\text{H}_2\text{AsO}_4]_2 \cdot \text{H}_2\text{O}$ (on the left) and their Fourier transform (on the right).

T [K]	shell	R [Å]	N	σ^2 [Å ²]	ΔE [eV]
298	U-O _{ax}	1.77	2.2(2)	0.0022	-1.2
	U-O _{eq}	2.38	5.1(4)	0.0068	/
	U-As	3.70	4.0(3)	0.0055	/
15	U-O _{ax}	1.79	1.9(1)	0.0015	6.5
	U-O _{eq}	2.35	4.7(4)	0.0044	0.7
	U-As	3.70	4.2(2)	0.0019	1.2
	U-U1	5.38	2.1(5)	0.0019	-14.0
	U-U2	5.73	6 (2)	0.0053	2.3

Tab. 2: EXAFS structural parameters of the U L_{III} -edge of $\text{UO}_2[\text{H}_2\text{AsO}_4]_2 \cdot \text{H}_2\text{O}$ at 289K and 15K (see Fig. 2).

Acknowledgments

We thank G. Grambole and M. Rutsch for sample preparation and K. Kroegner for chemical sample analysis.

FTIR SPECTROSCOPY OF WATER SOLUTIONS

R. Nicolai, K.H. Heise

Due to the low IR transmittance of common water (H_2O) in a wide wavelength range, it is often impossible to measure spectra in common water solutions. The higher IR transmittance of heavy water (D_2O) allows more sensitive measurements. Therefore, measurement in D_2O may be helpful, provided that the isotopic effects of deuterium are negligible.

Common water (H_2O) shows a high absorption in mid-infrared range. It shows strong bending vibrations, particularly at 900 cm^{-1} , and its transmittance is nearly zero. But the important stretching vibrations of metal ions are located in the range from 850 cm^{-1} to $1,000\text{ cm}^{-1}$. Thus, in H_2O it is often impossible to measure the stretching vibrations of metal ions in diluted solutions. However, heavy water (D_2O) shows a significantly lower absorption in this range. It is therefore often a better solvent, as its transmittance is higher and measurements can consequently be more sensitive. Hence this trick may be helpful with various experiments, provided that isotopic effects of deuterium in D_2O do not matter much.

In Fig. 1 the spectrum of H_2O is compared with the spectrum of D_2O in the above-mentioned wavelength range.

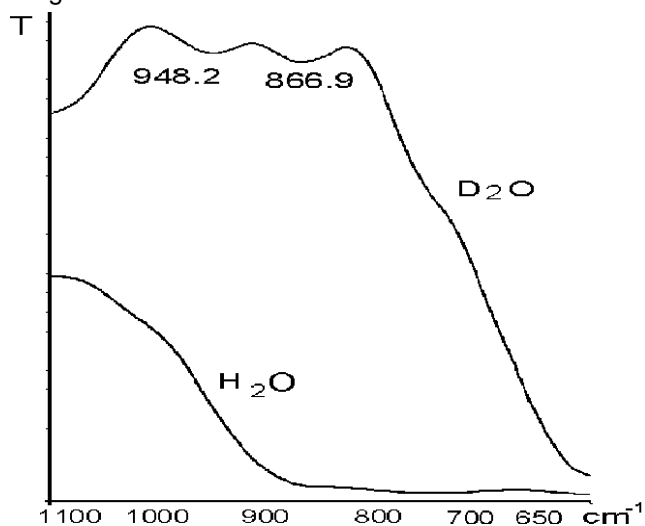


Fig. 1: Comparison of the FTIR spectra of common water (H_2O) and heavy water (D_2O)

By a simple experiment we compared the measuring sensitivity for the uranyl stretching vibration at 960 cm^{-1} in H_2O and in D_2O .

We measured uranyl nitrate solutions in the mid-infrared range from 800 to $1,100\text{ cm}^{-1}$, using a demountable Specac[®] ZnSe window cell /1/ with a path length of 0.025 mm (optical permeance $500 - 20,000\text{ cm}^{-1}$). The spectrometer was an FTIR Perkin-Elmer Mod 2000. Two series of descending concentrations of uranyl nitrate in solution were measured: a) uranyl nitrate dissolved in H_2O and b) uranyl nitrate dissolved in D_2O . The start concentration of both series was 1 mol/L .

Fig. 2 shows the series of IR spectra of uranyl nitrate dissolved in H_2O . The weak uranyl stretching vibration is visible at 961.1 cm^{-1} . But the uranyl nitrate spectra are noticeably superimposed by the H_2O spectrum. Furthermore, due to the high IR absorption of H_2O , the baseline drifts to zero transmittance at lower wave numbers. Below the concentration of $3 \cdot 10^{-2}\text{ mol/L}$, the uranyl stretching vibration is not longer detectable.

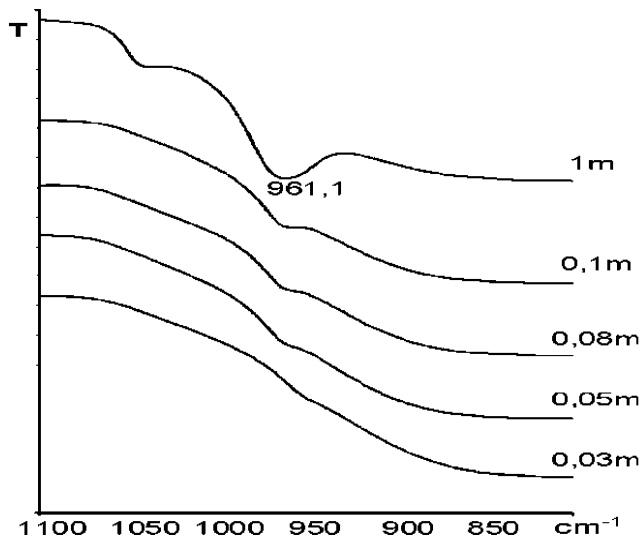


Fig. 2: Series of FTIR spectra of uranyl nitrate dissolved in H_2O (descending concentration, shifted along the y-axis)

Fig.3 shows the comparable series of IR spectra of uranyl nitrate dissolved in D_2O . The enrichment of deuterium was $>98\%$. Affected by the influence of D_2O , the uranyl stretching vibration shifted to the lower wave number at 953.6 cm^{-1} . However, in comparison with the H_2O solution, the uranyl stretching vibration was more pronounced. Furthermore, the sensitivity was much improved in D_2O , and the uranyl stretching vibration was clearly detectable even to $5 \cdot 10^{-3}\text{ mol/L}$. The sensitivity improved by a factor of >10 compared with measurement in H_2O .

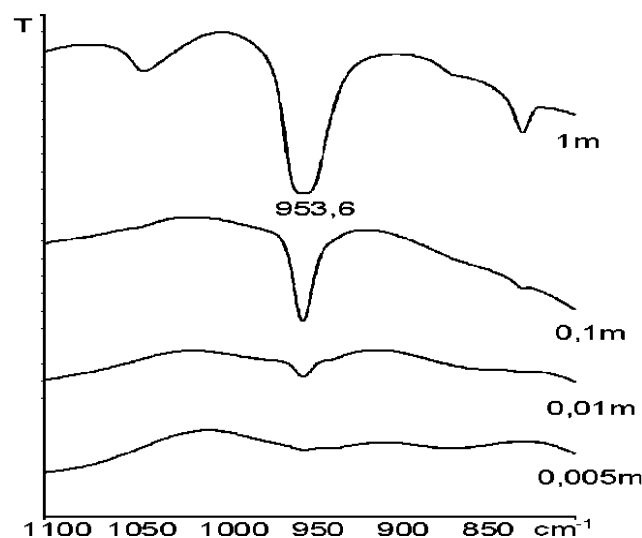


Fig. 3 : Series of FTIR spectra of uranyl nitrate dissolved in D_2O (descending concentration, shifted along the y-axis)

Reference

/1/ Firmenschrift: IR-Spektrometierzubehör für Dispersive und FTIR-Geräte; L.O.T.-Oriel, Darmstadt 10/2000, p. 5-8

LASER INDUCED BREAKDOWN DETECTION OF COLLOIDS

C. Walther, G. Geipel

The uncompressed laser pulses of a femtosecond laser system were used to get breakdown effects on colloids. Using a fast CCD camera we studied the time behavior of the plasma.

Colloids play an important role in the transport of pollutants in the environment. Harmful substances can undergo transport over large distances if bound to aerosols or colloids in aqueous surrounding. One example is the migration of the normally insoluble Pu(IV) at unexpected rates over several miles at the Nevada test site /1/.

For long-term safety assessments of waste disposal sites, it is crucial to know about the amounts, size distributions and chemical composition of colloids in the ground water. Standard methods as light scattering (PCS) can be applied for high concentrations and large sizes of particles. However, colloids smaller than 50 nm in size are detected with very low efficiency. The laser induced breakdown detection (LIBD) can fill this gap. Particles as small as 5 nm are detected down to concentrations below 1 ppt. Developed for the in situ control of process waters in the semi-conductor production, the method was used in a rather phenomenological manner. For the more advanced requirements defined above a deeper understanding of the underlying physical processes is essential.

A pulsed laser is focused into the (liquid) media to be investigated. At power densities of some 10^{10} W/cm² a dielectric breakdown occurs, i.e. the material is separated into electrons and positively charged ions - a plasma is created. However the threshold of this process depends strongly on the phase state of the substance. For solids plasma creation starts at power densities much lower than in the liquid phase. For particle detection the power density is chosen such, that no breakdown occurs in pure water, but as soon as a particle moves into the focal region the threshold for solids applies and a plasma is ignited, which can be detected by observing the emitted light and/or the shock wave created by the rapid plasma expansion. Particle concentrations can hence be measured by simply counting the relative frequency of breakdowns at a fixed laser-pulse repetition rate.

The whole process can be subdivided into two successive sequences: The plasma ignition and the following plasma heating and propagation. The former process is well understood and can be described by multi photon absorption leading to a few seed electrons which are accelerated in the laser (electric) field by inverse bremsstrahlung. These fast electrons (up to several 100 eV) create additional electrons via collisions with neutral atoms and hence the electron (and ion) density increases avalanche like within fractions of ns.

The heating and propagation of the plasma plume depends strongly on the pulse length of the laser and is investigated by observing the (optical) plasma emission with a ultrafast CCD camera (time resolution 250 ps). When the plasma is created by a 180 ps pulse of a Ti:Sa laser, optical emission is rather weak and ceases completely after some 7 ns. If the 30 ns pulse ($1/e^2$) of a Nd:YAG laser is used for plasma creation heating is much more effective, because the plasma creation happens within the first ns of the pulse, and the later

part of the pulse is absorbed by the plasma (which can be observed directly by use of two photodiodes in front and behind the plasma, see Fig.1).

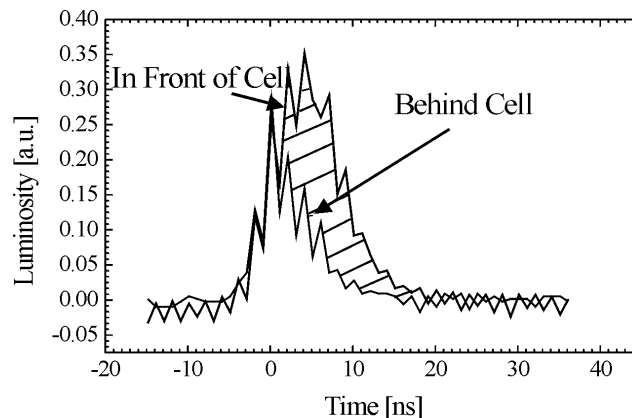


Fig. 1: Detection of laser pulse absorption by the plasma

In consequence emission is much brighter and is observed for up to 120ns after ignition. The diameter of the plasma plume typically reaches 60 μ m after 40–80 ns. While directly after formation the plume exhibits spherical shape, it is elongated towards the laser beam, because with increasing electron density the plasma becomes opaque for the laser light and only the part of the plume turned towards the laser is heated further (Fig. 2).

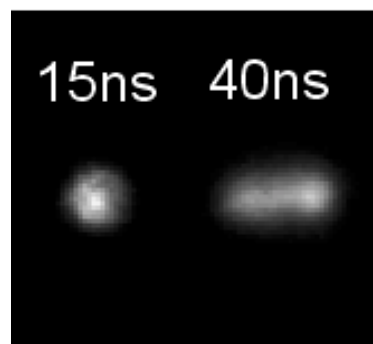


Fig. 2: Expansion of the plasma with time

Later on the plasma collapses and the energy release into the surrounding water leads to formation of gas bubbles which expand at sonic speed and are observed up to 250 μ s after plasma ignition.

This process is important for colloid detection in a twofold manner. First, bubble formation limits the maximum repetition rate of the laser and therefore the time required for getting sufficient statistics. Second, the acoustic wave is suited very well for detection of the breakdown event, even when - in the case of ps laser-pulses - the optical emission is too weak to be detected. In continuation of this work material dependencies of the optical emission and the heating processes are to be investigated.

References

- /1/ Honeyman; Nature **397**, 23-24 (1999)
- /2/ Scherbaum, K., Kim, J.I.; Appl. Phys. B **63**, 299-306 (1996)

THE USE OF DEFLOCCULANTS AND SURFACTANTS TO STABILIZE CONCRETE SUSPENSIONS FOR THE PREPARATION OF ALPHA-SOURCES

C. Nebelung, B. Barz

The direct α -spectrometry of thin large area concrete sources is a fast method of determining actinide activities of ≥ 0.02 Bq/g [1]. Stable concrete suspensions are required to prepare of homogenous sources. The stability of suspensions is measured by the streaming potential with a particle charge detector (PCD).

Experimental

The thin (0.6 - 6.0 μm) and large (314 mm^2) α -sources for direct α -spectrometry are prepared by spraying of concrete suspensions onto plates and then drying them. To obtain homogeneous thin sources, the agglomeration of particles during this process has to be prevented by deflocculants and surfactants. The stability of a suspension depends on the particle charge in the electrochemical double layer. This particle charge can be measured by the relative movement of the solid and the liquid phase. By generating this movement by means of a drive-out piston in the measuring cylinder in the PCD, a part of the diffuse layer of the particles is sheared off. The so-called zeta or PCD potential [2] can be measured at the shear plane. If this potential is near zero, the suspension begins to agglomerate.

Results

Some deflocculants shift the PCD potential and thus stabilize the suspension. Fig. 1 shows the titration of a concrete suspension (440 mg / 15 mL) by various deflocculants (10 g/L). As one can see, the suspension becomes very stable after the addition of 1.7 to 2.0 mL of the deflocculant solutions.

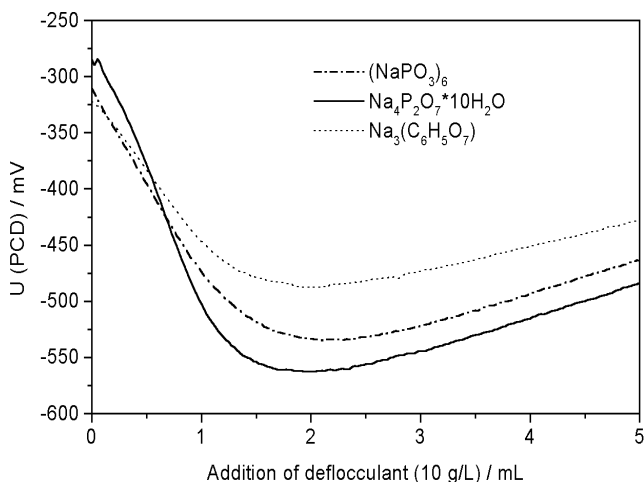


Fig. 1: Influence of deflocculants on the PCD potential of concrete suspensions

Some surfactants were tested whether they permitted the wetting the plate by the concrete suspension using the most efficient deflocculant $\text{Na}_4\text{P}_2\text{O}_7 \cdot 10\text{H}_2\text{O}$. Fig. 2 shows that the PCD potential was near zero if the cation active surfactant Hyamin is used. All other surfactants made the PCD potential more negative and thus stabilized the concrete suspension.

Fig. 3 shows that the higher the CaCO_3 content in the concrete, the more $\text{Na}_4\text{P}_2\text{O}_7 \cdot 10\text{H}_2\text{O}$ is required to reach the minimum of the PCD potential, i.e. to obtain stable suspensions.

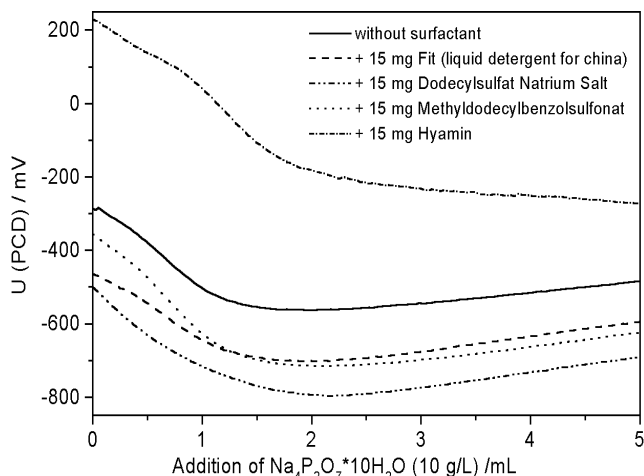


Fig. 2: Variation of the PCD potential of the RCNS concrete suspension containing various surfactants by titration with $\text{Na}_4\text{P}_2\text{O}_7 \cdot 10\text{H}_2\text{O}$ (RCNS = Rossendorf radiochemical laboratory)

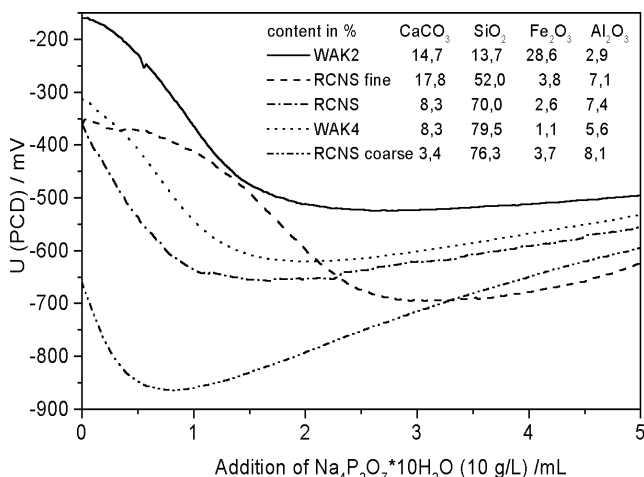


Fig. 3: Titration of various concrete samples with $\text{Na}_4\text{P}_2\text{O}_7 \cdot 10\text{H}_2\text{O}$ (WAK = reprocessing plant Karlsruhe)

Acknowledgment

This work was supported by the Bundesministerium für Bildung und Forschung (BMBF) under contract number 02 S 7768/6.

References

- 1/ Nebelung, C., Nitsche, H. *Stilllegung und Rückbau: Direktmessung alpha-aktiver Nuklide in Bauschutt zur Freigabeentscheidung*, Schlußbericht BMBF Fördervorhaben 02 S 7655 (1999)
- 2/ Müller, R.H., *Zetapotential und Partikelladung in der Laborpraxis*. Wissenschaftliche Verlagsgesellschaft mbH Stuttgart, Band 37, 1996

MINIMIZING OF THE BACKGROUND SPECTRUM OF A GRID IONIZATION CHAMBER

C. Nebelung

Alpha-spectra of sources with diameters of 200 mm can be measured with a grid ionization chamber (GIC). The application of this device is the best way for direct alpha spectrometry of actinides without chemical separation and concentration in the region of the clearance levels. Its accuracy is determined by its background spectrum.

The GIC from Münchner Apparatebau (mab) /1/ is used for the direct measurement of actinides in thin (0.6 - 6 μm) and large (314 cm^2) concrete samples /2/. The detection limit depends on the background counts of the device. Two devices are used for the measurements of alpha spectra. The background level in the newer GIC was increasing during the operation time of 6 years. The older GIC shows a constant low background effect at the same working conditions with the same specimens.

Fig. 1 presents the background spectra versus the lifetime. The ^{210}Po peak is increasing remarkably within a period of 4 years. ^{210}Po is a daughter product of natural uranium with a half-life period of 138 d which is built-up in the course of time.

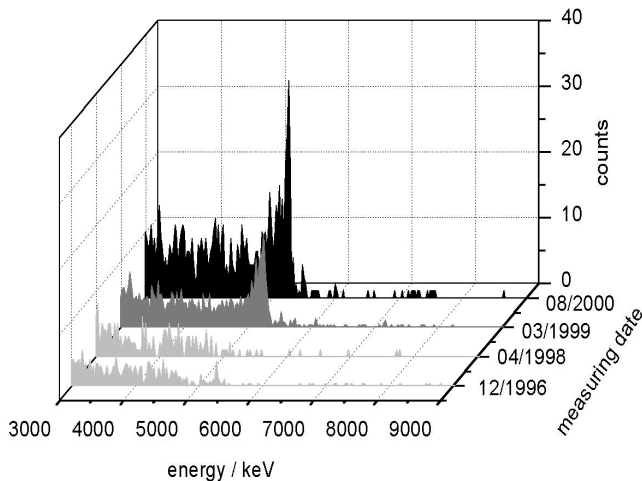


Fig. 1: Development of the alpha background spectrum of a GIC within 4 years

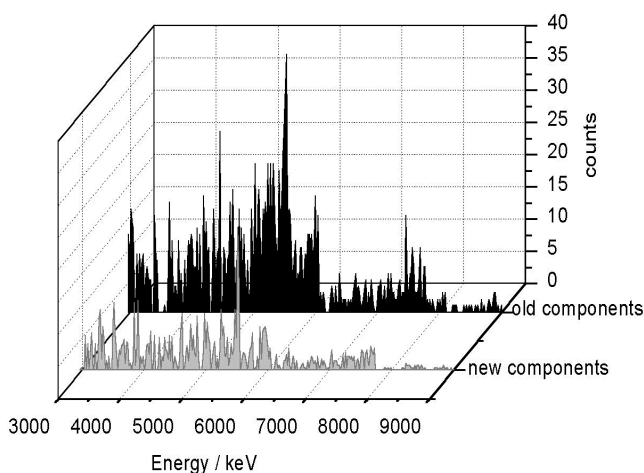


Fig. 2: Spectra of the plastic components of the GIC

After opening the GIC with the high background, the alpha-spectra of all components were measured in the elder GIC with the low background in order to find ^{238}U , the source of the radon and polonium generation. The metallic components, measured after the decay of the long-lived daughter ^{210}Po , have alpha-spectra

near the background spectrum. The plastic components (3 acrylic cylinders with microcracks and 3 teflon pieces) seemed to be the sources of the high background, because they show ^{238}U and its daughters in the spectra measured after the time of the ^{210}Po decay.

In Fig. 2 alpha spectra of the old plastic components and new components from mab are compared. The activities were caused by ^{238}U and its daughters. They are given in Tab. 1.

Nuclide	Half-life period years	Activity / mBq	
		6 old components	6 new components
^{238}U	$4.468 \cdot 10^9$	1.8	0.2
^{230}Th	$7.538 \cdot 10^4$	2.1	0.4
$^{234}\text{U} / ^{226}\text{Ra}$	$2.455 \cdot 10^5 / 1600$	1.8	0.4
^{222}Rn	0.01	6.5	1.7
^{218}Po	$5.9 \cdot 10^{-6}$	3.2	0.9
^{214}Po	$3.1 \cdot 10^{-10}$	1.7	0.3
^{210}Po	0.379	4.2	0.7

Tab. 1: Content of ^{238}U and its daughters in the plastic components

The content of ^{238}U and its daughters is lower in the new components but still too high for low-level measurements in an alpha-chamber. We were searching for alternative electrically insulating materials (various brands of PVC, acrylic, teflon and ceramics). However, no significant reduction of the background levels could be reached (^{222}Rn activities, for instance, varied between 1.3 to 9.5 mBq). As a compromise we will use the material of the still lowest background in the future (acrylic material after thermal treatment).

Acknowledgment

This work was supported by the Bundesministerium für Bildung und Forschung of the Federal Republic of Germany under the contract number 02 S 7768/6.

References

- /1/ Hötzl, H., Winkler, R.; Nucl. Instr. Meth. **150**, 177 (1978)
- /2/ Nebelung, C., Nitsche, H.; *Stilllegung und Rückbau: Direktmessung alpha-aktiver Nuklide in Bauschutt zur Freigabeentscheidung*, Schlußbericht BMBF Fördervorhaben 02 S 7655 (1999)

Chemistry of the Heaviest Elements

A FIRST ATTEMPT TO CHEMICALLY IDENTIFY ELEMENT 112

A.B. Yakushev¹, G.V. Buklanov¹, M.L. Chelnokov¹, V.I. Chepigin¹, S.N. Dmitriev¹, V.A. Gorshkov¹, V.Ya. Lebedev¹, O.N. Malyshev¹, Yu.Ts. Oganessian¹, A.G. Popeko¹, E.A. Sokol¹, S.N. Timokhin¹, V.M. Vasko¹, A.V. Yeremin¹, I. Zvara¹, S. Hübener, A. Türler²

¹Flerov Laboratory of Nuclear Reactions, Dubna, Russia

²Paul Scherrer Institut, Villigen, Switzerland

A first experiment to chemically identify a previously discovered long-lived superheavy isotope of element 112 was conducted at the U-400 cyclotron of Flerov Laboratory of Nuclear Reactions, Dubna. Even though the experiment reached a sensitivity of a few picobarns, no decay that could be attributed to an isotope of element 112 was observed.

Introduction

The relatively long half-lives of isotopes of superheavy elements obtained in ⁴⁸Ca induced reactions allow for the first time to study their chemical properties. The chemical identification of the proton number is very important, since none of the members of the observed decay chains are known. The nuclide ²⁸³112 ($T_{1/2} \approx 3$ min) can be produced in the reaction ²³⁸U(⁴⁸Ca, 3n) with a cross section of about 5 pb /1/. Element 112 (E112) should belong to group 12 of the periodic table like Zn, Cd, and Hg and exhibit some unique chemical properties. Some theoretical works predict, that E112 is very volatile and chemically inert and resembles thus more Rn than Hg /2/. Two different approaches are thus necessary. In a first step we developed a separation and detection method for Hg, expecting E112 to behave similarly and thus to strongly adsorb on some metal surfaces due to inter-metallic bonds.

Experimental

Tests with both long- and short-lived Hg isotopes showed, that an almost quantitative transport through a 30 m long teflon capillary is possible at room temperature. Next, the chemisorption of Hg on various metal surfaces in pure He was studied at room temperature or slightly below it, in order to deposit E112 directly on metal coated Si detector surfaces. Adsorption of Hg was quantitative on Au, Pt or Pd. The rate of chemisorption was highest on Au. Only 1 cm² of Au or Pd surface sufficed for quantitative chemisorption of Hg from He at room temperature and flow rates up to 1 L/min. The adsorption yield of Hg on Au at 243 K decreased to 50%. For the experiments with short-lived Hg isotopes at the U-400 cyclotron a flow-through detection chamber was constructed with a pair of square (2x2 cm) PIPS (passivated ion-implanted planar silicon) detectors, which were coated with about 40 µg/cm² of Au or Pd. The distance between the detectors was 1 mm, which resulted in a detection efficiency of 80% at a resolution of about 100 keV for 6 MeV α-particles. The residence time of the gas in each detector chamber was only a fraction of a second. Several chambers were connected in series with short PTFE capillaries.

A first attempt to chemically identify E112 was performed at the Dubna U-400 cyclotron in January 2000. A 2-mg/cm² ²³⁸U₃O₈ target containing 100 µg of natural Nd on a 2 µm HAVAR foil (which served also as vacuum window) was irradiated with 6.85×10^{17} ⁴⁸Ca ions ($E_{lab} = 230-244$ MeV). Recoils were thermalized in pure He at atmospheric pressure and transported through a 25 m long PTFE capillary to the

detection apparatus. The transport time was 25 s at a gas flow rate of 500 mL/min. Eight detection chambers were connected in series. Detectors 1 through 6 were coated with Au, the last two chambers contained Pd coated detectors. The chambers were positioned inside an assemblage of 84 ³He-filled detectors (in a moderator) to register neutrons from spontaneous fission decays. The detection efficiency for a single neutron was about 50%. Decay events in the fission fragment energy range triggered the measurement of prompt neutrons, which lasted 128 µs. Neutrons were detected in this period with a time resolution of 1 µs. The α-decay count rate in a single detector ($E_{\alpha} > 6$ MeV) was 4.5 min⁻¹. All peaks in the spectra were identified and attributed to the decay of ^{211,220}Rn and its descendants.

Results and Discussion

In our experiment no spontaneous fission events were observed. If the efficiencies measured for Hg held for E112, we could have expected detection of some 3 events based on a 5 pb production cross section. This experiment undoubtedly showed the possibility of chemical identification of nuclei produced with picobarn cross sections. The experiment does not give an unambiguous answer about physical and chemical properties of element 112. In a next step, we plan to increase the beam dose by at least a factor of two and to upgrade our detector system to measure α-decays and SF events in the gas exiting the chambers with the PIPS detectors using a special ionization chamber.

References

- /1/ Oganessian, Yu.Ts. et al., Eur. Phys. J. **A5**, 63 (1999)
- /2/ Pitzer, K. S., J. Chem. Phys. **63**, 1032 (1975)

ATTEMPT TO CHARACTERIZE ELEMENTAL LAWRENCIUM BY THERMOCHROMATOGRAPHY

S. Taut, S. Hübener, A. Vahle, B. Eichler¹, A. Türler¹, D.T. Jost¹, H.W. Gäggeler¹, C.A. Laue², K.E. Gregorich²
¹ Labor für Radio- und Umweltchemie, Paul Scherrer Institut Villigen (CH)
² Lawrence Berkeley National Laboratory (USA)

²⁶¹Lr was produced in the ²⁴⁹Bk(¹⁸O, α 2n)²⁶¹Lr reaction. In the thermochromatographic fraction of the metallic trivalent actinides on a tantalum column one spontaneous fission event which might be attributed to a ²⁶¹Lr decay was observed. This implies a production cross section of 2 nb with an upper limit of 7.5 nb (5 % error probability).

Experimental

A target containing 317 $\mu\text{g}/\text{cm}^2$ of ²⁴⁹Bk and 353 $\mu\text{g}/\text{cm}^2$ of ²⁴⁹Cf was irradiated for 123 min with $2.1 \cdot 10^{16}$ ¹⁸O ions at the PSI Philips cyclotron. A beam energy of 93 MeV was used, assuming that the α 2n de-excitation channel has the cross section maximum at the same energy as the 4n channel /1/. A Be catcher foil was mounted behind the target to collect the recoiling nuclear reaction products. This foil was used as the thermochromatography sample without further preparation.

We used the same thermochromatography setup as in /2/. In contrast to /2/, Ta served as the column metal as actinides are adsorbed on it at higher temperatures than on Nb, resulting in a narrower chromatographic peak. The temperature maximum in the column was 1920 K, the He carrier gas flow was 50 mL/min, and the chromatography time was 15 min.

Results and Discussion

The alpha spectroscopic analysis of the column started 51 minutes after the end of bombardment. Within 195 min only one spontaneous fission (108 MeV) was detected (life time 78 min).

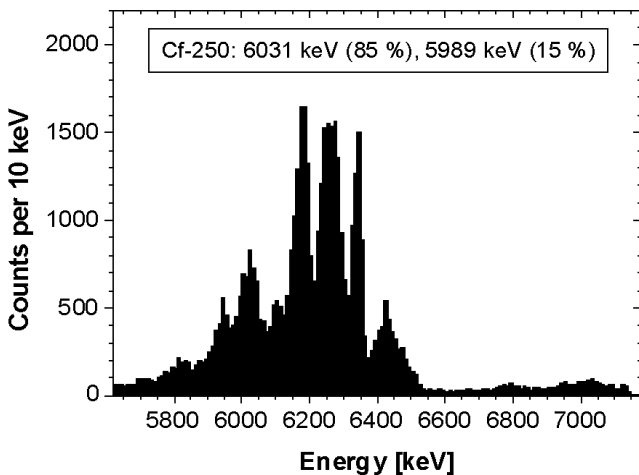


Fig. 1: Alpha spectrum of the high temperature column part acquired within 56 h directly after thermochromatography

Fig. 1 and Fig. 2 show alpha spectra of the trivalent actinide fraction taken at various times. The decontamination factors of ²⁵⁰Cf and ^{252/253}Es in the trivalent actinide fraction were calculated from these spectra, assuming these nuclides to be produced with the experimental cross sections from /3,4/. Es is separated by a factor of 1000, but Cf only by a factor of 5. The much lower Cf decontamination is possibly caused by the trivalency of Cf within the Be catcher foil bulk metal. The difference between this result and the one reported in /2/ might have been caused by a

slower evaporation kinetics from Be in comparison to that from Zr used in /2/.

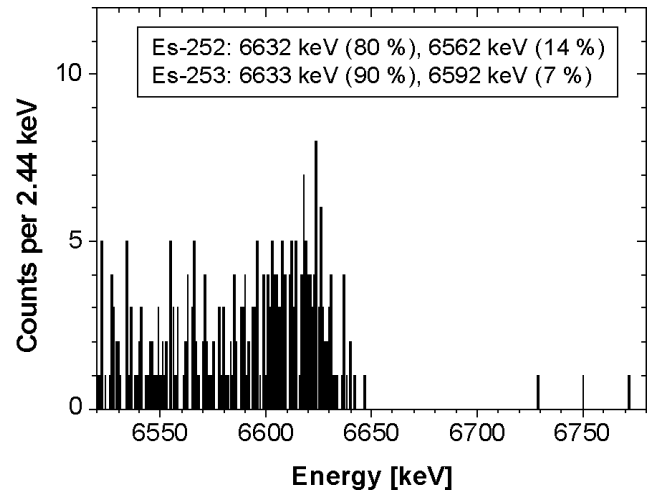


Fig. 2: ^{252/253}Es region of an alpha spectrum of the high temperature column part acquired within 168 h 50 days after the thermochromatography

The spontaneous fission background in the sample which produced the 78 min event was 0.0037 min^{-1} . Assuming that ²⁵⁶Fm (main source of fission events) is separated like Es, this would be consistent with the decontamination factor of Es given above.

A statistical analysis showed that the spontaneous fission event might with 77 % probability have been caused by a ²⁶¹Lr decay while there is 23 % probability that it is background. Thus, it cannot be unambiguously assigned to ²⁶¹Lr.

The maximum probability production cross section of ²⁶¹Lr was calculated from our experimental data to be 2 nb. Its upper limit (5 % error probability) is 7.5 nb. Both values are consistent with the 8-10 nb cross section of the ²⁶⁰Lr formation in the α 3n de-excitation channel /4,5/.

Acknowledgments

We are indebted to US DOE for making the ²⁴⁹Bk available to us through the transplutonium element program at ORNL.

References

- /1/ Zimmermann, H.P., PhD thesis, Report GSI 92-04 (1992), p. 90
- /2/ Taut, S. et al., Report FZR-285, p. 83; Vahle, A. et al., same report p. 81
- /3/ Lee, D. et al., Phys. Rev. C **27**, 2656 (1983)
- /4/ Gäggeler, H. et al., Report EIR TM-44-87-04 (1987)
- /5/ Hoffman, D.C. et al., J. Radioanal. Nucl. Chem. (Articles) **124**, 135 (1988)

ADSORPTION STUDIES WITH HOMOLOGS OF SUPERHEAVY ELEMENTS

A. Vahle, S. Hübener, S. Taut, E. Jäger¹, M. Schädel¹, B. Schausten¹, B. Eichler²
¹GSI Darmstadt, ²PSI Villigen

The adsorption of the SHE homologs Tl, Pb, Bi, and Po on Ti, V, Nb, Ta, Mo, and Ni was studied by thermochromatography.

Introduction

In preparation of chemical studies with superheavy elements around $Z = 114$ the adsorption behavior of these elements and their lighter homologs on different metals has been predicted based on (semi-) empirical models and extrapolations (see e.g. /1, 2/).

Adsorption studies with SHE homologs were performed on various metals, especially metals of group 10 and 11 (see e.g. /3/). The experimental results mainly confirmed the calculated data, but in a few cases great differences between predicted and experimental data were observed. Therefore, the adsorption behavior of SHE homologs on further metals is of great interest to prove the validity of the predictions.

In the present work the adsorption of Tl, Pb, Bi, and Po on the group 5 metals V, Nb, Ta as well as on Mo, Ni, Ti has been studied by thermochromatography. Experimental data have been compared to predictions.

Experimental

Bi, Pb, and Tl isotopes were produced by bombarding an ^{nat}Ir target (0.3 mg/cm²) with a ¹²C beam (90 MeV on target) at the GSI UNILAC. The recoil nuclei of the nuclear reactions were caught in catcher foils made of 9 μm Cu. These foils were preconditioned by heating them up to 800°C for 15 min in a 100 mL/min gas flow of N₂/H₂ (ratio 90:10). Hydrogen was used to reduce the surface layer of Cu oxide to Cu. The catcher foils served as the thermochromatographic samples without further preparation.

²¹⁰Po was obtained by neutron activation of ^{nat}Bi at the TRIGA Mainz reactor and subsequent decay of the produced ²¹⁰Bi. Po was separated from Bi by thermochromatography according to /4/ and deposited on a Ta column. One cm pieces of the Ta column with the adsorbed Po were used as samples for the thermochromatography experiments.

The experimental setup was similar to that described in detail in /5/. Thermochromatographic columns were made from 20 - 25 μm thick Ti, V, Nb, Ta, Mo, and Ni foils. Quartz glass columns served as support tubes. The inside of these tubes was lined with thin Ta foils in order to adsorb the oxygen emitted from the quartz glass at high temperatures. A carrier gas flow of 25 or 50 mL/min He was established. The starting temperature was varied between 700 and 950°C. After 15 or 30 min thermochromatography time the nuclide distribution along the column was determined by γ- or α-spectroscopy of 1 cm column pieces.

Results

Po was nearly completely (> 98 %) volatilized from the Ta foils. Tl, Pb, and Bi partly remained in the catcher foils.

Thermochemical data were determined by two methods: (1) Adsorption entropy and enthalpy were calculated according to /6/ with $\tau_0 = 10^{-12}$ s. (2) $\Delta S^{\circ}_{\text{ads}}$ and $\Delta H^{\circ}_{\text{ads}}$ were determined according to /7/ using an individual τ_0 for each adsorpt-adsorbent combination.

As an example, predicted and experimentally determined adsorption enthalpies for Tl on several adsorbent metals are depicted in Fig. 1.

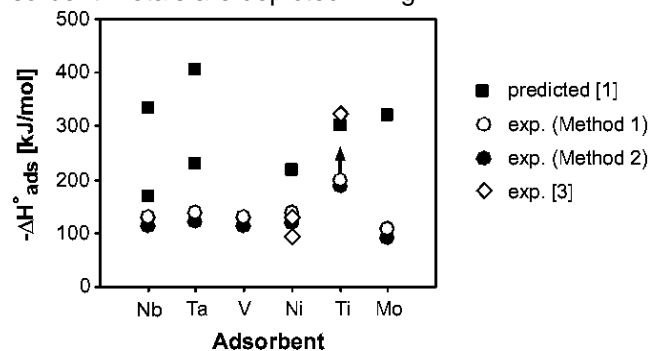


Fig. 1: Adsorption enthalpies of Tl on several metals.

The two different values on Nb and Ta were obtained by different models.

The main results of our adsorption studies can be summarized as follows:

- Irrespective of the used method, significantly less negative adsorption enthalpies were obtained than predicted by /1/.
- Our results correspond quite well with the experimental data given in /3/.
- As predicted, less negative or similar adsorption enthalpies were found for all studied elements on Nb compared to Ni, Ta, and Ti. However, the least negative adsorption enthalpies of all studied elements were surprisingly obtained on Mo. This might be an erroneous result caused by an oxide layer on the column surface which could not be removed by heating in a He flow.
- On titanium, Tl and Pb were deposited in the starting position and only an upper limit of $\Delta H^{\circ}_{\text{ads}}$ can be given. On all other adsorbent metals, less negative adsorption enthalpies were obtained for Tl than for Pb.

Acknowledgments

This work was performed in cooperation with the GSI. The preparation of the Ir target by the "Targetlabor" of GSI is gratefully acknowledged. We thank the staff of the TRIGA Mainz reactor for the irradiation of Bi.

References

- /1/ Roßbach, H. et al., Report ZfK-527 (1984)
- /2/ Eichler, B., Report PSI 00-09 (2000)
- /3/ Eichler, B. et al., Dubna Report P12-81-717 (1981)
- /4/ Hübener, S. et al., Report ZfK-510 (1983), p.123
- /5/ Taut, S. et al., Radiochim. Acta **78**, 33 (1997)
- /6/ Eichler, B. et al., Radiochim. Acta **30**, 233 (1982)
- /7/ Taut, S. et al., submitted to J. Chem. Phys.

A GEOMETRIC MODEL FOR DIRECT CONDENSATION

A. Vahle, R. Dressler¹

¹Institut für Kern- und Hadronenphysik

A geometric model is proposed to estimate the deposition yield in gas chromatographic experiments using direct condensation as the deposition mode.

Direct condensation has been established as a well-suited deposition mode for high temperature gas chromatography experiments. Unfortunately, there is no simple model of this process in the literature until now. The model proposed here neglects the exact flow pattern near the deposition foil as well as diffusion processes which might influence the yield. A flow pattern of an underexpanded supersonic jet is formed during the efflux of the reaction gas into a low pressure region, e.g. the ROMA device. Such jets are characterized by a shock cell, the so-called zone of silence, in which the flow velocity is much greater than the local speed of sound and a boundary region between the jet and the ambient gas, in which the gas moves slightly faster than at the exit (see e.g. /1, 2/). The zone of silence consists of a barrel-shaped shock surrounding the jet and a nearly planar normal shock, or Mach disk, downstream. Pressure and temperature decrease dramatically in the zone of silence, whereas the mass flow rate is nearly unchanged. Behind the Mach disk the flow velocity drops down to a subsonic flow. Good conditions for direct condensation of chemical compounds exist within the zone of silence.

The radius of the Mach disk is $r_{\text{mach}} = \frac{0.67 \text{ bar} \cdot r_{\text{in}}}{\sqrt{P_0 P_{\text{ROMA}}}}$

and its distance from the outlet is $d_{\text{mach}} = 4 r_{\text{mach}}$

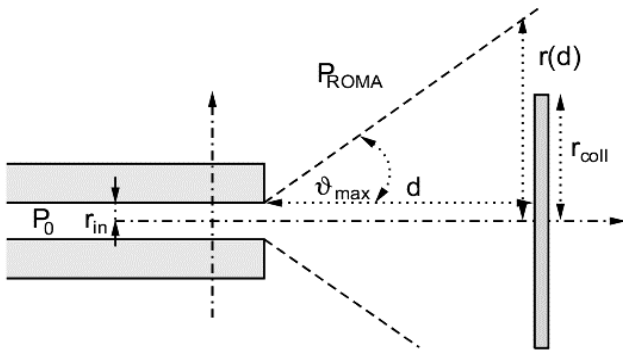


Fig. 1: Geometric model for the evaluation of the deposition yield (symbols are explained below)

A simple geometrical model (Fig. 1) is used to estimate the deposition yield. This model is based on four assumptions: 1) The gas velocity v_{\parallel} in the direction of the axis of the chromatography column after passing the end of the column is constant. 2) The flow pattern is a sharp cone. The axis of the cone has the same direction as the axis of the chromatography column; the cone has an opening angle of $2\vartheta_{\text{max}}$. 3) The gas density in a disk perpendicular to the axis of the flow cone is constant. 4) The gas flow perpendicular to the axis of the cone has a constant velocity.

The yield ε is defined by $\varepsilon = \frac{\dot{m}_{\text{coll}}}{\dot{m}_{\text{out}}}$. The mass flow

rates \dot{m}_{coll} and \dot{m}_{out} can be calculated by integrating the local gas density $\rho(d)$ over the collection and the outlet cross section, respectively.

This leads to $\dot{m}_{\text{out}} = \pi r_{\text{in}}^2 v_{\parallel} \rho_L$

$$\dot{m}_{\text{coll}} = \int_0^{r_{\text{coll}}} 2\pi r v_{\parallel} \rho(d) dr$$

The mass flow rate is constant. $\rho(d)$ can be calculated by

$$\rho(d) = \left(\frac{r_{\text{out}}}{r(d)} \right)^2 \rho_L$$

The exit velocity v_{\parallel} of the gas for $P_{\text{ROMA}} < P_0$ is given by

$$v_{\parallel} = \sqrt{\kappa \frac{P_L}{\rho_L}}$$

and the velocity component v_{\perp} perpendicular to the direction of the out flow can be calculated by

$$v_{\perp} = \sqrt{\frac{2\kappa}{\kappa-1} \frac{P_L}{\rho_L} \left[1 - \left(\frac{P_{\text{ROMA}}}{P_L} \right)^{\frac{\kappa-1}{\kappa}} \right]}$$

The opening angle ϑ_{max} of the flow cone can be calculated by $\tan(\vartheta_{\text{max}}) = \frac{v_{\perp}}{v_{\parallel}}$

Combining these formulas yields

$$\dot{m}_{\text{coll}} = \begin{cases} \pi r_{\text{in}}^2 v_{\parallel} \rho_L & \text{for } r(d) < r_{\text{coll}} \\ \pi \left(\frac{r_{\text{coll}}}{r(d)} \right)^2 r_{\text{in}}^2 v_{\parallel} \rho_L & \text{for } r(d) > r_{\text{coll}} \end{cases}$$

for the collected mass flow.

Finally, the yield ε can be obtained by

$$\varepsilon = \begin{cases} \frac{\kappa-1}{2} \left(\frac{r_{\text{coll}}}{d} \right)^2 \left[1 - \left(\frac{P_{\text{ROMA}}}{P_L} \right)^{\frac{\kappa-1}{\kappa}} \right]^{-1} & \text{for } r(d) > r_{\text{coll}} \\ 1 & \text{for } r(d) < r_{\text{coll}} \end{cases}$$

Experimental data (ε , optimum d , spot diameter) could be reproduced well with the proposed geometrical model /3/. For instance, the spots observed experimentally at the pressure optimum can be explained by the zone of silence. The Mach disk has a diameter of 3.3 mm close to the observed diameter of about 3 mm.

Acknowledgments

This work was performed in cooperation with the GSI.

References

- /1/ Trigg, G.L. (ed.): *Encyclopedia of Applied Physics*, Vol. 4, VCH, Weinheim 1992, pp. 43
- /2/ Tejada, G. et al., *Phys. Rev. Lett.* **76**, 34 (1996)
- /3/ Vahle, A. et al., submitted to *Nucl. Instr. Meth.*

Symbols: m_{coll} = mass collected on the catcher foil, m_{out} = mass flowing out of the tip of the chromatography column (cc), r_{in} = inner radius at the end of the cc, $\rho(d)$ = density at the distance d from the outlet, r_{coll} = radius of the catcher foil, d = distance between cc and catcher foil, $r(d)$ = diameter of the cone = $d \tan(\vartheta_{\text{max}})$, κ = POISSON coefficient = C_p / C_v , P_0 = back pressure in the cc, P_{ROMA} = ambient pressure in the ROMA device, ρ_0 = gas density at P_0 , P_L = Laval pressure = $P_0 \left(\frac{2}{\kappa+1} \right)^{\frac{\kappa}{\kappa-1}}$, ρ_L = Laval density = $\rho_0 \left(\frac{2}{\kappa+1} \right)^{\frac{1}{\kappa-1}}$

SEMI-EMPIRICAL CALCULATION OF METAL ADSORPTION ENTROPIES AND ENTHALPIES

S. Taut, S. Hübener, B. Eichler¹

¹ Labor für Radio- und Umweltchemie, Paul Scherrer Institut Villigen (CH)

Metal adsorption entropies can be calculated using a statistical thermodynamics model, an empirical correlation between force constants and adsorption enthalpies, and the long known compensation effect between τ_0 and the adsorption enthalpy.

Symbols

A	molar standard surface area of adsorbed substance
d	inner column diameter
f	force constant
f_{hindr}	hindrance factor
g	temperature gradient along the chromatography column
h	Planck constant
J	electron system magnetic quantum number
k	Boltzmann constant
m	mass of adsorpt atom
q_{2trans}	partition function of two-dim. translation
R	gas constant
t	chromatography time
T	temperature
T_0	ambient temperature
T_{ads}	adsorption temperature
T_{start}	temperature at starting position
u_0	carrier gas speed at ambient temperature T_0
V	molar standard volume of substance to be adsorbed
v	adsorpt vibration frequency normal to surface
τ_0	frequency factor in the FRENKEL equation
ΔH_{ads}^0	differential molar standard adsorption enthalpy
ΔS_{ads}^0	differential molar standard adsorption entropy

$$f_{hindr} = \frac{q_{2trans,ads,mob}}{q_{2trans,ideal}}$$

It can be calculated from the frequency factor τ_0 of the FRENKEL equation /2/

$$\tau_0 = f_{hindr} \cdot \frac{h}{kT \cdot \left\{ 1 - \exp\left(-\frac{h \cdot v}{kT}\right) \right\}} \cdot \frac{2J_{ads} + 1}{2J_{gas} + 1}$$

and from experimental adsorption entropies with the equation derived above. Thus, the well-known compensation effect between experimental τ_0 and adsorption enthalpy values /4/ can be used to establish a correlation between hindrance factor and adsorption enthalpy with literature adsorption data of lanthanoids and actinoids on bcc metals:

$$\log(f_{hindr}) = 1.79 + 0.0062 \cdot \Delta H_{ads} [kJ/mol]$$

Calculations of Adsorption enthalpies

Adsorption enthalpies can be calculated from thermochromatographic data /5/:

$$t = \frac{T_0}{g \cdot u_0} \cdot \ln \frac{T_{ads}}{T_{start}} - \frac{4 \cdot T_0 \cdot \frac{V}{A} \cdot f_i \cdot \exp\left(\frac{\Delta S_{ads}^0}{R}\right)}{d \cdot g \cdot u_0} \cdot \int_{T_{start}}^{T_{ads}} \frac{1}{T} \cdot \exp\left(\frac{\Delta H_{ads}^0}{R \cdot T}\right) \cdot dT$$

Calculation of Adsorption Entropies

Applying statistical partition functions for both gaseous and adsorbed state /1/ and considering the non-ideal behavior of the two-dimensional adsorpt gas /2/, an expression for the entropy of mobile adsorption was derived:

$$\Delta S_{ads,mob}^0 = \frac{1}{2}R + R \cdot \ln \left\{ \frac{f_{hindr} \cdot A \cdot \left(\frac{2J_{ads} + 1}{2J_{gas} + 1}\right)}{V \cdot \left(\frac{kT \cdot 2\pi \cdot m}{h^2}\right)^{\frac{1}{2}} \cdot \left\{ 1 - \exp\left(-\frac{h \cdot v}{kT}\right) \right\}} \right\}$$

In /3/ was shown that experimental adsorpt stretching frequencies follow the oscillation equation:

$$v = \frac{1}{2\pi} \cdot \sqrt{\frac{f}{m}}$$

An empirical correlation between force constants and adsorption enthalpies was derived from literature data:

$$\log(f [N/cm]) = -1.78 - 0.0036 \cdot \Delta H_{ads} [kJ/mol]$$

The stretching frequency can now be calculated. The hindrance factor considers the non-ideal and ideal translation of the two-dimensional gas on the surface:

As has been shown, the adsorption entropy is not a simple parameter, but a function of the adsorption enthalpy. The program TECRAD /6/ was modified such that its iteration loop for the enthalpy calculation considers the dependence of the adsorption entropy on the adsorption enthalpy.

Acknowledgments

We gratefully acknowledge the support by BMBF, contract 06 DR 824.

References

- /1/ Atkins, P.W.; *Physikalische Chemie*; 2nd edition, Weinheim 1996, p.640
- /2/ De Boer, J.H.; *Advances in Catalysis* **8**, 17 (1956)
- /3/ Astaldi, C. et. al.; *Solid State Commun.* **75**, 847 (1990)
- /4/ Bauer, E.; *Chemisorption Systems*, Woodruff, D. P., King, D.A. (eds.); Elsevier 1984, p.51
- /5/ Eichler, B., Zvara, I.; *Radiochim. Acta* **30**, 233 (1982)
- /6/ Funke, H. et. al.; *Report FZR-43* (1994) p.53

VOLATILITY STUDIES OF ACTINIDE OXIDE HYDROXIDES

S. Hübener, S. Taut, A. Vahle

Uranium trioxide was chosen as a reference material to study the volatility of oxide hydroxides of hexavalent actinides. Some first results of thermochromatographic experiments are interpreted as an indication of surface reactions of $\text{UO}_3/\text{UO}_2(\text{OH})_2$ in the $\text{O}_2\text{-H}_2\text{O}(\text{g})/\text{SiO}_2(\text{s})$ system.

Introduction

The oxidation of PuO_2 to PuO_{2+x} by water and humid oxygen, as recently reported by Haschke et al. /1/, is a new feature of plutonium chemistry with enormous consequences for both industrial applications and the long-term storage of plutonium. For more than 50 years PuO_2 has been recognized to be the highest plutonium oxide. In PuO_{2+x} ($x \leq 0.27$) a considerable portion of the plutonium ions exist as $\text{Pu}(\text{VI})$ which is far more mobile than $\text{Pu}(\text{IV})$. $\text{Pu}(\text{VI})$ is more water soluble than $\text{Pu}(\text{IV})$ and should form an oxide hydroxide which is expected to be volatile at high temperatures as known from the group 6 elements /2/ and uranium /3/. Indeed, already formerly /4/ PuO_2 was found to be volatile in the presence of humid oxygen. The Pu volatility was assigned to $\text{PuO}_3(\text{g})$ and $\text{PuO}_2(\text{OH})_2(\text{g})$. It was found to be very low, e.g., $< 10^{-10}$ bars at 1300 K, which is four orders of magnitude lower than the volatility of uranium. Volatile plutonium oxide species were also reported by Domanov et al. /5/. In thermochromatographic experiments with ^{238}Pu and ^{239}Pu several volatile plutonium species were identified, one of them having a volatility as high as that of OsO_4 . The experimental results were interpreted with the formation of PuO_3 and $\text{PuO}_4(\text{l})$.

These contradictory experimental findings motivated us to study the volatility of oxidic actinide species in humid oxygen by thermochromatography. In a first series of experiments U is studied as a reference element.

Experimental

The experimental setup resembles that used earlier to study molybdenum and tungsten oxide hydroxides /2/. The commercial gradient oven HTM LORA 36 was used. Open tubular quartz glass columns of an inner diameter of 3.5 mm were used. The thermochromatographic samples were prepared from a solution of ^{234}U in 0.01 N HCl. A quartz wool plug was soaked with 100 μL of a solution containing about $3 \cdot 10^{16}$ atoms ^{234}U . The solution was evaporated to dryness. Fuming with nitric acid was three times repeated to remove residual chloride ions. The quartz wool plug loaded with ^{234}U was inserted into the column in the starting position of thermochromatography. To start thermochromatography the carrier gas flow through the column was started. A mixture of helium and oxygen in the ratio 1:1 was used as the carrier gas at a total flow rate of 100 $\text{cm}^3 \text{min}^{-1}$. The carrier gas was moistened by bubbling through water at defined temperatures. To end a thermochromatography experiment the carrier gas flow was interrupted and the column removed from the oven within 10 seconds. Then, the column was cut into 1 cm sections which were leached with hot nitric acid. Thin-layer samples were prepared from the acidic solution by evaporation

on glass disks. The ^{234}U concentration of these samples was determined by alpha spectrometry.

Results and Discussion

Fig. 1 shows as an example a chromatogram at a water vapor pressure of 2 kPa after 30 min chromatography time.

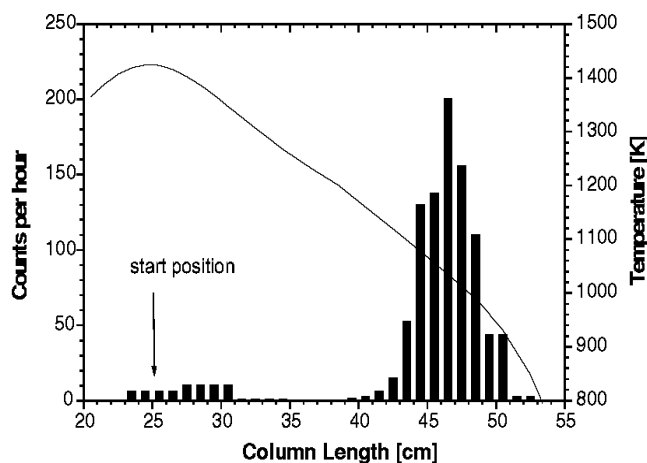


Fig. 1: Thermochromatogram of ^{234}U at a water vapor pressure of 2 kPa.

As can be seen from Fig. 1, the chromatographic peak is relatively broad, which is typical of reaction gas chromatography. The broad peak shape indicates that reaction (1) is the basic reaction of chromatography in the $\text{O}_2\text{-H}_2\text{O}(\text{g})/\text{SiO}_2(\text{s})$ system.



Further evidence in support of this explanation comes from a Monte Carlo simulation. Assuming reaction (1) a chromatogram analogous to Fig. 1 was calculated at a reaction entropy $\Delta S^\circ_{\text{diss.ads}} = -41 \text{ J}/(\text{K} \cdot \text{mol})$ and an enthalpy $\Delta H^\circ_{\text{diss.ads}} = -71.5 \text{ kJ}/\text{mol}$.

References

- /1/ Haschke, J.M., Allen, T.H., Morales, L.A.; *Science* **287**, 285, (2000)
- /2/ Vahle, A. et al.; *Radiochim. Acta* **84**, 43 (1999)
- /3/ Dharwadkar, S.R. et al., in: *Thermodynamics of Nuclear Materials, Vol. II*, IAEA-SM-190/32, p.455 (1974)
- /4/ Krikorian, O.H. et al.; *J. Nucl. Materials* **247**, 161 (1997)
- /5/ Domanov, V.P., Buklanov, G.V., Lobanov, Yu.V.; *Ext. Abstracts 5th Int. Conf. Nuclear and Radiochemistry*, Pontresina, CH, 3.-8.9.2000, Vol. 1, p.93 (2000)

II. PUBLICATIONS, PATENTS, LECTURES AND POSTERS

PUBLICATIONS

Buckau, G., Hooker, P., Moulin, V., Schmeide, K., Maes, A., Warwick, P., Moulin, Ch., Pieri, J., Bryan, N., Carlsen, L., Klotz, D., Trautmann, N.

Main Conclusions of the EC-Humics Project: Effects of Humic Substances on the Migration of Radionuclides: Complexation and Transport of Actinides

In: E.A. Ghabbour, G. Davies (eds.): Humic Substances, Versatile Components of Plants, Soils and Water; The Royal Society of Chemistry (2000) p.235-260

Buckau, G., Hooker, P., Moulin, V., Schmeide, K., Maes, A., Warwick, P., Moulin, Ch., Pieri, J., Bryan, N., Carlsen, L., Klotz, D., Trautmann, N.

Effects of Humic Substances on the Migration of Radionuclides: Complexation and Transport of Actinides

Proceedings of Euradwaste '99: "5th European Commission Conference on Radioactive Waste Management and Disposal and Decommissioning", Luxembourg, 15.-18.11.1999

Report EUR 19143 EN (2000), p.460-463

Bundschuh, T., Knopp, R., Müller, R., Kim, J.I., Neck, V., Fanghänel, Th.

Application of LIBD to the determination of the solubility product of thorium(IV)-colloids

Radiochim. Acta **88**, 625-629 (2000)

Eichler, R., Brüchle, W., Dressler, R., Düllmann, Ch.E., Eichler, B., Gäggeler, H.W., Gregorich, K.E., Hoffman, D.C., Hübener, S., Jost, D.T., Kirbach, U.W., Laue, C.A., Lavanchy, V.M., Nitsche, H., Patin, J.B., Piguët, D., Schädel, M., Shaughnessy, D.A., Strellis, D.A., Taut, S., Tobler, L., Tsyganov, Y.S., Türler, A., Vahle, A., Wilk, P.A., Yakushev, A.B. Chemical characterization of bohrium (element 107)

Nature **407**, 63 (2000)

Fanghänel, Th., Neck, V.

Comment on 'Behaviour of Europium(III) and its Hydroxo and Carbonate Complexes in a Solvent Extraction System with HDBM in 2 M NaCl at 303 K' by M. Jiménez-Reyes, M. Solache-Rios and A. Rojas-Hernández.

Radiochim. Acta **88**, 499-501 (2000)

Geipel, G., Bernhard, G., Rutsch, M., Brendler, V., Nitsche, H.

Speciation in Water released from Mining and Milling Facilities

In: T.E. Baca and T. Flokowski (eds.), The Environmental Challenges of Nuclear Disarmament, Kluwer Academic Publishers, Netherlands (2000), p.323-332

Geipel, G., Bernhard, G., Rutsch, M., Brendler, V., Nitsche, H.

Spectroscopic properties of uranium(VI) minerals studied by time-resolved laser-induced fluorescence spectroscopy (TRLFS)

Radiochim. Acta **88**, 757-762 (2000)

Hennig, C., Reich, T., Roßberg, A., Funke, H., Bernhard, G.

EXAFS as a Tool for Bond-Length Determination in the Environment of Heavy Atoms (Abstract)

Z. Krist. Suppl. **17**, 81 (2000)

Hensen, K., Mayr-Stein, R., Stumpf, Th., Pickel, P., Bolte, M., Fleischer, H.

Halogen Exchange and Expulsion: Ligand Stabilized Dihalogen Silicon Dications

J. Chem. Soc., Dalton Trans., 473-477 (2000)

Hensen, K., Kettner, M., Stumpf, Th., Bolte, M.

Synthese und Kristallstrukturbestimmung von Silicium-Komplexen der Koordinationszahl sechs mit Dimethylpyridinen

Z. Naturforschung **55b**, 901-906 (2000)

Kim, J.I., Fanghänel, T., Regan, L., Nitsche, H., Brendler, V., Grenthe, I., Glaser, F., Bruno, J., Saxena, S.

Joint European Thermodynamic Database for Environmental Modelling (JETDEM)

Report EUR 19131 (2000), Final report EC, DG RTD/D.II.3

Knöfler, R., Mattig, S., Deussen, A., Heise, K.H., Bubner, M., Weisbach, G.

Adenosine Diphosphate as mediator of Interaction between Platelets and Erythrocytes in Human Blood

Platelets **11**, 116 (2000)

Moll, H., Reich, T., Hennig, C., Roßberg, A., Szabó, Z., Grenthe, I.

Solution Coordination Chemistry of Uranium in the Binary UO_2^{2+} - SO_4^{2-} and the Ternary UO_2^{2+} - SO_4^{2-} - OH^- System

Radiochim. Acta **88**, 559-566 (2000)

Moll, H., Reich, T., Szabó, Z.

The Hydrolysis of Dioxouranium(VI) Investigated using EXAFS and ^{17}O -NMR

Radiochim. Acta **88**, 411-415 (2000)

- Nebelung, C., Henniger, J.
Schnelles Freimeßverfahren für alpha-aktive Nuklide in Bauschutt durch Direktmessung großflächiger dünner Meßpräparate
VI. Stilllegungskolloquium Hannover und 5. Statusbericht Stilllegung und Rückbau kerntechnischer Anlagen, 13.-14.04. 2000, Hannover; Tagungsband S. 293-304
- Neuweiler, F., Rutsch, M., Geipel, G., Reimer, A., Heise, K.H.
Soluble humic substances from in situ precipitated microcrystalline calcium carbonate, internal sediment, and in spar cement in a Cretaceous carbonate mud-mound
Geology **28**, 851 (2000)
- Panak, P., Raff, J., Selenska-Pobell, S., Geipel, G., Bernhard, G., Nitsche, H.
Complex formation of U(VI) with *Bacillus*-isolates from a uranium mining waste pile
Radiochim. Acta **88**, 71-76 (2000)
- Pompe, S., Schmeide, K., Bubner, M., Geipel, G., Heise, K.H., Bernhard, G., Nitsche, H.
Investigation of Humic Acid Complexation Behavior with Uranyl Ions Using Modified Synthetic and Natural Humic Acids
Radiochim. Acta **88**, 553-558 (2000)
- Pompe, S., Bubner, M., Schmeide, K., Heise, K.H., Bernhard, G., Nitsche, H.
Influence of Humic Acids on the Migration Behavior of Radioactive and Non-Radioactive Substances under Conditions Close to Nature. Synthesis, Radiometric Determination of Functional Groups, Complexation
Report FZR-290, Forschungszentrum Rossendorf (2000)
- Pompe, S., Bubner, M., Schmeide, K., Heise, K.H., Bernhard, G., Nitsche, H.
Synthesis, Radiometric Determination of Functional Groups, Complexation. In: Influence of Humic Acids on the Migration Behavior of Radioactive and Non-Radioactive Substances under Conditions Close to Nature. Final Report.
Report FZKA 6557, Forschungszentrum Karlsruhe, p.125-235 (2000)
- Reich, T., Bernhard, G., Geipel, G., Funke, H., Hennig, C., Roßberg, A., Matz, W., Schell, N., Nitsche, H.
The Rossendorf Beamline ROBL - A Dedicated Experimental Station for XAFS Measurements of Actinides and other Radionuclides
Radiochim. Acta **88**, 633-637 (2000)
- Reich, T., Geipel, G., Funke, H., Hennig, C., Roßberg, A., Bernhard, G.
Plutonium. XAFS Measurements of Plutonium Hydrates
ESRF Highlights 1999, 32 (2000)
- Reich, T.
Grundlagen der Röntgenabsorptionsspektroskopie (EXAFS) und ihre Anwendung auf die Untersuchung der Chrom-Kollagen-Wechselwirkung
Tagungsband „2. Freiburger Kollagensymposium“, 25.-26.05.2000, Freiberg, S. M/1-M/9
- Roßberg, A., Baraniak, L., Reich, T., Hennig, C., Bernhard, G., Nitsche, H.
EXAFS Structural Analysis of Aqueous Uranium(VI) Complexes with Lignin Degradation Products
Radiochim. Acta **88**, 593-597 (2000)
- Schmeide, K., Pompe, S., Bubner, M., Heise, K.H., Bernhard, G., Nitsche, H.
Uranium(VI) Sorption onto Phyllite and Selected Minerals in the Presence of Humic Acid
Radiochim. Acta **88**, 723-728 (2000)
- Schmeide, K., Brendler, V., Pompe, S., Bubner, M., Heise, K.H., Bernhard, G.
Kinetic Studies of the Uranium(VI) and Humic Acid Sorption onto Phyllite, Ferrihydrite and Muscovite
Report FZKA 6524, Forschungszentrum Karlsruhe, p.149-170 (2000)
- Schmeide, K., Brendler, V., Pompe, S., Bubner, M., Heise, K.H., Bernhard, G.
Influence of Sulfate on the Kinetics of Uranium(VI) Sorption onto Ferrihydrite/Humic Acid Systems
Report FZKA 6524, Forschungszentrum Karlsruhe, p.171-188 (2000)
- Schmeide, K., Pompe, S., Bubner, M., Reich, T., Heise, K.H., Bernhard, G.
Structural Investigation of the Interaction of Uranium(VI) with Modified and Unmodified Humic Substances by EXAFS and FTIR Spectroscopy
Report FZKA 6524, Forschungszentrum Karlsruhe, p.189-209 (2000)
- Schmeide, K.
Complementary Information on the Characterization of Material Used within the Project. Part 3: Characterization of Natural and Synthetic Humic Substances, Rock Material and Minerals at FZR-IfR
Report FZKA 6524, Forschungszentrum Karlsruhe, p.385-394 (2000)

Seifert, S., Künstler, J.-U., Gupta, A., Funke, H., Reich, T., Hennig, C., Roßberg, A., Pietzsch, H.-J., Alberto, R., Johannsen, B.

EXAFS Analyses of Technetium(I) Carbonyl Complexes - Stability Studies in Solutions
Radiochim. Acta **88**, 239-245 (2000)

Szabó, Z., Moll, H., Grenthe, I.

Structure and Dynamics in the Complex-ion $(\text{UO}_2)_2(\text{CO}_3)(\text{OH})_3^-$
Dalton Transactions **18**, 3158-3161 (2000)

Vejmelka, P., Fanghänel, Th., Kienzler, B., Korthaus, E., Römer, J., Schüssler, W., Artinger, R.

Sorption and Migration of Radionuclides in Granite (ÄSPÖ, Sweden)
Report FZKA 6488, Forschungszentrum Karlsruhe (2000) p.1-34

Zänker, H., Richter, W., Hüttig, G., Brendler, V., Moll, H.

Charakterisierung der Kolloidpartikel in den Wasserfließsystemen stillgelegter sächsischer Bergbauanlagen.
Ergebnisbericht an die DFG für den Zeitraum Januar 1999 bis Februar 2000. Rossendorf, 28.03.2000

Zänker, H., Richter, W., Brendler, V., Nitsche, H.

Colloid-borne uranium and other heavy metals in the water of a mine drainage gallery
Radiochim. Acta **88**, 619-624 (2000)

PATENTS

Förster, E., Heise, K.H., Nitsche, H.

Verfahren zur elektrochemischen Mineralisierung von organischen, insbesondere C-14-markierten Abfallstoffen
Patent DE 196 46 049 C2 erteilt am 28.12.2000 von Deutsches Patent- und Markenamt

LECTURES

Babanov, Yu.A., Zayarnaya, T.Ye, Reich, T., Funke, H.

EXAFS Study of U(VI) Compounds: A New Approach to Data Analysis
2nd Euroconference and NEA Workshop on Speciation, Techniques, and Facilities for Radioactive Materials at
Synchrotron Light Sources. Actinide-XAS-2000
Grenoble, France, 10.-12.09.2000

Bernhard, G.

Uranium mining and milling in Eastern Germany B Radioecological Aspects
30^{èmes} Journées des Actinides
Dresden, Germany, 04.-06.05.2000

Bernhard, G.

Uran in der Umwelt - Ursachen und Konsequenzen
Tag der offenen Tür
Rossendorf, Germany, 16.09.2000

Bernhard, G., Günther, A., Roßberg, A., Reich, T., Nitsche, H.

Determination of uranium speciation in plants
5th International Conference on Nuclear and Radiochemistry, NRC5
Pontresina, Switzerland, 03.-08.09.2000

Bernhard, G.

Natürliche und künstliche Radioaktivität in der Umwelt
Lehrerfortbildung 2000
Rossendorf, Germany, 17.08.2000

Brendler, V. Arnold, Th.

Speciation und Sorption für Risikoanalysen B Modellierung und Datenbanken
GRS Sorptionsworkshop
Köln, Germany, 07.12.2000

Brendler, V. Arnold, Th.

Speciation und Sorption für Risikoanalysen B Modellierung und Datenbanken
DFG Workshop 'Skalenwechsel in Messung und Modellierung'
Tübingen, Germany, 13.12.2000

Fanghänel, Th.

Aquatische Chemie der Actiniden - Ein Baustein für die Bewertung der Langzeitsicherheit von Endlagern
hochradioaktiver Abfälle
Anorganisch-Chemisches Institutskolloquium der Technischen Universität München
Garching, Germany, 28.02.2000

- Fanghänel, Th.
Verhalten von Actiniden in natürlichen aquatischen Systemen
Kolloquium 'Isotope in den Geowissenschaften', Institut für Interdisziplinäre Isotopenforschung
Leipzig, Germany, 09.03.2000
- Fanghänel, Th.
Aquatische Chemie der Actiniden - Ein Baustein für die Bewertung der Langzeitsicherheit von Endlagern hochradioaktiver Abfälle
GDCh-Vortrag, Technischen Universität Clausthal
Clausthal, Germany, 10.11.2000
- Fanghänel, Th., Stumpf, Th.
Interaction of trivalent actinides (Cm(III)) with clay and calcite mineral surfaces
2000 International Chemical Congress of Pacific Basin Societies, (PACIFICHEM 2000)
Honolulu Hawaii, USA, 14.-19.12.2000
- Hennig, C.
EXAFS-Strukturuntersuchungen an Uranylkomplexverbindungen
PSI Villigen
Villigen, Switzerland, 23.05.2000
- Hennig, C., Panak, P.J., Reich, T. Raff, J., Selenska-Pobell, S., Bernhard, G. Nitsche, H.
Uranium(VI) Complexation by Bacillus Species Isolated from Uranium Mining Waste Pile - A Comparative EXAFS Study.
2nd Euroconference Bacterial-Metal/Radionuclide Interaction
Rossendorf, Germany, 30.8.-01.9.2000
- Hennig, C., Panak, P.J., Reich, T. Raff, J., Selenska-Pobell, S., Roßberg, A., Funke, H., Merroun, M.L., Bernhard, G.
EXAFS Investigation of U(VI) Interaction with Bacteria
2nd Euroconference and NEA Workshop on Speciation, Techniques, and Facilities for Radioactive Materials at Synchrotron Light Sources. Actinide-XAS-2000
Grenoble, France, 10.-12.09.2000
- Hübener, S.
Entdeckung und Charakterisierung der schwersten Elemente
TU Dresden, Institut für Werkstoffwissenschaft
Dresden, Germany, 15.06.2000
- Hübener, S., Taut, S., Vahle, A., Eichler, B., Jost, D.T., Türler, A., Trautmann, N.
Thermochromatographic Adsorption Studies of Berkelium
30^{èmes} Journées des Actinides
Dresden, Germany, 04.-06.05.2000
- Klöcking, H.-P., Mahr, N., Klöcking, R., Heise, K.H.
Influence of naturally occurring humic acids and synthetic humic acid-like polymers on the protein C anticoagulant pathway
10th International Meeting of the International Humic Substances Society
Toulouse, France, 24.-28.07.2000
- Klöcking, H.-P., Mahr, N., Klöcking, R., Heise, K.H.
Factor Xa inhibition by naturally occurring humic acids and synthetic humic acid-like Polymers
11th International Peat Congress
Québec City, Canada, 06.-12.08.2000
- Krawczyk-Bärsch, E.
Untersuchungen zur Sorption von Uran an Gesteinen und Mineralen am Beispiel des Granits von Eibenstock
Vortragsreihe Forum Hydrogeologie des Institut für Geowissenschaften der Friedrich Schiller Universität Jena
Jena, Germany, 16.11.2000
- Merroun, M.L., Selenska-Pobell, S.
Complexation of Uranium by three eco-types of *Acidithiobacillus ferrooxidans*
2nd International Biometals Symposium 'Biometals 2000'
Tübingen, Germany, 24.-29.04.2000
- Merroun, M.L., Tzvetkova, T., Selenska-Pobell, S.
Complexation of Uranium by different *Acidithiobacillus ferrooxidans* Types
2nd Euroconference on Bacterial-Metal/Radionuclide Interaction
Rossendorf, Germany, 30.8.-01.09.2000
- Pompe, S., Schmeide, K., Bubner, M., Heise, K.H., Bernhard, G.
Melanoidins as Model Compounds for Humic Acids - Synthesis, Characterization, Complexation

Meeting EU-COST-Project (Melanoidins in Food and Health)
Berlin, Germany, 07.-08.04.2000

Reich, T.
Scientific Activities in Radiochemistry of the ROBL-CRG at the ESRF
Environmental Geochemistry Group, LGIT B IRIGM, University of Grenoble
Grenoble, France, 17.02.2000

Reich, T.
Principles of X-ray Absorption Spectroscopy and its Application to Actinides
School on the Chemistry and Physics of the Actinides
Dresden, Germany, 02.-03.05.2000

Reich, T., Geipel, G., Funke, H., Hennig, C., Roßberg, A., Bernhard, G.
XANES and EXAFS Measurements of Pu(III) and Pu(VI) Hydrates
30^{èmes} Journées des Actinides
Dresden, Germany, 04.-06.05.2000

Reich, T.
EXAFS Measurements of Actinides at the Rossendorf Beamline ROBL
Workshop on Synchrotron Radiation Techniques in the Environmental Sciences
Forschungszentrum Karlsruhe
Karlsruhe, Germany, 11.-12.05.2000

Reich, T.
Grundlagen der Röntgenabsorptionsspektroskopie (EXAFS) und ihre Anwendung auf die Untersuchung der Chrom
- Kollagen - Wechselwirkung
2. Freiburger Kollagensymposium
Freiberg, Germany, 25.-26.05.2000

Reich, T.
Röntgenabsorptionsspektroskopie von Actiniden
Johannes Gutenberg-Universität Mainz, Institut für Kernchemie
Mainz, Germany, 27.06.2000

Reich, T.
XAFS-Untersuchungen von Actiniden am Rossendorfer Synchrotronstrahlrohr ROBL
Forschungszentrum Karlsruhe, Institut für Nukleare Entsorgung
Karlsruhe, Germany, 05.07.2000

Reich, T.
Study of Radioactive Compounds by Synchrotron-Based X-ray Absorption Spectroscopy
5th International Conference on Nuclear and Radiochemistry, NRC5
Pontresina, Switzerland, 03.-08.09.2000

Reich, T., Bernhard, G., Funke, H., Hennig, C., Schell, N., Matz, W.
Opportunities for XAFS Spectroscopy on Actinides at the Rossendorf Beamline (ROBL) at the European
Synchrotron Radiation Facility
2nd Euroconference and NEA Workshop on Speciation, Techniques, and Facilities for Radioactive Materials at
Synchrotron Light Sources. Actinide-XAS-2000
Grenoble, France, 10.-12.09.2000

Reich, T., Bernhard, G., Bubner, M., Nefedov, V.I., Pompe, S., Schmeide, K.
EXAFS and XPS Investigations of Actinide Complexes with Humic Substances
Workshop 'Surface Chemical Processes in Natural Environments'
Monte Verità, Ascona, Switzerland, 01.-06.10.2000

Reich, T.
Röntgenabsorptionsspektroskopie von Actinoiden mittels Synchrotronstrahlung
Technische Universität München, Institut für Radiochemie
Garching, Germany, 20.11.2000

Selenska-Pobell, S., Raff, J., Wahl, R., Pompe, W.
Metal nanoclusters on a bacterial surface layer protein
4th Balcan Conference on Pure and Applied Physics
Velika Tarnovo, Bulgaria, 19.-24.08.2000

Selenska-Pobell, S., Radeva, G., Flemming, K., Raff, J., Merroun, M., Tzvetkova, I., Tzvetkova, T., Hennig, C.,
Reich, T., Wahl, R., Pompe, W.
Bacteria from uranium wastes and their interactions with U(VI) and other metals
2nd Euroconference on Bacterial-Metal/Radionuclide Interaction

Rosendorf, Germany, 30.8.-01.09. 2000

Selenska-Pobell, S., Radeva, G., Flemming, K., Merroun, M., Raff, J.
Bacteria from uranium wastes and their interactions with uranium and other metals
Biotechnology 2000, 11th International Biotechnology Symposium and Exhibition
Berlin, Germany, 03.-08.09.2000

Taut, S., Hübener, S., Vahle, A., Eichler, B., Jost, D.T., Türlér, A., Gregorich, K.
Thermochromatography of Fermium, Mendeleevium, and Nobelium
30^{èmes} Journées des Actinides
Dresden, Germany, 04.-06.05.2000

Taut, S., Hübener, S., Vahle, A., Eichler, B., Türlér, A., Jost, D.T., Gäggeler, H.W., Trautmann, N.
Metal Adsorption Studies of the Heaviest Actinides
5th International Conference on Nuclear and Radiochemistry, NRC5
Pontresina, Switzerland, 03.-08.09.2000

Türlér, A., Wilk, P.A., Eichler, R., Gregorich, K.E., Jost, D.T., Laue, C.A., Ninov, V., Adams, J.L., Brüche, W.,
Dressler, R., Düllmann, Ch.E., Eichler, B., Gäggeler, H.W., Hoffman, D.C., Hübener, S., Kirbach, U.W., Lane,
M.R., Lavanchy, V.M.H., Lee, D.M., Nitsche, H., Patin, J.B., Schädel, M., Shaugnessy, D.A., Strellis, D.A., Taut,
S., Tobler, L., Tsyganov, Yu., Vahle, A., Yakushev, A.B.
Two new isotopes of element 107: ²⁶⁶Bh and ²⁶⁷Bh.
7th International Conference on Nucleus Collisions
Strasbourg, France, 03.-07.07.2000

Vahle, A.
Gas Chromatographic Studies of the Heaviest Elements (invited)
Tours Symposium on Nuclear Physics IV
Tours, France, 04.-07.09.2000

Zänker, H., Richter, W., Brendler, V., Kluge, A., Hüttig, G.
Kolloidpartikel in fließenden Grubenwässern und in Acid Rock Drainage (Lettenwasser)
6. Kolloquium des DFG-Schwerpunktprogramms 'Geochemische Prozesse mit Langzeitfolgen im anthropogen
beeinflussten Sickerwasser und Grundwasser'
Berlin, Germany, 02.-03.03.2000

Zeevaert, Th., Bousher, A., Brendler, V., Hedemann Jensen, P., Nordlinder, S.
Restoration strategies for radioactively contaminated sites and their close surroundings
10th International Congress of the International Radiation Protection association (IRPA-10)
Hiroshima, Japan, 14.-19.05.2000

Zeevaert, Th., Bousher, A., Brendler, V., Hedemann Jensen, P., Nordlinder, S.
A ranking methodology of restoration strategies for radioactively contaminated sites
Radiation Legacy of the 20th Century: Environmental Restoration (MINATOM and IAEA)
Moscow, Russia, 30.10.-03.11.2000

POSTERS

Amayri, S., Geipel, G., Reich, T., Matz, W., Bernhard, G.
Synthesis, Characterization and Solubility of Bayleyite, Mg₂[UO₂(CO₃)₃]·18H₂O
5th International Conference on Nuclear and Radiochemistry, NRC5
Pontresina, Switzerland, 03.-08.09.2000

Amayri, S., Reich, T., Bernhard, G.
EXAFS Investigations of Earth Alkaline Metal Uranyl Tricarbonato Complexes
2nd Euroconference and NEA Workshop on Speciation, Techniques, and Facilities for Radioactive Materials at
Synchrotron Light Sources. Actinide-XAS-2000
Grenoble, France, 10.-12.09.2000

Baraniak, L., Abraham, A., Mack, B., Geipel, G., Bernhard, G., Nitsche, H.
Über die Möglichkeit der reduktiven Uran- und Arsenimmobilisierung in Bergbauwässern als Folge des natürlichen
Holzabbaus
Internationale Konferenz zur Bergbausanierung
Schlema, Germany, 11.-14.07.2000

Bubner, M., Meyer, M., Jander, R., Heise, K.H., Matucha, M., Vlasakova, V., Fuksova, K., Nitsche, H.
Radiolabelling of Polychlorinated Biphenyls: Synthesis of [¹⁴C]PCB Congeners No. 11 and No. 77
7th International Symposium on the Synthesis and Application of Isotopes and Isotopically Labelled Compounds
Dresden, Germany, 18.-22.06.2000

Geipel, G., Brendler, V., Bernhard, G.
 Complex Formation of Uranium(VI) with Phosphate in Acidic Media
 30^{ièmes} Journées des Actinides
 Dresden, Germany, 04.-06.05.2000

Geipel, G., Bernhard, G., Brendler, V., Reich, T.,
 Complex Formation between Uranium(VI) and Adenosine Phosphate
 5th International Conference on Nuclear and Radiochemistry, NRC5
 Pontresina, Switzerland, 03.-08.09.2000

Günther, A., Bernhard, G., Geipel, G., Roßberg, A., Reich, T.
 Untersuchungen zur chemischen Speciation von Uran(VI) in Pflanzen
 Botanikertagung 2000
 Jena, Germany, 17.-22.09.2000

Hennig, C., Reich, T., Roßberg, A., Funke, H., Bernhard, G.
 EXAFS as a Tool for Bond-Length Determination in the Environment of Heavy Atoms
 8. Jahrestagung der Deutschen Gesellschaft für Kristallographie (DGK)
 Aachen, Germany, 13.-16.3.2000

Hennig, C., Reich, T., Funke, H., Roßberg, A., Rutsch, M., Bernhard, G.
 EXAFS as a Tool for Bond-Length Determination in the Environment of Heavy Atoms
 11th Internat. Conference on X-ray Absorption Fine Structure (XAFS XI)
 Aki, Japan, 26.-31.7.2000

Hennig, C., Reich, T., Funke, H., Roßberg, A., Rutsch, M., Bernhard, G.
 Analysis of Atomic Distances in Inaccurately Determined Heavy-Atom Crystal Structures Using EXAFS Spectroscopy
 2nd Euroconference and NEA Workshop on Speciation, Techniques, and Facilities for Radioactive Materials at Synchrotron Light Sources. Actinide-XAS-2000
 Grenoble, France, 10.-12.09.2000

Hübener, S., Bröchle, W., Dressler, R., Eichler, B., Gäggeler, H.W., Grantz, M., Heyne, H., Jäger, E., Jost, D.T., Kirbach, U., Nitsche, H., Piguet, D., Schädel, M., Schimpf, E., Taut, S., Trautmann, N., Türler, A., Vahle, A., Yakushev, A.B.
 On-Line Gas Chemistry Studies of Seaborgium Oxide Hydroxide
 5th International Conference on Nuclear and Radiochemistry, NRC5
 Pontresina, Switzerland, 03.-08.09.2000

Matucha, M., Uhlířova, H., Fuksova, K., Bubner, M.
 Application of ¹⁴C-Labeling in Investigation of Forest Decline: Uptake, Translocation and Fate of Trichloroacetic Acid in Norway Spruce (*Picea abies*)
 7th International Symposium on the Synthesis and Application of Isotopes and Isotopically Labelled Compounds
 Dresden, Germany, 18.-22.06.2000

Merroun, M.L., Flemming, K., Selenska-Pobell, S.
 Microdiverse types of *A. ferrooxidans* and their interactions with uranium
 2nd International Biometals Symposium 'Biometals 2000'
 Tübingen, Germany, 24.-29.04.2000

Merroun, M.L., Reich, T., Hennig, C., Selenska-Pobell, S.
 EXAFS Investigation of Uranium (VI) Complexes formed at the *A. ferrooxidans* Types
 European Workshop on X-ray Absorption for Biology
 Orsay, France, 03.-04.07.2000

Merroun, M.L., Hennig, C., Reich, T., Selenska-Pobell, S.
 EXAFS Investigation of Uranium (VI) Complexes formed at the *A. ferrooxidans* Types.
 2nd Euroconference on Bacterial-Metal/Radionuclide Interaction
 Rossendorf, Germany, 30.08.-01.09.2000

Merroun, M.L., Flemming, K., Tzvetkova, T., Reich, T., Hennig, C., Selenska-Pobell, S.
 Microdiverse Types of *A. ferrooxidans* and their Interactions with Uranium
 Biotechnology 2000, 11th International Biotechnology Symposium and Exhibition
 Berlin, Germany, 03.-08.09.2000

Merroun, M.L., Reich, T., Hennig, C., Selenska-Pobell, S.
 EXAFS Investigation of Uranium (VI) Complexes Formed at the *A. ferrooxidans* Types
 2nd Euroconference and NEA Workshop on Speciation, Techniques, and Facilities for Radioactive Materials at Synchrotron Light Sources. Actinide-XAS-2000
 Grenoble, France, 10.-12.09.2000

Merroun, M.L., Reich, T., Hennig, C., Selenska-Pobell, S.
Spectroscopic Characterization of Uranium (VI) Complexes with *A. ferrooxidans* Types.
7th International Summer School on Biophysics
Istria, Croatia, 14.-25.09.2000

Moll, H., Reich, T., Szabó, Z.
The Hydrolysis of Uranium(VI) Investigated by EXAFS and ¹⁷O-NMR
30^{ièmes} Journées des Actinides
Dresden, Germany, 04.-06.05.2000

Moll, H., Zänker, H., Richter, W., Brendler, V., Reich, T., Hennig, C., Roßberg, A., Funke, H.
XAS Study of Acid Rock Drainage Samples From an Abandoned Zn-Pb-Ag Mine at Freiberg, Germany
2nd Euroconference and NEA Workshop on Speciation, Techniques, and Facilities for Radioactive Materials at
Synchrotron Light Sources. Actinide-XAS-2000
Grenoble, France, 10.-12.09.2000

Moll, H., Zänker, H., Richter, W., Brendler, V., Kluge, A., Hüttig, G.
Ausscheidung von Sekundärmineralen aus Lettenwasser der Himmelfahrt Fundgrube Freiberg
6. Kolloquium des DFG-Schwerpunktprogramms ‚Geochemische Prozesse mit Langzeitfolgen im anthropogen
beeinflußten Sickerwasser und Grundwasser‘
Berlin, Germany, 02.-03.03.2000

Pompe, S., Schmeide, K., Bubner, M., Geipel, G., Heise, K.H., Choppin, G.R., Bernhard, G.
Influence of Phenolic OH Groups on Humic Acid Complexation with Uranium(VI)
30^{ièmes} Journées des Actinides
Dresden, Germany, 04.-06.05.2000

Pompe, S., Bubner, M., Schmeide, K., Heise, K.H., Choppin, G.R., Bernhard, G.
¹³C-CP/MAS-NMR Spectroscopy of Chemically Modified and Unmodified Synthetic and Natural Humic Acids
Symposium on Refractory Organic Substances in the Environment - ROSE II
Karlsruhe, Germany, 01.-03.08.2000

Pompe, S., Schmeide, K., Reich, T., Hennig, C., Funke, H., Roßberg, A., Geipel, G., Brendler, V., Heise, K.H.,
Bernhard, G.
Neptunium(V) Complexation by Various Humic Acids in Solution Studied by EXAFS and UV-Vis Spectroscopy
2nd Euroconference and NEA Workshop on Speciation, Techniques, and Facilities for Radioactive Materials at
Synchrotron Light Sources. Actinide-XAS-2000
Grenoble, France, 10.-12.09.2000

Radeva, G., Flemming, K., Tzvetkova I., Selenska-Pobell, S.
Molecular analysis of bacterial communities in uranium polluted waste piles
Biotechnology 2000, 11th International Biotechnology Symposium and Exhibition
Berlin, Germany, 03.-08.09.2000

Raff, J., Wahl, R., Matys, S., Flemming, K., Mertig, M., Selenska-Pobell, S., Pompe, W.
Interactions of the S-layer protein of the uranium waste pile isolate *Bacillus sphaericus* JG-A12 with metals
2nd Euroconference on Bacterial-Metal/Radionuclide Interaction
Rossendorf, Germany, 30.08.-01.09.2000

Raff, J., Wahl, R., Matys, S., Flemming, K., Mertig, M., Selenska-Pobell, S., Pompe, W.
Interactions of the S-layer protein of the uranium waste pile isolate *Bacillus sphaericus* JG-A 12 with metals
Biotechnology 2000, 11th International Biotechnology Symposium and Exhibition
Berlin, Germany, 03.09.-08.09.2000

Roßberg, A., Reich, T.
The Application of Iterative Transformation Factor Analysis to Resolve Multicomponent EXAFS Spectra of
Uranium(VI) Complexes with Acetic Acid as a Function of pH
2nd Euroconference and NEA Workshop on Speciation, Techniques, and Facilities for Radioactive Materials at
Synchrotron Light Sources. Actinide-XAS-2000
Grenoble, France, 10.-12.09.2000

Schmeide, K., Pompe, S., Bubner, M., Heise, K.H., Bernhard, G.
Uranium(VI) and Humic Acid Sorption onto Phyllite and Ferrihydrite
30^{ièmes} Journées des Actinides
Dresden, Germany, 04.-06.05.2000

Schmeide, K., Brendler, V., Pompe, S., Bubner, M., Heise, K.H., Bernhard, G.
Sorption Kinetics in the System Uranium / Sulfate / Humic acid / Ferrihydrite
Symposium on Refractory Organic Substances in the Environment - ROSE II
Karlsruhe, Germany, 01.-03.08.2000

Schmeide, K., Pompe, S., Reich, T., Hennig, C., Funke, H., Roßberg, A., Geipel, G., Brendler, V., Heise, K.H., Bernhard, G.

Complexation of Neptunium(IV) by Various Humic Substances Studied by X-Ray Absorption Spectroscopy
2nd Euroconference and NEA Workshop on Speciation, Techniques, and Facilities for Radioactive Materials at Synchrotron Light Sources. Actinide-XAS-2000
Grenoble, France, 10.-12.09.2000

Selenska-Pobell, S., Merroun, M., Hennig, C., Reich, T., Tzvetkova, T.
Bacteria from uranium waste piles and their interactions with uranium (VI)
2nd International Biometals Symposium 'Biometals 2000'
Tübingen, Germany, 24.-29.04.2000

Vahle, A., Hübener, S., Taut, S., Gregorich, K.E., Kirbach, U., Eichler, B., Gäggeler, H.W., Jost, D.T., Türlér, A., Trautmann N.

Separation of Heavy Actinoides by Thermochromatography
5th International Conference on Nuclear and Radiochemistry, NRC5
Pontresina, Switzerland, 03.-08.09.2000

Yakushev, A.B., Buklanov, G.V., Chelnokov, M.L., Chepigin, V.I., Dmitriev, S.N., Gorshkov, V.A., Lebedev, V.Ya., Malyshev, O.N., Oganessian, Yu.Ts., Popeko, A.G., Sokol, E.A., Timokhin, S.N., Vasko, V.M., Yeregin, A.V., Zvara, I., Hübener, S., Türlér, A.

First Attempt to Chemically Identify Element 112
5th International Conference on Nuclear and Radiochemistry, NRC5
Pontresina, Switzerland, 03.-08.09.2000

Zayarnaya, T.Ye., Reich, T., Hennig, C., Funke, H., Babanov, Yu.A.
Application of the Tikhonov Regularization Method to the EXAFS Analysis of $\text{UO}_2\text{HAsO}_4 \cdot 4\text{H}_2\text{O}$ and $\text{UO}_2(\text{H}_2\text{AsO}_4)_2 \cdot \text{H}_2\text{O}$

2nd Euroconference and NEA Workshop on Speciation, Techniques, and Facilities for Radioactive Materials at Synchrotron Light Sources. Actinide-XAS-2000
Grenoble, France, 10.-12.09.2000

III. SEMINARS, CONFERENCES AND WORKSHOPS

INSTITUTE SEMINARS

Dr. Thomas Neu

Umweltforschungszentrum Leipzig-Halle, Sektion Gewässerforschung Magdeburg
Erfahrung mit der Anwendung des Confocalen Laser Scanning Mikroskopes in Bezug auf Biofilme
18.01.2000

Dr. Tobias Reich

FZR, Institut für Radiochemie; FZR-Beamline Grenoble
XAFS-Untersuchungen an der Rossendorfer Beamline von Np- und Pu-Hydraten
20.01.2000

DC Andre Roßberg

FZR, Institut für Radiochemie; FZR-Beamline Grenoble
Anwendung der EXAFS-Spektroskopie zur Bestimmung der Speziation von Uranylkomplexen in Lösungen
20.01.2000

Dr. Joachim Oelichmann

Perkin-Elmer Bodenseewerk, Überlingen
Prinzipien und Anwendungen der Infrarot-Mikrospektroskopie
11.02.2000

Dr. Siegfried Hübener

Universität Bern, Labor für Radio- und Umweltchemie; FZR, Institut für Radiochemie
Radionuklidmessungen am Jungfrauoch zum Studium atmosphärischer Prozesse
15.02.2000

Dr. Andreas Lehmann

Universität Hohenheim, Institut für Bodenkunde
Beitrag der Bodenkunde bei der Beurteilung von Uranbelastungen der Umwelt
22. 02. 2000

Dr. Thorsten Stumpf

FZ Karlsruhe, Institut für Nukleare Entsorgungstechnik
Aufklärung chemischer Reaktionen im Spurenbereich: Laserspektroskopische Untersuchungen (TRLFS) mit Cm(III)
23.02.2000

Prof. Joan de Pablo

Universitat Politecnica Catalunya Barcelona, Chemical Engineering Department
Nuclear and Hazardous Waste Management: Environmental Impacts
07.03.2000

Prof. D.C. Koningsberger

Universiteit Utrecht, Department of Inorganic Chemistry and Catalysis
XAFS Spectroscopy in Catalysis Research: AXAFS and Fano Resonances
04.04.2000, CRG-ROBL, ESRF, Grenoble, France

Dr. S. Tsushima

The University of Tokyo, Department of Quantum Engineering and System Science
Quantum Chemical Calculations on Actinide Complexes - From Structure to Solubility
10.04.2000, CRG-ROBL, ESRF, Grenoble, France

Prof. Dr. Susan Clark

Washington State University, Chemistry Department, USA
Chemistry of Uranium(VI) Solid Phases in Environmental Systems
03.05.2000

Prof. Dr. Susan Stipp

University of Copenhagen, Geological Institute, Denmark
Reactions at Interfaces: What can we see at molecular scale?
17.05.2000

Dr. Wolfgang Dedek

Universität Leipzig
Entdeckung von Tritium und Kohlenstoff-14
31.05.2000

Dr. Clemens Walther

Forschungszentrum Karlsruhe
Ultraspurenachweis von Kolloiden mittels LIBD - Grundlagen der Laser-induzierten Plasmaerzeugung
26.07.2000

Prof. Dr. M. Kosmulski
Technical University Lublin, Department of Electrical Engineering, Poland
Electrokinetic potential in adsorption modeling
10.08.2000

Prof. Dr. M. Kosmulski
Technical University Lublin, Department of Electrical Engineering, Poland
Ambient Temperature Ionic Liquids
25.08.2000

Dr. Satoru Tsushima
University of Tokyo, Department of Quantum Engineering and System Science, Japan
The Structure and Thermochemistry Study of Uranium Complexes with the Gaussian98 Program
28.08.2000

Dr. Reiner Schmid
BTU Cottbus, Lehrstuhl für Physikalische Chemie und Analytik
Infrarotspektroskopische Untersuchungen von Anilin-X Clustern und ihrer korrespondierenden Cluster-Kationen im Frequenzbereich der NH₂-Streckschwingungen
29.09.2000

Dr. Shoichi Tachimori
Japan Atomic Energy Research Institute
Japanese OMEGA Program and Recent Topics of Separation Chemistry for Partitioning at JAERI
13.11.2000

Dr. Holger Fleischer
Johannes Gutenberg Universität Mainz, Institut für Anorg. u. Analyt. Chemie
Ab initio Computer Chemie: Möglichkeiten und Grenzen
14.11.2000

Dr. Winfried Hoffmüller
Daimler-Crysler Aerospace, München
Peptidsynthese und Peptidkomplexe des Pd, Ru und Ir
05.12.2000

Dr. Peter Vejmelka
Forschungszentrum Karlsruhe, INE
Nuklidmigration im Deckgebirge des Endlagers für radioaktive Abfälle Morsleben
12.12.2000

INTERNAL SEMINARS (open for the public)

Institutsseminar ‚Actinidenchemie, Speziation, Sorption, Modellierung‘
14.-15.03.2000

K. Krogner
Vorstellung der Abteilung Analytik im Überblick

W. Wiesener, U. Schäfer
Methoden der Elementaranalytik

D. Birnstein
Komponentenanalytik

V. Brendler
Speziation und Sorption für Risikoanalysen: Modellierung und Datenbanken

T. Arnold
Untersuchungen zur Sorption von U(VI) auf Gesteine und Minerale

E. Krawczyk-Bärsch
Untersuchungen zur Sorption von U(VI) an Gesteinen des Erzgebirges in Gegenwart von Huminsäuren

K. Schmeide
Zur Sorptionskinetik im System Uran/Sulfat/Huminsäure/Mineral

S. Pompe
NMR-Untersuchungen an synthetischen und natürlichen Huminsäuren

M. Bubner
Feste Metallkomplexe von Huminsäuren

G. Schuster
Untersuchungen zur thermischen Stabilität von Huminsäuren und Uranylhumatkomplexen

M. Rutsch
Zeitaufgelöste laserinduzierte Fluoreszenzspektroskopie an Huminsäuren

A. Abraham
Reduzierende Eigenschaften von Holzabbauprodukten und Huminstoffen

L. Baraniak
Uran(VI)-Komplexierung mit Phenolcarbonsäuren

M. Böttger
AFM-Messungen an Huminsäuren

G. Geipel
Komplexbildungsverhalten von Uran(IV) mit Phosphaten

S. Amayri
Erdalkaliuranylkomplexe: Synthese, Charakterisierung, Löslichkeit

A. Günther
Untersuchungen zur Speziation von Uran in Pflanzen

D. Rettig
Aerosolbildung durch Vakuum-UV-Bestrahlung von Siloxandämpfen

W. Richter
Kolloide in Grubenwässern

H. Moll
Die Hydrolyse des Uran(VI) untersucht mit EXAFS und NMR-Spektroskopie

T. Reich
Überblick über die Arbeiten der Abteilung Synchrotronstrahlungsanwendungen und ausgewählte Ergebnisse

H. Funke
Neue methodische Ansätze zur Analyse von EXAFS Spektren

K.H. Heise
Konzeption zu infrarotspektroskopischen Messungen am FEL

C. Nebelung
Direktmessung von Actiniden in Beton

Institutsseminar ,Schwerste Elemente, Mikroorganismen'
24.05.2000

A. Vahle
Charakterisierung des Bohriums (Z=107) - Chemie und experimentelle Methoden

S. Taut
Metalladsorption der schwersten Elemente

S. Hübener
Gaschromatographische Untersuchungen oxidischer Verbindungen

M. Merroun
Microdiversity of *Acidithiobacillus ferrooxidans* in Uranium Wastes and their Interactions with Uranium

J. Raff
Metallclusterbildung auf dem S-Layer des Haldenisolats *Bacillus sphaericus* JG-A 12

S. Selenska-Pobell
Bacterial diversity and activity in uranium mining waste piles

H. Moll
Röntgenabsorptionsspektroskopie (XANES/EXAFS) an Lettenwasser-Proben
25.09.2000

H. Zänker, H. Moll, W. Richter, V. Brendler, T. Reich, G. Hüttig
Die Kolloidchemie von Acid Rock Drainage (Lettenwasser) aus einer stillgelegten Zn-Pb-Ag-Grube
25.09.2000

CONFERENCES / WORKSHOPS (organized by Institute of Radiochemistry)

2nd Euroconference on Bacterial-Metal/Radionuclide Interactions: Basic Research and Bioremediation
Rossendorf, Germany, 29.08.-01.09.2000

2nd Euroconference and NEA Workshop on Speciation, Techniques, and Facilities for Radioactive Materials at Synchrotron Light Sources
Grenoble, France, 10.9.-12.9.2000

Kolloquium im Institut für Radiochemie, FZ Rossendorf e.V., anlässlich des 65. Geburtstages von Dr. L. Baraniak
Rossendorf, Germany, 23.08.2000

G. Bernhard
Isotopenproduktion am Reaktor

S. Hübener
Vom Abbrand zum Californiumthiocyanat, Transuranchemie im ZfK Rossendorf

G. Geipel
Elektrochemische Oxidation von Cer im System Lanthanoidnitrate/Salpetersäure und extraktive Abtrennung des gebildeten Cer(IV)

Th. Arnold
Sorption von Uranyl an gesteinsbildenden Mineralen

Arbeitstreffen der WISMUT GmbH im Institut für Radiochemie, FZ Rossendorf e.V.
Rossendorf, Germany, 05.10.2000

G. Geipel
Uranspeziation in Wässern des Uranerzbergbaus

V. Brendler
Speziation und Sorption für Risikoanalysen - Modellierung und Datenbanken

Workshop anlässlich des Besuches einer Delegation des PSI / LSE
Rossendorf, Germany, 09.10.2000

V. Brendler
Schadstoff-Migration: Strategien, Prozesse, Modelle, Daten, Codes

Th. Arnold
Sorption von Uran auf Gesteinen

Th. Stumpf
TRLFS-Untersuchungen zu Wechselwirkungen von Cm(III)/Eu(III) mit Wasser/Ton-Grenzflächen

Workshop, Untersuchungen über die Komplexierung und die Migration von Actiniden und nichtradioaktiven Stoffen mit Huminsäuren unter geogenen Bedingungen - Komplexierung von Huminsäuren mit Actiniden in der Oxidationsstufe IV Th, U, Np'
Rossendorf, Germany, 19.-20.10.2000

S. Pompe
Festkörper-NMR-Spektroskopie an synthetischen und natürlichen Huminsäuren. Untersuchung von Synthese und Modifizierung.

K. Schmeide
EXAFS Untersuchungen der Wechselwirkung von Actiniden mit Huminstoffen.

Workshop anlässlich der Vorbereitung einer europäischen Initiative zur Einrichtung einer 'Französisch-Deutsch-Russischen Universität'
Rossendorf, Germany, 01.12.2000

K. Schmeide, S. Pompe
Interactions between Humic Substances and Actinides

G. Geipel
Laser-Induced Spectroscopic Methods in Chemistry of Actinides

V. Brendler, T. Arnold
Sorption Processes: Modeling and Databases

IV. PERSONNEL

PERSONNEL

Director

Prof. Dr. Th. Fanghänel (since February 1, 2000)

Administrative Staff

G. Kreusel

H. Pospischil

Scientific Staff

Dr. T. Arnold*
Dr. L. Baraniak*
Prof. Dr. G. Bernhard
DC D. Birnstein
Dr. V. Brendler
Dr. M. Bubner*
Dr. H.-J. Engelmann
Dr. E. Förster*
Dr. H. Funke
Dr. G. Geipel
Dr. A. Günther*

Dr. K.H. Heise
Dr. C. Hennig⁺
Dr. S. Hübener
Dr. A. Koban⁺
Dr. E. Krawczyk-Bärsch*
Dr. K. Krogner
Dr. P. Merker
Dr. M. Merroun⁺
Dr. H. Moll*
DC C. Nebelung
Dr. S. Pompe*

Dr. T. Reich
Dr. D. Rettig*
Dr. W. Richter*
Dr. S. Selenska-Pobell
Dr. K. Schmeide*
Dr. T. Stumpf⁺
Dr. S. Taut*
Dr. A. Vahle*
Dr. W. Wiesener*
Dr. H. Zänker

Technical Staff

DI(FH) B. Barz*
DI(FH) C. Eckardt
B. Eisold
DBC K. Flemming
J. Falkenberg
DI(FH) H. Friedrich
Ch. Fröhlich
DI(FH) G. Grambole
S. Heller*

DI(FH) K. Henkel
B. Heschel
H. Heyne
B. Hiller
DI(FH) G. Hüttig
DI(FH) R. Jander
P. Kluge
M. Leckelt*

DI(FH) M. Meyer
Ch. Müller
H. Neubert
DI(FH) K. Nicolai*
DI(FH) R. Nicolai*
A. Rumpel
R. Ruske
DI(FH) U. Schaefer

Graduate Students

DC A. Abraham
DC S. Amayri
DBT S. Kutschke

DB J. Raff
DC A. Roßberg
DC M. Rutsch

DI(FH) D. Vulpius
DM M. Walter
DC T. Zorn

Trainee

K. Berger
J. Bergmann
A. Duda
A. Grenner
K.-U. Hantsch

C. Heidel
P. Jählig
S. Krüger
M. Lange

K. Marschner
C. Möckel
N. Mühle
D. Westphal

* post doc
* term contract

DC: Dipl.-Chem.
DI: Dipl.-Ing.

DBC: Dipl.-Biochem.
DBT: Dipl.-Biotech.

DB: Dipl.-Biol.
DM: Dipl.-Mineral.

Guest Scientists

Dr. G. Arapis	Agricultural University of Athens, Athens, Greece
Prof. Dr. Yu.A. Babanov	Institute of Metal Physics, Russian Academy of Sciences, Ekaterinburg, Russia
Dipl.-Miner. F. Brand	Institut für Mineralogie, Universität Münster, Münster, Germany
Prof. Dr. I. Grenthe	Department of Chemistry, Inorganic Chemistry, The Royal Institute of Technology, Stockholm, Sweden
Dr. L. Kindermann	MACTEC-ERS (U.S. Dept. of Energy), Grand Junction, CO, USA
Prof. Dr. C.D. Koningsberger	Department of Inorganic Chemistry and Catalysis, Universiteit Utrecht, Utrecht, Netherlands
Prof. Dr. M. Kosmulski	Technical University Lublin, Department of Electrical Engineering, Poland
Dr. A. Lehmann	Universität Hohenheim, Institut für Bodenkunde
Prof. Dr. K.A. Matis	Aristotle University, Department of Chemistry, Thessaloniki, Greece
Prof. N. Medvedeva-Lyalikova	Institute of Microbiology, Russian Academy of Science, Moscow, Russia
Yu. Murakami	Hiroshima University, Higashi-Hiroshima, Japan
Prof. Dr. S. Rossbach	Western Michigan University, Department of Biological Science, Michigan, USA
Dr. Sh. Tachimori	Japan Atomic Energy Research Institute, Japan
Dr. Satoru Tsushima	The University of Tokyo, Department of Quantum Engineering and System Science, Tokyo, Japan
Dipl.-Biol. I. Tzvetkova	Department of Geomicrobiology, University of Sofia, Sofia, Bulgaria
Dipl.-Biol. Tz. Tzvetkova	Department of Geomicrobiology, University of Sofia, Sofia, Bulgaria
Dipl.-Phys. T.Ye. Zayarnaya	Institute of Metal Physics, Russian Academy of Sciences, Ekaterinburg, Russia

V. ACKNOWLEDGMENTS

ACKNOWLEDGMENT OF FINANCIAL SUPPORT

The Institute is part of the Forschungszentrum Rossendorf e.V., which is financed in equal parts by the Federal Republic of Germany and the Free State of Saxony.

Six projects were supported by the Bundesministerium für Bildung, Wissenschaft, Forschung und Technologie (BMBF):

- Stilllegung und Rückbau: Schnelles Freimeßverfahren für α -aktive Nuklide in Bauschutt durch Direktmessung von großflächigen dünnen Meßpräparaten - Automatisierung des Verfahrens -
Contract No. BMBF 02 S 7768/6
- Chemie der schwersten Elemente: Hochtemperaturgaschromatographie der Elemente 106 und 107
Contract No. BMBF 06 DR 824 (2)
- Influence of humic acids on migration behavior of radioactive and non-radioactive heavy elements under natural conditions.
Contract No. BMBF 02 E 88150
- Biosorption of uranium by bacillus for remediation of uranium wastes
Contract No. DRL: BUL-014-97
- Integrierter Umweltschutz in der Textilindustrie: Abtrennung von Uranylionen aus Sicker- und Grundwässern mit uranophilen Calixarenen (Verbundprojekt)
Contract No. BMBF 0339917/3
- Untersuchungen über die Komplexierung und die Migration von Actiniden und nichtradioaktiven Stoffen mit Huminsäuren unter geogenen Bedingungen - Komplexierung von Huminsäuren mit Actiniden in der Oxidationsstufe IV Th, U, Np (Verbundprojekt)
Projektförderung durch BMWi/BMBF
Contract No. PTE 02E92999

The Commission of the European Communities supported two projects:

- Building confidence in deep disposal: the BOREhole Injection Sites at Krasnoyarsk-26 and Tomsk-7 (BORIS)
In collaboration with:
Galson Sciences Limited, United Kingdom; United Kingdom Nirex Limited, Nirex Safety Assessment Research Program, United Kingdom; FZ Karlsruhe, Institut für Nukleare Entsorgungstechnik, Germany; Studiecentrum voor Kernenergie / Centre d'Étude de L'Énergie Nucléaire, Waste & Disposal Department/SCKACEN, Belgium; Institut de Protection et de Sûreté Nucléaire, France; All-Russian Designing and Research Institute of Production Engineering, VNIPIPT, Laboratory for Liquid industrial waste underground disposal, Russia; The Environment Agency, EA, National Centre for Risk Analysis and Options Appraisal, United Kingdom; AEA Technology plc, United Kingdom; Universitat Politècnica de Catalunya, Spain
Contract No.: FIS5-1999-00336
- ACTAF B Aquatic Chemistry and Thermodynamics of Actinides and Fission Products Relevant to Nuclear Waste Disposal
In collaboration with:
FZ Karlsruhe, Germany; Paul-Scherrer-Institut (PSI) Villigen, Switzerland; Kungl. Tekniska Högskolan (KTH) Stockholm, Sweden; Universitat Politècnica Catalunya (UPC) Barcelona, Spain; Københavns Universitet (KU) Copenhagen, Denmark; Enterpris Ltd. (EP) Reading, Great Britain; CIEMAT (CM) Madrid, Spain
Contract No.: FILW-CT-2000-00035

The Sächsisches Staatsministerium für Wissenschaft und Kunst provided support for the following projects:

- Charakterisierung und Klassifizierung von Bakterien aus uranhaltigen Halden mit Hinblick auf Bioremediation: Bakterielle Diversität, Populationsdynamik und Bioakkumulation von Uran und ausgewählten Radionukliden durch Bakterien
Contract No. SMWK 4-7531.50-03-FZR/607
- Untersuchung der Bildung von kolloidalen organischen Partikeln in Bergwerkswässern.
Contract No. SMWK 4-7533.70-FZR/704
- Chemische Konvertierung der Altbestände Kohlenstoff-14-markierter Verbindungen zu Bariumcarbonat. Förderung im Rahmen des Vorhabens 'Nukleare Entsorgung des Forschungsstandorts Rossendorf' Altlastenfonds 2000 des SMWK

- Gastaufenthalt T.Ye. Zayarnaya; Förderung durch SMWK - Forschungsförderung 2000
Contract No. SMWK 4-7531.50-04-844-00/18

Six projects were supported by Deutsche Forschungsgemeinschaft (DFG):

- Identifizierung und Charakterisierung von Komplexierungsprodukten des U(VI) in Pflanzen.
Contract No. DFG BE 2234/1-1
- Komplexierung von Uranyl- und Neptunylionen mit phenolischen Monomeren des natürlichen Ligninabbaus als Grundlage für die Beschreibung der Radionuklid Ausbreitung
Contract No. DFG BE 2234/3-1
- Biocere mit spezifischer Metallbindungsaktivität
Contract No.: DFG SE 671/7-1
- Heterogene Reaktionsmechanismen und deren Kinetik an Schichtsilikatoberflächen
Contract No. DFG BE 2234/4-2
- Charakterisierung der Kolloidpartikel in den Wasserfließsystemen stillgelegter sächsischer Bergwerke
Contract No. DFG ZA 238/1-3
- Untersuchung der Sorptionsmechanismen von Uran(VI) auf Gesteins- und Mineraloberflächen. Identifizierung und Modellierung der sorbierten Oberflächenspezies auf molekularer Ebene.
Contract No. DFG NI 210/6-1

Four projects were supported by the following sponsors:

- Development of experimental arrangements and methods for on-line high temperature gas-chromatography of the heaviest elements.
In cooperation with GSI.
GSI DRNITK.
- Euroconference 'Speciation, techniques, and facilities for radioactive materials at synchrotron light sources'
Contract No. EU/ERBFMMACT98-0331
- Euroconference 'Bacterial-Metal/Radionuclide Interaction: Basic Research and Bioremediation'
Contract No. EU/ERBFMMACT98-0339
- Structure, Bonding and Thermodynamics in Binary and Ternary Dioxouranium Complexes
Marie Curie Individual Fellowship within the Fifth Framework Program of the European Union
(Improving human research potential and the socio-economic knowledge base)
Contract No. HPMF-CT-1999-00342